

Use of absorption and fluorescence spectroscopic techniques for different applications by the newly designed chemosensors

**THESIS SUBMITTED FOR THE DEGREE OF
DOCTOR OF PHILOSOPHY (SCIENCE)
JADAVPUR UNIVERSITY**



BY

MUKUL BIKASH MAITY, M. Sc

Registration No. SCHEM1102921

Index No. - 29/21/Chem./27

**DEPARTMENT OF CHEMISTRY
JADAVPUR UNIVERSITY
KOLKATA – 700 032
WEST BENGAL, INDIA**

2023

Prof. (Dr.) C. Sinha, Ph.D.
Professor & Former Head
Department of Chemistry

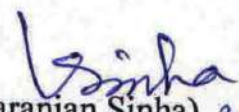


JADAVPUR UNIVERSITY KOLKATA -
7 0 0 0 3 2, I N D I A Telephone: 91+033+
2414-6666. Ext. 2453 (O), Mobile: +91-
9433621872/ 7044231277
e-mail: crsjuchem@gmail.com

To Whom It May Concern

This is to certify that the thesis entitled “Use of absorption and fluorescence spectroscopic techniques for different applications by the newly designed chemosensors” submitted by Mr. Mukul Bikash Maity, M.Sc., who got his name registered on 19.03.2021 (Ph.D. Registration No.- SCHEM1102921) for the award of Ph.D. (Science) degree of Jadavpur University, is absolutely based upon his own work under the supervision of Dr. Chittaranjan Sinha, Professor, Department of Chemistry, Jadavpur University, Kolkata-700 032 and that neither this thesis nor any part of it has been submitted for either any degree / diploma or any other academic award anywhere before. Each Chapter is reviewed by iThenticate software in c/o Jadavpur University and similarity of introductory chapter, Chapter I lies within 10% as recommended by UGC rule. Other Chapters show self-citation only.

It is also certified that he has fulfilled all the requirements of the regulations relating to the nature, period and ethical guideline of research.


(Chittaranjan Sinha) 30/06/2023

(Signature of the Supervisor, date with official Seal)

Professor of Chemistry
D. partment of Chemistry
Jadavpur University
Kolkata-700 032

Declaration of the Scholar

I declare that this written submission suggests my creative approaches in my own words and where other's ideas have been included, I have properly cited with suitable reference from the authentic sources. I also declare that I have adhered to all origins of academic principle and honesty and have not misled or fabricated or falsified any approach/ data/ concept in my submission. I understand such violation of the above will cause for disciplinary action by University and can evoke legal action from the sources which have thus not been properly cited or from whom proper permission has not been taken when needed.

Mukul Bikash Maity
Mukul Bikash Maity 30/06/2023
Department of Chemistry
Jadavpur University

Dedicated to Baba and Maa ...

"Chemistry is a Mystery of
Chemicals,
Chemists are the Detectives
who solve this Mystery."



Acknowledgement

It is one of the best moments in my academic life when I get the opportunity to express my gratitude to all of my near and dear ones and to all who have been attached to my academic career.

First and foremost, I sincerely convey my deepest gratitude to my Supervisor Prof. Chittaranjan Sinha, Professor, Department of Chemistry, Jadavpur University, Kolkata - 700 032, who allowed me to be one of the Research Scholars under his supervision. It's been a privileged and integral part of my academic phase to be under his constant guidance and support during the course of my Ph.D. degree. His sharp intelligence and attention to the work and incisive decision has guided me to accomplish my research project successfully. Thank you very much Sir for giving me that opportunity, believing in me and most importantly for being such a wonderful guide at every stage of my Ph.D. career.

I record my sincere thanks to Prof. Subratanath Koner, Head, Department of Chemistry; Prof. Saurabh Das, Section-in-Charge, Inorganic Chemistry Section and Prof. Ambikesh Mahapatra, Prof. Sujoy Baitalik, Prof. Jnan Prakas Naskar, Prof. Partha Roy, Prof. Samaresh Bhattacharya, Prof. Subrata Mukhopadhyay, Dr. Partha Mahata, Prof. Mahammad Ali, Prof. K. K. Rajak, Prof. K. S. Pramanik, Dr. Bibhuti Bhushan Show, Prof. Tapan Kumar Mondal, Prof. Amrita Saha, Prof. Shouvik Chattopadhyay and other faculty members of the Department of Chemistry, Jadavpur University; I remember my indebtedness to all the staff members of this department for their help in various respects.

I am also extremely thankful to my Research Advisory Committee (RAC) members, Prof. Chirantan Roy Choudhury (WBSU, Kolkata-126), Prof. Chittaranjan Sinha (JU, Dept. of Chemistry, Kolkata-32) and Prof. Subratanath Koner (JU, HOD, Dept. of Chemistry, Kolkata-32) for their valuable suggestions, advices and support during the RAC meetings.

It has been a great pleasure for me to be a part of the Research group of Prof. Sinha. I fail to utter my heartfelt thanks with appropriate words to Dr. Basudeb Dutta, Mr. Suprava Bhunia and Mr. Gurupada Bairy for their constant co-operation and kind support at every stage of my research tenure. I express my gratitude towards Dr. Debasis Mallick for his generous support and contribution throughout my research career.

I am also thankful to all the past and present members of this research group *viz.*, Dr. Sukanya Paul, Mr. Arka Patra, Mr. Koushik Saha, Mr. Manik Shit, Ms. Sangita Ghosh, Mr. Abhisake Karmakar, Dr. Angeera Chandra, Dr. Suwendu Maity, Dr. Srikanta Jana, Dr. Ananya Das mahapatra, Mr. Samrat Dev, Mr. Himadri Shekhar Chatterjee, Mr. Soumya Jyoti Ghosh, Mr. Sambhunath Bera, Dr. Abhijit Das, Mr. Sabir Ahmed, Mrs. Nivedita Roy, Mr. Kumarjit Chowdhury, Dr. Nilima Sahu, Dr. Arup Kumar Adak, Dr. Sunanda Dey.

I am extremely thankful to Mr. Ashikur Rahaman, Mr. Debojit Talukdar, Mr. Panchanan Sahoo for their contribution in my research. I sincerely thank to all my collaborators - Prof. Deba Prasad Mandal, Dr. Shamee Bhattacharjee (Department of Zoology, West Bengal State University, Kolkata 700126) and Dr. Nabendu Murmu, Dr. Gaurav Das (Department of Signal Transduction and Biogenic Amines, Chittaranjan National Cancer Institute (CNCI), Bhowanipore, Kolkata - 700026), Dr. Snehasis Mishra (School of Materials Science and Nanotechnology, Jadavpur University, Jadavpur, Kolkata 700 032, India) for their kind cooperation in research works. I would like to acknowledge Council of Scientific and Industrial Research (CSIR), New Delhi for the Financial Assistance. I would also like to thank Wiley, Elsevier for the research articles that I managed to publish during the tenure of my Ph.D. career.

I am also thankful to my sister Shrabanti and Basanti and my friends Arijit, Supriya, Krishanuda, Abir for their pleasant association, which directly or indirectly helped me in both academic and non-academic affairs.

Whatever I am and whatever I intend to be in future are because of the goodwill and unstinted encouragements that I have received from my parents, Mr. Niharendu Maity and Mrs. Monjuri Maity for their selfless sacrifices, motivation and emotional support which help me a lot throughout the whole academic career and in pursuing the Ph.D. study and no words are enough to acknowledge them. Last but not the least, my sincere acknowledgement to Jadavpur University Administration for providing academic, financial and administrative support for this research.

Mukul Bikash Maity
(Mukul Bikash Maity) 30/06/2023

Preface

The present dissertation entitled “**Use of absorption and fluorescence spectroscopic techniques for different applications by the newly designed chemosensors**” is hereby submitted to fulfill the requirements for the Degree of Doctor of Philosophy (Science) of Jadavpur University. This study mainly based on the synthesis and characterization of some probes which selectively detect biologically important cations. Absorption of light of particular energy will excite the molecule/material and the excited species may either release energy in the form of emission or execute some mechanical motion such as isomerization, rotation, vibration, cleavage etc. The synthesized probe mainly based on Rhodamine, Coumarin, Diformylphenol and Chromone moiety, which have been characterized by different analytical techniques. These species showed significant sensitivity and selectivity towards Cu^{2+} , Al^{3+} , Zn^{2+} , Cr^{3+} and Fe^{3+} ions. Interestingly these synthesized species exhibited anti-cancer activity against different cancer cell lines and the intracellular live cell imaging on various cations also observed. In some cases, the structures have been confirmed by the Single Crystal X-ray crystallographic measurement. The energy gap calculation of optimized structures has been done by DFT (Density Functional Theory) computation. Additionally, a complex based on Hg(II) has been synthesized which has exhibited intense photochromic property and also some comparative discussion on different parameters with some published literature.

The thesis contains six chapters. **Chapter I** contains a discussion on the use and toxicity of the several biological important cations on health and environment. The various fluorescent mechanisms, biological applications and a review on some probes for the detection of Cu^{2+} , Al^{3+} , Zn^{2+} , Cr^{3+} and Fe^{3+} ions related to the present work mentioned in this chapter are delineated in this research. Effect of light on excitation of the probe and also photochromic efficiency of azoimidazoles are briefly described. **Chapter II** contains a coumarin based probe which can serve as fluorescent turn-on Al^{3+} -sensor in acetonitrile-water medium with the enhancement of emission intensity

and LOD is 0.62 μM . It also covers detailed experimental observation on the anti-metastatic potential of the probe on Human skin carcinoma and Human lung carcinoma cells. **Chapter III** deals with rhodamine appended chromone based Schiff base which exhibited efficient sensitivity towards Al^{3+} (LOD, 0.0029 ppm), Cr^{3+} (LOD, 0.0052 ppm), and Fe^{3+} (LOD, 0.0051 ppm) in methanol-water medium with the significant enhancement of fluorescence intensity. The study also covers the detailed characterization process and concise sensing experiments and the results also compared with the published literature. Additionally, the cell imaging in presence of Al^{3+} , Cr^{3+} and Fe^{3+} ions and the action of probe on human breast cancer cell lines also mentioned in this chapter. **Chapter IV** covers on a diformylphenol based Schiff base which selectively detect Zn^{2+} (LOD, 0.30 μM) ions in DMSO-water. The Intracellular Zn^{2+} ions in living cells have also been identified by the probe using fluorescence microscopic imaging technique. **Chapter V** comprises the UV light assisted photochromic behaviour of ligands and the Hg(II) complexes. The rate and quantum yield of E-to-Z isomerisation of the complexes and free ligand also calculated by the experimental data. **Chapter VI** is concerned with a chromone-based molecule, which selectively recognize Cu^{2+} ion (LOD, 0.6 μM) in EtOH- H_2O medium by colorimetrically. The naked eye change of color of the probe upon addition of Cu^{2+} ion in presence of different competitive metal ions is very convincing and helps to design paper kits.

From my research work, I have published some of the above works in high impact SCI journals and more results will be published shortly.

Mukul Bikash Maity

Mukul Bikash Maity

30/06/2023

Index No. 29/21/Chem./27

Registration No. SCHEM1102921

Department of Chemistry

Jadavpur University

Abstract

Index No. 29/21/Chem./27

Registration No. SCHEM1102921

Title of Thesis: Use of absorption and fluorescence spectroscopic techniques for different applications by the newly designed chemosensors.

Our main objective of the research is to explore a special type of molecules who may be excited by absorbing light of definite energy and the excited species may change their emission or mechanical characteristics (structural isomerization, photoisomerization, rotation, cleavage, radical formation etc.) by interacting with specific ions/molecules intricately and can selectively, specifically and sensitively identify the analyte. The Schiff bases (-C=N-) and azo (-N=N-) functions have received much attention in this direction due to their ease of synthesis and structural characterization, use of environmentally benign molecules like, aldehydes/ketones and amines appended with fluorogenic or chromophoric moiety. The Schiff bases are a group of compounds having exocyclic C=N bond(s). The -C=N- can act as a ligating centre and binds to M^{n+} selectively. Hence the Schiff base can act as efficient probe for the detection of several bio-relevant cations at a very low concentration (μM level). The abnormal level of various bio-relevant cations can cause serious health issue. Hence, the recognition of these cations is challenging task for researcher and this can be nicely monitored by the functionalized Schiff bases with fluorogenic moiety. Extensive efforts have been devoted for the design and development of effective chemosensor based on imine moiety (-C=N-) for the selective recognition for sensitive detection of cations. In addition, the UV assisted photochromic behavior is very interesting for researcher because this follows photo-isomerisation which leads to change in

various physicochemical properties like refractive index, redox potential and geometrical structure. Due to these change in molecular property, the photochromism i.e. mostly photo-isomerisation can be applied to various photo-switching devices and optical memory media. Our synthesised species also exhibited UV light assisted photochromic behavior. In my research work, four probes based on Rhodamine, Coumarin, Diformylphenol and Chromone moiety, which have been characterized by different spectroscopic techniques (IR, Mass, NMR, elemental analysis) and some of the structure confirmed by Single Crystal X-Ray Diffraction measurements and Hg(II)-halide complexes of 1-alkyl-2-(*p*-nitro-phenylazo)imidazoles also characterized by Single Crystal X-Ray Diffraction measurements and it exhibited UV light assisted photochromic behavior. Benzimidazolyl-hydroxy-coumarinyl diad, serves as fluorescent turn-on Al³⁺-sensor in acetonitrile-water (2:1, v/v) of pH, 7.2 (HEPES buffer) medium and with the addition of Al³⁺ ions the emission intensity enhanced by twelve times and is detailed in **Chapter II**. The probe showed limit of detection (LOD) as 0.62 μM for Al³⁺ ions. The anti-metastatic potential of the probe on Human skin carcinoma (A431) and Human lung carcinoma (A549) cells are also examined. Another probe Rhodamine based Schiff base with two fluorogenic motifs is described in **Chapter III**. The probe has been characterized through various spectroscopic techniques. The probe exhibits efficient sensitivity and selectivity towards Al³⁺, Cr³⁺ and Fe³⁺ ions with the enhancement of fluorescence intensity by 350 fold (Fe³⁺), 250 fold (Al³⁺) and 220 fold (Cr³⁺), in methanol-water (99:1, v/v; HEPES buffer, pH, 7.2) medium. The limits of detection (LOD) are 0.0051 ppm (Fe³⁺), 0.0029 ppm (Al³⁺) and 0.0052 ppm (Cr³⁺); and in addition the probe has been utilized for cell imaging in presence of Al³⁺, Cr³⁺ and Fe³⁺ ions and the action of probe on human breast cancer cell lines and other different assay like wound healing capacity, nuclear fragmentation, Growth

inhibition analysis also examined. Diformylphenol based probe is delineated in **Chapter IV** and it emits light at 610 nm upon excitation at 380 nm and the emission is strongly intensified on interacting with Zn^{2+} ion in DMSO-water (99:1, v/v; HEPES buffer, pH, 7.2) medium and also in solid state. The limit of detection of Zn^{2+} , 0.30 μM and the binding constant (K_d) is $4.2585 \times 10^4 \text{ M}^{-1}$. The Intracellular Zn^{2+} ions in living cells of HEK293 have also been identified by the probe using fluorescence microscopic imaging technique. Impact of light on the probe does not only excite to execute emission but also does some mechanical performance like structural isomerization such as trans(E)-cis(Z) isomerization of 1-alkyl-2-(arylo)imidazoles and their Hg(II) complex which is known as photochromism. **Chapter V** describes the effect of light irradiation on Hg(II)-halide complexes of 1-alkyl-2-(*p*-nitro-phenylazo)imidazoles. They have been characterized and the structures have been confirmed by single crystal X-ray diffraction. UV light assisted photochromic behaviour of ligands and the complexes are checked. The rate and quantum yield of E-to-Z isomerisation of the complexes and free ligand also calculated by the experimental data. DFT and TD-DFT calculations also support the experimental data of the rate and quantum yields. Chromone-based probe is noted in **Chapter VI** and has been used for the chromogenic selective recognition of Cu^{2+} ion in EtOH- H_2O (99:1, v/v) medium. The sensor shows excellent selectivity towards Cu^{2+} ion at very low limit of detection, 0.6 μM and the binding constant for Cu^{2+} also determined as $4.9346 \times 10^4 \text{ M}^{-1}$. The naked eye change of color of the probe upon the addition of Cu^{2+} ion is very convincing and helps to design paper kits.

From my research work, I have published a total of four original research articles and more results will be published shortly. I have attended a number of national and international conferences and have presented my research results.

Contents

Contents	Page No.
<hr/> <i>Chapter I: Introduction</i> <hr/>	
I. Abstract	2
I.1. Introduction	3
I.2. Cations in Biological System	4
I.3. Preference towards Optical Sensing over other analytical techniques	7
I.4. Photochromism	15
I.5. Biological Applications	16
I.6. Use of chemosensors toward detections of bio-relevant cations	17
I.7. Aims and scope of the present research	36
I.8. Physical measurement	39
I.9. References	40
<hr/> <i>Chapter II: Double advantages of Benzimidazolyl-hydroxy-coumarinyl diad - “turn-on” sensing of Al³⁺ and preventing metastasis in cancer</i> <hr/>	
II. Abstract	53
II.1. Introduction	53
II.2. Experimental	55
II.3. Results and Discussion	68
II.4. Conclusion	86
II.5. References	86

Chapter III: Application of a Rhodamine-Chromone Schiff Base Probe for the Sensing of Fe³⁺, Al³⁺, Cr³⁺ at Low Concentration and Exploration of the Anticancer Activity and Bio-imaging

III. Abstract	90
III.1. Introduction	91
III.2. Experimental section	93
III.3. Results and discussion	102
III.4. Conclusion	133
III.5. References	133

Chapter IV: Use of Diformyl-triazolo Schiff base for Zn²⁺ Sensing and intracellular Live Cell Imaging

IV. Abstract	138
IV.1. Introduction	139
IV.2. Experimental Section	140
IV.3. Results and discussion	145
IV.4. Conclusion	167
IV.5. References	168

Chapter V: Structure and Photoisomerisation of Halo-bridged dimeric Mercury (II) complexes of 1-alkyl-2-(p-nitro-phenylazo) imidazoles

V. Abstract	174
V.1. Introduction	175
V.2. Experimental	175
V.3. Results and discussion	179
V.4. Conclusion	190
V.5. References	191

Chapter VI: Use of chromone based probe as colorimetric sensor for the detection of Cu²⁺ ion: design of test paper kit

VI. Abstract	195
VI.1. Introduction	196
VI.2. Experimental Section	197
VI.3. Results and discussion	201
VI.4. Conclusion	213
VI.5. Reference	214

Chapter VII: Conclusion

VII.1. Conclusion	219
VII.2. Chapter II	219
VII.3. Chapter III	222
VII.4. Chapter IV	225
VII.5. Chapter V	227
VII.6. Chapter VI	230

Chapter I

Introduction

CHAPTER I

Abstract

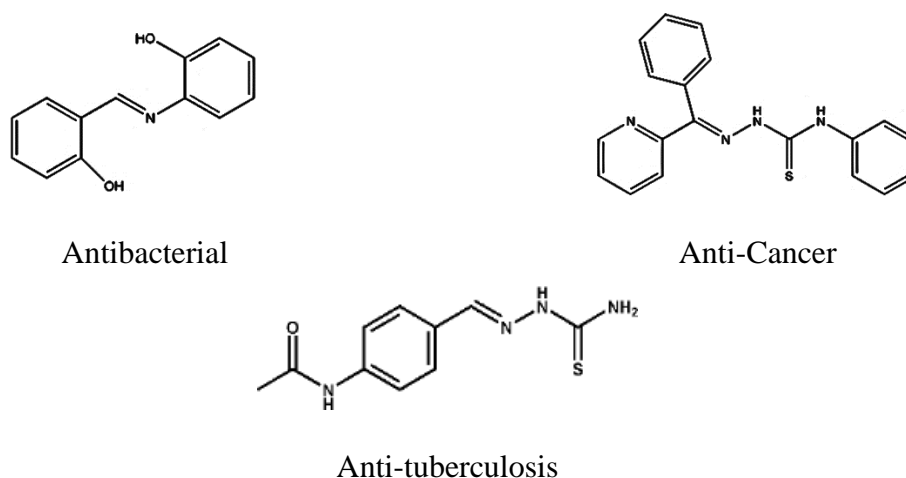
Design and application of chemosensors towards the detections of biologically significant cations: A partial Review

Chemosensor, a synthetic or semi-synthetic and structurally established chemical compound, can recognize various types of analytes selectively, specifically and sensitively by changing color with the change in absorption and/or emission characteristics (like wavelength, intensity, life time). In last two decades the field is undergoing mammoth progress mainly its application in diseases diagnosis, environmental monitoring, toxicological analysis, and usefulness as marker in biology and chemistry [1].

In the field of chemosensors, the Schiff bases have received much attention due to their ease of synthesise and structural characterization, use of environmentally benign aldehydes/ketones and amines appended with fluorogenic or chromophoric moiety. We have designed fluorescence active Schiff bases based on rhodamine, coumarin, diformylphenol and chromone moiety which offer O, N, S donating sides towards the analytes. These chemosensors recognize Cu^{2+} , Al^{3+} , Zn^{2+} , Cr^{3+} and Fe^{3+} ions by Fluorometric as well as colorimetric techniques. The synthesized probes have a different application such as preventing metastasis in cancer, live cell imaging etc.

I.1. Introduction

The Schiff bases are a group of compounds having a double bond connecting between the carbon and nitrogen atoms (-C=N-) [2,3]. During the progression of scientific research Schiff bases have been significantly exciting to both chemists/biochemists/environmental analysts. In the year 1864 Hugo Schiff reported the first Schiff base and synthesized from the reaction of -NH₂ (an amino) and carbonyl compound (aldehyde or ketone) which has an active, imine (-C=N-) group. This imine (-C=N-) function, in general, is stable but it can be susceptible to hydrolysis in acidic or basic medium and sometime catalysed by metal ions. Schiff bases may easily be functionalized and may act as a multidentate chelating agent and can form coordination complexes with transition and post-transition metal ions of innumerable stereochemistry [4,5]. The Schiff bases (**Scheme I.a**) show extensive application in the field of pharmacology, dye industry, catalysis, agrochemical [6,7], biology and chemistry, [8-10] and they also show different biological applications like analgesic, [11] anticancer activity, [12-14] anti-inflammatory, [15,16] antifungal, [17,18] antibacterial, [19,20] activity. Several types of amines and carbonyl moieties forms various multidentate and structurally unique Schiff bases which plays a significant role in broad area of coordination chemistry, sensing, biological activity, coordination polymer etc.



Scheme I.a. Some biologically active drugs having C=N group

I.2. Cations in Biological System

Cations i.e., the metal ions, these are nonbiodegradable, exist everywhere and plays a vital role [21,22] in all forms of life. They can smoothen the normal functioning of various biological processes like metabolism, immune system improvement, catalysis oxygen metabolism, nervous system, osmotic regulation etc. Different transition, non-transition, alkali/alkaline earth metals such as Iron (Fe), Copper (Cu), Chromium (Cr), Zinc (Zn), Cobal (Co), Nickel (Ni), Molybdenum (Mo), Aluminum (Al), Sodium (Na), Potassium (K), Magnesium (Mg), Calcium (Ca) contribute a significant activity in biological process. In human body Iron occupies the most abundant and significant transition trace element. It exists in both ferrous (Fe^{2+}) and ferric (Fe^{3+}) form which play a crucial biological function [23]. These two forms of iron actively participated in energy production, cell growth, electron transportation etc. Iron also presents in hemoglobin and myoglobin which are involved in the oxygen transport and oxygen storage process respectively. Fe^{3+} ion helps to transport electrons. However, the labile $\text{Fe}^{2+/3+}$ ions are very much toxic to cells and causes degenerative diseases [24]. Again, the iron deficiency can cause anemia, which can be harmful or even deadly [25,26]. But excessive consumption of iron leads to dysfunction of different organs as well. Additionally, the presence of Iron has severe effects on the quality of crops and agricultural activities [27]. Copper mainly exists in two oxidation forms cuprous (Cu^+) and cupric (Cu^{2+}) and copper is the third most available (next to Fe and Zn) essential nutrient in human body. In human body copper is found in liver, bone [28], and muscle. Cu^{2+} plays a diverse role as an active centres and catalytic co-factors for metalloenzymes like, superoxide dismutase (SOD), cytochrome oxidase, energy transport processes and other several biochemical processes. Copper involves in the formation of red blood cells, stimulates the immune system of human body to fight against infections. The deficiency of copper can cause bone, arterial, and anaemia abnormalities while the excessive level of copper can cause toxicity due to the formation of ROS which give rise to

neurodegenerative disease like Wilson's Alzheimer's and Parkinson's disease etc. Additionally, Copper is also an essential micronutrient for plants cellular process which on excessive causes chlorosis [29-35]. The common oxidation state of chromium is + 3 which is less toxic, however the higher oxidation states (Cr^{4+} and Cr^{6+}) are potentially toxic [36]. The Cr^{3+} ion is considered as the essential trace element in nutritional diet for human and it activates the insulin to reduce blood sugar [37,38]. The US Environmental Protection Agency (USEPA) has classified chromium species as a mutagenic and carcinogenic agent [39,40]. Below the tolerable level of Cr^{3+} in living system leads to diabetes and cardiovascular diseases. However, the excessive presence of Cr^{3+} ions can bind with DNA through guanine N7 and phosphate backbone and affect and damage the cellular components [41,42]. The Zinc commonly exists in divalent form (Zn^{2+}) and in this form it is the second most essential micronutrient in biological system. The Zn^{2+} involves in more than 300 enzymes [43] and that's why it is called the mother of metalloenzyme. Notably the Zn^{2+} ion present at the active site of various enzymes like carbonic anhydrase, carboxypeptidase etc. In addition, zinc assists a structural role in various proteins and proteins acts as catalytic co-factor for vital process like regulation of enzymes, gene expression, DNA binding cellular metabolism, apoptosis, neural signal transmission. Lower level of Zinc can cause metabolic disorder like retarded and impaired growth, weaker immune response, dermatitis, hypotension, and hypothermia. However, the excess presence of Zinc in body is detrimental to vital organs and are responsible for Parkinson's and Alzheimer's disease [44-47]. Aluminium is the third most abundant element in the earth crust and it has been extensively used in our daily life. The most common oxidation state of Aluminium is Al^{3+} which can be widely used in pharmaceuticals [48-54], water purification systems, food supplements etc. But it is well known that Al^{3+} is a nonessential element while excess of Al^{3+} causes neurological disorders, such as Parkinson's disease [55-58], Alzheimer and dementia. The high concentration of Al^{3+} effects on plants growth as a result decreases the production of

the agriculture. Sodium metal exists as Na^+ ion and it is the sixth most abundant element in Earth's Crust (about 2.83%). Sodium ion (Na^+) found in the extracellular part of animal cells and it regulates electrostatic charge transportation, osmotic equilibrium and it also maintains the blood pressure, pH level, and helps in neurotransmission [59,60]. Lower concentration of Na^+ causes an electrolytic disorder while an excess concentration exhibits an adverse effect on Kidney and increases blood pressure [61]. Potassium (K^+) existing as 0.4% of the mass of body depending on K^+ concentration inside the cells or in the extracellular fluid plays diverse roles in the intracellular part and is related with the maintenance of electrolytic balance with the Na^+ . Potassium (K^+) ion plays an important role for the signal transduction in the nervous system [62,63]. Potassium consumption is very much essential for plants and animals for the regular functioning of the system. The imbalances in potassium (K^+) level cause a serious health problem and high concentration leads to severe cardiac disorder while its deficiency causes nausea, muscle weakness and fatigue [64]. Magnesium, a member of the alkaline earth series, is the fourth-most-abundant metal ion in cells. Magnesium mainly exists as Mg^{2+} ions and it is a key component of chlorophyll and performs the photosynthetic process in plants and it also acts as a cofactor on cell proliferation, numerous enzymatic catalysis like DNA Synthesis [65-67], phosphorylation of proteins etc. Various distributions of Mg^{2+} ions in sub-cellular compartments accomplish their varying biological functions. Irregular concentrations of Mg^{2+} ions cause different diseases such as diabetes, Epilepsy, Alzheimer and hypertension [68-70]. Calcium exists as the largest intracellular concentration of the alkaline earth series with around 100 nM in its free form in living systems. Primarily 99% of the calcium exists in bones and teeth. The Ca^{2+} monitors hormonal secretion, gene transcription, fertilization, nerve impulse transmission, signal transduction and muscle contraction. Additionally, the imbalances in intracellular concentration levels of Ca^{2+} ions can cause physiological disorders like obesity and Alzheimer's disease [71,72]. (**Table I.1**)

Table I.1. Acceptable limits of few elements in drinking water (in the unit of mg/liter) [73]

Element	WHO (mg/day)	ICMR (mg/day)	ISI (mg/day)	USEPA (mg/day)	CPCB (mg/day)
Iron	0.1	1.0	0.3	-	1.0
Copper	1.0	1.5	0.05	1.3	1.5
Aluminum	0.03	-	-	-	-
Zinc	5.0	0.10	5.0	-	15.0
Chromium	-	-	0.05	0.1	No relaxation
Sodium	200	1100-3300	-	20	-
Potassium	-	1100-3750 mg/day	-	-	-
Magnesium	50	-	30	-	100
Calcium	75	200	75	-	200

WHO: World Health Organization; ICMR: Indian Council of Medical Research; ISI: Indian Standard Institute; USEPA: US Environment and Protection Agency; CPCB: Central Pollution Control Board

I.3. Preference towards Optical Sensing over other analytical techniques

For the detection of ultra-trace concentration of analytes some common techniques such as Electrochemical, Gravimetry and Spectrophotometric methods are used. The Classical Techniques which involved so many techniques like inductively coupled plasma-atomic emission spectrometry (ICP-AES) [74,75], voltammetry [76], atomic absorption spectroscopy (AAS) [77], inductively coupled plasma mass spectrometry (ICPMS) [78], flame atomic absorption spectroscopy (FAAS) [79], thin chitosan films [80,81] and functionalized metal nanoparticles [82,83] and all these techniques are involves an expensive and laborious and are very much complicated for estimation. However Spectrophotometric method based on optical chemosensor involves UV-Visible and Fluorescence technique which have emerged as the

most convenient method for recognition of biologically important analytes with a low detection limit and intracellular imaging of analyte for biological applications. Mainly the Fluorescence and Absorption Methods are effective over other because these Fluorescence and Absorption Methods are cost-effectiveness, feasible synthetic route, rapid responsive, substantial selectivity and sensitivity, easy to analysis, operational simplicity, significant detection limit etc.

I.3.1. Chemosensor

A device which deals with a physical quantity and transforms to measurable and a distinct “signal” that can be detected by a viewer or by an analytical instrument is called sensor. A chemosensor is a device which can detect different chemical components such as ions, molecules, compounds and different analytical samples employing chemical principles. To ensemble a chemosensor three key units are required: (a) a receptor which is composed of mainly two units one part attached to spacer and another part i.e., binding unit which performs a major role to bind with the specific analytes according to its selectivity and sensitivity; (b) a signaling unit, which provides a specific distinguishable signal when an analyte interacts with the receptor; (c) analytical instruments and methods which can recognize this distinguishable signal and transformed it into a valued information (**Fig.I.1**). When an analyte binds with a chemosensor then a change in fluorescence and absorption spectra takes place which indicates the nature of response towards analytes. When an analyte interacts with the fluorogenic receptor then a change in fluorescence emission intensity takes place which can be measured by Fluorometric spectrophotometer whereas an analyte when binds with a chromogenic receptor then it responses via colorimetric change that can be easily measured by UV-Visible absorption spectra.

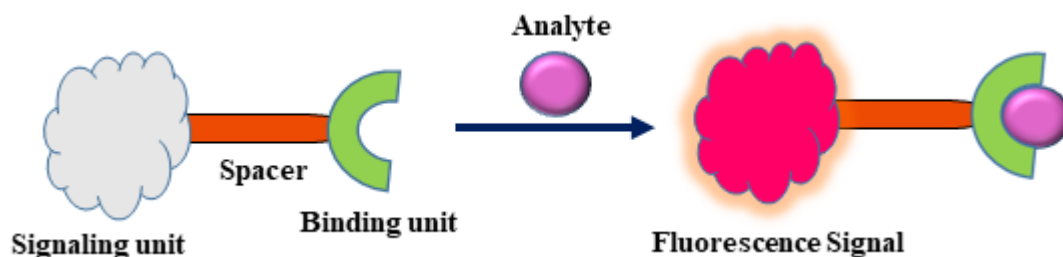


Fig.I.1. Pictorial representation of binding an analyte (guest) with the chemosensor via host-guest interaction.

I.3.2. Different Fluorescence Sensing Mechanism

In case of fluorescence active molecules, the absorption of light at a specific wavelength effects the radiative emission from excited state. In case of fluorescence chemosensors mainly two types of responses take place i.e., “Turn On” and “Turn Off”. In case of “Turn On” response, commonly the fluorescence emission intensity significantly enhanced at a particular wavelength or with the shifting of wavelength or the ratiometric enhancement takes place whereas for the “Turn Off” sensing the lowering or the quenching of emission intensity takes place sometimes with the shifting of wavelength.

I.3.2.1. Photoinduced Electron Transfer (PET)

The PET active chemosensor composed of three moieties i.e., fluorophore-spacer-receptor unit. This mechanism exhibits mainly the charge transfer from the lone pair present in the HOMO of the heteroatom (O, N, S and P) to the LUMO of acceptor. In case of free probe i.e., the unbound state of the probe the intramolecular electron transfer takes place from the HOMO of the free receptor to LUMO of the fluorophore moiety, this electronic transition follows the non-radiative pathway and hence no such fluorescence observed. When the analyte interacts with the probe, the electron pair of the receptor interact with the analyte as a consequence the energy of the HOMO of the bound receptor decreases and lower than the HOMO of receptor and hence

the PET process is inhibited and producing a “Turn On” fluorescence enhancement phenomena (**Fig.I.2**). The solvent polarity makes an important role for the PET mechanism, as the solvent polarity increases the electron transfer is also facilitated [84].

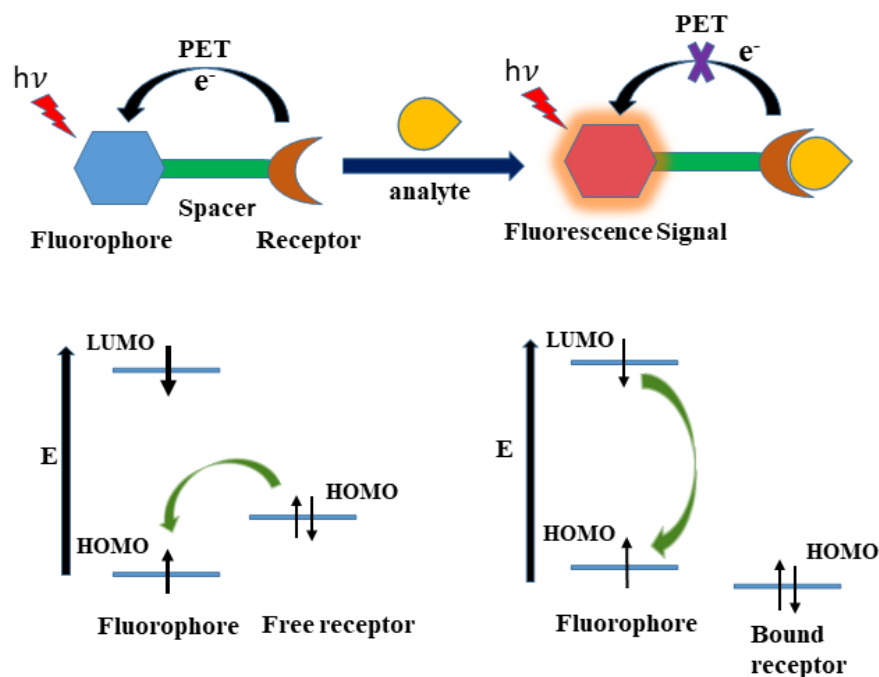


Fig. I.2. Schematic representation of PET process

I.3.2.2. Excited-State Intramolecular Proton Transfer (ESIPT):

In biological system proton transfer mode in terms of ESIPT extensively exists in nature. If the proton donor (amino and hydroxyl group) present nearby the proton acceptor ($-C=O$, $-N=$), then the intramolecular hydrogen bonding in an ESIPT molecules becomes favorable [85]. The fundamental concept of ESIPT process was first reported by Weller in 1950s [86]. The ESIPT process is best explained by the relaxation of photoexcited molecules via tautomerization by transfer of protons. A molecule follows the ESIPT mechanism when the molecule is capable of forming a five/six membered ring transition state during the tautomerization followed by a significantly large Stokes' shift (**Fig.I.3**). This process follows the four-state photochemical route where the ground state represents as enol (E) form which on photo excitation undergoes

tautomerization to keto (K) form and this process can be represented as $E^*(S_1) \rightarrow K^*(S_1)$ and this pathway passes through the intramolecular hydrogen bonding with a five/six membered cyclic transition state [87]. Then, it reverts back to initial enol form with the reverse protons transfer (RPT) mechanism and this process happens at a very fast rate. However, radiative decay and the non-radiative ESIPT process follows similar pathway from excited keto (K^*) form into the ground state keto (K) form. But ESIPT is relatively faster than the radiative decay. The ESIPT chromophores show fluorescence because the keto tautomer (K) with a few exceptions and are substantially sensitive to its surroundings. The polar and hydrogen-bonding donating solvents inhibits the ESIPT mechanism [88].

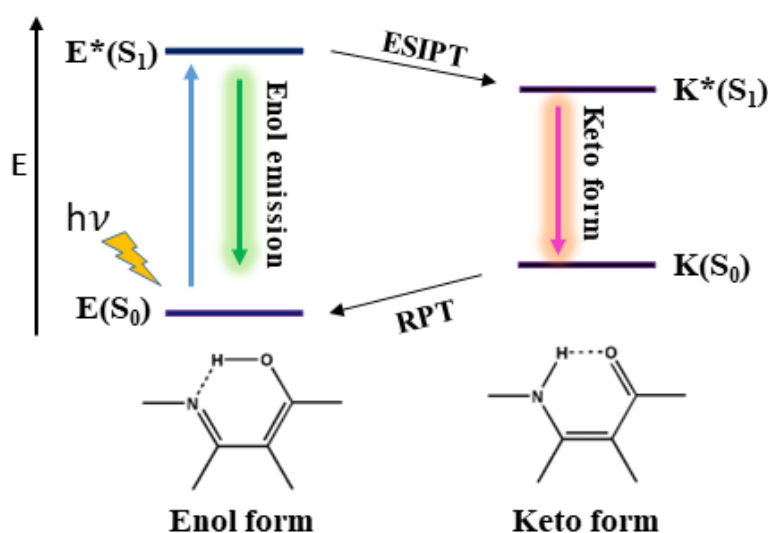


Fig. I.3. Schematic Representation of ESIPT pathway

I.3.2.3. Intra and Intermolecular Charge Transfer (ICT)

ICT is a mechanism by which a molecule in its excited state undergoes energy relaxation via charge transfer process and this process carried out by both intermolecular and intramolecular pathway (**Fig.I.4**). The intermolecular charge transfer process happens when an excited

molecule and a neighboring molecule act as an acceptor and donor but the intramolecular process happens when the charge redistribution occurs in the excited state within the same molecule having both donor and acceptor moieties and generate a great dipole moment. In case of ICT system, a fluorophore moiety is in direct interaction with a receptor and comprises of electron rich and electron deficient moieties resembling a ‘push–pull’ mechanism. The fluorescence output during the detection processes of interaction between the receptor and the analyte dictates the change in electron density in the fluorophore. The ICT mechanism causes considerable shifts in absorption and fluorescence spectra of the probe upon the binding with the analyte and it may exhibit ratiometric fluorescence shifts [89].

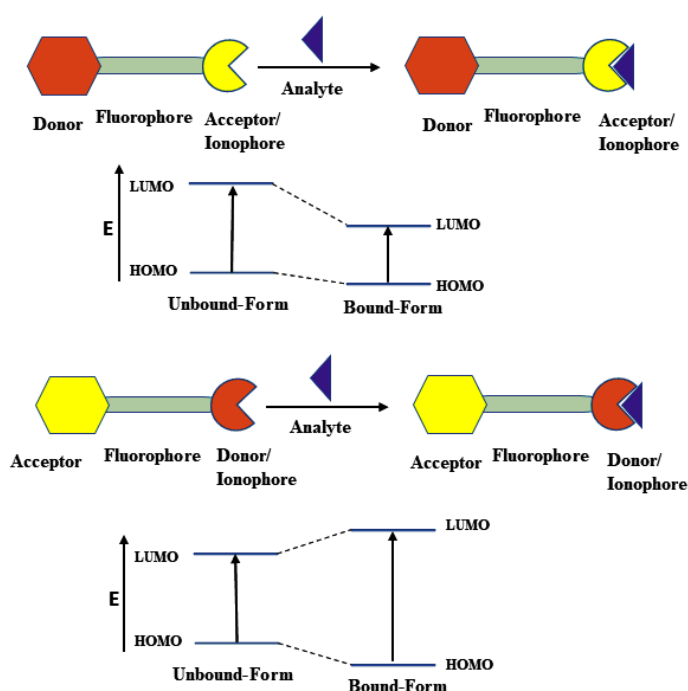


Fig. I.4. Schematic representation of ICT phenomena.

I.3.2.4. Fluorescence Resonance Energy Transfer (FRET)

The FRET process occurs by the energy transfer from an excited fluorophore (donor) to another fluorophore (acceptor). This mechanism is basically a distance-dependent phenomenon. The FRET proficiency depends upon the strength of overlap of the donor emission spectra and

acceptor absorption spectra and the proximity between two specifically lies within Förster radius (3-6 nm), dipole-dipole interaction (**Fig. I.5**). In FRET process the transfer of energy occurs from the excited donor (D^*) fluorophore to the acceptor fluorophore (A) having longer-wavelength ($D^* + A \rightarrow D + A^*$), and acceptor emits light with the resulting loss of emission from donor. The efficiency of FRET (E_{FRET}) is depends by the inverse relation with sixth power of intermolecular distance ($E_{\text{FRET}} = 1/[1 + (r/R_0)^6]$; R_0 is the Förster radius and it's the distance where E exhibits at its 50% of its maximum intensity.) for analytes that produces changes in molecular proximity with the receptor [90,91].

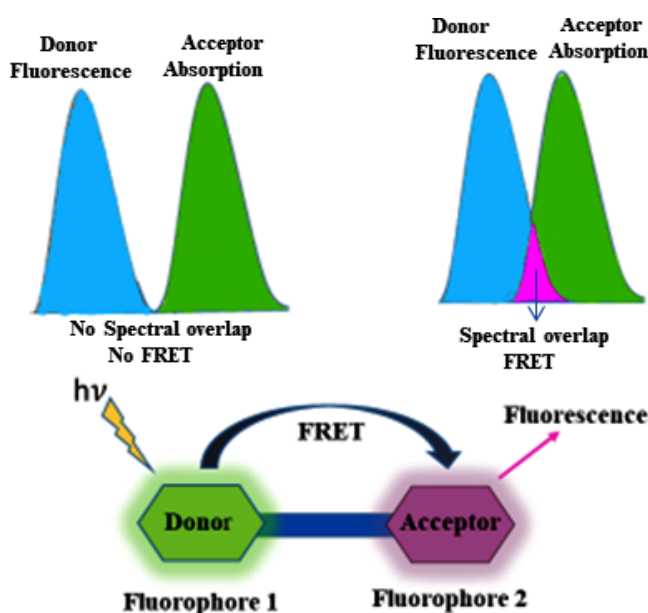


Fig. I.5. Schematic Representation of FRET Mechanism.

I.3.2.5. Chelation Enhanced Fluorescence (CHEF) and Chelation Enhanced Quenching

(CHEQ): When a fluorogenic probe bears two or more accessible donor centres and can bind metal ion simultaneously forming five or six-member ring then a change in fluorescence response takes place and this process occurs by two ways i.e., CHEF and CHEQ. When the fluorescence intensity increases upon the interaction with metal ion then the process is called CHEF and when the fluorescence intensity decreases upon the interaction with metal ion then

the process is called CHEQ (**Fig. I.6**). A red or blue shift in the emission band could be observed because of CHEF and CHEQ process. Due to the Chelation in CHEF process the rigidity of the resulting complex increases which also enhances the radiative process. However, in case of CHEQ due to the existence of paramagnetic substance (transition metal ion or radical) the species with the close proximity to the fluorogenic probe and on excitation, it may undergo ISC from S1 to T1 state of the fluorophore and subsequently deactivated through the non-radiative pathway [92].

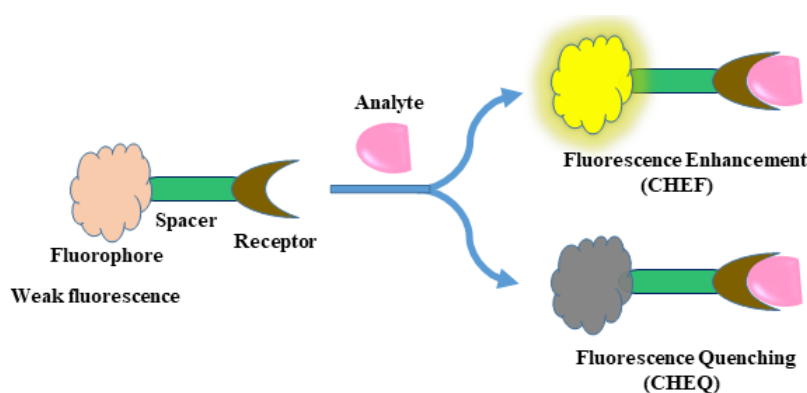


Fig. I.6. Schematic Diagram of CHEF and CHEQ process.

The quenching process (**Fig. I.7**) affects the lifetime profile of the probe and this quenching further classified into two types (i) Dynamic and (ii) Static

(i) **Dynamic Quenching:** when $Q > A$, collisional quenching happens; excited-state of the fluorophore, A^* , becomes deactivated in presence of Q , $[A^*Q]$. Heavy atoms have large number of L-S coupled states, quenching happens due to spin-orbit coupling and inter-system crossing to the triplet state. Dynamic Quenching i.e. Collisional quenching diminishes the lifetime of the fluorophore.

(ii) **Static Quenching:** In presence of large excess ($Q \gg A$) of quencher (Q) with the analyte (A) a stable ground state complex ($A + Q \rightarrow AQ$) may be formed and the resulting component may be non-fluorescent then in this case the emission is quenched statically. This type

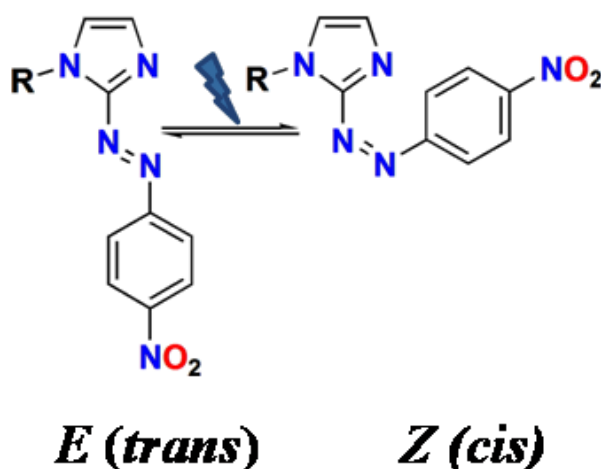
quenching i.e., Static quenching will not change or reduce the lifetime of the sample because it forms the non-fluorescent ground state complex with the quencher. Hence, they will have normal excited state characteristics. As the quencher is reducing the quantity of fluorophores hence the emission from the sample is decreased.



Fig. I.7. Schematic Diagram of Quenching Response.

I.4. Photochromism

Photochromism is a reversible photo-isomerization (Scheme I.b) of two different isomers having two different absorption spectra and color. With the photo-irradiation this process induces in both the direction or in one direction [93-97]. However, this photo-isomerisation leads to change in several physicochemical properties like redox potential, refractive index and geometrical structure. Due to these change in molecular property, this phenomenon can be applied to several photo-switching devices and optical memory media [98-101].



Scheme I.b. Photo-isomerization with the irradiation of light

Inorganic materials have been used to design erasable memory devices which is mainly based on magneto-optic effect or on phase transformation. Due to the inadequate reliability the organic constituents, they have not exhibited such applications. But now a day such concept is completely reversed because some organic dyes are used as a building block of CD-R (compact disk-recordable). Photochromic substances have been exhibited a favourable constituents for the next generation erasable memory device. Different types of organic materials such as azobenzene, stilbene etc., having a photo-isomerizable chromophores can change their conformation by photo-irradiation [102, 103]. Some organic polymers which are able to change their refractive index [104-108] by thermal heating and they have been currently used in optical fiber as the switching components. Hence, these types of materials can be effectively substituted by photochromic materials [109-112], which can change their refractive index. Rate, efficiency and various activity of photochromism have been regulated by molar mass, structural flexibility, solvent polarity and presence of apparently innocent molecules associated around the photochrome. In this regard, metal complexes of arylazoimidazoles ($RaaiR'$) have been studied in our laboratory in different dimension [113-122].

I.5. Biological Applications

Metal ions, a non-biodegradable integral part of evolution of cells, regulate the cell growth and the metabolic processes. Therefore, the measurement of ion concentration in cell is of urgent important for human health. Design of ion selective probe those are non-toxic to living cell and diffusible to living cells via cell membrane is a focused area of research. In addition, the chemosensors penetrates through the different cancer cells and prevents the metastasis in cancer. The live cell imaging is so much significant because from this study we can directly recognize the presence of biologically important metal ions in intracellular position. Now a days the prevention of the metastasis in cancer is relevant because out of 1.35 billion Indian

populations, 1.4 million are diagnosed with cancer every year and in a developing country like India, mortality from cancer is as high as 1.2 million. Our synthesized probes those are mentioned in the different chapters show potent anticancer activity in various cancer cell lines. To examine this anticancer activity, we have successfully performed different assay. We went through several cellular studies after checking its cytotoxicity through MTT assay to address the question that whether the chemosensor has any anticancer effect. As cancer mainly shows uncontrolled proliferation (hyperplasia) due to mutation in certain proto-oncogenes and inhibited cell death pathways, we checked for the effect of the synthesized chemosensor on the proliferation of the cancer cells through colony formation assay. So, our synthesized chemosensors shows multi-functional characteristics in biological fields.

I.6. Use of chemosensors toward detections of bio-relevant cations.

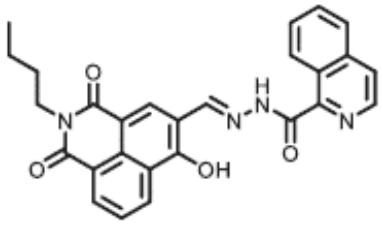
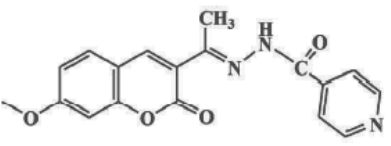
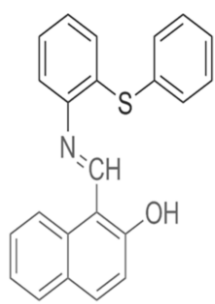
I.6.1. Al³⁺ sensing probe

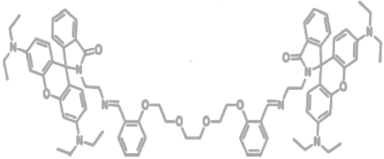
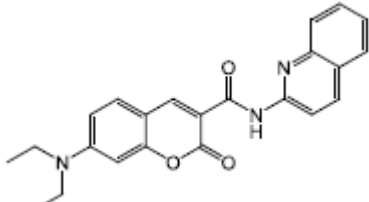
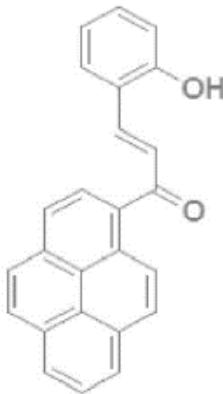
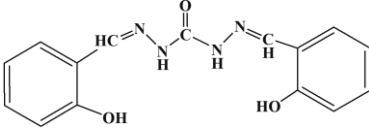
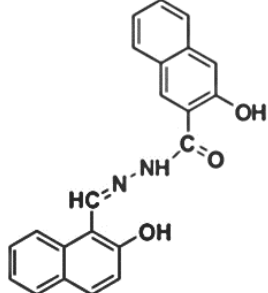
The 3rd most abundant bio-relevant metal ion, Al³⁺ in the earth crust has been commonly used in our everyday life. Al³⁺ enters into living body through different activities and exposure to environment, biology, food as supplements, pharmaceuticals etc. Hence the detection of Al³⁺ ions (**Table I.2**) is very challenging task for the researchers. In 2022, H. Xu et al. reported [123] a probe on Al³⁺ sensing where Schiff base receptor based on naphthalimide and isoquinoline units (**A-1**) that can selectively detect Al³⁺ ions. The probe (**A-1**) shows visible color change and significant enhancement of emission intensity in presence of Al³⁺ ions in DMSO/H₂O solution with detection limit of 52×10^{-9} M for Al³⁺ ions. D. Ravichandran et. al. in 2023 reported [124] a probe (**A-2**) which shows an efficient fluorescent selectivity towards Al³⁺ ions in presence of different competitive cations. The probe (**A-2**) selectively sense Al³⁺ ions in methanolic (10 μ M) solution with the detection limit of 0.0490 μ M. In 2020 W. A. Durai et. al. designed [125] a new chemosensor (**A-3**) which is selectively detect Al³⁺ ions in

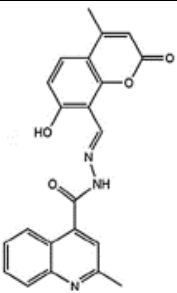
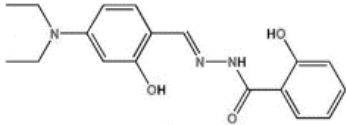
DMSO medium. The 1:1 stoichiometry of complexation between the probe and Al^{3+} has been studied by using Job's plot analysis. The limit of detection (LOD) was evaluated as 13×10^{-7} M. R. Manjunath et. al. in 2018 synthesized [126] a rhodamine-based chemosensor (**A-4**) detects Al^{3+} ions by colorimetrically as well as and fluoremetrically. The mechanism of complexation between the probe and Al^{3+} was explained by the cleavage of spirolactam ring and as a result fluorescence enhancement takes place. Y. Li and co-authors in 2020 efficiently designed [127] a Quinoline carboxamides based on coumarin derivatives which showed the fluorescence quenching in presence of Al^{3+} ions in MeCN/ H_2O (95:5, v/v) medium. The reported probe (**A-5**) shows the good selectivity and sensitivity towards Al^{3+} ions and form 2:1 complex with Al^{3+} ions in MeCN/ H_2O (95:5, v/v) medium. S. Suresh et. al. in 2018 synthesised [128] a pyrene based chemosensor (**A-6**) by an aldol type of condensation reaction. The chemosensor detect Al^{3+} ions selectively with the enhancement of fluorescence intensity and the probe (**A-6**) formed 1:1 stoichiometric complex with Al^{3+} ions which was established by the job's plot analysis. The detection limit towards Al^{3+} ions was evaluated as 4.13×10^{-6} M. M. V. Kaveri and co-authors in 2021 reported [129] a probe (**A-7**) which has been synthesized by the condensation between salicylaldehyde and carbohydrazide. The probe (**A-7**) specifically and selectively sense Al^{3+} ions with the enhancement of fluorescence intensity and the probe forms 1:1 complex with Al^{3+} ions. The limit of detection (LOD) value of the probe towards Al^{3+} was reported as 32 nM. The probe (**A-7**) can used as a cell imaging study of Al^{3+} ions in MCF-7 cells lines and real water samples. A. Saravanan et. al. in 2020 reported [130] a probe (**A-8**) which can selectively sense Al^{3+} ions with the enhancement of emission intensity. The limit of detection of the probe (**A-8**) towards Al^{3+} ions evaluated as 1.2×10^{-7} M. Additionally the probe (**A-8**) can be used as the detection of Al^{3+} ions in real water sample. L. Fan and coauthors in 2014 reported [131] a coumarin based probe (**A-9**) which has selectively sense Al^{3+} ions. The probe selectively detects Al^{3+} ions with the 200-fold enhancement of emission

intensity. The probe (**A-9**) shows 2:1 stoichiometric binding with Al^{3+} ions. The limit of detection value of the probe (**A-9**) towards Al^{3+} ions was reported as 8.2×10^{-7} M. M. Kumar et. al. in 2022 reported [132] a new salicylaldehyde based chemosensor (**A-10**) which selectively detect Al^{3+} ions. The probe shows 20 times enhancement of emission intensity in existence of only Al^{3+} ions. The chemosensor (**A-10**) also shows similar trend for Al^{3+} ions in presence of various type solvents. Additionally, the limit of detection of **A-10** for Al^{3+} ions was evaluated as 1.2×10^{-6} M. The Job's plot calculations showed the 2:1 complexation between the probe (**A-10**) and Al^{3+} ions.

Table I.2. Some Reported Probes on Al^{3+} sensing

Probe	Solvent	LOD (M)	Reference
 <p>A-1</p>	DMSO/H ₂ O (9/1, v/v, pH 7.4, HEPES buffer, 0.2 mM)	5.2×10^{-8}	[123]
 <p>A-2</p>	Methanol (10 μM) solution	4.9×10^{-8}	[124]
 <p>A-3</p>	DMSO medium	13×10^{-7} M	[125]

Probe	Solvent	LOD (M)	Reference
 <p>A-4</p>	CH ₃ CN:H ₂ O (80:20, v/v) solution	-	[126]
 <p>A-5</p>	MeCN/H ₂ O (95:5, v/v) solution	-	[127]
 <p>A-6</p>	EtOH-H ₂ O solution (1:1 v/v, HEPES = 50 mM, pH = 7.4)	4.13×10^{-6} M	[128]
 <p>A-7</p>	CH ₃ OH : H ₂ O (1:2, v/v)	32×10^{-9} M	[129]
 <p>A-8</p>	DMSO-H ₂ O	1.2×10^{-7} M	[130]

Probe	Solvent	LOD (M)	Reference
 <p>A-9</p>	EtOH	8.2×10^{-7} M	[131]
 <p>A-10</p>	DMF	1.2×10^{-6} M	[132]

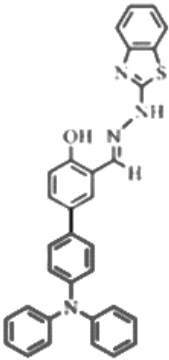
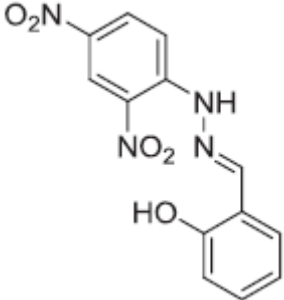
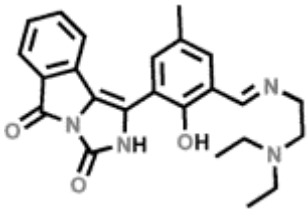
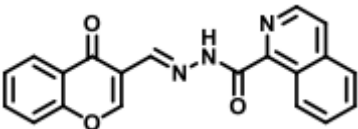
I.6.2. Zn²⁺ ion sensing probe

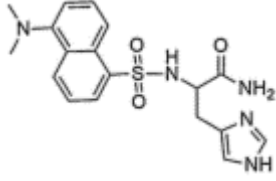
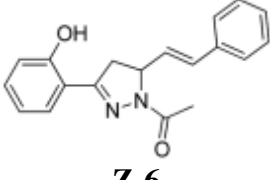
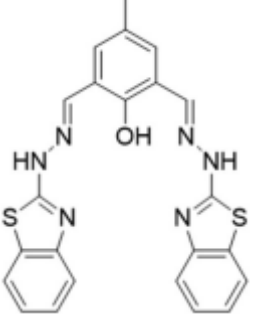
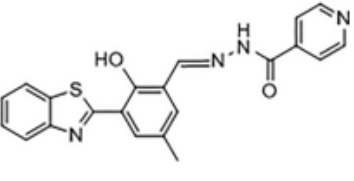
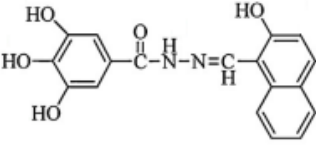
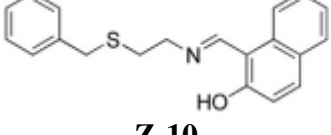
Zinc ion (Zn²⁺), being a very essential element, plays an important role in different biochemical and environmental activities. So, the detection of Zn²⁺ (**Table I.3**) is very interesting task for the researchers. G. Xu et. al. in 2023 reported [133] a hydrazone-based Schiff base (**Z-1**) which has been selectively detects Zn²⁺ ions in DMSO/H₂O with the strong yellow-green emission. The probe (**Z-1**) forms 1:1 stoichiometric adduct with Zn²⁺ ions which has been established by Job's Plot study. The detection limit (LOD) as well as binding constant value was evaluated as 112 μM and 184 M⁻¹ respectively. Additionally, the reported probe (**Z-1**) detects Zn²⁺ ions on test paper strips. R. Behura et. al. in 2022 reported [134] a dinitrophenyl-based Schiff base (**Z-2**) which sense Zn²⁺ ions selectively in DMSO-H₂O solvent mixture. The binding constant and the limit of detection are evaluated as 6.35 × 10⁷ M⁻¹ and 1.1 × 10⁻⁸ M, respectively. Additionally, the chemosensor (**Z-2**) can be used to detect Zn²⁺ ions in living Hela cells. S. Sahu et. al. in 2022 reported [135] an isoindole-imidazole containing probe (**Z-3**). The probe (**Z-3**) selectively sense Zn²⁺ ions via fluorescence turn-on pathway. The chemosensor (**Z-3**) showed very low detection limit as 0.073 μM towards Zn²⁺ ions. The stoichiometric study has been studied by Job's method which indicated the 1:1 complexation between the probe (**Z-3**)

+ Zn²⁺ ions. X. Chen and co-authors in 2022 reported [136] a chemosensor (**Z-4**) which was selectively detect Zn²⁺ ions by colorimetric as well as fluorimetric pathway. The probe (**Z-4**) exhibited outstanding fluorescent sensing toward Zn²⁺ ions in EtOH/H₂O medium. The probe showed very low limit of detection (34 nM) toward Zn²⁺ ions. The chemosensor (**Z-4**) used to recognize Zn²⁺ ions in real water samples and living cells. P. Wang et. al. in 2020 reported [137] a new fluorescent chemosensor (**Z-5**) which showed an excellent selectivity toward Zn²⁺ ions and it exhibited a “turn-on” emission specifically for Zn²⁺ ions. Interestingly chemosensor (**Z-5**) detect Zn²⁺ ions in 100% aqueous medium. The detection limit for Zn²⁺ ions was evaluated as 19.25 nM. Y. S. Yang et. al. in 2018 synthesized [138] a fluorescence probe (**Z-6**) mainly based on cinnamyl pyrazoline which was detect selectively Zn²⁺ ions with a 56-fold increase in emission intensity. The reported probe significantly and selectively detects Zn²⁺ ions and the detection limit and binding constant value was evaluated as 2.95×10^{-8} M and 1.468×10^4 M⁻¹ respectively. The chemosensor used to recognize Zn²⁺ ions in baby hamster kidney (BHK)-21 cells. L. Chen et. al. in 2022 synthesized [139] a probe (**Z-7**) by grafting 2-hydrazinobenzothiazole onto 2,6-diformyl-4- methylphenol, which was selectively sense Zn²⁺ ions with the significant enhancement of fluorescent intensity and distinguishable change in color from light yellow-green to strong green. The detection limit (LOD) for Zn²⁺ ions was reported as 1.9×10^{-8} M. The probe can be effectively used as a paper based indicator of Zn²⁺ ions as well as live cell imaging of Zn²⁺ ions. Z. Liu and co-authors in 2023 reported [140] a benzothiazole based probe (**Z-8**) which was selectively recognize Zn²⁺ ions with a very low limit of detection towards Zn²⁺ ion as 0.678 μM. Y. Sun and co-authors in 2015 reported [141] a chemosensor (**Z-9**) mainly based on acylhydrazone group which selectively sense Zn²⁺ ions but in existence of different competitive cations no such distinguishable change in emission intensity takes place. The detection limit (LOD) for Zn²⁺ ions was evaluated as 9.3×10^{-8} M. In addition, the probe (**Z-9**) can be used in biological systems for the monitoring of Zn²⁺ ions.

J. Zhu et. al. in 2017 synthesized [142] a Schiff base (**Z-10**) showed excellent turn-on fluorescence response selectively for Zn^{2+} ions. From the Job's plot analysis, the stoichiometry of complexation determined as 2:1 ratio between the probe (**Z-10**) and Zn^{2+} . The detection limit (LOD) for Zn^{2+} ions was evaluated as 5.03×10^{-7} M. The chemosensor (**Z-10**) can be used as fluorescence live cell imaging to detect Zn^{2+} ions.

Table I.3. Some Reported Probes on Zn^{2+} sensing.

Probe	Solvent	LOD (M)	Reference
 <p>Z-1</p>	DMSO/H ₂ O	112×10^{-6}	[133]
 <p>Z-2</p>	DMSO:H ₂ O (10:90 v/v)	1.1×10^{-8}	[134]
 <p>Z-3</p>	3:7 HEPES buffer:DMSO	7.3×10^{-8}	[135]
 <p>Z-4</p>	EtOH/H ₂ O	3.4×10^{-8}	[136]

 <p style="text-align: center;">Z-5</p>	HEPES buffer solutions (20.0 mM, pH 7.4).	1.92×10^{-8}	[137]
 <p style="text-align: center;">Z-6</p>	EtOH-H ₂ O (1 : 1, v/v, pH = 7.2)	2.95×10^{-8}	[138]
 <p style="text-align: center;">Z-7</p>	DMSO-H ₂ O	1.9×10^{-8}	[139]
 <p style="text-align: center;">Z-8</p>	DMSO/Tris-HCl buffer solution	6.78×10^{-7}	[140]
 <p style="text-align: center;">Z-9</p>	H ₂ O/DMSO (8:2, v/v)	9.3×10^{-8}	[141]
 <p style="text-align: center;">Z-10</p>	EtOH/HEPES buffer (95:5, v/v, pH 7.4)	5.03×10^{-7}	[142]

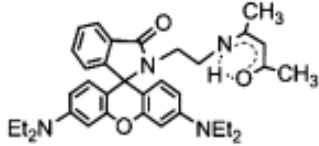
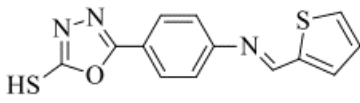
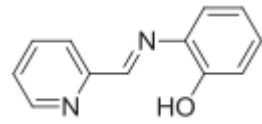
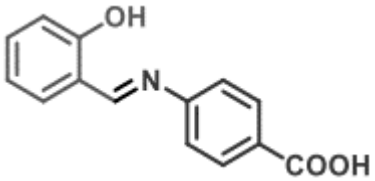
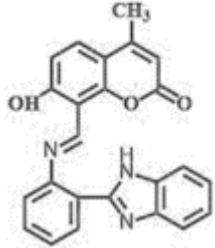
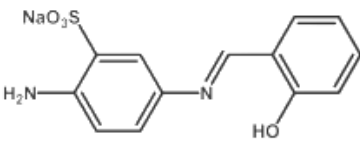
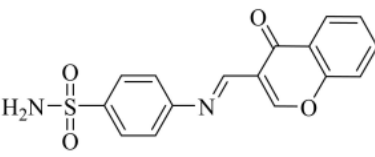
I.6.3. Fe³⁺ ion sensing probe

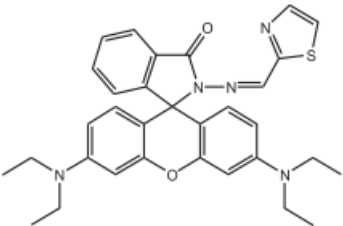
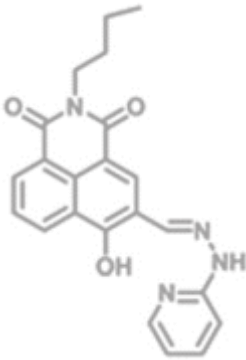
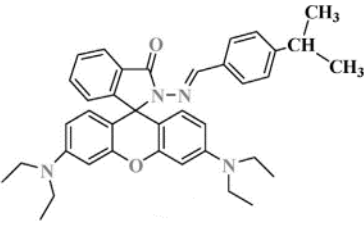
Iron is an essential trace element which performs a vital function in different physiological actions like oxygen-transport in haemoglobin and myoglobin, electron transfer process in

photosynthesis etc. In human body most abundant oxidation state of iron is Fe (III) and it plays an important function in chemistry, environment and biology. Hence the detection of Fe (III) ions (**Table I.4**) is very exciting task for the researchers. L. Dong et. al. in 2010 reported [143] a rhodamine based Schiff base (**F-1**) which showed very high sensitivity and selectivity towards Fe³⁺ ions. The chemosensor (**F-1**) detected Fe³⁺ ions by fluorometric as well as colorimetric method. The probe showed significant color change upon the addition of Fe³⁺ ions with a very low limit of detection (LOD) for Fe³⁺ ions as 0.11 μM (fluorescence experiment) and 1.6 μM (UV–vis experiment). R. Mehandi et. al. in 2023 reported [144] a Oxadiazole based chemosensor (**F-2**) which showed a significant and selective detection towards Fe³⁺ ions. The 1:1 stoichiometry of binding between the probe (**F-2**) and Fe³⁺ has been established by Job's plot analysis. The detection limit (LOD) for Fe³⁺ ions was evaluated as 0.113 μM. The probe (**F-2**) showed antifungal activity and good scavenging antioxidant property against DPPH and H₂O₂ free radicals. A. T. Wu and co-authors in 2013 reported [145] a novel chemosensor (**F-3**) which exhibited selective recognition towards Fe³⁺ ions in MeOH solution. The chemosensor (**F-3**) alone showed very weak fluorescence response but in existence of Fe³⁺ ions the emission intensity enhanced significantly and the chemosensor exhibited very high association constant with Fe³⁺ ions. The chemosensor (**F-3**) showed very low detection limit (LOD), which was determined as 8.5×10^{-10} M. G. Singh et. al. in 2019 designed [146] a new Schiff base (**F-4**) which selectively sense Fe³⁺ ions with a turn-off response and it showed good reversibility upon the addition of EDTA in its fluorescence response profile. The detection limit (LOD) for Fe³⁺ ions was evaluated as 0.77 μM. Z. Y. Yin in 2020 reported [147] a new coumarin based chemosensor (**F-5**) which was used to recognize Fe³⁺ selectively. The chemosensor (**F-5**) showed an important aggregation-induced emission (AIE) and upon the addition of Fe³⁺ to the probe, the distinguishable color change takes place with the significant increase in emission intensity. The probe (**F-5**) showed very low limit of detection (LOD) for

Fe³⁺ ions as 4.88×10^{-7} M. S. Serin and co-authors in 2021 developed [148] a water soluble probe (**F-6**) which exhibited a remarkable decrease in fluorescence intensity upon the addition of Fe³⁺ ions. The detection limit (LOD) for Fe³⁺ ions was evaluated as 1.29 μ M and the 1:1 stoichiometry of complexation between **F-6** and Fe³⁺ was evaluated from Job's plot analysis. S. Sharma and co-authors in 2021 synthesized [149] an effective chemosensor (**F-7**) by the condensation of sulfanilamide and 3- formyl chromone. The probe (**F-7**) sense Fe³⁺ ions by fluorimetrically as well as colorimetrically and the probe showed significant sensitivity for Fe³⁺ ions and the detection limit (LOD) for Fe³⁺ ions was evaluated as 9.3×10^{-7} M. The probe (**F-7**) can be used as a molecular logic operation (INHIBIT) and also used for the detection of Fe³⁺ ions by test paper strips. L. Wang et. al. in 2018 developed [150] a rhodamine based chemosensor (**F-8**) which showed turn-on fluorescence response for Fe³⁺ ions. The chemosensor (**F-8**) showed high sensitivity and selectivity for Fe³⁺ ions with the low limit of detection (LOD) value as 92 nM. The probe (**F-8**) binds with Fe³⁺ ions with 2:1 stoichiometric ratio which was determined from Job's plot analysis. In addition, the chemosensor (**F-8**) can be suitable for the mapping of Fe³⁺ ions in human colon cancer cells SW480. W. Liang and co-authors in 2020 reported [151] a fluorescent probe (**F-9**), which showed efficient selectivity towards Fe³⁺ ions. The emission intensity of the probe (**F-9**) enhanced significantly with the addition of Fe³⁺ ions. The limit of detection (LOD) for Fe³⁺ ions is very low as 38.3 nM. Additionally, the probe can be effectively used for exogenous and endogenous detection of Fe³⁺ ions in living cells. P. S. Nayab et. al. in 2017 synthesized [152] a rhodamine based probe (**F-10**) which selectively sense Fe³⁺ ions with a 48-fold enhancement of emission intensity. The probe (**F-10**) formed 1:1 complex with Fe³⁺ ions which was confirmed by the Job's plot analysis. The detection limit (LOD) for Fe³⁺ was evaluated as 5.05 μ M.

Table I.4. Some Reported Probes on Fe³⁺ sensing

Probe	Solvent	LOD (M)	Reference
 <p>F-1</p>	Ethanol–water (4/6, v/v, Tris–HCl buffer, pH = 7.0)	0.11 μM (fluorescence measurement) 1.6 μM (UV–vis measurement).	[143]
 <p>F-2</p>	DMSO–H ₂ O (1:1, v/v)	1.13×10^{-7}	[144]
 <p>F-3</p>	MeOH	8.5×10^{-10}	[145]
 <p>F-4</p>	MeOH	7.7×10^{-7}	[146]
 <p>F-5</p>	DMSO/H ₂ O (1:9, v/v, pH = 7.2)	4.88×10^{-7}	[147]
 <p>F-6</p>	Water	1.29×10^{-6}	[148]
 <p>F-7</p>	ACN/H ₂ O (1:1, v/v)	9.3×10^{-7}	[149]

Probe	Solvent	LOD (M)	Reference
 <p>F-8</p>	HEPES buffer solution (1.0 mM, pH 7.0)	9.2×10^{-8}	[150]
 <p>F-9</p>	DMSO/H ₂ O (7 : 3, v/v, pH 7.4)	3.83×10^{-8}	[151]
 <p>F-10</p>	CH ₃ CN - aq. HEPES buffer. (5:5, v/v; pH = 7.2)	5.05×10^{-6}	[152]

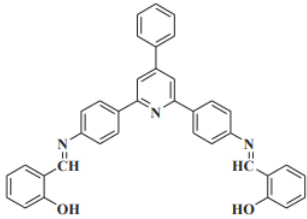
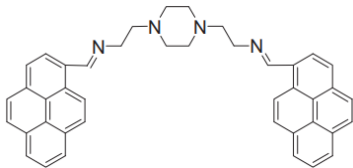
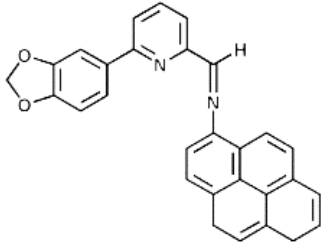
I.6.4. Cr³⁺ ion sensing probe

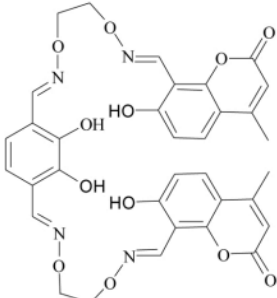
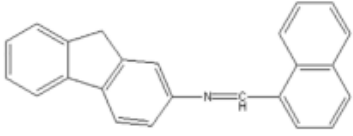
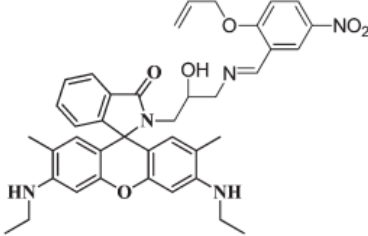
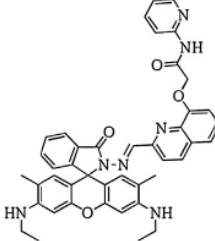
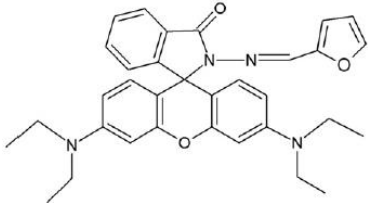
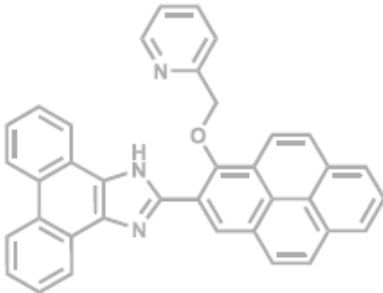
Chromium exists at a very trace level in our human body and it plays very major role for the metabolism of proteins, fats and carbohydrates and it also controls the activity of insulin in human body. In soil and water samples most common oxidation state is Cr (III). Hence there is a vital need to estimate such Cr (III) ions (**Table I.5**). G. B. Chalmardi et. al. in 2018 reported [153] a Schiff base (**C-1**) which showed a selective detection of Cr³⁺ ions in CH₃CN/H₂O (95/5%) solution. The emission intensity enhanced remarkably with the addition of Cr³⁺ ions. The 1:1 stoichiometry of binding between the probe (**C-1**) and Cr³⁺ was determined by Job's plot analysis. The association constant (K_a) and the detection limit (LOD) was evaluated as

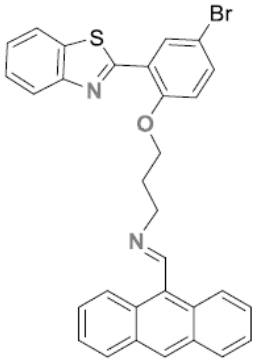
$2.28 \times 10^5 \text{ M}^{-1}$ and $1.3 \times 10^{-7} \text{ M}$ respectively. Y. S. Wu et. al. in 2014 designed [154] a pyrene based chemosensor (**C-2**) which recognize Cr^{3+} ions selectively in Tris- HNO_3 buffered solution (pH 7.0). The probe (**C-2**) showed ratiometric fluorescence response with a significant selectivity towards Cr^{3+} ions. The detection limit (LOD) for Cr^{3+} ions was evaluated as $4 \times 10^{-8} \text{ M}$. The experimental observation revealed that the sensing behavior of **C-2** for Cr^{3+} is pH independent. The probe can be used for the recognition of Cr^{3+} in real water sample. S. Mukherjee et. al. in 2020 designed [155] a pyrene based chemosensor (**C-3**) which detects Cr^{3+} ions in DMSO/ H_2O (2:1, v/v) medium. The chemosensor (**C-3**) significantly detects Cr^{3+} ions with the distinguishable change in color. The detection limit (LOD) for Cr^{3+} was evaluated as $4.925 \times 10^{-9} \text{ M}$. P. Zhang in 2021 reported [156] a chemosensor (**C-4**) which showed a significant sensitivity towards Cr^{3+} ions. The limit of detection (LOD) for Cr^{3+} ions was determined as $4.87 \times 10^{-7} \text{ M}$. T. Hu et. al. in 2021 synthesized [157] a new probe (**C-5**) which sense Cr^{3+} ions in $\text{CH}_3\text{CN}-\text{H}_2\text{O}$ (v/v, 7:3) medium. The limit of detection of the probe (**C-5**) for Cr^{3+} ion evaluated much lower value as $6.31 \times 10^{-8} \text{ M}$. The mechanism of detection of **C-5** for Cr^{3+} ion was confirmed by MS and ^1H NMR. A. K. Bhanja et. al. in 2017 reported [158] a rhodamine based platform (**C-6**) which selectively and specifically detects Cr^{3+} ions with the enhancement of fluorescence intensity. The chemosensor (**C-6**) exhibited strong fluorescence turn on emission with a clear band appears at 557 nm. The limit of detection for Cr^{3+} ions was evaluated as 33 nM. X. M. Li et. al. in 2017 developed [159] a rhodamine-based probe (**C-7**) which showed colorimetric and fluorescence responses selectively with Cr^{3+} ions with the distinguishable color change with the enhancement of emission intensity up to 13-fold. The chemosensor (**C-7**) showed the detection limit for Cr^{3+} ions as $5.6 \times 10^{-6} \text{ M}$. Y. Zhou et. al. in 2013 designed [160] a rhodamine-based chemosensor (**C-8**) which showed high selectivity toward Cr^{3+} ions with a very low detection limit (LOD) as 0.023 μM . The chemosensor (**C-8**) can be used for the recognition of Cr^{3+} ions in real water samples and it also used to intracellular

Cr³⁺ imaging in living cells. Z. Lu and co-authors in 2015 synthesized [161] a pyrene based chemosensor (**C-9**) which sense Cr³⁺ ions selectively and the mechanism of sensing was well explained by intramolecular-charge transfer (ICT) process. The detection limit (LOD) and the association constant (K_a) of the chemosensor for Cr³⁺ ions were evaluated as 0.23 μM and 7.52 × 10⁴ M⁻¹ respectively. The 1:1 stoichiometry of complexation between the probe (**C-9**) and Cr³⁺ was confirmed by the Job's plot analysis. S. Erdemir et. al. in 2016 designed [162] a new anthracene based chemosensor (**C-10**) which showed sensitivity toward Cr³⁺ ions by both fluorimetric as well as colorimetric experiments in CH₃CN medium. The limit of detection (LOD) toward Cr³⁺ ions was evaluated as 0.46 μM. The probe (**C-10**) also used as a fluorescence bio-imaging study of Cr³⁺ ions in human prostate cancer cell lines.

Table I.5. Some Reported Probes on Cr³⁺ sensing.

Probe	Solvent	LOD (M)	Reference
 <p>C-1</p>	CH ₃ CN/H ₂ O (95/5%)	1.3 × 10 ⁻⁷	[153]
 <p>C-2</p>	Tris-HNO ₃ buffered solution (pH 7.0)	4 × 10 ⁻⁸	[154]
 <p>C-3</p>	DMSO/H ₂ O (2:1, v/v)	4.925 × 10 ⁻⁹	[155]

 <p>C-4</p>	Tris-HCl buffer solution with pH = 7.4.	4.87×10^{-7}	[156]
 <p>C-5</p>	CH ₃ CN-H ₂ O (v/v, 7:3)	6.31×10^{-8}	[157]
 <p>C-6</p>	CH ₃ CN/H ₂ O, 1:4, v/v, HEPES buffer, pH = 7.4	3.3×10^{-8}	[158]
 <p>C-7</p>	CH ₃ CN/Tris-HCl (0.01 mol/L, pH 7.4; v/v = 9:1)	5.6×10^{-6}	[159]
 <p>C-8</p>	Tris-HCl (10 mM, pH = 7.2)	2.3×10^{-8}	[160]
 <p>C-9</p>	THF-H ₂ O (1:1, v/v) at pH= 7 (HEPES 10 mM).	2.3×10^{-7}	[161]

 <p style="text-align: center;">C-10</p>	CH ₃ CN	4.6×10^{-7}	[162]
--	--------------------	----------------------	-------

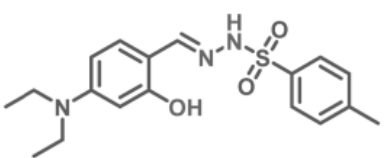
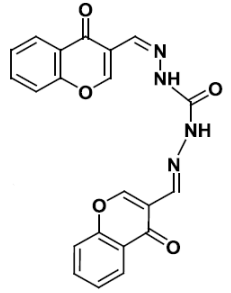
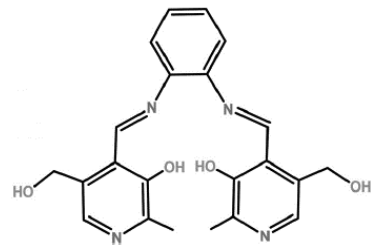
I.6.5. Cu²⁺ ion sensing probe

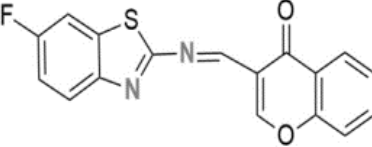
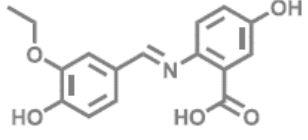
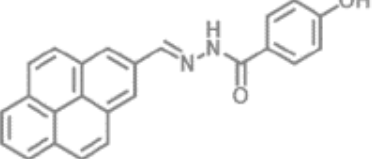
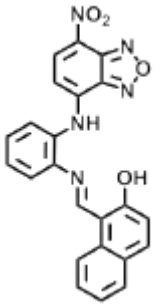
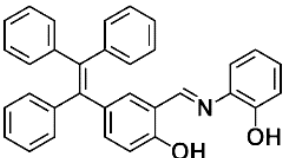
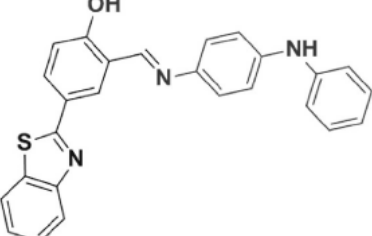
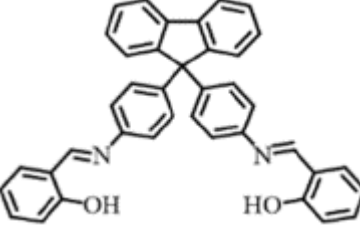
The transition metal offers a vital role in biological system because of their participation in many physiological functions. Cu (II) being an essential species plays a significant role in enzymes, proteins and various biological processes. Hence the detection of Cu²⁺ ions (**Table I.6**) is an interesting topic for the researchers. R. Tamizhselvi et. al. in 2022 synthesized [163] a new sulfonohydrazide based Schiff base (**S-1**) which selectively sense Cu²⁺ ions. Interestingly the chemosensor (**S-1**) selectively detect Cu²⁺ ions by colorimetrically in existence of other various cations. The 2:1 stoichiometry of binding between the probe and Cu²⁺ was supported by the Job's plot analysis. The detection limit (LOD) for Cu²⁺ ions was evaluated as 2.74×10^{-7} M. Additionally the probe (**S-1**) can be used as the efficient chemosensor for the detection Cu²⁺ using test paper strips. N. Tomer et. al. in 2022 reported [164] a chromone based chemosensor (**S-2**) which exhibited colorimetric recognition of Cu²⁺ ions. The detection limit (LOD) for Cu²⁺ was evaluated as 11.4×10^{-7} M. Additionally the probe (**S-2**) can be applied for the recognition of p-nitrotoluene. V. Bhardwaj et. al. in 2022 synthesized [165] a Schiff base (**S-3**) which exhibited an aggregation-induced emission upon the addition of water. The chemosensor (**S-3**) selectively detect Cu²⁺ ions and it exhibited turn off sensing in presence of Cu²⁺ ions with a detection limit (LOD) as 5.31×10^{-7} M for Cu²⁺ ions. The reported probe (**S-3**) formed 1:1 complex with Cu²⁺ ions. The developed Schiff base (**S-3**) also detect Cu²⁺ in test paper strips and it can be used for the recognition of Cu²⁺ ions in real water samples. R. Kouser

et. al. in 2022 designed [166] a chemosensor (**S-4**) which selectively sense Cu^{2+} ions in THF: Ethanol medium. The 2:1 complexation between the probe (**S-4**) and Cu^{2+} was supported by the job's plot analysis. The reported chemosensor (**S-4**) showed limit of detection (LOD) for Cu^{2+} as 0.273×10^{-6} M. In addition, the probe can be applied to recognize Cu^{2+} ions in different tissues of biological samples. B. Shruthi et. al. in 2023 developed [167] a chemosensor (**S-5**) which selectively sense Cu^{2+} ions. The probe (**S-5**) showed 1:1 complexation with Cu^{2+} and chemosensor (**S-5**) selectively detect Cu^{2+} ions with the reduction of emission intensity. The detection limit (LOD) for Cu^{2+} ions was evaluated as $0.39 \mu\text{M}$. A. A. Napoleon and co-author in 2023 reported [168] a new pyrene based Schiff base (**S-6**) which was used as an excellent colorimetric sensor selectively for Cu^{2+} ions. Upon the addition of Cu^{2+} to the probe (**S-6**), the colorless probe changes to yellow which was supported by UV–Visible spectroscopic analysis. The 1:1 complexation formed between the probe (**S-6**) and Cu^{2+} ions. The detection limit (LOD) for Cu^{2+} ion was determined as 2.19×10^{-7} M. Interestingly the reported chemosensor also detect Cu^{2+} ions in real samples by test paper strips. J.Y. Yang. et. al. in 2023 reported [169] a novel chemosensor (**S-7**) which exhibited as a colorimetric and fluorescent probe for the selective recognition of Cu^{2+} ions with the 25-fold increase in emission intensity. The chemosensor (**S-7**) formed a complex with 1:1 stoichiometric ratio with Cu^{2+} ions. The detection limit (LOD) for Cu^{2+} was evaluated as 42.2 nM . The probe (**S-7**) was also used to sense Cu^{2+} in living cells. J. Jia and co-authors in 2023 developed [170] a new tetraphenylethene based chemosensor (**S-8**). The probe was a significant AIE-active species and it showed significant selectivity toward Cu^{2+} ions in DMSO/PBS (70% fw) medium. The 1:1 stoichiometric complexation between the probe and Cu^{2+} was confirmed by the Job's plot analysis. The probe exhibited very low detection limit (LOD) for Cu^{2+} as 4.5 nM . The probe (**S-8**) also used for the estimation of Cu^{2+} ions in various real water samples. D. Aydin et. al. in 2022 designed [171] a benzothiazole-based probe (**S-9**) which showed an excellent candidate

for the selective recognition of Cu^{2+} ions. The detection limit (LOD) for Cu^{2+} was evaluated as 2.23 nM. The stoichiometry of binding between the probe (**S-9**) and Cu^{2+} was determined as 2:1 ratio. Interestingly the chemosensor (**S-9**) covered silica plates were used to recognize Cu^{2+} ions. S. Majeed et. al. in 2022 developed [172] a chemosensor (**S-10**) which exhibited aggregation induced emission (AIE) followed by excellent selectivity towards Cu^{2+} ions. The detection limit (LOD) for Cu^{2+} was evaluated as 2.13 nM. Interestingly upon the addition of glutathione (GSH) to the probe (**S-10**)- Cu^{2+} complex instantly an enhancement of emission intensity taken place which was explained by the replacement of Cu^{2+} ions by GSH and release of probe (**S-10**). Additionally, the chemosensor (**S-10**) can detect Cu^{2+} and GSH in various real water and food samples.

Table I.6. Some Reported Probes on Cu^{2+} sensing.

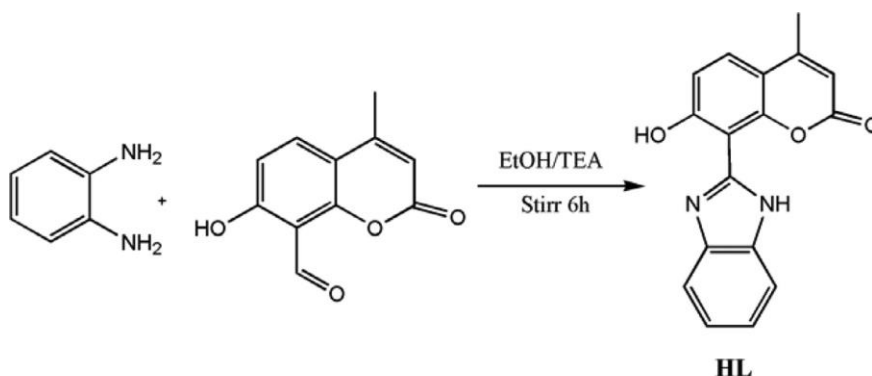
Probe	Solvent	LOD (M)	Reference
 <p>S-1</p>	$\text{CH}_3\text{CN} : \text{H}_2\text{O}$ (7:3, v/v)	2.74×10^{-7}	[163]
 <p>S-2</p>	DMSO	11.4×10^{-7}	[164]
 <p>S-3</p>	$\text{EtOH} : \text{HEPES buffer}$ (5% EtOH, pH = 7.4)	5.31×10^{-7}	[165]

 <p style="text-align: center;">S-4</p>	THF: Ethanol	0.273×10^{-6}	[166]
 <p style="text-align: center;">S-5</p>	EtOH-H ₂ O (v/v, 8:2) (HEPES 0.01 M, pH = 7.4) solution.	0.39×10^{-6}	[167]
 <p style="text-align: center;">S-6</p>	DMSO: H ₂ O (7:3, v/v)	2.19×10^{-7}	[168]
 <p style="text-align: center;">S-7</p>	CH ₃ CN/H ₂ O, 1:1, v/v, pH=7.4	4.22×10^{-8}	[169]
 <p style="text-align: center;">S-8</p>	DMSO/PBS (70% fw)	4.5×10^{-9}	[170]
 <p style="text-align: center;">S-9</p>	HEPES/ ACN (v:v, 3:7, pH:7)	2.23×10^{-9}	[171]
 <p style="text-align: center;">C-10</p>	DMF/H ₂ O (2:8, v/v)	2.13×10^{-9}	[172]

I.7. Aims and scope of the present research

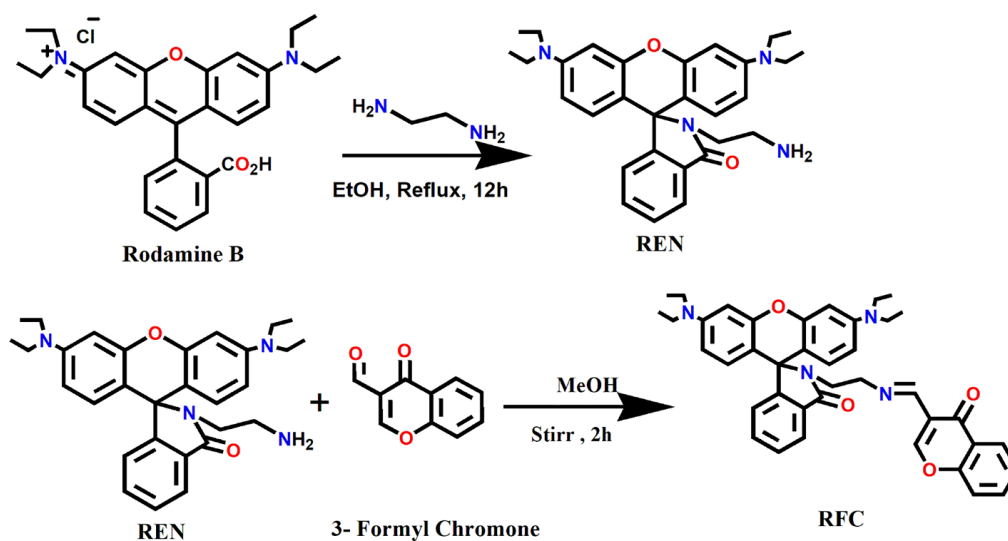
Our aim of the research is to design some molecules those will absorb light and be excited; at this stage the active species may interact with specific ions so that a characteristic emission may be found to identify them and in some cases the excited species may show mechanical performance like structural isomerization or photochromism. This thesis contains the synthesis, characterization and applications of different species functionalized with fluorescent chromophores, which have shown efficient sensitivity for Cu^{2+} , Al^{3+} , Zn^{2+} , Cr^{3+} and Fe^{3+} ions and one azoimidazole based Hg(II) complex which have shown photo-mechanical activity by *trans-cis* isomerization those can be used as an optical sensor. The dissertation is focused on: (i) Design, synthesis and characterization of various Schiff bases appended with a photoactive motif, (ii) Exploring the role of such synthesized chemosensor in sensing of various metal ions, (iii) Exploring the optical sensing of structural isomers of azoimidazole based Hg (II) complex, (iv) Exploring the role of such chemosensor for live cell imaging and biological and medicinal activity. Herein, we explore the characterization of four Schiff bases and one azoimidazole based Hg (II) complex in relevance to my thesis work. This Schiff bases are mainly based on rhodamine, coumarin, diformylphenol and chromone moiety which have been developed, synthesized and characterized by different analytical techniques. These developed probes act as an efficient sensor for the detection of Cu^{2+} , Al^{3+} , Zn^{2+} , Cr^{3+} and Fe^{3+} ions. Cations exist as essential, beneficial as well as non-essential and toxic elements. An optimum concentration of ions must be present for the usual functioning of biological system and its presence must be monitored carefully. When the concentration of different metal ions increases or reduces then the survivability or the proper functioning of cells are somewhat hindered. Therefore, a positive effort should be applied towards the detection and quantitative estimation of various ions at ultra-low concentration level. The designed probe follows the usual sensing mechanism like ICT, PET, ESIPT, FRET, MLCT etc. Hence the probe has been used for the optical sensing of various analytes which mainly follows the primary photophysical properties of the synthesized fluorescent chemosensors.[173]

Chapter II: A benzimidazolyl–hydroxy- coumarinyl diad (**HL**) acts as an efficient fluorescence turn-on sensor for Al^{3+} ions. The probe (**HL**) has been synthesized by the following procedure (**Scheme I.c**).



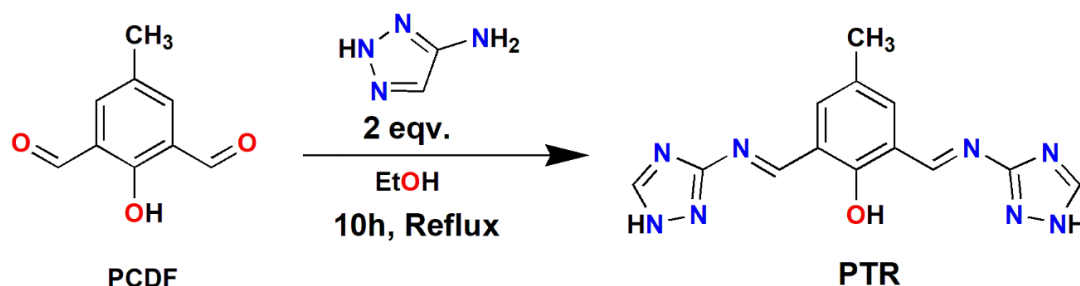
Scheme I.c. Synthesis of Ligand, HL

Chapter III: The chapter contains a rhodamine based chemosensor (**RFC**) which exhibits the fluorescent turn-on response for trivalent (Al^{3+} , Cr^{3+} and Fe^{3+}) metal ion. The probe (**RFC**) has been synthesized by the following procedure (**Scheme I.d**).



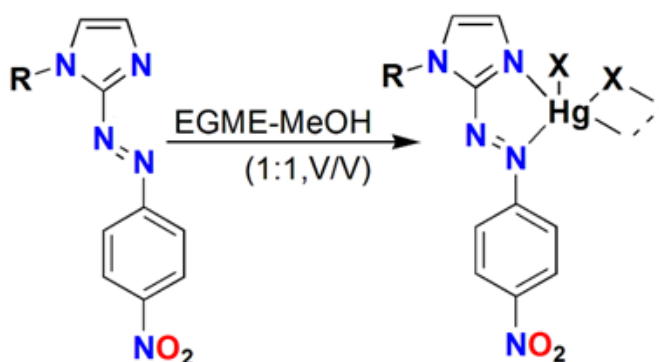
Scheme I.d. Synthesis of Probe RFC

Chapter IV: This chapter consist of a diformylphenol based Schiff base (**PTR**), which can selectively detect Zn^{2+} ions and the probe has been synthesized by the following procedure (**Scheme I.e**)



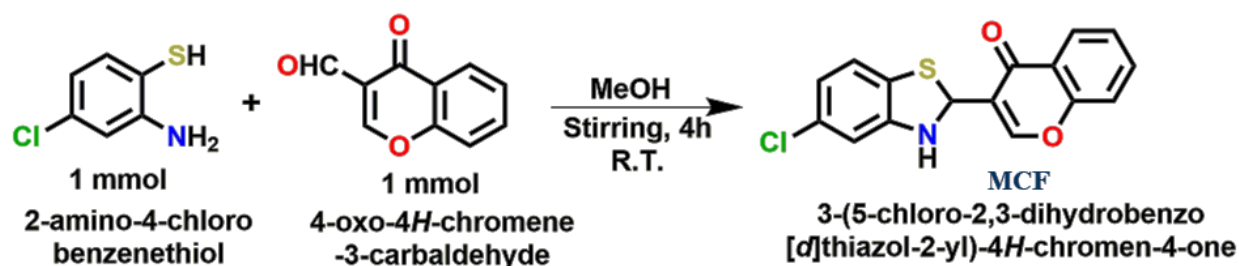
Scheme I.e. Synthesis of PTR probe

Chapter V: This chapter contains Structure and Photoisomerisation of Halo-bridged dimeric Mercury (II) complexes (**Scheme I.f**) of 1-alkyl-2-(p-nitro-phenylazo) imidazoles. The structure of the Hg-compound has been confirmed by Single Crystal X-ray diffraction study.



Scheme I.f. Synthetic route of Hg (II)- halide complexes

Chapter VI: This chapter contains a colorimetric chromone-based platform (**MCF**) which can detect selectively Cu^{2+} ions. The designed probe (**MCF**) has been synthesized by the following procedure (**Scheme I.g**)



Scheme I.g. Synthesis of Probe MCF

I.8. Physical measurement:

- (i) **Elemental analysis:** Microanalytical data (C, H, N) were collected on Perkin Elmer 2400 Series-II CHN analyzer, USA elemental analyzer using the pure solid sample.
- (ii) **FT-IR spectra:** FT-IR spectra ($4000\text{--}400\text{ cm}^{-1}$) by Perkin Elmer LX-1 FTIR and LITA FT-IR spectrophotometer with samples.
- (iii) **UV-Vis spectra:** UV-vis experiments were studied by using Perkin Elmer UV-vis spectrophotometer with model Lambda 25 using the solution as required concentration. The prepared solution with a required concentration has been kept in a quartz cell with 1 cm path length and the absorption spectra were recorded starting from visible to UV region.
- (iv) **Fluorescence Spectra:** Spectrofluorometric experiments were studied by using Perkin Elmer Spectrofluorimeter with model LS-55 using the solution as required concentration. The prepared solution with a required concentration has been kept in a quartz cell with 1 cm path length and the absorption spectra were recorded starting from visible to UV region.

- (v) **¹H-NMR spectra:** ¹H NMR spectra were studied by using Bruker (AC) 300, 400 MHz FT-NMR spectrometer with trimethyl silane (TMS) as internal standard.
- (vi) **Single crystal X-ray diffraction study:** Single crystals of the synthesized probes has been obtained by the slow evaporation process and the data collected on a Bruker SMART Apex CCD area detector by graphite monochromated MoK α radiation with wavelength of 0.71073 Å. X-ray data reduction, solution of structure and refinement were done by using ORTEP- 32 [174], SHELXL-97 [175], and PLATON-99 [176] programs. The structures were solved by direct method.
- (vii) **Mass Spectroscopy:** To record ESI mass spectra a Water HRMS model XEVO-G2QTOF#YCA351 spectrometer has been used.
- (viii) **Theory and Computational Methods:** Optimization of ground-state structures and energy calculations for all the synthesized fluorescence probe and their complexes were carried out by DFT (density functional theory) method using the Gaussian 09W, where B3LYP was chosen as the basis function [177,178]. The fraction of contributions of different groups in each molecular orbital were calculated by carrying out GAUSSSUM [179]
- (ix) **Live cell imaging and anticancer activity:** Cell images were taken using fluorescence microscope. To investigate the anticancer activity different cell lines (MCF-7, WI-38, A549, A431) were used which is mentioned in different chapter.

I.9. References:

- [1]. B. Wang, E. V. Anslyn (Eds), John Wiley & Sons, Inc., 2011.
- [2]. E. Raczuk, B. Dmochowska, J. Samaszko-Fiertek, J. Madaj, *Molecules*, 27 (2022) 787.

- [3]. M. S. More, P. G. Joshi, Y. K. Mishra, P. K. Khanna, *Mater. Today Chem.*, 14 (2019) 100195.
- [4]. A. B. P. Lever, I. M. Walker, P. J. McCarthy, K. B. Mertes, A. Jircitano, R. Sheldon, *Inorg. Chem.*, 22 (1983) 2252-2258
- [5]. L. Fabbrizzi, *J. Org. Chem.* 85 (2020) 12212-12226.
- [6]. S. Gaur, *Asian J. Chem.*;15 (2003) 250.
- [7]. M. J. Gemi, C. Biles, B. J. Keiser, S. M. Poppe, S. M. Swaney, W. G. Tarapley, D. L. Romeso, Y. Yage, *J. Med. Chem.* 43 (2000) 1034.
- [8]. P. G. Cozzi, *Chem. Soc. Rev.*, 33 (2004) 410-421.
- [9]. M. S. Karthikeyan, D. J. Prasad, B. Poojary, K. S. Bhat, B.S. Holla, N.S. Kumari, *Bioorganic Med. Chem.*, 14 (2006) 7482-7489.
- [10]. K. Singh, A. Prakash, H.K. Rajour, N. Bhojak, D. Adhikari, *Spectrochim. Acta A Mol. Biomol. Spectrosc.*, 76 (2010) 376-383.
- [11]. A. M. Alafeefy, M. A. Bakht, M. A. Ganaie, M. N. Ansarie, N. N. El-Sayed, A. S. Awaad. *Bioorganic Med. Chem. Lett.*, 25 (2015) 179-183.
- [12]. C.T. Supuran, M. Barboiu, C. Luca, E. Pop, M.E. Brewster, A. Dinculescu, *Eur. J. Med. Chem.*, 31 (1996) 597.
- [13]. L.H. Abdel-Rahman, R.M. El-Khatib, L.A.E. Nassr, A.M. Abu-Dief, M. Ismael, *Spectrochim. Acta, Part A.* 117 (2014) 366-378.
- [14]. M. Abu-Dief, L.A.E. Nassr, *J. Iran. Chem. Soc.*, 12 (2015) 943-955.
- [15]. A. A. Bekhit, H.T.Y. Fahmy, S.A.F. Rostom, A.M. Baraka, *Eur. J. Med. Chem.*, 38 (2003) 27-36.
- [16]. B. M. Sahoo, S. C. Dinda, BVV R. Kumar, J. Panada, *Lett. Drug Des. Discov.*, 11 (2014) 82-89.
- [17]. A. Bacchi, M. Carcelli, P. Pelagatti, G. Pelizzi, M. C. Rodriguez-Arguelles, D. Rogolino, C. Solinas, F. Zani, *J. Inorg. Biochem.*, 99 (2005) 397-408.
- [18]. Y. Liu, L. Yang, D. Yin, Y. Dang, L. Yang, Q. Zou, J. Li, J. Sun, *J. Organomet. Chem.*, 899 (2019) 120903.

- [19]. W. H. Mahmoud, R. G. Deghadi, G. G. Mohamed, *Appl. Organomet. Chem.*, 30 (2016) 221-230.
- [20]. M. Rao, L. Shadap, V. Banothu, *J. Organomet. Chem.*, 915 (2020) 121246.
- [21]. X. Zheng, W. Cheng, C. Ji, J. Zhang, M. Yin, *Rev. Anal. Chem*, 39 (2020) 231-246.
- [22]. M. K. Goshisht, G. K. Patra, N. Tripathi, *Materials Advances*, 3 (2022) 2612-2669.
- [23]. P.J. Aggett, Wiley-Blackwell, 10th Edition, 2012.
- [24]. J. Xu, Z. Jia, M. D. Knutson, C. Leeuwenburgh, *Int. J. Mol. Sci.* 13 (2012) 2368-2386.
- [25]. A. Luo, H. Wang, Y. Wang, Q. Huang, Q. Zhan., *Spectrochim. Acta A: Mol. and Biomol. Spec.*, 168 (2016) 37-44
- [26]. S. Sen, S. Sarkar, B. Chattopadhyay, A. Moirangthem, A. Basu, K. Dhara, P. Chattopadhyay, *Analyst*, 137 (2012) 3335-3342
- [27]. J. Hofmann, V. Watson, B. Scharaw, *Environ. Earth. Sci*, 73 (2014) 629-648.
- [28]. RS Porter, MD Kaplan, BP Homeier., *Merck Manual Home Health Handbook*; Merck & Company, 2009
- [29]. G.-Bi Li, H.-C. Fang, Y.-P. Cai, Z.-Y. Zhou, P. K. Thallapally, J. Tian *Inorg. Chem.*, 49 (2010) 7241–7243
- [30]. B. Wang, W. Xu, K. Gan, K. Xu, Q. Chen, W. Wei, W. Wu., *Spectrochim. Acta A: Mol. and Biomol. Spectrosc.*, 277 (2022) 121245
- [31]. C. Joel, D. J. Livingston, R. B. Bennie, D. Jeyanthi, R.V. Solomon *J. Photochem. Photobiol. A: Chem.*, 423 (2022) 113612
- [32]. P. Srisuwan, A. Sappasombut, W. Thongyod, T. Jantararat, V. Tipmanee, N. Leesakul, D. Sooksawat. *J. Photochem. Photobiol. A: Chem.*, 427 (2022) 113841
- [33]. X. Liu, P. Xu, X. Zhao, J. Ge, C. Huang, W. Zhu, C. Li, L. Du, M. Fang, *Inorg. Chim. Acta*, 495 (2019) 118975.
- [34]. H. So, J. B. Chae, C. Kim, *Inorg. Chim, Acta* 492 (2019) 83-90.
- [35]. S. Anbu, A. Paul, K. Surendranath, N. Shaikh, S. Armando J. L. Pombeiro., *Sens. Actuators. B: Chem.*, 337 (2021) 129785.

- [36]. D. Bagchi, S. J. Stohs, B. W. Downs, M. Bagchi, H.G. Preuss. *Toxicology*, 180 (2012) 5-22
- [37]. A. K. Singh, V. K. Gupta, B. Gupta, *Anal. Chim. Acta*, 585 (2007) 171-178.
- [38]. J. Mao, L. Wang, W. Dou, X. Tang, Y. Yan, W. Liu., *Org. Lett.*, 9 (2007) 4567-4570
- [39]. J.B. Vincent. *Nutr. Rev.*, 58 (2000) 67-72.
- [40]. D. Li, C.-Y. Li, H.-R. Qi, K.-Y. Tan, Y-F. Li, *Sens. Actuators. B*, 223 (2016) 705-712.
- [41]. H. Arakawa, R. Ahmad, M. Naoui, H. Ali, T. Riahi, *J. Biol. Chem.*, 275 (2000) 10150-10153.
- [42]. X. Hu, X. Zhang, G. He, C. He, C. Duan., *Tetrahedron*, 67 (2011) 1091-1095.
- [43]. B. L. Vallee, K. H. Falchuk., *Physiol Rev.*, 73 (1993) 79-118
- [44]. P. Jiang and Z. Guo, *Coord. Chem. Rev.*, 248 (2004) 205-229.
- [45]. J. M. Berg and Y. Shi, *Science*, 271 (1996) 1081-1085.
- [46]. C. J. Frederickson, *Int. Rev. Neurobiol.*, 31 (1989) 145-238.
- [47]. A. Takeda, *BioMetals*, 14 (2001) 343-351.
- [48]. S. Das, M. Dutta, D. Das, *Anal. Methods* 5 (2013) 6262.
- [49]. Q. Diao, P. Ma, L. Lv, T. Li, Y. Sun, X. Wang, D. Song, *Sens. Actuators B Chem.* 229 (2016) 138-144.
- [50]. J. Malini, M. Sayed, *J. Photochem. Photobiol., A* 418 (2021) 113431
- [51]. H. Xu, W. Chen, L. Ju, H. Lu, *Spectrochim. Acta. A Mol. Biomol. Spectrosc.* 247 (2021) 119074.
- [52]. D. Anu, P. Naveen, R. Rajamanikandan, M.V. Kaveri, *J. Photochem. Photobiol., A* 405 (2021) 112921.
- [53]. Z. Li, W. Chen, L. Dong, Y. Song, R. Li, Q. Li, D. Qu, H. Zhang, Q. Yang, Y, Li, *New J. Chem.* 44 (2020) 3261-3267.
- [54]. F. Zhou, H. Wang, P. Liu, Q. Hu, Y. Wang, C. Liu, J. Hu, *Spectrochim, Acta Part A: Mol. Biomol. Spectrosc.* 190 (2018) 104-110.
- [55]. G.D. Fasman, *Coordin. Chem. Rev.* 149 (1996) 125-165.

- [56]. Y. Li, K. Xu, Y. Si, C. Yang, Q. peng, J. He, Q. Hu, K. Li, *Dyes Pigm.* 179 (2019) 107682.
- [57]. J.R. Walton, *Inorg. Biochem.* 101 (2007) 1275-1284.
- [58]. D.R.C. McLachlan, *Environmetrics* 6 (1995) 233-275.
- [59]. M. Constantin, I. Alexandru, *Balneo-Research*, 2 (2011) 70-74
- [60]. P. Nandhikonda, M. P. Begaye, M. D. Heagy, *Tetrahedron Lett.*, 50 (2009) 2459-2461.
- [61]. T. Clausen, *Physiol. Rev.*, 83 (2003) 1269-1324.
- [62]. J. M. Burnell, B. H. Scribner, B. T. Uyeno, M. F. Villamil, *J. Clin. Invest.*, 35 (1956) 935-939.
- [63]. J. M. Berg, J. L. Tymoczko and L. Stryer, *Biochemistry*, W. H. Freeman, New York, 5th edn, 2002
- [64]. H.-R. Yu, X.-J. Ju, R. Xie, W. Wang, B. Zhang and L.-Y. Chu, *Anal. Chem.*, 85 (2013) 6477-6484.
- [65]. N. Singh, N. Kaur, R. C. Mulrooney, J. F. Callan, *Tetrahedron Lett.*, 49 (2008) 6690-6692.
- [66]. F. H. Nielsen, H. C. Lukaski, *Magnesium Res.*, 19 (2006) 180-189.
- [67]. J. R. Moll, A. Acharya, J. Gal, A. A. Mir, C. Vinson, *Nucleic Acids Res.*, 30 (2002) 1240-1246.
- [68]. H. Komatsu, N. Iwasawa, D. Citterio, Y. Suzuki, T. Kubota, K. Tokuno, Y. Kitamura, K. Oka, K. Suzuki, *J. Am. Chem. Soc.*, 126 (2004) 16353-16360.
- [69]. O. B. Stepura, A. I. Martynow, *Int. J. Cardiol.*, 134 (2009) 145-147
- [70]. T. Shoda, K. Kikuchi, H. Kojima, Y. Urano, H. Komatsu, K. Suzukic, T. Nagano, *Analyst*, 128 (2003) 719-723.
- [71]. S. Kim, J. Kim, N. H. Lee, H. H. Jang, M. S. Han, *Chem. Commun.*, 47 (2011) 10299-10301.
- [72]. H. M. Kim, B. R. Cho, *Acc. Chem. Res.*, 42 (2009) 863-872.
- [73]. M. Kumar, A. Puri. *Indian J. Occup. Environ. Med.*, 16 (2012) 40-44.

- [74]. K. Pomazal, C. Prohaska, I. Steffan, G. Reich, J. F. K. Huber, *Analyst*, 124 (1999) 657-663.
- [75]. P. Vanloot, B. Coulomb, C. Brach-Papa, M. Sergent, J. L. Boudenne, *Chemosphere*, 69 (2007) 1351-1360.
- [76]. C. M. G. Berg, *Anal. Chem.*, 78 (2006) 156-163.
- [77]. G. Cerchiaro, T. M. Manieri, F. R. Bertuchi, *Metallomics*, 5 (2013) 1336-1345.
- [78]. A. A. Ammann, *J. Mass Spectrom.*, 42 (2007) 419-427.
- [79]. T. Shamspur, I. Sheikhshoae, M. H. Mashhadizadeh, *J. Anal. At. Spectrom.*, 20 (2005) 476-478.
- [80]. H. A. McIlwee, C. L. Schauer, V. G. Praig, R. Boukherroub, S. Szunerits, *Analyst*, 133 (2008) 673-677.
- [81]. T. I. Nasution, I. Nainggolan, D. Dalimunthe, M. Balyan, R. Cuana, S. Khanifah, *IOP Conf. Ser.: Mater. Sci. Eng.*, 309 (2018) 012080.
- [82]. V. N. Mehta, S. K. Kailasa, H. F. Wu, *New J. Chem.*, 38 (2014) 1503-1511.
- [83]. Z. Z. Yin, Y. Li, L. P. Jiang, R. K. Rana, J. J. Zhu, *Anal. Chim. Acta*, 781 (2013) 48-53.
- [84]. R. A. Marcus, *Angew. Chem. Int. Edit.*, 32 (1993) 1111-1121.
- [85]. a) C.-C. Hsieh, C.-M. Jiang, P.-T. Chou, *Acc. Chem. Res.*, 43 (2010) 1364; b) J. E. Kwon, S. Y. Park, *Adv. Mater.*, 23 (2011) 3615; c) A. P. Demchenko, K.-C. Tang, P.-T. Chou, *Chem. Soc. Rev.*, 42 (2013) 1379; d) M. Mohapatra, A. K. Mishra, *Photochem. Photobiol. Sci.*, 18 (2019) 2830.
- [86]. a) A. Weller, *Elektrochemie*, 56 (1952) 662; b) A. Weller, *Prog. React. Kinet.*, 1 (1961) 187.
- [87]. L. Chen, P. Y. Fu, H. P. Wang, M. Pan, *Advanced Optical Materials*, 9 (2021) 2001952.
- [88]. T. Iijima, A. Momotake, Y. Shinohara, T. Sato, Y. Nishimura, T. Arai, *J. Phys. Chem. A*, 114 (2010) 1603-1609.
- [89]. Y. Jiao, B. Zhu, J. Chen, X. Duan, *Theranostics*, 5 (2015) 173-187.

- [90]. M. A. Rizzo, G. H. Springer, B. Granada, D. W. Piston, *Nat. Biotechnol.*, 22 (2004) 445-449.
- [91]. W. M. Shih, Z. Gryczynski, J. R. Lakowicz, J. A. Spudich, *Cell*, 102 (2000) 683-694.
- [92]. P. Li, X. Zhou, R. Huang, L. Yang, X. Tang, W. Dou, Q. Zhao, W. Liu, *Dalton Trans.*, 43 (2014) 706-713.
- [93]. H. Agarkar, D. Dave, D. Das, *Spectrochim. Acta Part A: Mol. Biomol. Spectrosc.*, 242 (2020) 118735.
- [94]. K. Naskar, S. Maity, S. Jana, B. Dutta, S. Tanaka, D. Mallick, T. Akitsu, C. Sinha, *Cryst. Growth Des.*, 18 (2018) 2986-2997.
- [95]. M. Irie, Y. Yokoyama, T. Seki, *New Frontiers in Photochromism*; Springer: Tokyo, 2013.
- [96]. C. C. Ko, V. W. W. Yam, *J. Mater. Chem.*, 20 (2010) 2063-2070.
- [97]. B. Chowdhury, K. Naskar, D. Mallick, C. Sen, K. K. Sarkar, C. Sinha, *J. Indian Chem. Soc.*, 95(2018) 405-416.
- [98]. S. Chen, F. Jiang, Z. Cao, G. Wang, Z.-M. Dang, *Chem. Commun.*, 51 (2015) 12633-12636.
- [99]. E. J. Harbron, *Isr. J. Chem.*, 53 (2013) 256-266.
- [100]. K. D. Singer, C. Ryan, J. Shan, J. Lott, C. Weder, B. Valle, R. Baer, *Optical Information Storage Medium*. U.S. Patent US 2016/ 0336035 A1, 2016.
- [101]. M. H. Sharifian, A. R. Mahdavian, H. Salehi-Mobarakeh, *Langmuir*, 33 (2017) 8023-8031.
- [102]. C. C. Ko, V. W. W. Yam, *Acc. Chem. Res.*, 51(2018) 149-159.
- [103]. M. Irie, T. Fukaminato, K. Matsuda, S. Kobatake, *Chem. Rev.*, 114 (2014) 12174-12277.
- [104]. L. Oggioni, C. Toccafondi, G. Pariani, L. Colella, M. Canepa, C. Bertarelli, A. Bianco, *Polymers*, 9 (2017) 462.
- [105]. C. Wiebeler, C. A. Bader, C. Meier, S. Schumacher, *Phys. Chem. Chem. Phys.*, 16 (2014) 14531-14538.
- [106]. A. Szukalski, A. Korbut, E. Ortyl, *Polymer*, 192 (2020) 122311.

- [107]. M. C. Mantero, L. Oggioni, G. Pariani, F. Ortica, S. Tosi, M. Canepa, C. Bertarelli, M. Tommasini, A. Bianco, *RSC Adv.*, 10 (2020) 26177-26187.
- [108]. Q. Zhang, J. Li, L. Niu, Z. Chen, L. Yang, S. Zhang, L. Cao, F. Zhang, *Chinese Science Bulletin*, 58 (2013) 74-78.
- [109]. D. Mallick, K. K. Sarker, R. Saha, T. K. Mondal, C. Sinha, *Polyhedron*, 54 (2013) 147-157.
- [110]. G. Saha, P. Datta, K. K. Sarkar, R. Saha, G. Mostafa, C. Sinha, *Polyhedron*, 30 (2011) 614-623.
- [111]. J. Garcia-Amorós, M. C. R. Castro, S. Nonell, S. Vílchez, J. Esquena, M. M. M. Raposo, D. Velasco, *J. Phys. Chem. C*, 123 (2019) 23140-23144.
- [112]. S. Zielińska, M. Larkowska, S. Kucharski, *Dyes Pigm.*, 92 (2012) 1018-1024.
- [113]. P. Gayen, A. Karmakar, N. Sepay, C. Sinha, *J. Indian Chem. Soc.*, 99 (2022) 100295
- [114]. C. Sinha, *Indian J. Chem. A*, 57 (2020) 418-426.
- [115]. B. Chowdhury, K. Naskar, D. Mallick, K. K. Sarkar, C. Sen, C. Sinha, *Inorganica Chim. Acta*, 483 (2018) 87-92
- [116]. D. Mallick, U. Panda, S. Jana, C. Sen, T. K. Mondal, C. Sinha, *Polyhedron*, 117 (2016) 318-326
- [117]. U. Panda, D. Mallick, C. Sen, A. Nandi, T. K. Mondal, C. Sinha, *J. Indian Chem. Soc.*, 92 (2015) 1925-1938
- [118]. S. Saha, C. Sen, S. Roy, D. Mallick, E. López-Torres, C. Sinha, *Polyhedron*, 97 (2015) 240-247
- [119]. C. Sen, S. Roy, T. K. Mondal, R. Ghosh, J. A. Mondal, D. K. Palit, C. Sinha, *Polyhedron*, 85 (2015) 900-911
- [120]. P. Gayen, C. Sinha, *J. Lumin.*, 132 (2012) 2371-2377
- [121]. K. K. Sarker, D. Sardar, K. Suwa, J. Otsuki, C. Sinha, *Inorg. Chem.*, 46 (2007) 8291-8301
- [122]. K. K. Sarker, B. G. Chand, K. Suwa, J. Cheng, T. H. Lu, J. Otsuki, C. Sinha, *Inorg. Chem.*, 46 (2007) 670-680

- [123]. H. Xu, S. Zhang, Y. Gu, H. Lu, *Spectrochim. Acta A Mol. Biomol. Spectrosc.*, 265 (2022) 120364.
- [124]. D. Ravichandran, M. Ranjani, G. P. Sankar, R. Shankar, M. Karthi, S. Selvakumar, R. Prabhakaran, *J. Mol. Struct.*, 1273 (2023) 134329.
- [125]. W. A. Durai, A. Ramu, A. Dhakshinamoorthy, *Inorg. Chem. Commun.*, 121 (2020) 108191.
- [126]. R. Manjunath, P. Kannan, *Optical Materials*, 79 (2018) 38-44.
- [127]. Z. Zhou, W. Niu, Z. Lin, Y. Cui, X. Tang, Y. Li, *Inorg. Chem. Commun.*, 121 (2020) 108168.
- [128]. S. Suresh, N. Bhuvanesh, J. Prabhu, A. Thamilselvan, S. R. J. Rajkumar, K. Kannan, V. R. Kannan, R. Nandhakumar, *J. Photochem. Photobiol. A*, 359 (2018) 172-182.
- [129]. D. Anu, P. Naveen, R. Rajamanikandan, *J. Photochem. Photobiol. A*, 405 (2021) 112921.
- [130]. A. Saravanan, S. Shyamsivappan, N. K. Kalagatur, T. Suresh, N. Maroli, N. Bhuvanesh, P. Kolandaivel, P. S. Mohan, *Spectrochim. Acta A Mol. Biomol. Spectrosc.*, 241 (2020) 118684.
- [131]. J. C. Qin, T. R. Li, B. D. Wang, Z. Y. Yang, L. Fan, *Spectrochim. Acta A Mol. Biomol. Spectrosc.*, 133 (2014) 38-43.
- [132]. M. Kumar, A. Kumar, S. Kishor, S. Kumar, N. Manav, A. K. Bhagi, S. Kumar, R. P. John, *J. Mol. Struct.*, 1247 (2022) 131257.
- [133]. G. Xu, S. J. Ma, H. H. Zhang, J. Jing, X. H. Chen, X. P. Zhang, *J. Fluoresc.*, 33 (2023) 1183-1189.
- [134]. R. Behura, P. P. Dash, P. Mohanty, S. Behera, M. Mohanty, R. Dinda, S. K. Behera, A. K. Barick, B. R. Jali, *J. Mol. Struct.*, 1264 (2022) 133310.
- [135]. S. Sahu, Y. Sikdar, R. Bag, J. Cerezo, J. P. Cerón-Carrasco, S. Goswami, *Molecules*, 27 (2022) 2859.
- [136]. H. Xu, S. Zhang, C. Zhang, Y. Wang, X. Chen, *Spectrochim. Acta A Mol. Biomol. Spectrosc.*, 282 (2022) 121697.
- [137]. P. Wang, J. Wu, *J. Photochem. Photobiol. A*, 386 (2020) 112111.

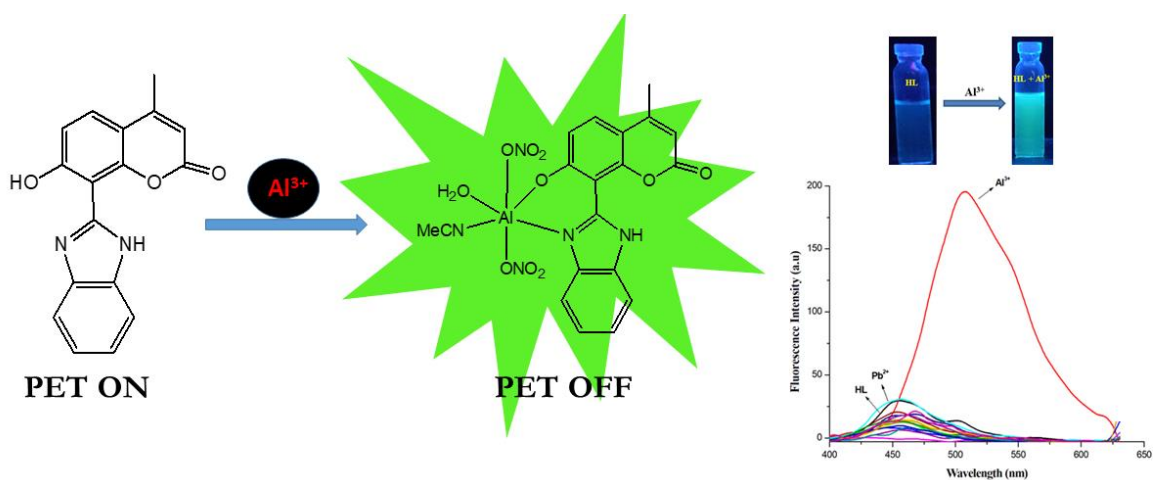
- [138]. Y. S. Yang, C. M. Ma, Y. P. Zhang, Q. H. Xue, J. X. Ru, X. Y. Liu, H. C. Guo, *Anal. Methods*, 10 (2018) 1833-1841.
- [139]. L. Chen, H. Jiang, N. Li, Q. Meng, Z. Li, Q. Han, X. Liu, *Spectrochim. Acta A Mol. Biomol. Spectrosc.*, 268 (2022) 120704.
- [140]. Z. Li, J. Wang, Y. Chen, L. Xiao, Z. Liu, *Inorganica Chim. Acta*, 545 (2023) 121275.
- [141]. J. H. Hu, J. B. Li, J. Qi, Y. Sun, *Sens. Actuators B Chem.*, 208 (2015) 581-587.
- [142]. J. Zhu, Y. Zhang, Y. Chen, T. Sun, Y. Tang, Y. Huang, Q. Yang, D. Ma, Y. Wang, M. Wang, *Tetrahedron Lett.*, 58 (2017) 365-370.
- [143]. L. Dong, X. Zeng, L. Mu, S. F. Xue, Z. Tao, J. X. Zhang, *Sens. Actuators B Chem.*, 145 (2010) 433-437.
- [144]. R. Mehandi, R. Sultana, S. Ahmedi, M. Rana, N. Manzoor, S. Javed, N. Nishat, *J. Fluoresc.*, 33 (2023) 751-772.
- [145]. C. H. Chen, P. J. Hung, C. F. Wan, A. T. Wu, *Inorg. Chem. Commun.*, 38 (2013) 74-77.
- [146]. G. Singh, J. Sindhu, V. Kumar, V. Sharma, S. K. Sharma, S. K. Mehta, M. H. Mahnashi, A. Umar, R. Kataria, *J. Mol. Liq.*, 296 (2019) 111814.
- [147]. Z. Y. Yin, J. H. Hu, K. Gui, Q. Q. Fu, Y. Yao, F. L. Zhou, L.L. Ma, Z. P. Zhang, *J. Photochem. Photobiol. A.*, 396 (2020) 112542.
- [148]. G. G. Çelik, E. Şenkuytu, O. Şahin, S. Serin, *Inorganica Chim. Acta*, 527 (2021) 120556.
- [149]. D. Utreja, K. Singh, S. Sharma, *ChemistrySelect*, 6 (2021) 12323-12330.
- [150]. L. Wang, W. Li, W. Zhi, Y. Wang, J. Han, Z. Cao, L. Ni, H. Li, J. Jing, *J. Lumin.*, 196 (2018) 379-386.
- [151]. L. Hou, T. Liu, Y. Gong, J. Li, C. Deng, C. Zhang, Y. Wang, S. Shuang, W. Liang, *New J. Chem.*, 44 (2020) 19642-19649.
- [152]. P. S. Nayab, M. Shkir, P. Gull, S. AlFaify, *J. Photochem. Photobiol. A.*, 347 (2017) 209-217.
- [153]. G. B. Chalmardi, M. Tajbakhsh, N. Hasani, A. Bekhradnia, *Tetrahedron*, 74 (2018) 2251-2260.

- [154]. Y. S. Wu, C. Y. Li, Y. F. Li, J. L. Tang, D. Liu, *Sens. Actuators B Chem.*, 203 (2014) 712-718.
- [155]. S. Mukherjee, S. Betal, A. P. Chattopadhyay, *Spectrochim. Acta A Mol. Biomol. Spectrosc.*, 228 (2020) 117837.
- [156]. P. Zhang, X. Xu, Y. F. Cui, X. H. Wei, Y. X. Sun, *J. Photochem. Photobiol. A.*, 408 (2021) 113066.
- [157]. T. Hu, L. Wang, J. Li, Y. Zhao, J. Cheng, W. Li, Z. Chang, C. Sun, *Inorganica Chim. Acta*, 524 (2021) 120421.
- [158]. A. K. Bhanja, S. Mishra, K. Naskar, S. Maity, K. D. Saha, C. Sinha, *Dalton Trans.*, 46 (2017) 16516-16524.
- [159]. X. M. Li, R. R. Zhao, Y. Yang, X. W. Lv, Y. L. Wei, R. Tan, J. F. Zhang, Y. Zhou, *Chin. Chem. Lett.*, 28 (2017) 1258-1261.
- [160]. Y. Zhou, J. Zhang, L. Zhang, Q. Zhang, T. Ma, J. Niu, *Dyes Pigm.*, 97 (2013) 148-154.
- [161]. X. Huang, C. Fan, Z. Wang, X. Zhan, M. Pei, Z. Lu, *Inorg. Chem. Commun.*, 57 (2015) 62-65.
- [162]. S. Erdemir, O. Kocyigit, *Talanta*, 158 (2016) 63-69.
- [163]. R. Tamizhselvi, A. A. Napoleon, *Inorg. Chem. Commun.*, 139 (2022) 109330.
- [164]. N. Tomer, A. Goel, P. Bhalla, P. Bhagat, R. Malhotra, *J. Photochem. Photobiol. A.*, 427 (2022) 113823.
- [165]. V. Bhardwaj, L. Hindocha, S. A. Kumar, S. K. Sahoo, *New J. Chem.*, 46 (2022) 3248-3257.
- [166]. R. Kouser, A. Rehman, S. M. A. Abidi, F. Arjmand, S. Tabassum, *J. Mol. Struct.* 1256 (2022) 132533.
- [167]. B. Shruthi, H. D. Revanasiddappa, B. Jayalakshmi, A. Syed, A. M. Elgorban, R. Eswaramoorthy, R. G. Amachawadi, C. Shivamallu, S. P. Kollur, *Inorg. Chem. Commun.*, 150 (2023) 110467.
- [168]. K. Dhanasekaran, A. A. Napoleon, *Inorg. Chem. Commun.*, 151 (2023) 110481.

- [169]. J. Y. Yang, W. Y. Gao, J. H. Wang, Z. M. Dong, Y. Wang, S. M. Shuang, *J. Lumin.*, 254 (2023) 119549.
- [170]. J. Bai, J. Peng, T. Xu, M. Bu, W. Chen, Y. Nie, J. Jia, *Spectrochim. Acta A Mol. Biomol. Spectrosc.*, 290 (2023) 122190.
- [171]. D. Aydin, I. B. Gunay, O. Alici, *J. Lumin.*, 242 (2022) 118561.
- [172]. S. Majeed, T. A. Khan, M. T. Waseem, H. M. Junaid, A.M. Khan, S. A. Shahzad, *J. Photochem. Photobiol. A.*, 431 (2022) 114062.
- [173]. C. I. David, N. Bhuvanesh, H. Jayaraj, A. Thamilselvan, D. P. devi, A. Abiram, J. Prabhu, R. Nandhakumar, *ACS Omega*, 5 (2020) 3055-3072.
- [174]. L. J. Farrugia, *J. Appl. Crystallogr.*, 30 (1997) 565.
- [175]. G. M. Sheldrick, *Acta Crystallogr., Sect. A: Found. Crystallogr.*, 64 (2008) 112-122.
- [176]. A. L. Spek, *J. Appl. Cryst.*, 36 (2003) 7-13.
- [177]. M. J. Frisch, G. W. Trucks, H. B. Schlegel, P. M. W. Gill, B. G. Johnson, M. A. Robb, J. R. Cheeseman, T. A. Keith, G. A. Petersson, J. A. Montgomery, K. Raghavachari, M. A. Al-Laham, V. G. Zakrzewski, J. V. Ortiz, J. B. Foresman, J. Cioslowski, B. B. Stefanov, A. Nanayakkara, M. Challacombe, C. Y. Peng, P. Y. Ayala, W. Chen, M. W. Wong, J. L. Andres, E. S. Replogle, R. Gomperts, R. L. Martin, D. J. Fox, J. S. Binkley, D. J. Defrees, J. Baker, J. P. Stewart, M. Head-Gordon, C. Gonzalez, J. A. Pople, *Gaussian 98*, Gaussian Inc. Pittsburgh, PA, (1998).
- [178]. C. Lee, W. Yang, R. G. Parr, *Phys. Rev. B.*, 37 (1988) 785-789.
- [179]. N. M. O'Boyle, A. L. Tenderholt, K. M. Langner, *J. Comput. Chem.*, 29 (2008) 839-845.

Chapter II

Double advantages of Benzimidazolyl-hydroxy-coumarinyl diad - “turn-on” sensing of Al^{3+} and preventing metastasis in cancer



CHAPTER II

Abstract

8-(1H-Benzoimidazol-2-yl)-7-hydroxy-4-methyl-chromen-2-one (**HL**), a benzimidazolyl-hydroxy-coumarinyl diad, serves as fluorescent turn-on Al^{3+} -sensor in acetonitrile-water (2:1, v/v) at pH, 7.2 (HEPES buffer) medium. The intensity of emission on binding with Al^{3+} is enhanced by twelve times of probe with limit of detection (LOD) 0.62 μM . The structure of the probe has been established by the spectroscopic data (FT-IR, ^1H NMR, Mass spectra) and is confirmed by Single Crystal X-ray structure determination. The co-ordination environment of the complex, $[\text{Al}(\text{L})(\text{NO}_3)_2(\text{H}_2\text{O})(\text{NCCH}_3)]$, has been supported by Mass, FT-IR, NMR spectra and the Job's plot supports 1:1 composition. The anti-metastatic potential of **HL** on Human skin carcinoma (A431) and Human lung carcinoma (A549) cells are examined. Wound healing and Zymography assay suggest that **HL** has anti-migratory properties. The RT-PCR and Immunoblotting data suggest that **HL** down-regulates the expression of mesenchymal markers (Vimentin, Snail, Slug, MMP, and MMP9) and induces the expression of the epithelial marker (E-Cadherin).

II.1. Introduction

Towards achievement of sustainable health - quality of air, water, essential goods, pharmaceuticals, cosmetics etc. are very important. So, quality control of the food products and other consuming materials, along with precise and accurate analytical determination are significant (**Chapter I**). Different high value analytical techniques and instruments are used in this regard in the R & D sector of the industries and research institutes. Fluorescence sensing [1-7] is one of the widely accepted techniques that is widely used due to high selectivity, sensitivity, simple instrumentation technique, low cost etc. By the way sensing of biologically active metal ions has practical utility on the issues of human health. Aluminium (Al), third

most abundant metal present in the earth's crust (8% of its mass) [8], has used in large quantity in domestic purposes, cooked food supply and transportation. Al(III) ingestion causes diverse abnormality in human body such as neurotoxicity, Alzheimer's and Parkinson's diseases, and also obstructs the protein transportation in respiratory system, softening of bone, anemia in living actualities etc. [9,10]. Al(III) impedes the acceptance of Ca²⁺ and inhibits to delay the growth rate of biological systems. Moreover, the harmfulness of Al(III) is a threat towards aquatic lives and slows down the agriculture production in acidic lands. Dose-response impact of Al(III) shows adverse effects with respect to human health and plant growth. As a consequence, developing of new and practical multigesturing chemosensor for Al³⁺ is very important. Till date, several analytical techniques are available for recognition of Al³⁺ including titrimetric, chromatography, atomic absorption spectra, mass spectrometry, electrochemical detection, and Al-NMR technologies. Fluorescence spectroscopic technique is considered in recent literature as one of the most powerful analytical technique [11-15]. Many fluorescent based probes have been considered and some of them are utilized successfully in Al-neurochemistry. Most of the molecules have been constructed on quinoline, pyridyl, bipyridyl, coumarinyl, imine, pyrene, nitrobenzoxadiazole, carbazole, naphthalimide, benzoxazole, pyrazoline, tripyrrins, BINOL, fluorescein, rhodamine fluorophores [16-21]. benzimidazolyl and coumarinyl groups are strongly fluorogenic motifs and inclusion of these two in a single molecule may prepare analytically and biologically useful agent which may be applied for optical detection of metal ions. Besides, coumarin belongs to interesting class of natural ingredients and shows anticancer, anticoagulant and antioxidant activity [22]. Benzimidazolyl motif serves as fungicides, anthelmintic, anticancer, anti-tubercular, anti-HIV and inhibits microtubule assembly [23]. Therefore, a molecular diad with benzimidazolyl and coumarinyl groups may be a suitable biomedically significant fluorogenic system and may have biological effect against cancer and can be a promising anticancer drug. In this work, we characterize 8-

(1H-Benzoimidazol-2-yl)-7-hydroxy-4-methyl-chromen-2-one (**HL**), a diad composed of benzimidazolyl and hydroxy-coumarinyl, which is used for the sensing of Al³⁺ with low detection limit (0.62 μM). The composition of the complex is established by spectroscopic data (FT-IR, Mass, Job's plot, ¹H NMR). We have examined the biological efficiency of **HL** against metastasis of two human cancer cell lines, A431 and A549; anti-migratory property is assessed following wound healing and Zymography assay analysis. Besides, the probe down-regulates the expression of mesenchymal markers (Vimentin, Snail, Slug, MMP, and MMP9) and induces the expression of the epithelial marker (E-Cadherin).

II.2. Experimental

II.2.1 Materials and methods

Benzene-1,2-diamine was purchased from Himedia and 7-hydroxy-4-methyl-2-oxo-2H-chromene-8-carbaldehyde was prepared following published method [24]. Thiazolyl Blue Tetrazolium Bromide (MTT), Propidium Iodide (PI), RNase and Ethidium Bromide was purchased from Sigma (St. Louis, Missouri, USA). MuLV Reverse Transcriptase was purchased from Bio Bharati (Kolkata, India). GoTaq master mix was purchased from Promega (Madison, USA). Anti-E Cadherin, Anti-Vimentin, and Anti-GAPDH antibodies were purchased from Cell Signaling Technology (Danvers, Massachusetts, USA). Polyvinylidene Fluoride membrane was purchased from Pall (New York, USA). Human Lung Carcinoma (A549) and Human Skin Carcinoma (A431) cell lines were purchased from National Centre for Cell Science (Pune, India) and maintained in Dulbecco's Phosphate Eagle Medium (DMEM) in a humidified chamber maintaining 5 % CO₂ at 37°C. Analytical grade chemicals and solvents were used in this research.

II.2.2 Physical measurements

Melting point apparatus used to check melting point of the probe. Perkin Elmer RX-1 spectrophotometer (KBr disk, 4000-400 cm⁻¹) was used to collect IR spectra. Bruker 300 MHz FT-NMR spectrometer with TMS as internal standard in DMSO-d₆ was used to collect the ¹H NMR spectra. Water HRMS model XEVO-G2QTOF#YCA351 spectrometer was used to record mass spectra. Perkin Elmer Lambda 25 spectrophotometer was used to collect absorption spectra and emission spectra were measured in Perkin Elmer LS55 fluorescence spectrophotometer at room temperature (298K). The solution spectral measurements were carried out at pH, 7.2 (HEPES buffer) in acetonitrile-water (2:1, v/v) medium.

II.2.3. Quantum Yield Calculation

The fluorescence quantum yield was measured using standard quinine sulfate solution as reference with a known quantum yield, $\phi_R = 0.54$ in 0.5 M H₂SO₄. The sample under experiment and reference were excited at the same wavelength, keeping almost the same absorbance. Using the software available in the instrument area of the fluorescence spectra were measured and the quantum yield was calculated by following the formula

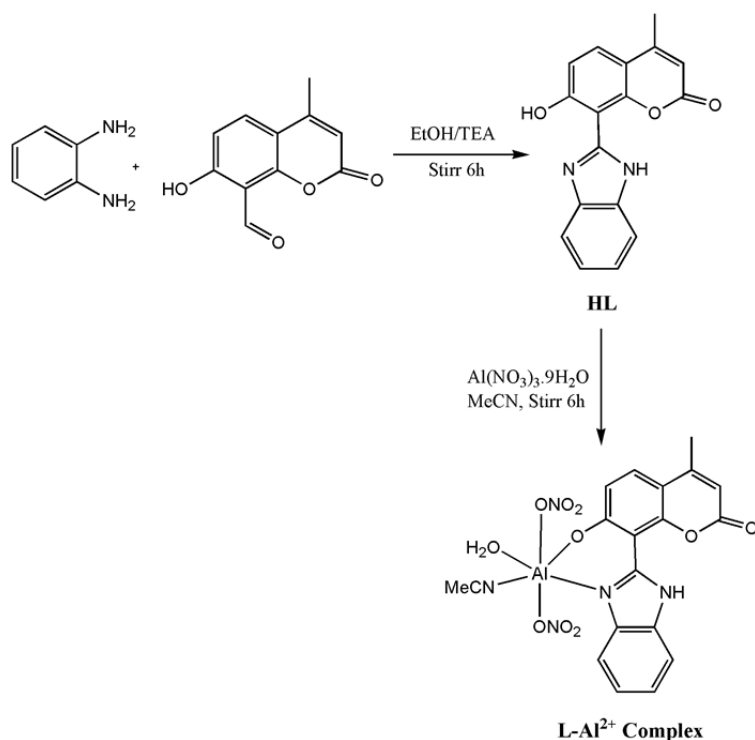
$$\phi_S/\phi_R = [A_S/A_R] \times [(Abs)_R / (Abs)_S] \times [\eta_S^2/\eta_R^2]$$

Where, ϕ_S and ϕ_R are the fluorescence quantum yield of the samples and reference respectively; the areas under emission spectra of the sample and references are represented by A_S and A_R respectively. $(Abs)_R$, $(Abs)_S$ are the absorbance of sample and reference at the required excitation wave length. The refractive index of the solvent (η_S^2) and reference (η_R^2) were collected from literature report [25, 26]

II.2.4. Synthesis of 8-(1H-Benzoimidazol-2-yl)-7-hydroxy-4-methyl-chromen-2-one (HL)

7-Hydroxy-4-methyl-2-oxo-2H-chromene-8-carbaldehyde (0.228 g, 1.12 mmol) was dissolved in ethanol (20 ml) by adding triethylamine in drops along with ethanol solution of Benzene-1,2-diamine (0.13 g, 1.2 mmol). The mixture was then stirred for 6 h at room temperature. The precipitate formed was filtered and recrystallized from CHCl₃ to isolate yellow crystalline 8-(1H-Benzoimidazol-2-yl)-7-hydroxy-4-methyl-chromen-2-one (**HL**) (**Scheme II.a**). TLC experiment was performed to check purity of the product; yield, 0.13 g (62%); M.P. 175°C.

Monoanalytical data of C₁₇H₁₂N₂O₃ (M.wt. 292) Calcd. for C₁₇H₁₂N₂O₃: C, 69.86; H, 4.14; N, 9.58 %. Found: C, 69.78; H, 4.24; N, 9.44 %., MS: m/z for [M+H⁺] = 293.08 (calc.), m/z for [M+H⁺] = 293.088 (found) (**Fig.II.1**); FT-IR: ν 3444, 3358, 1726, 1615 cm⁻¹ (**Fig.II.2**). ¹H NMR (300 MHz, DMSO-d₆): δ 13.72 (1H, brs); 7.81-7.78 (3H, m); 7.35-7.32 (2H, m); 7.08 (1H, d); 6.33 (1H, s); 2.46 (3H, s) (s, singlet; brs, broad singlet; d, doublet; m, multiplet) (**Fig.II.3**).



Scheme II.a. Synthesis of **HL** and its probable Al(III) complex.

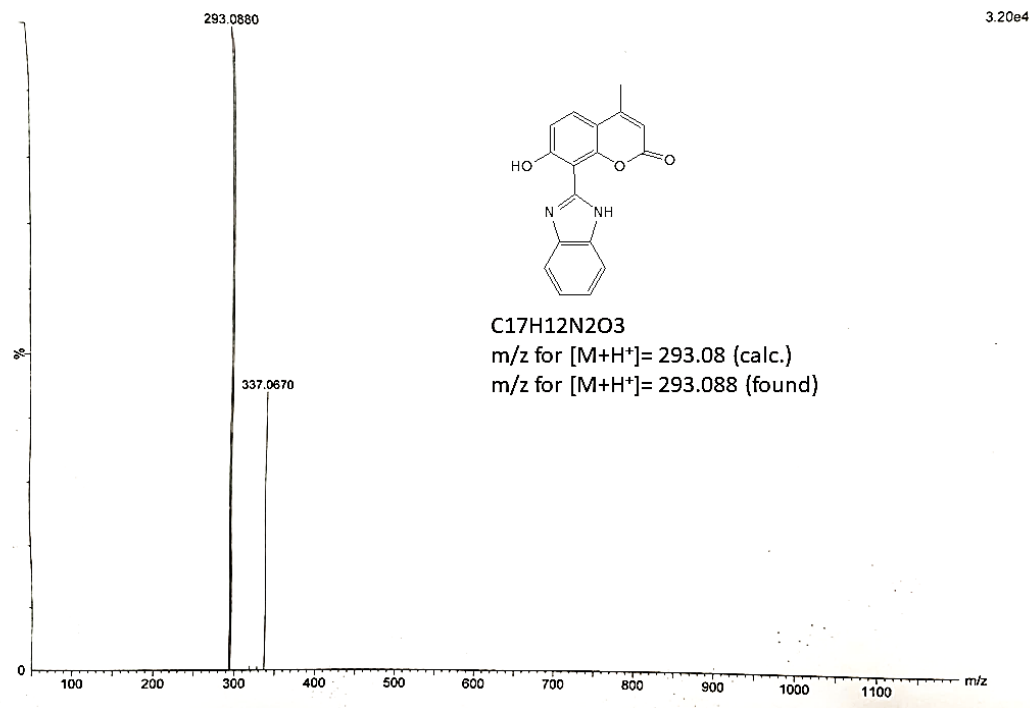


Fig.II.1. ESI- MS spectrum of HL.

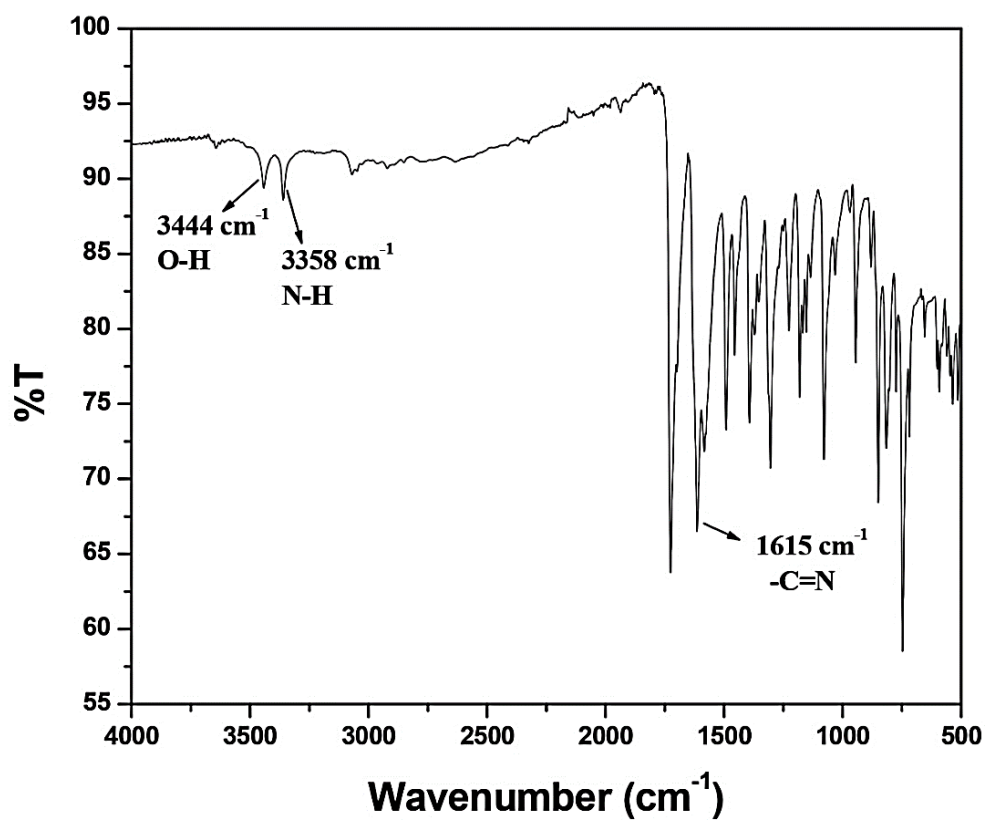


Fig.II.2. FT-IR spectrum of HL

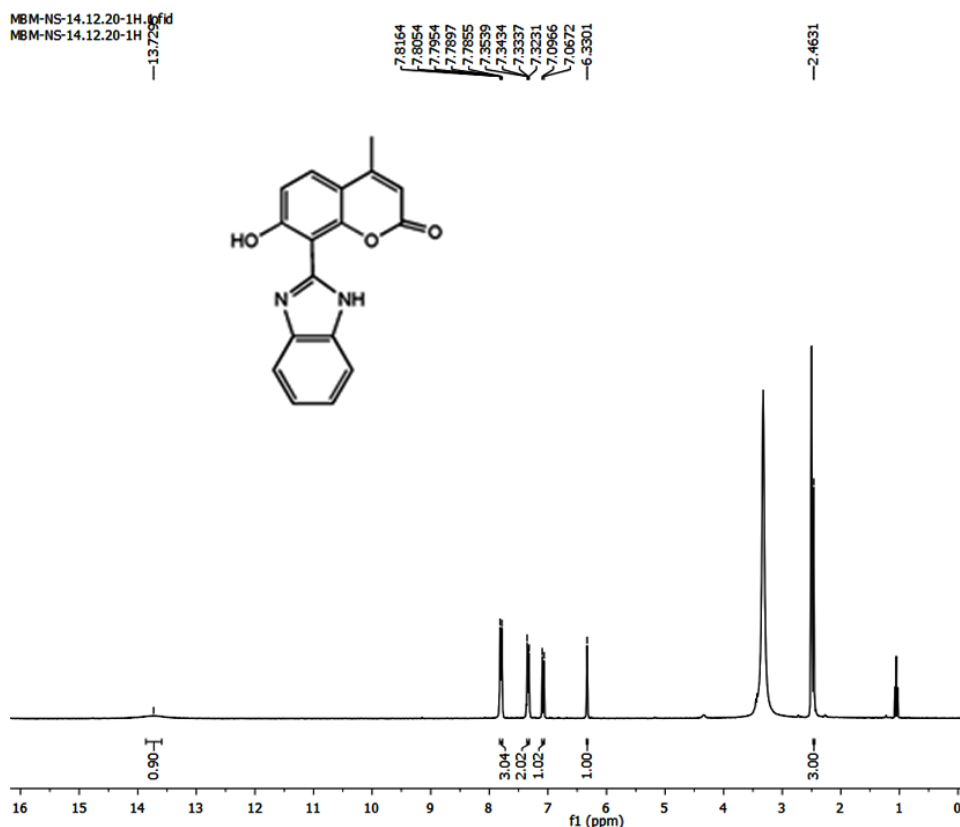


Fig.II.3. ¹H NMR spectrum of **HL** in DMSO-d₆.

II.2.5. Synthesis of Al³⁺ complex of HL

The probe, **HL** (0.114 g, 0.392 mmol) in acetonitrile (30 ml) and Al(NO₃)₃ · 9H₂O (0.147 g, 0.392 mmol) in methanol (15 ml) was added dropwise with constant stirring. The yellowish colored solution of **HL** turned orange after complete addition of Al(NO₃)₃ and the stirring was continued for 6 h (**Scheme II.a**). The solution was evaporated to dryness and the mass was washed with water for several times. The purity was checked by TLC.

Microanalytical data revealed that Calcd. (%): C₁₉H₁₆AlN₅O₁₀ : C, 45.52; H, 3.22; N, 13.97 % Found: C, 45.49; H, 3.29; N, 14.08 %, MS: m/z for [M+Na⁺] = 524.06 (calc.) , m/z for [M+Na⁺]=524.12(found) (**Fig.II.4**); IR: 3300-3500(b), 2257(s), 1680(s), 1590(s), 1304 (**Fig.II.5**) ; which has supported the composition [Al(L)(NO₃)₂(CH₃CN)(H₂O)]. The ¹H NMR spectrum of the complex (300 MHz, DMSO-d₆) shows δ 8.14-8.10 (2H, m); 7.88-7.91 (1H, d);

7.63-7.60 (2H, m); 6.94-6.97 (1H, d); 6.24 (1H, s); 2.43 (3H, s) (s, singlet; d, doublet; m, multiplet) (Fig.II.6).

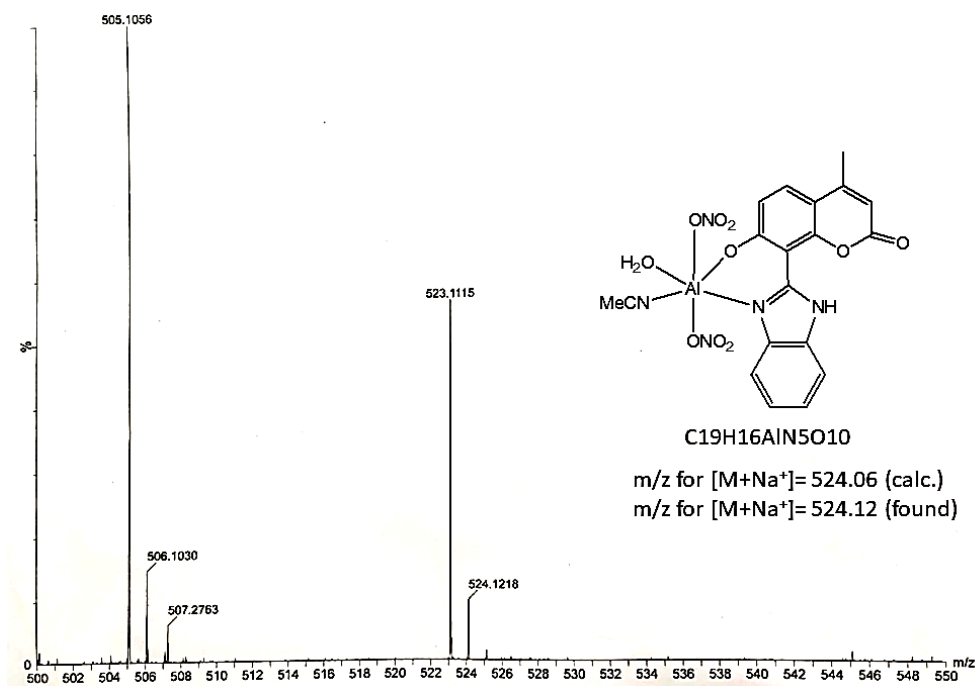


Fig.II.4. ESI-MS spectrum of $[Al(L)(NO_3)_2(H_2O)(NCCH_3)]$

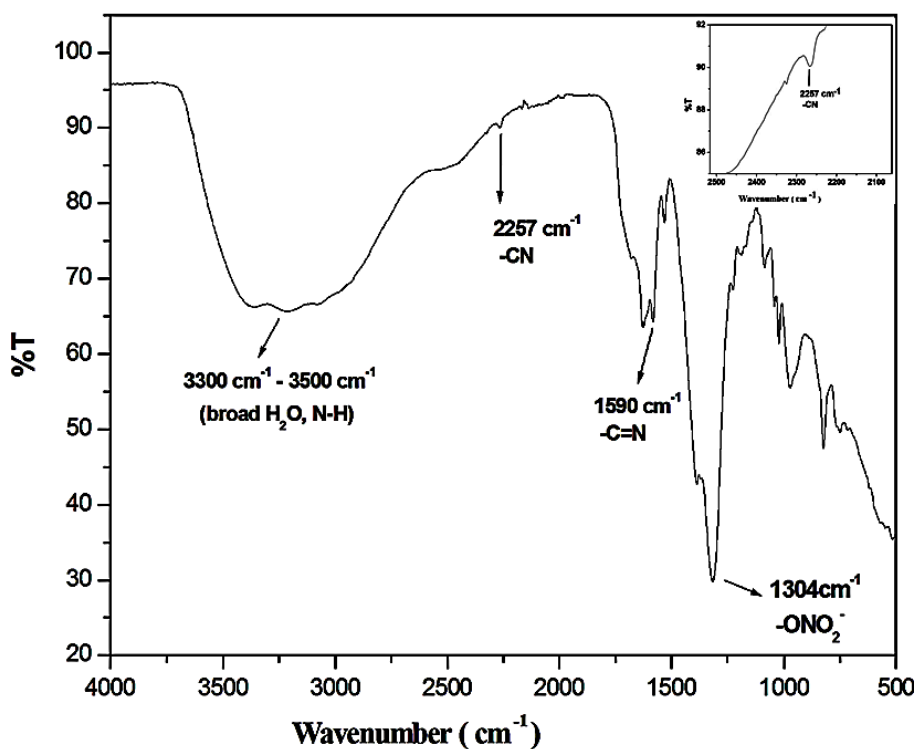


Fig.II.5. FT-IR spectrum of Al^{3+} complex of HL

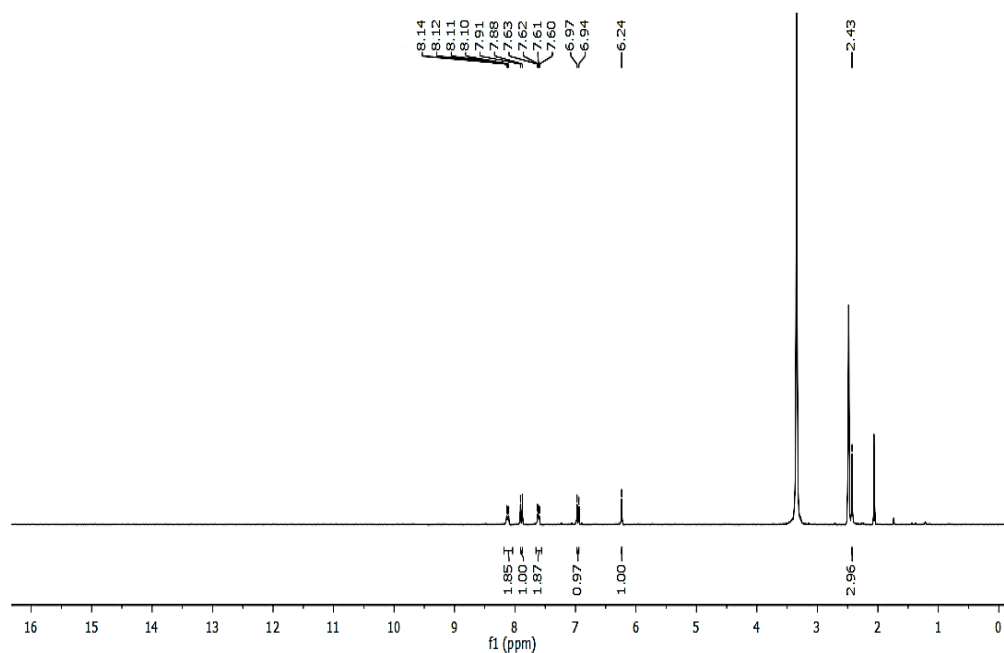


Fig.II.6. ¹H NMR spectrum of [Al(L)(NO₃)₂(H₂O)(NCCH₃)] in DMSO-d₆

II.2.6. General Method for the UV–vis and Fluorescence Experiments

Stock solutions of different metal ions ((CaCl₂·6H₂O, Al(NO₃)₃·9H₂O, NiCl₂·6H₂O, Zn(NO₃)₂·6H₂O, Hg(OAc)₂, FeCl₃·6H₂O, PdCl₂, NaCl, Co(NO₃)₂·6H₂O, Cu(OAc)₂·H₂O, CrCl₃·6 H₂O, Pb(NO₃)₂, MnCl₂·4H₂O, Cd(OAc)₂·2H₂O, NH₄Cl and KBr) (1 × 10⁻³ M) were prepared in deionized water. A stock solution of **HL** (1 × 10⁻³ M) was prepared in acetonitrile. The solution of **HL** was then diluted to 25 μM with acetonitrile-water (2:1, v/v) of pH, 7.2 (HEPES buffer) for the fluorescence experiments and UV-visible experiments, respectively. The different metal ions sensing by probe benzimidazolyl-hydroxy-coumarinyl diad was investigated using UV–vis and fluorescence spectrophotometer in mixed aqueous buffer (acetonitrile-water (2:1, v/v) of pH, 7.2 (HEPES buffer) solution at room temperature. An excitation wavelength at λ=309 nm was used for all fluorescence experiments.

II.2.7. General X-ray Crystallography

A block shaped crystal (0.24×0.16×0.05 Å³) of **HL** was taken for data collection from Bruker SMART APEX II [27] diffractometer equipped with graphite-monochromated MoKα radiation

(λ , 0.71073 Å). The hkl range $-22 \leq h \leq 22$, $-9 \leq k \leq 9$, $-23 \leq l \leq 23$ was used to determine the unit cell parameters and crystal-orientation matrices. Lorentz and polarization effects were used to correct the intensity of data [28]. The crystal data were collected by following the condition, $I > 2\sigma(I)$. The crystal structure was determined subsequent SHELXL 97 [29], ORTEP-3 [30], and PLATON 99 [31] programs. The non-hydrogen atoms (C,N,O) of the compound were refined by anisotropic thermal parameters. Crystal parameters and some selected bond lengths with bond angles are reported in **Table II.1** and **Table II.2**

Table II.1. Crystal data and refinement parameters for **HL**

Empirical formula	C ₃₄ H ₂₈ N ₄ O ₈
Formula weight	620.60
Temperature (K)	298(2)
System	Monoclinic
Space group	P 21/c
a (Å)	19.0176(16)
b (Å)	7.8418(7)
c (Å)	19.4841(16)
β /°	91.167(3)
V (Å) ³	2905.1(4)
Z	4
Dc/g cm ⁻³	1.419
μ /mm ⁻¹	0.103
λ (Å)	0.71073
R ₁ ^a [I>2 σ (I)]	0.0909
wR ₂ ^b	0.2245
GOF ^c	1.135

^aR₁ = $\Sigma||F_o| - |F_c|| / \Sigma|F_o|$; ^bwR₂ = $\{\Sigma[w(F_o^2 - F_c^2)^2] / \Sigma[w(F_o^2)]\}^{1/2}$; $w = [\sigma^2(F_o)^2 + (0.1142P)^2 + 2.4469P]^{-1}$ ($F_o^2 + 2F_c^2$)/3; ^c Goodness-of-fit

Table II.2. List of selected bond parameters of **HL**

Bond lengths, Å			
O5 – C21.	1.366(4)	O6 – C25	1.345(5)
O5 – C18	1.404(5)	O4 – C18	1.203(5)
O1 – C1	1.321(5)	N4 – C27	1.348(5)
O2 – C7	1.365(5)	N4 – C33	1.392(5)
O2 – C11	1.379(4)	N3 – C27	1.330(5)
N1 – C10.	1.367(5)	N3 – C28	1.380(5)
N1 – C17	1.378(5)	C7 – O3	1.228(5)
Bond angles (°)			
C21– O5– C18	121.3(3)	C7 – O2– C11	122.1(3)
C10 – N1 – C17	107.4(3)	C27 – N4 – C33	108.0(3)
C10 – N2 – C12	106.1(3)	C27 – N3 – C28	105.4(3)
O2 – C11 – C9.	116.7(3)	O5 – C21 – C26	115.7(3)
O2 – C11 – C4	119.4(3)	O5 – C21 – C22	121.4(3)
O6 – C25 – C26	122.0(4)	O1 – C1 – C9	122.9(3)
N2 – C10 – N1	111.3(3)	N3 – C27 – N4	112.3(3)

II.2.8. The biological effect of HL on carcinoma cell lines:

II.2.8.1. Hemolytic Assay

The toxicity of **HL** on Human erythrocytes was estimated by Hemolytic assay [32]. Fresh Human blood was drawn in a sterile tube and centrifuged at 3500 g (g: Relative Centrifugal Force) for 5 minutes. The supernatant was discarded and the pellet was washed twice in

Phosphate Buffer Saline (PBS), pH -7.4, and re-suspended in PBS at a final concentration of 2×10^8 cells/ml. An equal number of cells were incubated with various **HL** concentrations in a 1.5 ml microcentrifuge tube over a shaker at 37°C for 1 h. The cells were then centrifuged again at 3500 g for 5 minutes and the supernatant was collected and absorbance was measured at 540 nm. The percentage of Hemolysis was calculated using the following equation:

$$\% \text{ of Hemolysis} = (\text{Op}-\text{Ob}) / (\text{Om}-\text{Ob}) \times 100$$

Op = Absorbance in PBS; Ob = Absorbance in given drug concentration; Om = Absorbance in 0.1 % Triton X-100.

II.2.8.2. Cell Viability Assay

Fresh Human Peripheral blood was collected from one of the scholars volunteer in the research group and kept in a sterile Na₂EDTA coated tube and diluted with sterile PBS (1:1, v/v), pH - 7.4 under a sterile laminar hood. The diluted blood was then poured over Ficoll Histopaque (Sigma, USA) in a ratio of 4:1 of Ficoll: Blood and centrifuged at 2000 g for 15 min and the buffy layer of mononuclear cells were collected without disturbing other layers. These mononuclear cells were then washed twice in PBS and seeded in a 24 well plate at a concentration of 2×10^5 cells/ml. Cells were then incubated for 24 h at 37°C with various **HL** concentrations (3.42, 6.84, 17.12, 34.24, 68.49, 136.98, 205.47 μ M) and counted in a hemocytometer using the trypan blue exclusion method.

II.2.8.3. MTT assay

The cytotoxicity of **HL** was evaluated using MTT (3-(4, 5-Dimethyl-2-thiazolyl)-2, 5-diphenyl-2H-tetrazolium bromide) assay [33]. Cells were seeded in a 96 well plate at a

concentration of 1×10^4 cells/well and treated with variable **HL** concentrations (3.42, 6.84, 17.12, 34.24, 68.49, 136.98 μ M) in FBS free medium for 24 h at 5 % CO₂ and 37°C. Briefly, after that, the media was discarded and 100 μ l of PBS along with 10 μ l of MTT solution (5 mg/ml) was added and incubated for another 3 h at 37°C and 5 % CO₂. The formazan crystals formed were dissolved by adding another 100 μ l of DMSO and absorbance was taken at 595 nm.

II.2.8.4. Cell Cycle Analysis

Briefly, 1×10^6 cells were seeded in 12 well plates and followed by treatment with with 68.49 μ M of **HL** and incubated in a 5 % humidified chamber at 37°C for 24 h. Cells were trypsinized and washed with PBS suspended in 1 ml PBS and incubated with 10 μ l RNase (2.5 mg/ml) and 10 μ l Propidium Iodide (1 mg/ml) for 30 min at 37°C. The cells were then analyzed in Flow Cytometer (FACS Verse, Becton Dickinson, USA) and data were plotted in the histogram as DNA content vs Count.

II.2.8.5. Gelatin Zymography

Matrix metalloproteinases are enzymes that are capable of degrading the extracellular matrix. The expression of these molecules is low in the normal cell but in pathological conditions of cancer cells, their activity increases extensively which helps the cancer cells to metastasize [34]. The activity of these enzymes was studied by using non-reducing denatured SDS-PAGE [35]. Cells were cultured in 12 well plates and treated with 68.49 μ M of **HL** and incubated for 24 h in serum-free media in 5 % CO₂ at 37°C. The spent media was collected and centrifuged at 3500 g for 5 min. The supernatant was then taken and protein was precipitated using 10% TCA for 30 min at 4°C. It was then centrifuged at 12000 g for 15 min and the pellet was

collected and subjected to separation using 10 % SDS-PAGE containing 1mg/ml Gelatin. Gels were washed in 2.5 % Triton X-100 and incubated overnight in incubation buffer (Tris-HCl 50mM, CaCl₂ 10 mM, pH- 7.5) and stained with Coomassie brilliant blue G-250 stain followed by its removal. The gelatinase activity was observed as a clearer band over a blue background.

II.2.8.6. Wound Healing Assay

Cells were grown in a 6 well plate with 1×10^5 cell density and cultured until they reached sub-confluent density. A wound was created using a sterile micro tip and the cell plate was washed with sterile PBS and incubated in serum-free media containing 68.49 μ M of **HL** for 24 h at 37°C in 5 % CO₂. The image of the wound closure was captured using an inverted phase-contrast microscope (Leica Dmi8, Germany) and analyzed by ImageJ software (<https://imagej.nih.gov/ij/>).

II.2.8.7. RT-PCR

The gene expression of different Epithelial-Mesenchymal markers was analyzed by RT-PCR. The total RNA was isolated from 1×10^6 cells after treatment using Trizol (Thermo Fischer Scientific, USA) and quantified in UV-Vis Spectrophotometer. cDNA was prepared using MULV reverse transcriptase (Bio-Bharti, Kolkata). RT-PCR was performed using a Master cycler (Eppendorf, Germany) and are separated in 1 % agarose, stained with Ethidium Bromide (EtBr) and the image was captured using GelDoc (Bio-Rad, USA). The sequence of all primers was given in **Table II.3**.

Table II.3. Primer sequences used for RT-PCR

S. No.	Primers	Sequence (5'-3')
1	E-Cadherin (F)	TTCCAGGAACCTCTGTGATG
	E-Cadherin (R)	TCTTGGCTGAGGATGGTGTA
2	Vimentin (F)	AGGTGGACCAGCTAACCAAC
	Vimentin (R)	TCTCCTCCTGCAATTTCTCC
3	Snail (F)	CTAGGCCCTGGCTGCTAC
	Snail (R)	GACATCTCAGTGGGTCTGGA
4	Slug (F)	CTGGCCAAACACAAGCAG
	Slug (R)	ACCCAGGCTCACATATTCCT
5	MMP-2 (F)	AAGGGCATTTCAGGAGCTCTA
	MMP-2 (R)	TCCTGTTTGCAGATCTCAGG
6	MMP-9 (F)	CCGGACCAAGGATACAGTTT
	MMP-9 (R)	CGGCACTGAGGAATGATCTA
7	GAPDH (F)	ATCATCCCTGCCTCTACTGG
	GAPDH (R)	GTCAGGTCCACCACTGACAC

II.2.8.8. Immunoblotting

Cell lysates containing total protein were prepared after a brief treatment of 24 h and an equal amount of protein was separated using SDS-PAGE. Proteins in the gel were transferred to a polyvinylidene fluoride membrane (PVDF). The membrane was incubated with anti-E-cadherin, anti-vimentin, and anti-Gapdh primary antibodies followed by biotinylated secondary antibody and developed using NBT-BCIP as substrate.

II.3. Results and Discussion

II.3.1. General formulation of HL and its binding with Al³⁺

The probe (**HL**) is obtained by condensation of 7-hydroxy-4-methyl-2-oxo-2H-chromene-8-carbaldehyde with benzene-1, 2-diamine in ethanol under stirring condition by adding few drops of Et₃N at room temperature (**Scheme II.a**). The mass spectrum of **HL** shows peak at (m/z) 293.088 (**Fig.II.1**) which corresponds to molecular formula weight (Mwt, 292) and supports the composition of the probe. The characteristic stretching vibrations of **HL** are ν 3444 ($\nu(\text{O-H})$), ν 3358 ($\nu(\text{N-H})$), 1615 ($\nu(\text{C=N})$) cm⁻¹ (**Fig.II.2**) and accounts for condensation and cyclisation followed by areal oxidation. The ¹H NMR spectrum in DMSO-d₆ (**Fig.II.3**) identifies phenololato-OH at 13.72 ppm and benzimidazolyl protons appear at 7.78 -7.81 ppm; coumarinyl, -CH=CH(COO)- appear at 6.33 and 7.08 ppm along with phenolato aryl-H signal at 7.32-7.35 ppm.

Binding of **HL** to Al³⁺ has been examined by drop-casting Mass spectrum of [**HL**+Al(NO₃)₃] in acetonitrile-water (2:1, v/v) medium at pH, 7.2 and the mass peak at (M+Na), m/z) 524.12 (**Fig.II.4**) (M.wt, 524.06) proves the formation of the complex [Al(L)(NO₃)₂(H₂O)(CH₃CN)]. FT-IR spectral characteristic peaks have been compared with free ligand data and these are $\nu(\text{OH}_2)$, ($\nu(\text{N-H})$) 3300-3500(b), $\nu(\text{CH}_3\text{CN})$ 2257(s), $\nu(\text{C=N})$ 1590(s), $\nu(\text{ONO}_2)$ 1304(b) cm⁻¹ (**Fig.II.5**). The ¹H NMR spectrum of the complex in DMSO-d₆ (**Fig.II.6**) describes three coumarinyl-Hs at 6.24, 6.94-6.97, 7.88-7.91 ppm and four benzimidazolyl Hs appear in pairs at 7.60-7.63 and 8.10-8.14 ppm; imidazolyl-NH does not available which is probably involves in the proton exchange with solvent DMSO.

II.3.2. Molecular structure of HL

The single crystal structure determination reveals that the probe, **HL**, crystallizes in monoclinic crystal system with space group P 21/c and Z=4. The asymmetric unit contains two molecules (molecule-1, molecule-2; **Fig.II.7**) those are considered as conformational isomers as per their comparable bond parameters (**Table II.2**). The condensation of 7-hydroxy-4-methyl-2-oxo-2H-chromene-8-carbaldehyde and benzene-1,2-diamine followed by oxidation by air (O₂) has been supported by the formation of benzimidazolyl motif (**Fig.II.7**); where the corresponding C10–N1, 1.367(5); C10–N2, 1.323(5); C1–O1, 1.321(5); C7– O3, 1.228(5) (molecule-1) and C27–N4 , 1.348(5); C27–N3, 1.330 (5); C25–O6, 1.345(5); C18–O4, 1.203(5) Å (molecule-2) bond lengths are within the range of 0.01-0.02 Å).

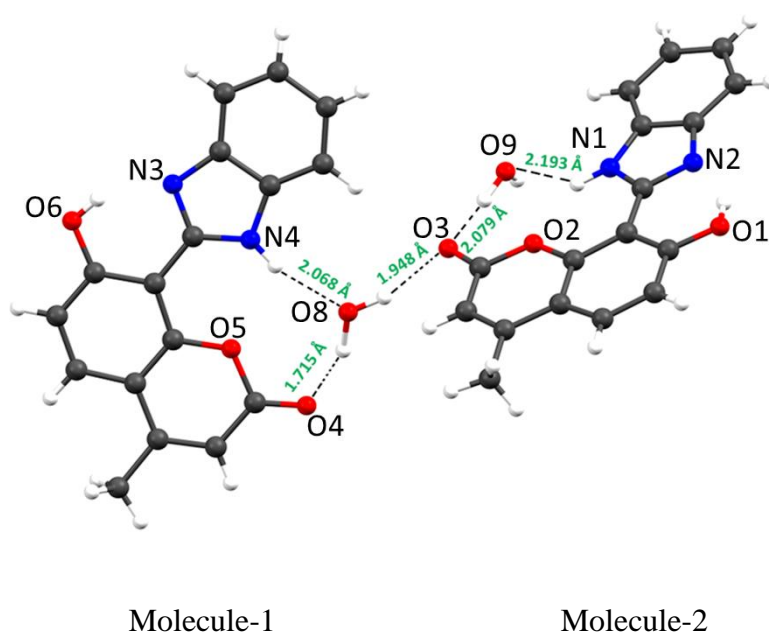


Fig.II.7. Molecular structure of two conformational isomers of probe **HL** with intermolecular Hydrogen bonding.

The asymmetric unit further contains two lattice water molecules those form hydrogen bonding interactions (H1A···O9 = 2.193 Å, H9A···O3=2.079 Å, H8E···O3=1.948 Å,

H8D \cdots O4=1.715 Å and H4 \cdots O8=2.068 Å) with **HL**. The structural architecture also reveals that the aldehyde and amine moieties are conformed almost planar structure, although the hydrogen bonded assembly is not planar. This hydrogen bonded dimeric assembly undergoes $\pi\cdots\pi$ interactions to generate supramolecular aggregate (**Fig.II.8**).

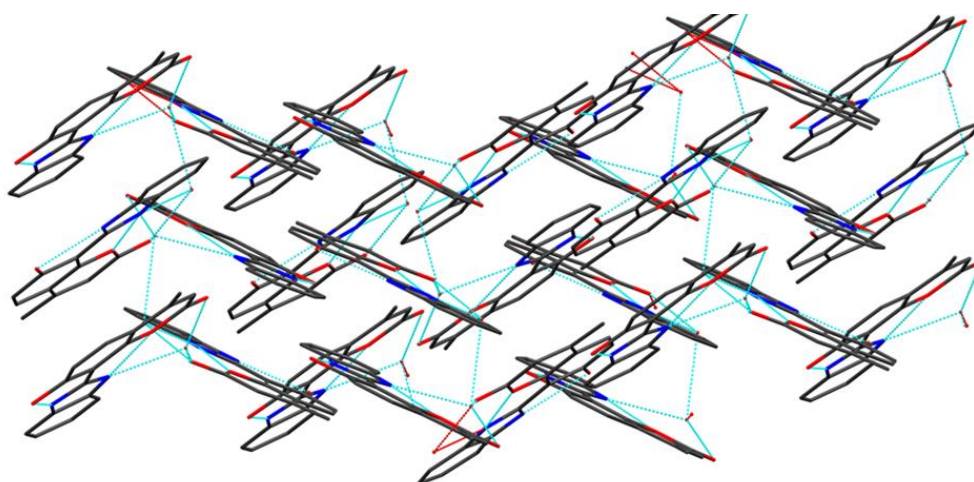


Fig.II.8. Supramolecular assembly of probe **HL**.

II.3.3. Spectroscopic studies

II.3.3.1. UV-vis Study

The probe **HL** shows strong absorption band at 309 nm (**Fig.II.9**) in acetonitrile-water (2:1, v/v; HEPES buffer, pH, 7.2, 25°C). Upon incremental addition of Al³⁺ to the solution of **HL** the absorption intensity gradually increases at 309 nm (**Fig.II.9**) and hence this UV-vis study

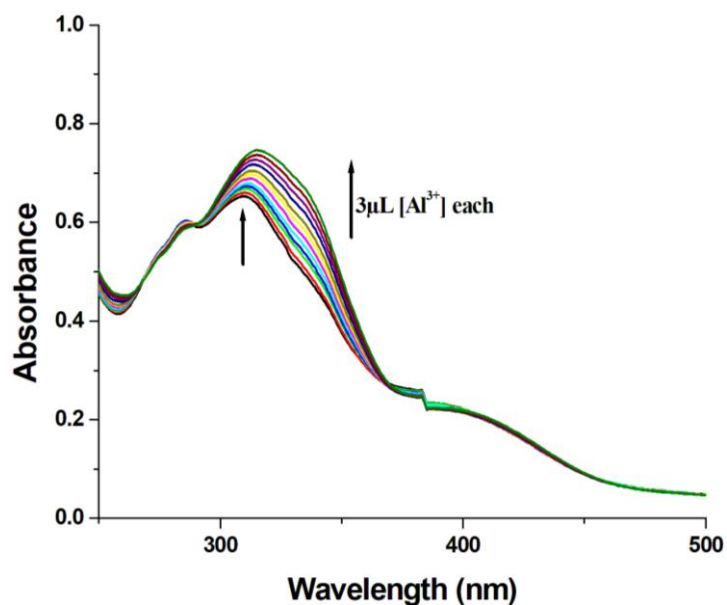


Fig.II.9. UV – VIS absorption spectra of **HL** in acetonitrile-water (2:1, v/v) of pH, 7.2 (HEPES buffer) on incremental addition of Al^{3+} .

reflects the interaction between **HL** and Al^{3+} . UV-vis study in presence of different metal ions (NH_4^+ , Na^+ , K^+ , Ca^{2+} , Hg^{2+} , Ni^{2+} , Co^{2+} , Cr^{3+} , Pb^{2+} , Pd^{2+} , Mn^{2+} , Cd^{2+} , Cu^{2+} , Fe^{3+} , and Zn^{2+} , Al^{3+}) was examined in acetonitrile-water (2:1, v/v; HEPES buffer, pH, 7.2) (**Fig.II.10**).

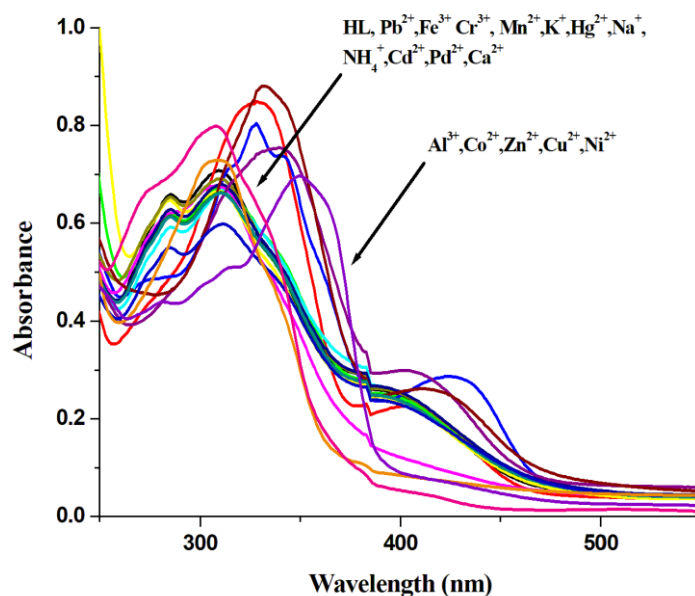


Fig.II.10. UV–vis absorption spectra of **HL** with various cations in acetonitrile-water (2:1, v/v) of pH, 7.2 (HEPES buffer) at room temperature.

In UV chamber pale yellow ligand solution turns into green upon addition of Al^{3+} (**Fig.II.11**) while other cations (NH_4^+ , Na^+ , K^+ , Ca^{2+} , Hg^{2+} , Ni^{2+} , Co^{2+} , Cr^{3+} , Pb^{2+} , Pd^{2+} , Mn^{2+} , Cd^{2+} , Cu^{2+} , Fe^{3+} , and Zn^{2+}) do not show observable color change in the sample vial in UV chamber (**Fig.II.12**). The naked eye view of **HL** in presence of different ions (**Fig.II.13**) in acetonitrile-water (2:1, v/v) of pH, 7.2 (HEPES buffer) was studied but no such significant color is observed.

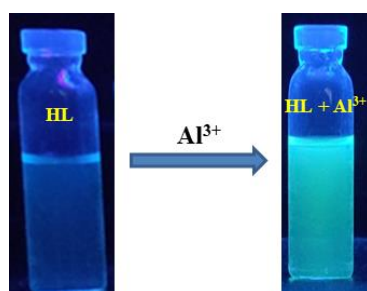


Fig.II.11. In acetonitrile-water (2:1, v/v) of pH, 7.2 (HEPES buffer) in UV chamber the colorless ligand (**HL**) solution turns into greenish yellow color.



Fig.II.12. In acetonitrile-water (2:1, v/v) of pH, 7.2 (HEPES buffer) UV chamber **HL** persists color in presence of Al^{3+} but disappears in presence of all other metals.



Fig.II.13. Naked eye view of **HL** in presence of different metal ions in acetonitrile-water (2:1, v/v) of pH, 7.2 (HEPES buffer)

II.3.3.2. Fluorescence study

The ligand, **HL**, emits weakly at 453 nm (quantum yield, ϕ_{HL} , 0.0091) and upon addition of Al³⁺ a new emission band appears at 508 nm (**Fig.II.14**) with twelve times enhancement of emission in acetonitrile-water (2:1, v/v; HEPES buffer, pH, 7.2). Upon complexation, the quantum yield of (**HL**+Al³⁺) is enhanced to $\phi_{\text{Complex}} = 0.0584$. The fluorescence spectra of **HL** with other cations (NH₄⁺, Na⁺, K⁺, Ca²⁺, Hg²⁺, Ni²⁺, Co²⁺, Cr³⁺, Pb²⁺, Pd²⁺, Mn²⁺, Cd²⁺, Cu²⁺, Fe³⁺, and Zn²⁺) have been examined (**Fig.II.14**) and no turn-on emission is observed. On gradual addition of Al³⁺ to the solution of **HL** the fluorescence intensity increases and becomes constant at 1:1 molar ratio of ligand and metal ion (**Fig.II.15**) (acetonitrile-water (2:1, v/v; HEPES buffer, pH, 7.2)). Excess of Al³⁺ does not show any effect on the emission intensity of the mixture. The fluorescence enhancement of [**HL**+Al³⁺] may be due to the elimination of photoinduced electron transfer (PET) and ESIPT in free **HL** followed by the attainment of structural rigidity through chelation of L⁻ to Al³⁺ with phenolato-O and imine-N(ring) (**Scheme II.b**).

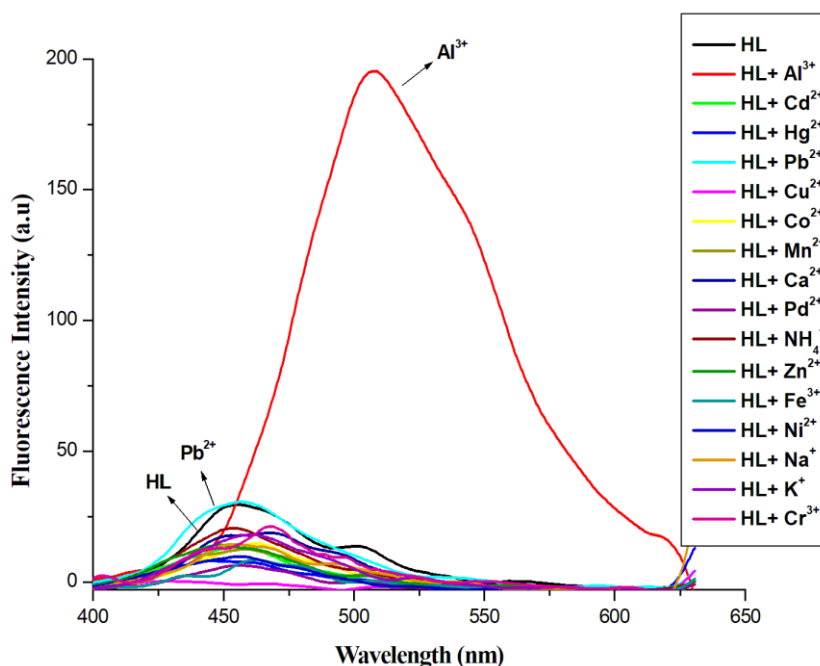


Fig.II.14. Fluorescence spectra of **HL** in acetonitrile-water (2:1, v/v) of pH, 7.2 (HEPES buffer) in presence of different cations.

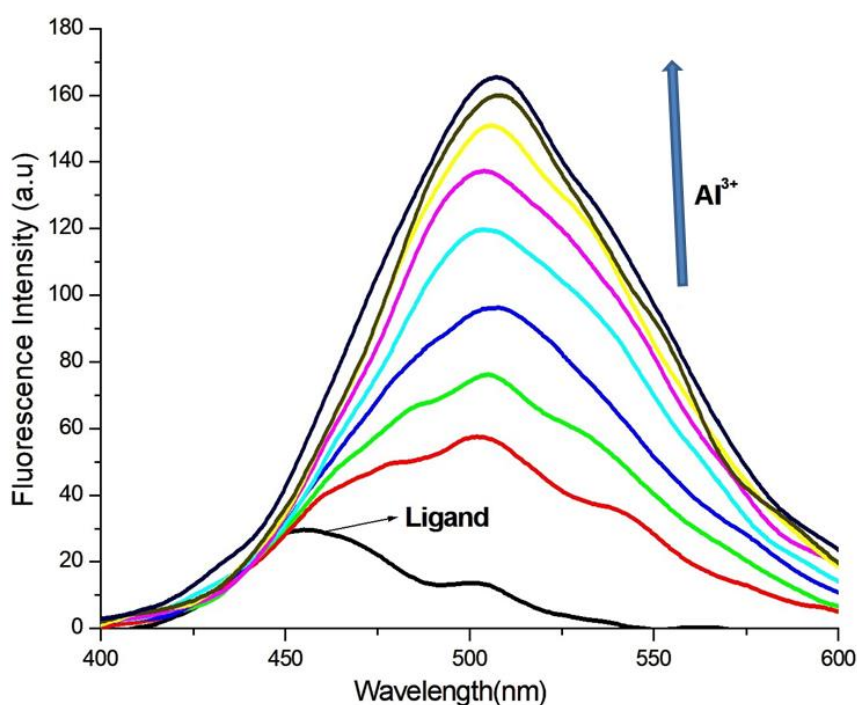
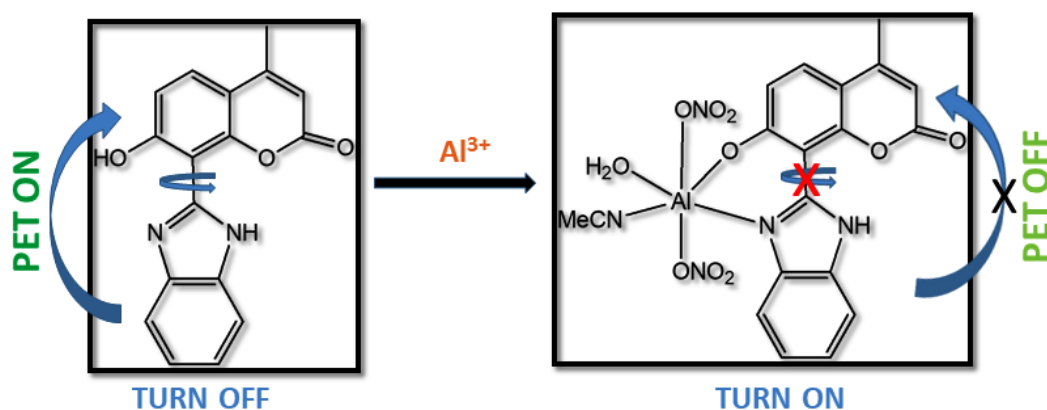


Fig.II.15. Fluorescence spectra of **HL** in acetonitrile-water (2:1, v/v) of pH, 7.2 (HEPES buffer) upon incremental addition of Al^{3+} .



Scheme II.b. Probable mechanism and binding mode of **HL** with Al^{3+} .

The comparative study (**Fig.II.16**) in presence of other competing metal ions (NH_4^+ , Na^+ , K^+ , Ca^{2+} , Hg^{2+} , Ni^{2+} , Co^{2+} , Cr^{3+} , Pb^{2+} , Pd^{2+} , Mn^{2+} , Cd^{2+} , Cu^{2+} , Fe^{3+} , and Zn^{2+}) the **HL** shows good selectivity towards Al^{3+} ; however, a little impact of quenching is observed upon addition of

Cu²⁺ and Fe³⁺ (**Fig.II.16**). The quenching may not be accounted from heavy atom effect or paramagnetism as other heavy atoms did not quench [36] the fluorescence.

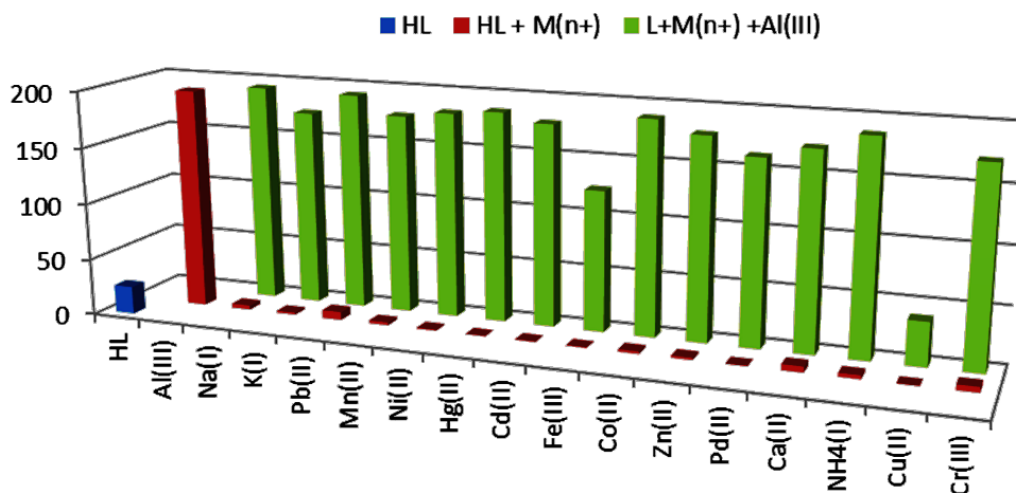


Fig.II.16. Selectivity studies of **HL** with Al³⁺ in the presence of competing

Metal ions in acetonitrile-water (2:1, v/v) of pH, 7.2 (HEPES buffer) at room temperature

The single crystal X-ray study has revealed that the synthesized ligand shows molecular assembly through various supramolecular interactions. It may be expected that in solution state this molecular aggregation may allow favorable communication to selective cations. It is observed that only Cu²⁺ and Fe³⁺ are invited to the assemble of [HL-Al³⁺] through some bonding interactions and assist quenching of emission of the complex. Therefore, the competitive fluorescence study ([HL-Al³⁺] + other metal ions) reveals the quenching of intensity when Cu²⁺ and Fe³⁺ ions are added which may be ascribed to secondary interactions in the molecular assembly (**Fig.II.17**). The quenching may be associated with excited state energy transfer or substitution of Al³⁺ by Cu²⁺/Fe³⁺ or chemical change of probe on interaction with the ions. We can't have solid prove to any of the reasons but we could say some interaction persist between ([HL-Al³⁺] and Cu²⁺/Fe³⁺ to quench emission.

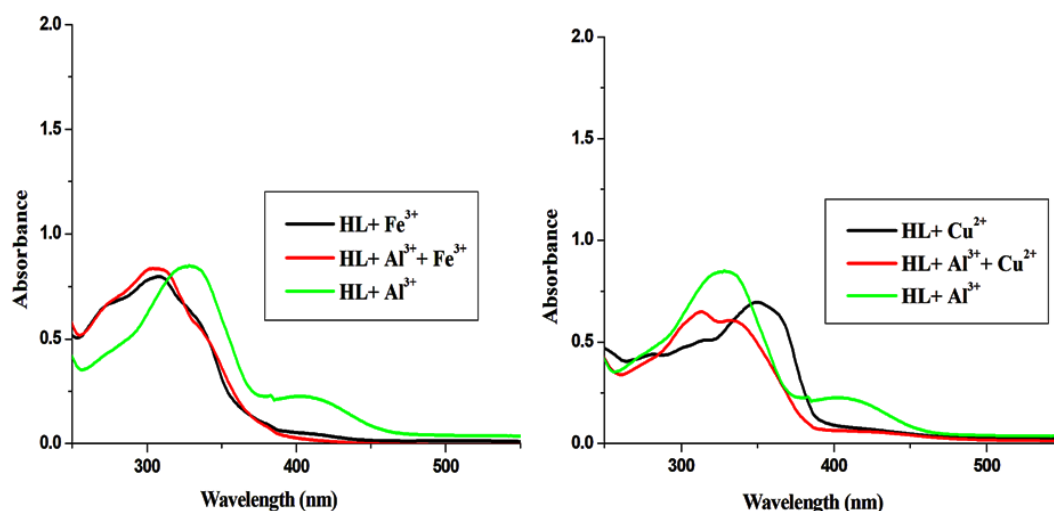


Fig.II.17. UV-vis absorption spectra of **HL** with Al^{3+} , Cu^{2+} and Fe^{3+} in acetonitrile-water (2:1, v/v) of pH, 7.2 (HEPES buffer) at room temperature.

Time resolved fluorescence measurement of **HL** in presence and absence of Al^{3+} shows that life time in complex state (τ_{complex} , 2.77 ns) is higher than the free ligand (τ_{HL} , 0.14 ns). The decay profile of **HL** and its [**HL**- Al^{3+}] complex (**Fig.II.18**) follow mono-exponential decay process.

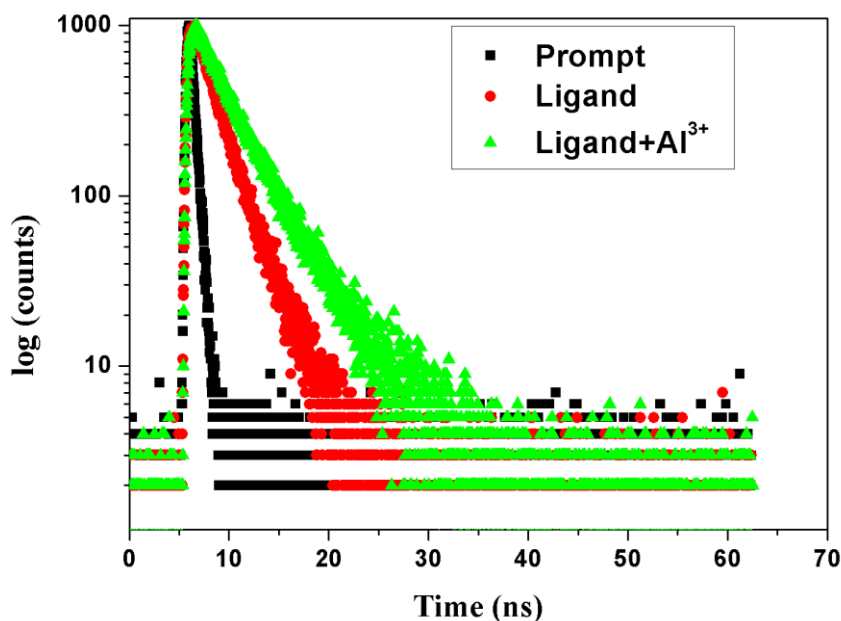


Fig.II.18. Fluorescence life time spectra of **HL** and its Al^{3+} complex in acetonitrile-water (2:1, v/v) of pH, 7.2 (HEPES buffer)

The probe (**HL**) binds with the Al^{3+} ion by 1:1 stoichiometric ratio which has been confirmed by the jobs plot (**Fig.II.19**) analysis.

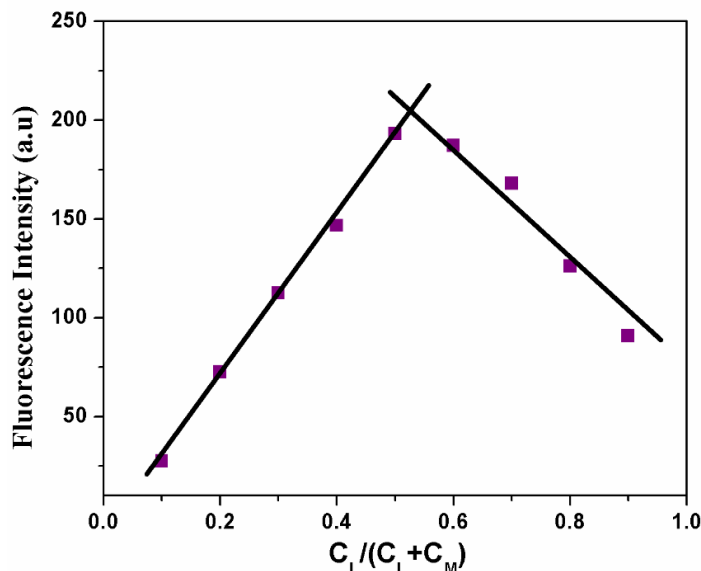


Fig.II.19. Job's plot for binding of Al^{3+} with **HL** in acetonitrile-water (2:1, v/v) of pH, 7.2 (HEPES buffer) by fluorometric method.

The binding constant, $1.43 \times 10^5 M^{-1}$ has been calculated by using modified Benesi-Hildebrand plot (**Fig.II.20**).

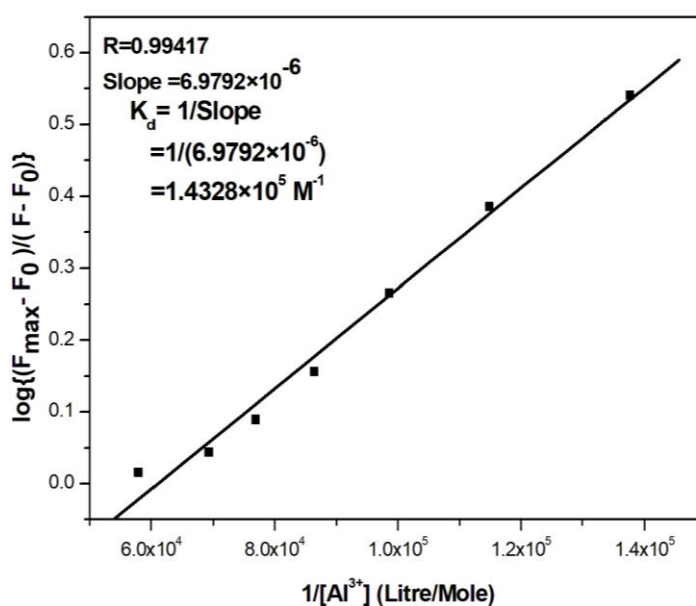


Fig.II.20. Modified Benesi-Hildebrand plot of $\log\{(F_{max}-F_0)/(F-F_0)\}$ vs. $1/[Al^{3+}]$

The limit of detection (LOD) of the probe **HL** (0.62 μM) has been studied in acetonitrile-water (2:1, v/v) of pH, 7.2 (HEPES buffer)) by 3σ/M method, where σ is the standard deviation and M is the slope between the fluorescence intensity versus [Al³⁺] (Fig.II.21).

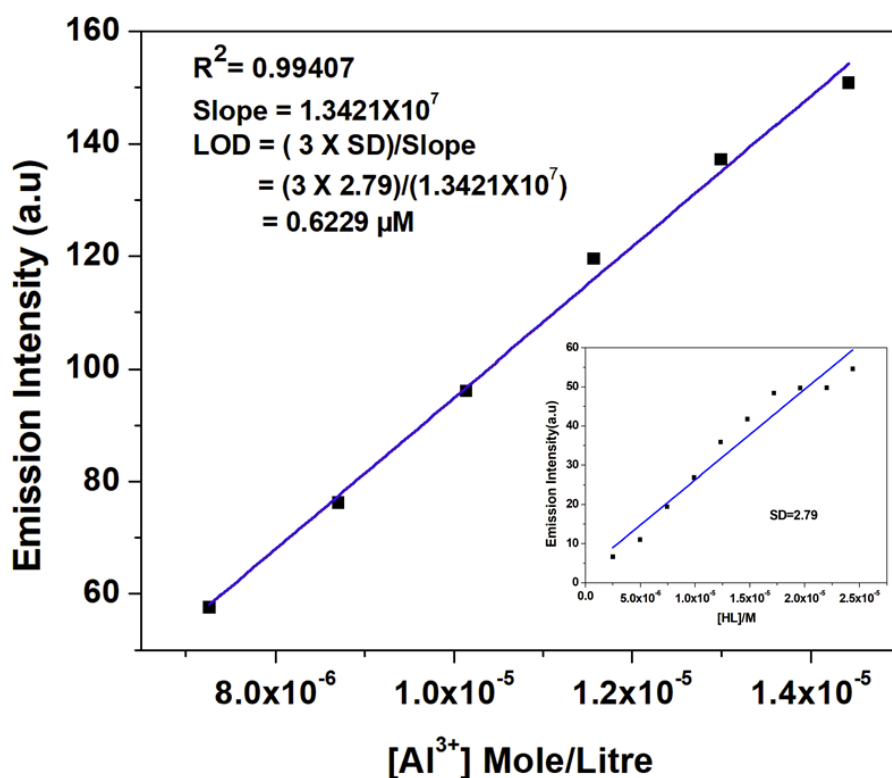


Fig.II.21. Determination of LOD of Al³⁺ by **HL** in acetonitrile-water (2:1, v/v) of pH, 7.2 (HEPES buffer) using 3σ method.

II.3.4. Probable Binding Mode of **HL** with Al³⁺

To investigate the interaction between **HL** and Al³⁺, the ¹H NMR spectrum has been recorded and shows the disappearance of coumarinyl –OH in the complex which was present in the ¹H NMR spectrum of **HL** at 13.72 ppm (Fig.II.22) and the aromatic protons are shifted towards downfield region. In FT-IR spectrum of **HL** (Fig.II.2) there is a sharp peak of –OH at 3444 cm⁻¹ which was disappeared in the FT-IR spectrum of Al³⁺ complex of **HL** (Fig.II.5). Hence

this observation clearly proves the formation of Al(III) complex with the replacement of proton from coumarinyl-OH. The binding of CH₃CN can be proved by FT-IR spectrum of Al³⁺ complex (inset of **Fig.II.5**) and $\nu(\text{CH}_3\text{CN})$ appears at 2257 cm⁻¹. Mass spectral data also supports binding of HL to Al³⁺ (**HL** (m/z), 293.088 (**Fig.II.1**); [Al(L)(NO₃)₂(H₂O)(NCCH₃)], (M+Na), m/z) 524.12 (**Fig.II.4**)).

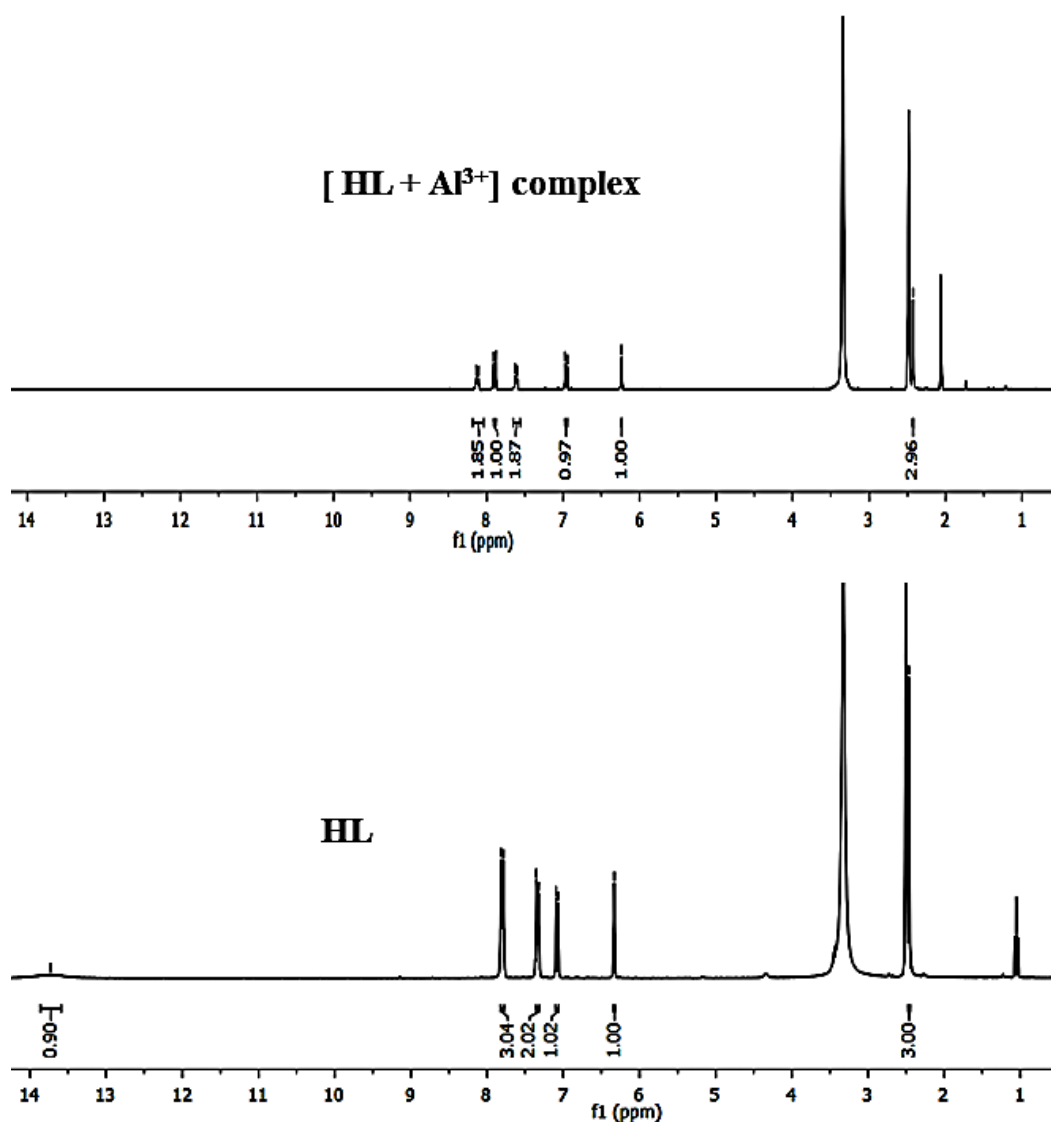
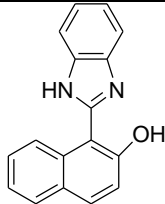
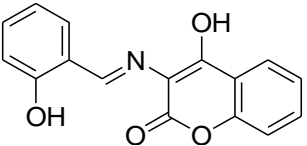
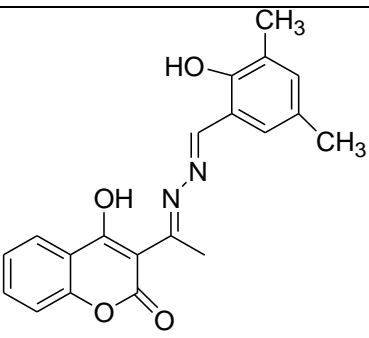
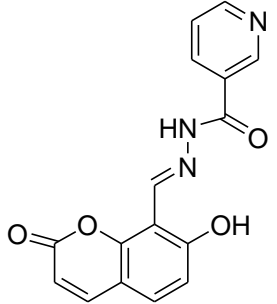


Fig.II.22. ¹H NMR spectrum of **HL** and **HL**+ Al³⁺ complex in DMSO-d₆

Intensive scrutiny of literature shows that Al³⁺ sensing probes with benzimidazolyl / coumarinyl group as transducer motif exhibits LOD within μM to nM range and stability constant (K_a) lies in 10^4 - 10^6 M^{-1} (Table II.4).

Table II.4. Comparison of LOD and K_a data of chemosensor to Al³⁺ available in literature with present probe having coumarinyl / benzimidazolyl group as transducer motif.

Sl no.	Structure of probe	Limit of Detection (LOD)	Binding Constant (K_a , M^{-1})	Solvent	Reference
1		0.99 μM	1.27×10^4	CH ₃ CN–H ₂ O 1:1 v/v	[37]
2		1.34 μM	$(1.06 \pm 0.2) \times 10^4$	MeOH: 0.01 M HEPES Buffer(9:1; v/v)	[38]
3		10.5 nM	8.5×10^5	1:5 v/v DMSO:H ₂ O	[39]
4		0.25 μM	9.64×10^4	EtOH-HEPES (95:5, v/v)	[40]

Sl no.	Structure of probe	Limit of Detection (LOD)	Binding Constant (K _a , M ⁻¹)	Solvent	Reference
5		1.62 μM	(9.9 ± 0.04) × 10 ³	(MeOH: 0.01 M HEPES Buffer; 9:1; v/v)	[41]
6		0.82 μM	3.3 × 10 ⁶	ethanol	[42]
7		3.3 μM	1.03 × 10 ⁴	ethanol and water (9 : 1, v/v)	[43]
8		0.39 μM	4.8 × 10 ⁵	1 : 1, v/v MeOH-H2O	[44]
10		0.62 μM	1.43 × 10 ⁵	acetonitrile-water (2:1, v/v)	This work

II.3.5. Effect of pH

In analytical and biological application pH of a medium plays a crucial role especially in the field of fluorescence chemosensors. Herein, the effect of pH study is determined in the pH

range of 2 to 12. The result clearly shows that the fluorescence emission intensity specially in case of (HL+Al³⁺) complex is remarkably high at around pH = 7 (Fig.II.23) but comparably

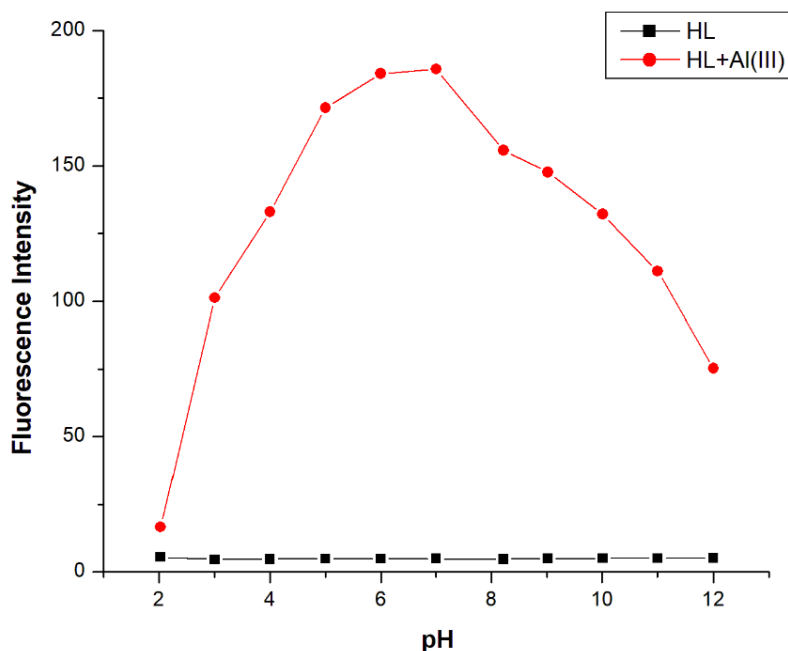


Fig.II.23. Effect of different pH on fluorescence intensity of HL and HL+ Al³⁺ complex.

low emission intensity is observed at high and low pH condition. Hence, the complexation between HL and Al³⁺ mostly favourable at around pH = 7 which is biologically efficient.

II.3.6. Biological application

II.3.6.1. Dose selection of HL

The activity of synthesized compounds has been exhibited its multifunctional activity on the biological systems. The active concentration was selected by hemolytic assay, Cell Viability assay on PBMC, and MTT assay, and Cell Cycle Assay on Cancer cells. The hemolytic activity (Fig.II.24A) suggests that HL was quite safe up to a concentration of 139.98 μ M as it induces a 6 % hemolysis at this concentration. The cell viability assay by trypan blue exclusion method

in PBMC (**Fig.II.24B**) suggests that **HL** at 68.49 μ M induces 6.7 % cytotoxicity whereas at 139.98 μ M it induces 32 % cytotoxicity.

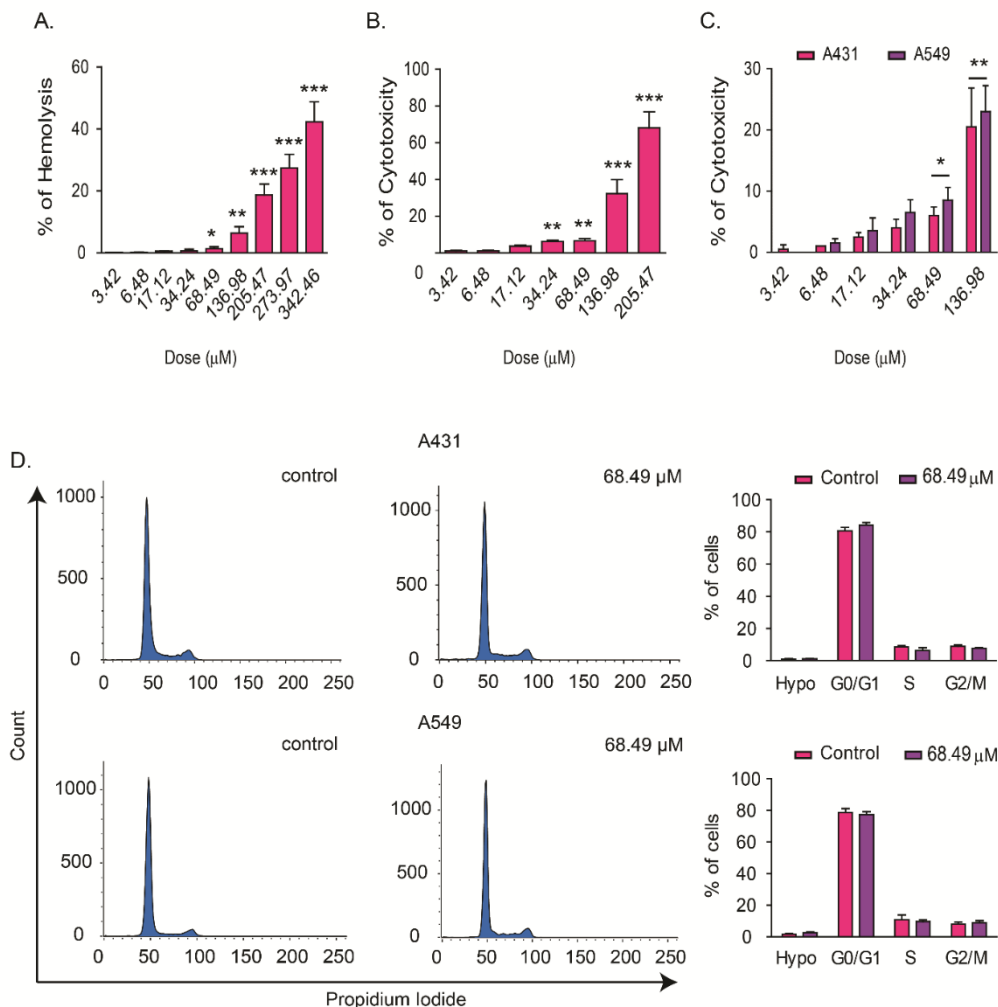


Fig.II.24. Effect of **HL** on cell viability on the percentage of hemolysis (A), on PBMC cell viability (B), on Human skin carcinoma (A431) and Human lung carcinoma cell viability by MTT assay (C). (D) The cell cycle phase distribution analysis displayed as a histogram of DNA content (X-axis) vs count (Y-axis) and bar plot of all phases of the cell cycle. The data were represented as mean \pm SD and performed in triplicate.

The MTT assay data (**Fig.II.24C**) indicate that **HL** induces significant toxicity in 139.98 μM but at 68.49 μM concentration it shows 6% cytotoxicity in A431 cells, and 8.5% in A549 cells. So, from these results, we have chosen 68.49 μM as critical dose for further study as it neither induces significant toxicity in normal cells nor in cancer cells. The effect of **HL** is further tested on cell cycle phase distribution (**Fig.II.24D**) of A431, and A549 cells in-vitro which reveals that **HL** doesn't induce the sub-G1 population in these cancer cell lines and even doesn't affect the cells in different phases of the cell cycle.

II.3.6.2. Effect of HL on Migration of Carcinoma Cell Lines

In order to metastasize from the primary site to distant secondary cells in the tumors, the drug, **HL**, induces the activity of Matrix Metalloproteinase (MMP) enzymes which digest the extracellular matrix surrounding the cell and helps to easily invade the bloodstream and travel to distant sites. The activity of MMP and MMP2 has been evaluated by gelatin zymography (**Fig.II.25A**), which suggest that the activity of these enzymes in both A549 and A431 has been significantly reduced in **HL** treated as compared to control cells. The anti-migratory potential of **HL** in these two cell lines were also evaluated using wound healing assay (**Fig.II.25B**), which reveals that upon treatment of **HL** in A431 cells had a wound closure of $26.33 \pm 7.5 \%$ as compared to the control, $81 \pm 7.6 \%$. In A549 cells the wound is closure to $45.66 \pm 10.01 \%$ as compared to control, $87 \pm 10.14 \%$ which indicates that **HL** has anti-migratory properties. For further investigation of anti-migratory effects, the gene expression of epithelial and mesenchymal markers was evaluated. The RT-PCR data (**Table II.3; Fig.II.25C**), suggest that **HL** downregulates the expression of mesenchymal markers (Vimentin, Snail, Slug, MMP2, and MMP9) and induces the expression of the epithelial marker (e-cadherin) in both these cell lines. The RT-PCR data were also fortified by immune-blotting (**Fig.II.25D**), which indicates

that **HL** downregulates the protein expression of Vimentin and upregulates the expression of E-Cadherin and for immunoblotting Gapdh was kept as loading control.

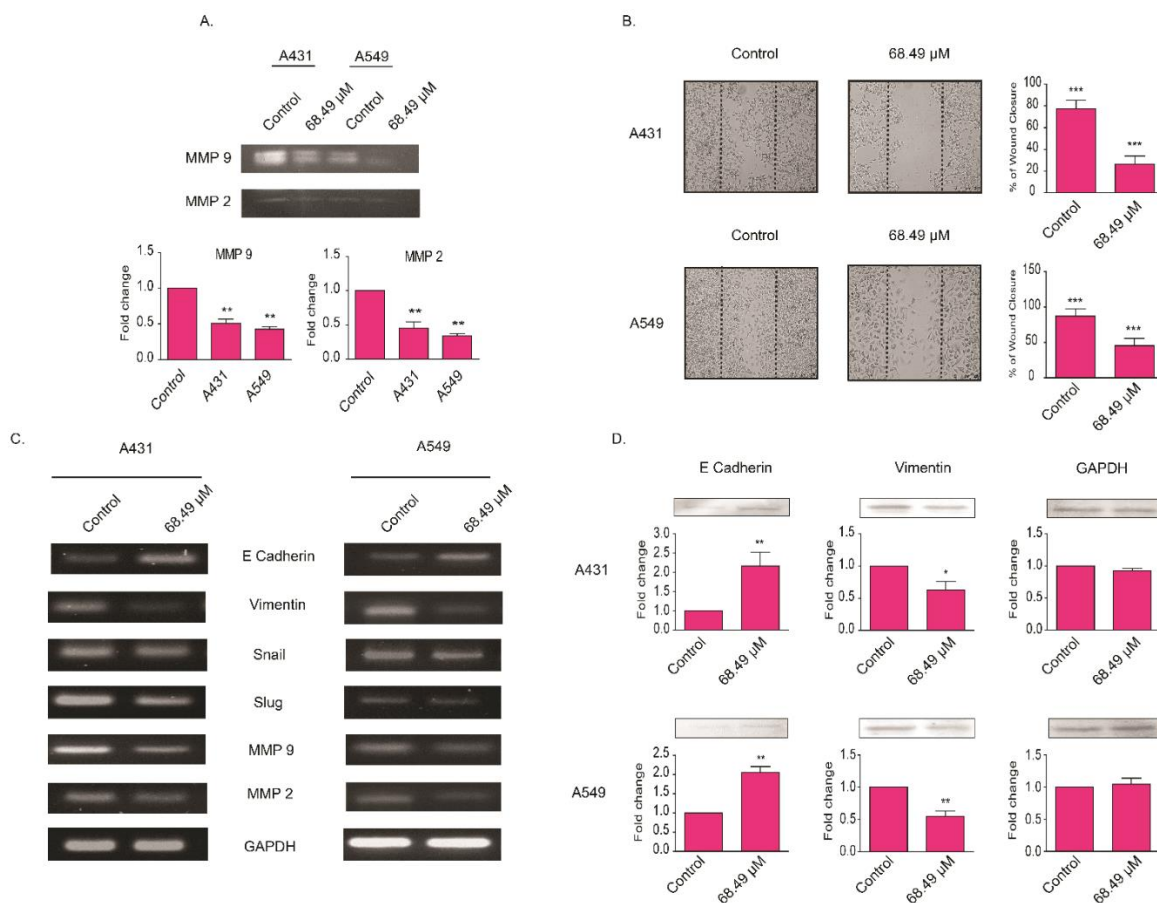


Fig.II.25. HL Inhibits the migration of carcinoma cell lines. (A) Effect of **HL** on the activity of matrix metalloproteinase enzyme by gelatin zymography. The MMP2 and MMP9 bands were displayed. (B) Wound healing assay displaying the migration of cells in 24 hours, with and without treatment with **HL** and the bar plots displaying % of wound coverage by cells. (C) The effect of **HL** on the EMT markers done by RT-PCR. (D) Effect of **HL** on E-Cadherin and Vimentin protein expression and bar plots represents the fold change in expression normalized with GAPDH. The data were represented as mean \pm SD and performed in triplicate.

II.4. Conclusion

Benzimidazolyl-hydroxy-coumarinyl (**HL**) diad constitutes two fluorogenic and biologically important groups and demonstrates high fluorogenic selectivity to Al³⁺ (LOD, 0.62 μM in acetonitrile-water (2:1, v/v) at pH, 7.2 (HEPES buffer)) over other cations (NH₄⁺, Na⁺, K⁺, Ca²⁺, Hg²⁺, Ni²⁺, Co²⁺, Pb²⁺, Pd²⁺, Mn²⁺, Cd²⁺, Cu²⁺, Fe³⁺, and Zn²⁺). **HL** shows promising anti-migratory activity against cancer cells without inducing toxicity in normal cells. It has reduced the activity of Matrix Metalloproteinase (MMPs) enzymes and is capable to modulate the epithelial to mesenchymal transitions by upregulating the gene expression of the epithelial markers and downregulating the gene expression of mesenchymal markers. It was also able to induce the protein expression of important epithelia marker, E-Cadherin and reduce the protein expression of Vimentin.

II.5. References:

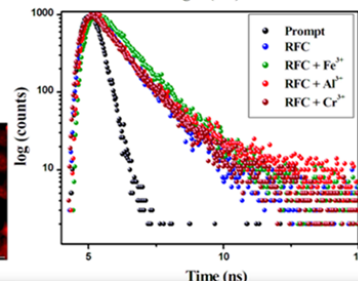
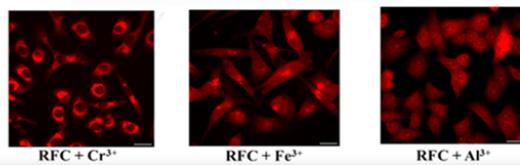
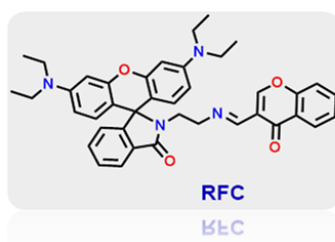
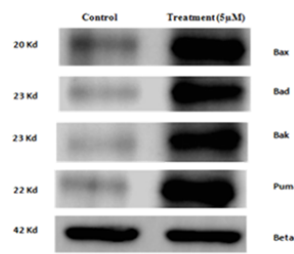
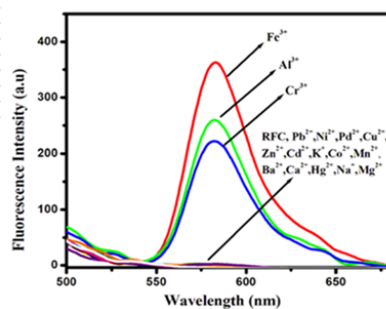
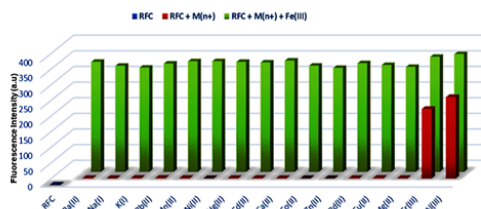
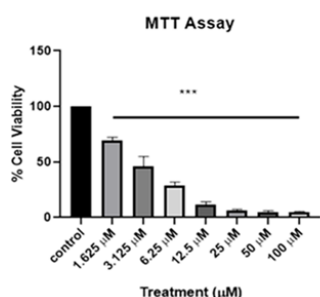
- [1]. A.W. Czarnik, American Chemical Society, Washington DC , 538 (1993) 1- 9.
- [2]. M. Shyamal, P. Mazumdar, S. Maity, S. Samanta, G. P. Sahoo, A. Misra, ACS Sens., 1 (2016) 739 -747.
- [3]. C. H. Chen, D. J. Liao, C. F. Wan, A. T. Wu, Analyst., 138 (2013) 2527-2530.
- [4]. B. Dutta, S. Dey, K. Pal, S. Bera, S. Naaz, K. Jana, C. Sinha, M. H. Mir, New J. Chem., 44 (2020) 13163-13171.
- [5]. K. Aich, S. Goswami, S. Das, C. Das Mukhopadhyay, RSC Adv., 5 (2015) 31189-31194.
- [6]. B Dutta, A Hazra, A Dey, C Sinha, PP Ray, P Banerjee, MH Mir, Cryst. Growth Des., 20 (2020) 765-776.
- [7]. M. A. Malik, O. A. Dar, P. Gull, M. Y. Wani, A. A. Hashmi, Med. Chem. Commun. 9 (2018) 409-436.
- [8]. P. Nayak, Environ. Res., 89 (2002) 101-115.
- [9]. J. R. Walton, Curr. Inorg. Chem., 2 (2012) 19-39.
- [10]. J. R. Walton, Neuro Toxicology, 27 (2006) 385-394.

- [11]. A. Dhara, A. Jana, N. Guchhait, P. Ghosh, S. K. Kar, *New J. Chem.*, 38 (2014) 1627-1634.
- [12]. R. Purkait, A. Dey, S. Dey, P. P. Ray, C. Sinha, *New J. Chem.*, 43 (2019) 14979-14990.
- [13]. L. Jin, W. Wang, Z. Shen, J. Xu, Q. Wang, C. Zhao, *J. Mol. Str.*, 1197 (2019) 73-79.
- [14]. Y. Choi, G. Park, Y. Na, H. Jo, S. Lee, G. You, C. Kim, *Sens. Actuators B Chem.* 194 (2014) 343-352.
- [15]. D. Karak, S. Lohar, A. Sahana, S. Guha, A. Banerjee, D. Das, *Anal. Methods.*, 4 (2012) 1906-1908.
- [16]. B. Sen, M. Mukherjee, S. Banerjee, S. Pal, P. Chattopadhyay, *Dalton Trans.* 44 (2015) 8708-8717.
- [17]. T. Ma, M. Dong, Y. Dong, Y. Wang, Y. Peng, *Chem. Eur. J.*, 16 (2010) 10313-10318.
- [18]. S. Dey, R. Purkait, K. Pal, K. Jana, C. Sinha, *ACS Omega.*, 4 (2019) 8451-8464.
- [19]. M. Shyamal, P. Mazumdar, S. Maity, G. P. Sahoo, G. Salgado-Morán, A. Misra, *J. Phys. Chem. A.*, 120 (2016) 210-220.
- [20]. X.-li. Yue, Z.-qing. Wang, C.-rui. Li, Z. -yin. Yang, *Tetrahedron Lett.*, 58 (2017) 4532-4537.
- [21]. J. Tian, X. X. Yan, H. Yang, F. Tian, *RSC Adv.*, 5 (2015) 107012-107019.
- [22]. Y. Chen, H.-R. Liu, H. -S. Liu, M. Cheng, P. Xia, K. Qian, P. -C. Wu, C. -Y. Lai, Y. Xia, Z. -Y. Yang, S. L. Morris-Natschke, K. -H. Lee, *Eur. J. Med. Chem.*, 49 (2012) 74-85.
- [23]. C. -Y. Hsieh, P. -W. Ko, Y. -J. Chang, M. Kapoor, Y. -C. Liang , H. -L. Chu , H. -H. Lin, J. -C. Horng, M. -H. Hsu, *Molecules*, 24 (2019) 3259-3277.
- [24]. D. M. Manidhar, K. U. M. Rao, N. B. Reddy, C. S. Sundar, C.S. Reddy, *J. Korean Chem. Soc.*, 56 (2012) 459-463.
- [25]. J.N. Demas, G.A. Crosby, *J. Phys. Chem.*, 75 (1971) 991-1024.
- [26]. C.S. Choi, M.K. Kim, K.S. Jeon, K.H. Lee, *J. Lumin.*, 109 (2004) 121-128.
- [27]. G. M. Sheldrick, *Acta Crystallogr., Sect. A: Found. Adv.*, 71 (2015) 3-8.
- [28]. SMART and SAINT; Bruker AXS Inc.: Madison, WI, 1998.

- [29]. G. M. Sheldrick, SHELXL 97: Program for the Solution of Crystal Structure; University of Göttingen: Göttingen, Germany, 1997.
- [30]. L. J. Farrugia, ORTEP-3 for windows. *J. Appl. Crystallogr.* 30 (1997) 565.
- [31]. A. L. Spek, PLATON: Molecular Geometry Program; University of Utrecht: Utrecht, The Netherlands, 1999.
- [32]. A. Sarkar, S. Bhattacharjee, D.P. Mandal, *Asian Pac J Cancer Prev.*, 16 (2015) 6753-6759.
- [33]. K. Patra, S. Jana, A. Sarkar, S. Karmakar, J. Jana, M. Gupta, G. Mukherjee, U.C. De, D.P. Mandal, S. Bhattacharjee, *Nutr and Cancer.*, 68 (2016) 689-707.
- [34]. T. Sorsa, L. Tjäderhane, T. Salo, *Oral Dis.*, 10 (2004) 311-318.
- [35]. A. Sarkar, A. Rahaman, I. Biswas, G. Mukherjee, S. Chatterjee, S. Bhattacharjee, D.P. Mandal, *J. Cell. Physiol.* 235 (2020) 7159-7172.
- [36]. Y.-G. Zhang, Z.-H. Shi, L.-Z. Yang, X.-L. Tang, Y.-Q. An, Z.-H. Ju, W.-S. Liu, *Inorg. Chem. Commun.*, 39 (2014) 86-89.
- [37]. K. Velmurugan, S. Mathankumar, S. Santoshkumar, S. Amudha, R. Nandhakumar, *Spectrochim. Acta A*, 139 (2015) 119-123.
- [38]. B. Sen, S. K. Sheet, R. Thounaojam, R. Jamatia, A. K. Pal, K. Aguan, S. Khatua, *Spectrochim. Acta A*, 173 (2017) 537-543.
- [39]. D. Sarkar, P. Ghosh, S. Gharami, T. K. Mondal, N. Murmu, *Sens. Actuators B Chem.* 242 (2017) 338-346.
- [40]. G. Zhu, Y. Huang, C. Wang, L. Lu, T. Sun, M. Wang, Y. Tang, D. Shan, S. Wen, J. Zhu, *Spectrochim. Acta A*, 210 (2019) 105-110.
- [41]. S. K. Sheet, B. Sen, R. Thounaojam, K. Aguan, S. Khatua, *J. Photochem. Photobiol. A*, 332 (2017) 101-111.
- [42]. J. -C. Qin, T. -R. Li, B. -D. Wang, Z. -Y. Yang, L. Fan, *Spectrochim. Acta A*, 133 (2014) 38-43.
- [43]. J. -C. Qin and Z. -Y. Yang, *Anal. Methods*, 7 (2015) 2036-2040.
- [44]. D. Sarkar, A. Pramanik, S. Biswas, P. Karmakar, T. K. Mondal, *RSC Adv.*, 4 (2014) 30666-30672.

Chapter III

Application of a Rhodamine-Chromone Schiff Base Probe for the Sensing of Fe^{3+} , Al^{3+} , Cr^{3+} at Low Concentration and Exploration of the Anticancer Activity and Bio-imaging



Western Blot Analysis

MCF-7 cell imaging

CHAPTER III

Abstract

Strategic design of fluorescent probe for the recognition of ions/molecules at very low concentration by fluorescence sensing is one of the stimulating current research topics with reference to health and sustainability. Towards this objective, Rhodamine based chemosensors are playing extraordinary protagonist. In this work, a Rhodamine appended chromone Schiff base (**RFC**), with two fluorogenic motifs, has been characterized through various spectroscopic techniques. The probe exhibits efficient sensitivity towards Analytical Group IIIA ions (Al^{3+} , Cr^{3+} and Fe^{3+}) in existence of other competitive analytes. The fluorescent intensity is enhanced by 350 fold (Fe^{3+}), 250 fold (Al^{3+}) and 220 fold (Cr^{3+}), respectively in methanol-water (99:1, v/v; HEPES buffer, pH, 7.2) medium. The limits of detection (LOD) ($3\sigma/M$ method; σ = standard deviation; M = slope) are 0.0051 ppm (Fe^{3+}), 0.0029 ppm (Al^{3+}) and 0.0052 ppm (Cr^{3+}); which are impressive and much below the WHO recommended data. In addition to this, the compound has been utilized for cell imaging in presence of these three cations. The action of probe on MCF-7 (human breast cancer) cell lines demonstrates IC_{50} , 2.53 μM that is far better than activity against WI-38 (normal cell line) (IC_{50} , 393.7 μM). The drug (**RFC**) minimizes the cellular proliferation and has significant wound healing capacity of the infected tissue with MCF-7 cells. The probe shows significant nuclear fragmentation with increase in the expression of apoptotic markers. Growth inhibition analysis in 3D tumor spheroid model showed the inhibition of breast cancer MCF-7 cells.

III.1. Introduction

The detection of cation in ecological as well as biological prominence is one of the issues of sustainable development [1-3]. The sensing application of organic molecules has exalted scientific, technological, and medicinal issues [4-6]. However, the design of a multifunctional fluorogenic probe is also a major concern. The ‘*turn-on*’ fluorescence property is practically more reliable than ‘*turn-off*’ to the probe-analyte interaction because of higher preciseness, sensitivity, and accuracy for direct laboratory-to-land application [7-10]. The interaction of metal ions has been directly controlled by the binding sites of chemosensor and hence the prominence of the fluorescence intensity [11-13].

Recently, the novel colorimetric and luminescent detection processes have been recognized in the sustainable development issues because of their efficacy in the critical phase of biology and environment in reference to the quantitative identification of non-biodegradable hazardous ions and persistent organic pollutants [14-17]. Principally, the following procedures may be intricate for the signaling manifestation of molecular chemosensors: photoinduced charge transfer (PCT), chelation-enhanced fluorescence (CHEF) following, in particular, the HSAB (Hard and Soft Acid Base) principle [18-20], PET and RET. The quantities of the analyte in the sample are the decisive cause for the regularization of ecological progression or the initiation of noxiousness. Hence, the trace level recognition of analyte concentration is a most trustworthy analytical task [21-23].

In this regard, the detection of very low concentration of trivalent metal ions (Analytical Group-III A) is vastly stimulating. These metal ions show mammoth role in living system and environs [24-26]. Besides, paramagnetic quenching effect of Cr^{3+} (d^3) and Fe^{3+} (d^5), in general, does not promote fluorescence enhancement; although Cr^{3+} has specific energy ordering of interelectronic interaction states in Oh symmetry and allows hetero-spin transition (${}^4T_2 \rightarrow {}^2T_2$)

followed by light-induced photochemical/photophysical impact. In most of the living cells the metalloenzymes containing Fe(II/III) redox state engage in O_2 -transportation and redox reactions. Any change in demand of biological concentration of living cells, either insufficiencies or overload, of these ions may originate potential irregularities and causes of ailments such as - Huntington's, Alzheimer's, Parkinson's, skin problems, anemia, etc [27-29]. World Health Organization recommends the daily acceptable limit of Al^{3+} in living system is 3–10 mg and the concentration level of Al^{3+} in drinking water must be below 7.41 μM . Excessive accumulation of these ions may cause different irregularities in neurodegenerative syndromes, for example, Alzheimer's, Parkinson's, weakening of bone, osteoporosis; sometimes gastrointestinal problems and waning of liver, stomach and kidney functions etc [30-32]. Cr^{3+} is one of the vital ions appears trace level in the living system and the 13th most rich metal ion in earth's crust. Biological action of human body has been regulated by insulin which is controlled by Cr^{3+} and also triggers secretion of some enzymes and stabilizing the activity of different biomolecules. The accessibility of Cr^{3+} ion in ecosystem is owing to erosion of Cr-containing rocks as well as restructuring by volcanic eruptions [33-35]. Some excellent chemosensors are designed in search of discussed metal ions (Fe^{3+} , Al^{3+} and Cr^{3+}) detection [36-40]. Recently, unnecessary industrial overflow and disorganized side products of these trivalent metal ions from chemical laboratory has also led to antithetical level of pollution. Again, insufficiency of any biological element is also harmful to general health of a living being. Therefore, a dynamic concentration of biologically important ions/molecules has to be maintained and is to be detected by selective, sensitive, cheap and easy processes. In the current study, we have designed a fluorescent molecule consisting of two fluorogenic units - rhodamine and chromone conjugated by C=N to get the probe (**RFC**) which has been spectroscopically characterized. Interestingly, the fluorescent probe, **RFC**, shows a 'turn-on' emission in presence of Fe^{3+} , Al^{3+} and Cr^{3+} (Group-IIIA analytical group) ions in methanol-water (99:1,

v/v; HEPES buffer, pH, 7.2) solution. It has also been utilized in the cell imaging study in presence of Fe³⁺, Al³⁺ and Cr³⁺ and also for anticancer activity assessment against breast cancer MCF-7 cells.

III.2. Experimental section

III.2.1. Materials

Rhodamine B, Ethylenediamine and other reagents were purchased from Merck and used in the experiment without further purification. All other chemicals (the metal salts such as: FeCl₃·6H₂O, Al(NO₃)₃·9H₂O, CrCl₃·6H₂O, NiCl₂·6H₂O, Cd(OAc)₂·2H₂O, CaCl₂·6H₂O, Zn(NO₃)₂·6H₂O, Hg(OAc)₂, Cu(OAc)₂·H₂O, NaCl, Co(NO₃)₂·6H₂O, PdCl₂, Pb(NO₃)₂, MnCl₂·4H₂O, BaCl₂·2H₂O, MgCl₂·6H₂O, KBr, LaCl₃, RuCl₃·xH₂O, KAuCl₄·2H₂O, SmCl₃·6H₂O, GdCl₃·6H₂O, EuCl₃·6H₂O, In(NO₃)₃·xH₂O, DyCl₃·6H₂O and TbCl₃·6H₂O were used for experiment) including solvents were of AR grade and used without further purification. Methanol, Di-methyl sulfoxide (DMSO -Cell culture Grade) and agarose were purchased from Sigma Aldrich. 3-(4,5-dimethylthiazol-2-yl)-2, 5-diphenyltetrazolium bromide (MTT), Crystal violet solution (Gram's Crystal violet) were purchased from Merck. Minimum Essential Media (Earle's) FBS and 1 % Pen-Strep were obtained from Gibco. Trypsin-EDTA was purchased from Invitrogen. All compounds were used subsequently used without any further rounds of purification.

III.2.2. General methods

In the understanding of functional moieties present in the structure different spectroscopic techniques have been employed: infrared (IR) spectrum (4000–500 cm⁻¹) was taken on a Bruker ALPHA II spectrometer in an attenuated total reflectance (ATR) mode; UV-Vis spectra have been recorded through a Perkin-Elmer Lambda 25 spectrophotometer instrument.

Emission data were collected on a Perkin-Elmer LS-55 fluorometer at room temperature (298K). Bruker 300 MHz FT-NMR spectrometer with TMS has been utilized as internal standard in DMSO- d_6 solvent was employed to collect the 1H NMR spectra. Water HRMS model XEVO-G2QTOF#YCA351 spectrometer was used to collect mass spectra.

III.2.3. Quantum yield calculation

The fluorescence quantum yields of the probe **RFC** and (**RFC** + Fe^{3+}), (**RFC** + Al^{3+}), (**RFC** + Cr^{3+}) were measured using standard quinine sulfate solution as a reference with a known quantum yield, $\phi_R = 0.54$ in 0.5 M H_2SO_4 . The reference and experimental sample were excited at the same wavelength, maintaining almost the same absorbance. Using the software available in the instrument area the fluorescence spectra were measured and the quantum yield was calculated by following the formula

$$\phi_S/\phi_R = [A_S/A_R] \times [(Abs)_R/(Abs)_S] \times [\eta_S^2/\eta_R^2]$$

Where ϕ_S and ϕ_R are the fluorescence quantum yield of the samples and reference respectively; A_S and A_R are the areas under emission spectra of the sample and references respectively. $(Abs)_R$, $(Abs)_S$ are the absorbance of reference and sample at the required excitation wavelength. The refractive index of the solvent (η_S^2) and reference (η_R^2) were collected from the literature report [41,42].

III.2.4. General experiment for the UV–vis and fluorescence spectra

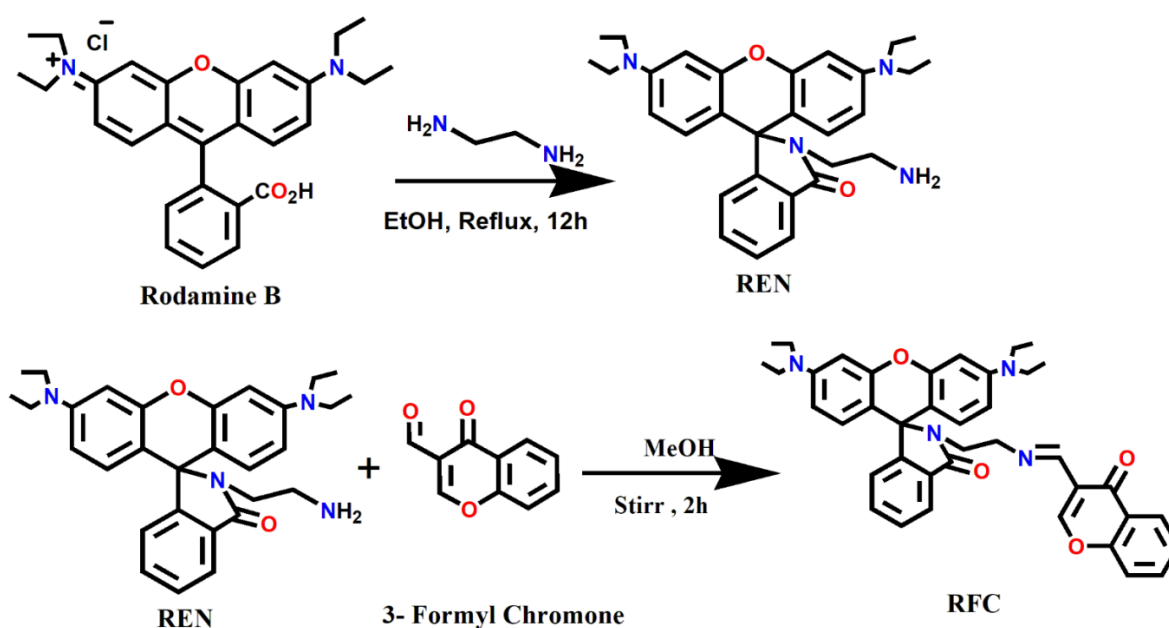
A solution of **RFC** (1×10^{-3} M) was prepared in methanol and the solution of **RFC** was diluted to 25 μ M with methanol-water (99:1, v/v) of pH, 7.2 (HEPES buffer) and this solution was used in the entire fluorescence and UV-visible experiment. The stock solution (1×10^{-3} M) of different metal ions were prepared in deionized water. The different metal ions sensing by the

probe **RFC** were studied using UV–vis and fluorescence spectrophotometer in mixed aqueous buffer (methanol-water (99:1, v/v) of pH, 7.2 (HEPES buffer) solution at room temperature. An excitation wavelength at $\lambda=350$ nm and slit: 10-10 was used for all fluorescence experiments. All the experiments have been done after small time gap of the addition of metal ions.

III.2.5. Synthesis of REN

Rhodamine B derivative, REN, has been synthesized as per the published procedure [43]. Rhodamine B (3.0 g, 6.3 mmol) was dissolved in ethanol (50 ml) after that ethylenediamine was added drop-by-drop to it for 30 min. The solution was then refluxed for 12 h (**Scheme III.a**) and evaporated to dryness. The product so formed was dissolved in DCM (100 ml) and washed well repeatedly with water (3×50 ml) and the product was dried over anhydrous Na_2SO_4 (2.76 g, 92% yield).

ESI-MS (m/z) $[M+H]^+$ calcd for $C_{30}H_{36}N_4O_2$, 485.29, found: 485.33 (**Fig.III.1**).



Scheme III.a. Synthetic route of **REN** and **RFC**.

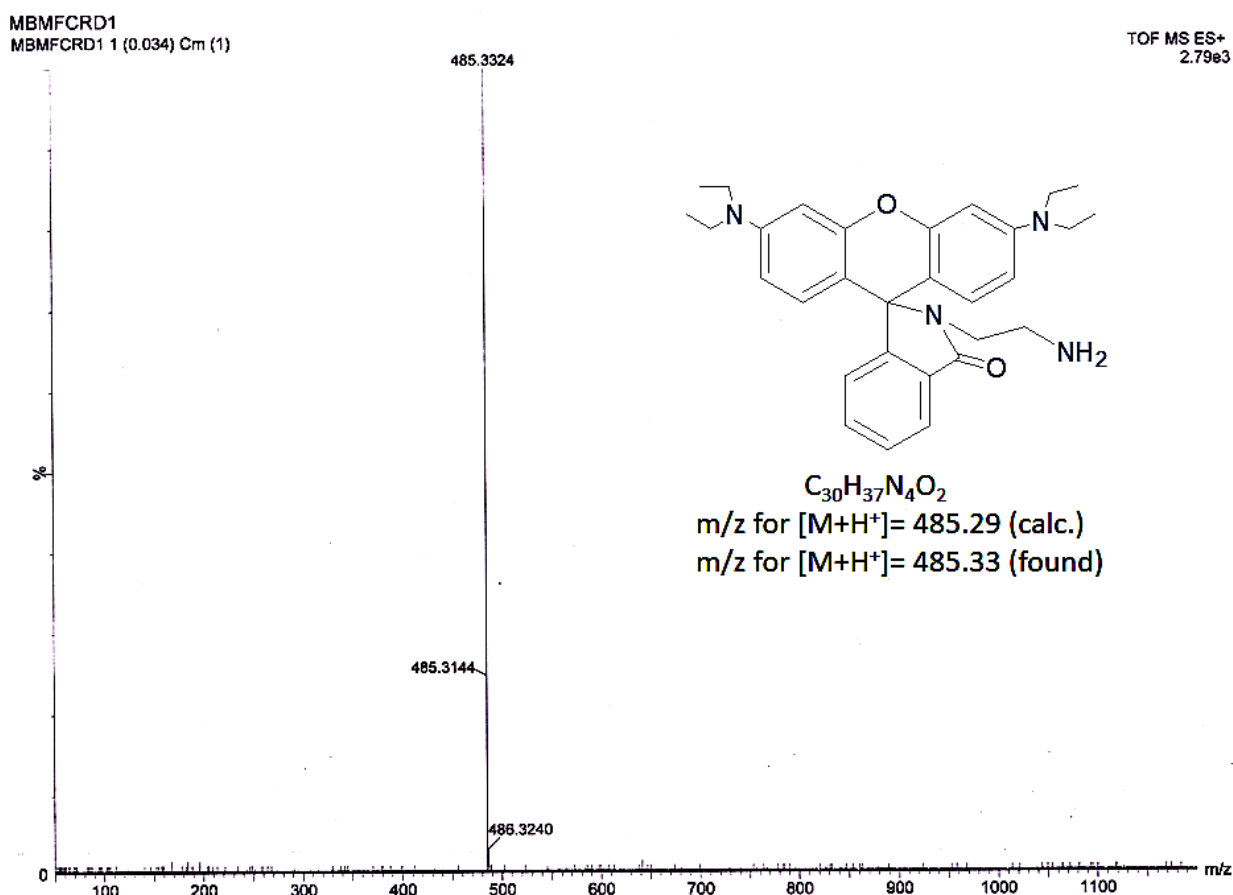


Fig.III.1. ESI- MS spectrum of **REN**

III.2.6. Synthesis of RFC

The rhodamine B derivative **REN** (396 mg, 0.82 mmol) was dissolved in CH_3OH (50 ml) and 3-formyl chromone (143 mg, 0.82 mmol) acidified with few drops of acetic acid was added to that solution. The resulting solution was stirred for 2 h (**Scheme III.a**) and evaporated to dryness. The product so formed was dissolved in dichloromethane (40 ml) and washed well with water (2×25 ml) and the product was dried over anhydrous Na_2SO_4 (579 mg, 88 % yield) and the product was recrystallized in DCM/hexane solution.

ESI-MS (m/z) $[M+H]^+$ calcd. for $C_{40}H_{41}N_4O_4$, 641.31, found: 641.35 (**Fig.III.2**).

FT-IR: ν 2929, 1688, 1611 cm^{-1} (**Fig.III.3**).

1H NMR (300 MHz, DMSO- d_6): δ 7.81 (dd, $J_1 = 6.2$ Hz, $J_2 = 1.5$ Hz, 1H), 7.73 (dd, $J_1 = 7.7$ Hz, $J_2 = 1.5$ Hz, 1H), 7.52 (d, $J = 8.4$ Hz, 1H), 7.51 (s, 1H), 7.47-7.41 (m, 1H), 7.06 (t, $J = 7.5$ Hz, 1H), 7.03 (d, $J = 2.7$ Hz, 1H), 7.02 (s, 1H), 7.01-6.92 (m, 2H), 6.40-6.34 (m, 6H), 3.34 (s, 8H), 3.28 (s, 2H), (there is a broad peak which is somewhat merged with the DMSO peak) 3.19 (s, 2H), 1.07 (t, $J = 6.0$ Hz, 12H). (**Fig.III.4** & **Fig.III.5**)

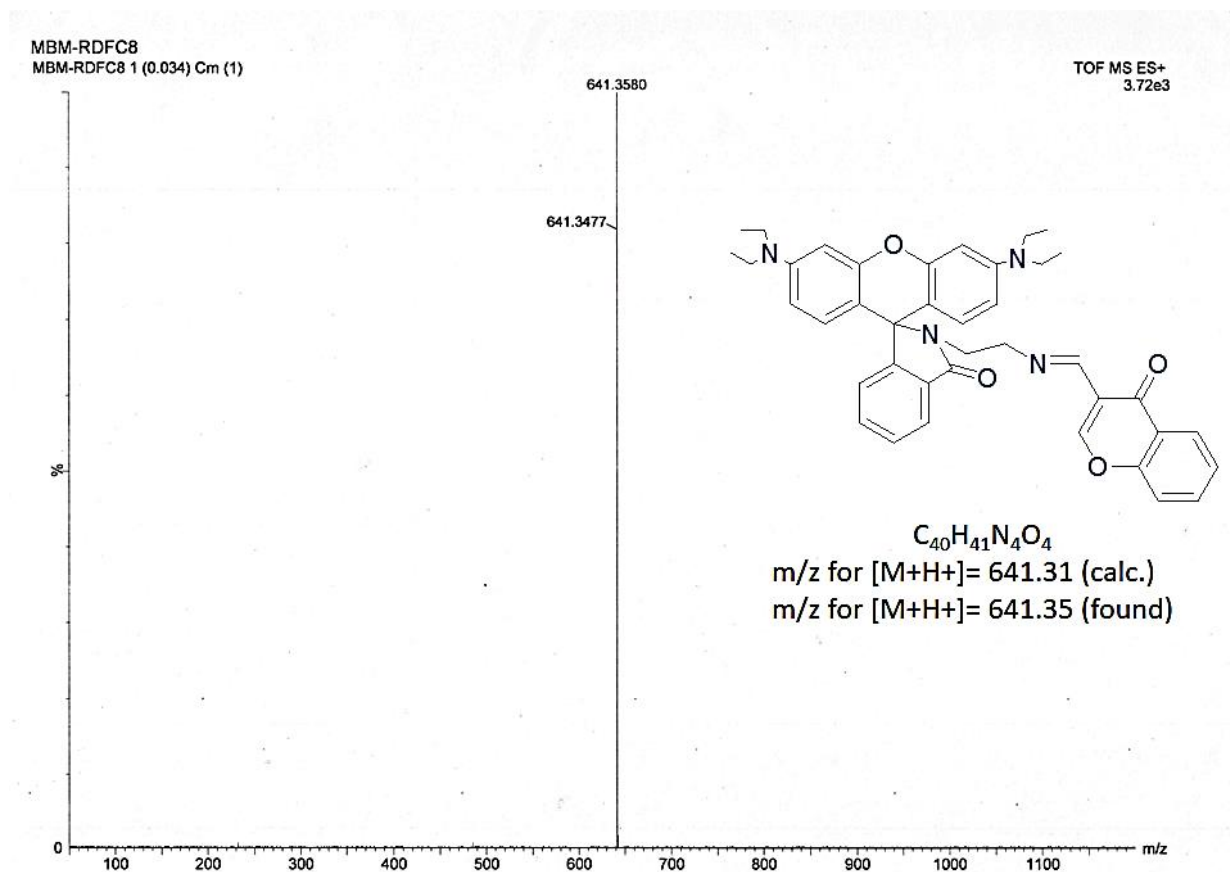


Fig.III.2. ESI- MS spectrum of RFC

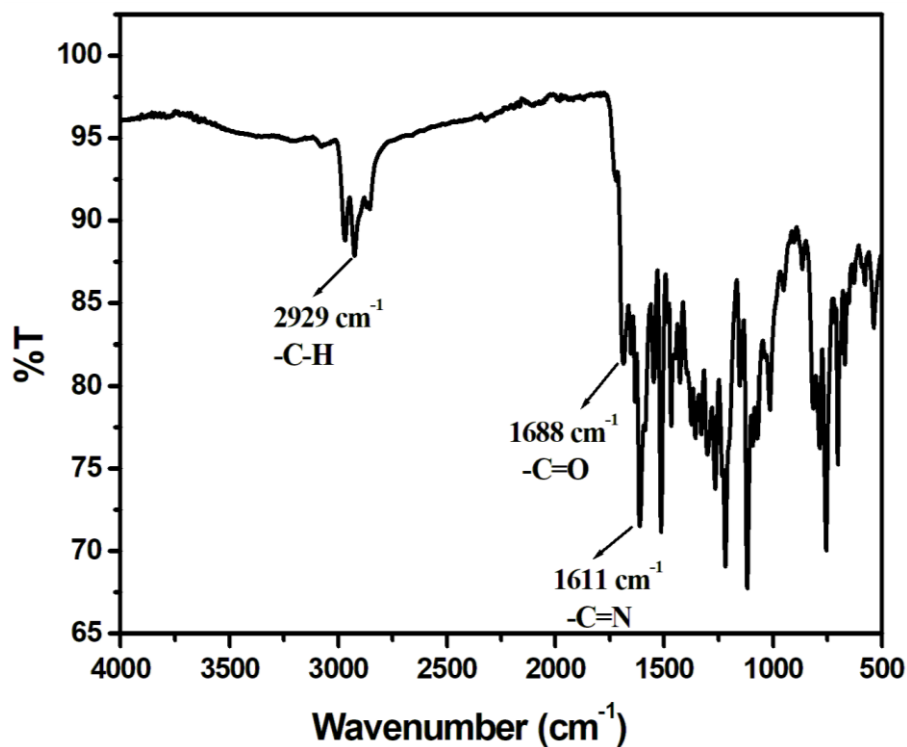
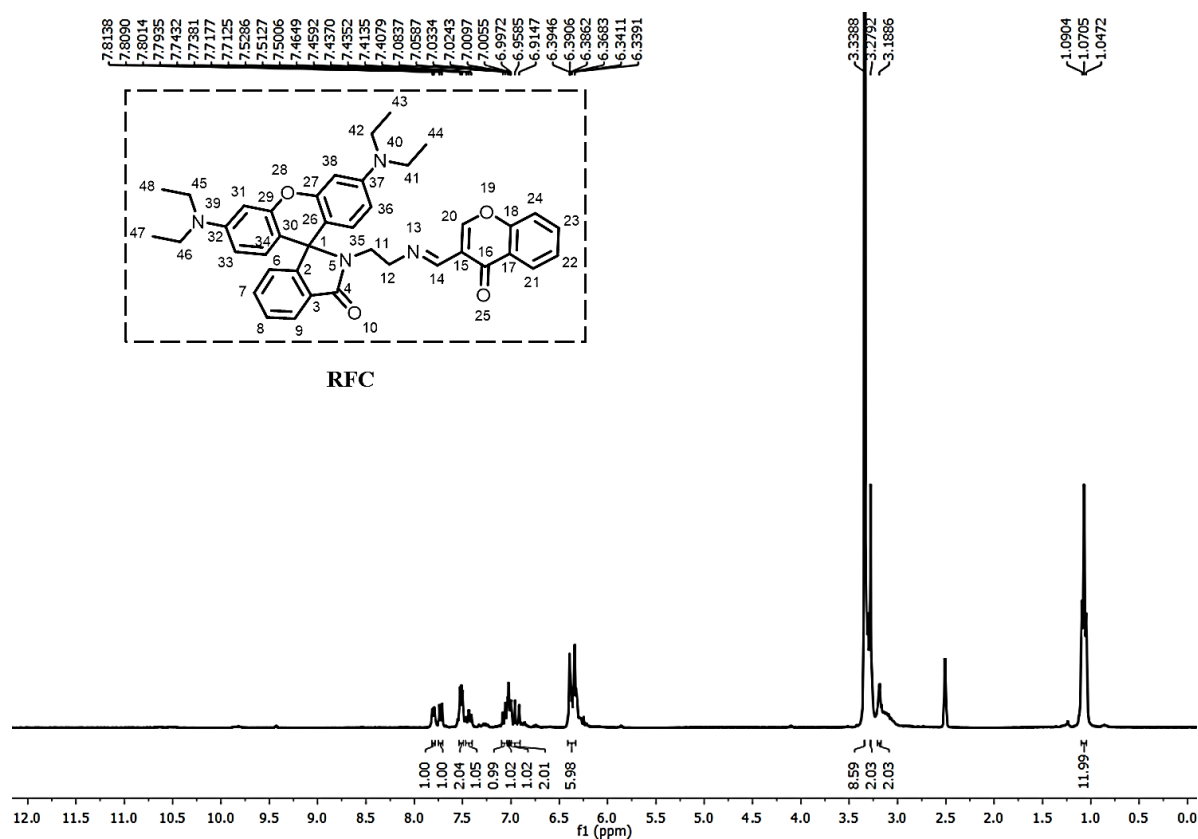


Fig.III.3. IR spectrum of RFC

Fig.III.4. 1H NMR spectrum of RFC

III.2.7. Biological Study

III.2.7.1. Cell culture

MCF-7 (Breast Adenocarcinoma) and WI-38 (Normal Lung Fibroblast) cells were procured from NCCS, Pune. MCF-7 cells were grown in MEM (Earle's) medium supplemented with 10% Fetal Bovine Serum (FBS, Gibco) and 1% Pen-Strep solution while WI-38 cells were cultured in Eagle's Minimum Essential Medium with 10% Fetal Bovine Serum (FBS, Gibco) and 1% Pen-Strep solution with a supply of 5% CO₂ at 37°C in a humidified environment of the CO₂ incubator. All successive investigations were carried out only after three passages.

III.2.7.2. Fluorescence imaging

The emission of the probe, **RFC** was examined in the presence of FeCl₃·6H₂O, Al(NO₃)₃·9H₂O, CrCl₃·6H₂O on MCF-7 cell line. For the assay, MCF-7 cells were seeded at a particular cell density on coverslips inside sterile 6 well plates. After 24 h, the cells were treated with the respective salts followed by incubation for 4 h. **RFC** was then added to the various groups except for control. There was also a experimental setup where only the **RFC** was added in the absence of salt. The addition of **RFC** was followed by incubation for 2 h and then the cells were fixed in methanol and observed by using a fluorescence microscope (Olympus) using the TRITC (Red) channel mirror.

III.2.7.3. Cytotoxicity analysis

The cytotoxic potential of **RFC** probe was studied by assessing the lessening capacity of 3-(4, 5-dimethylthiazol-2-yl)-2, 5-diphenyltetrazolium bromide (MTT). For this MCF-7 cells and WI-38 cells were seeded in a 96-well plate at a density of 1×10^4 followed by treatment after 24 h on varying concentration of **RFC** (1.6-100 μ M). MTT (5 mg/ml; 10 μ L) solution was added in each well and allowed for 4 h incubation (37°C). Formazan was reduced and then dissolved in DMSO/MeOH (1:1) and estimated by spectrophotometric data at 570 nm in a microtitre

plate reader (Spectramax i3x). Quantitative informations were gathered following equation: % Cell viability = [(A 570 (treated cells-background)/ (A 570 (untreated cells - background))] × 100. All statistical studies were carried out using GraphPad Prism 8.0.

III.2.7.4. Colony formation assay

The cytotoxic effects of the **RFC** probe were confirmed further through Colony Formation Assay on the MCF-7 cell line. MCF-7 cells were seeded in a sterile 6 well plate at a low density (500 cells in 2 ml/well) followed by treatment with two different doses of **RFC** i.e 2.5 μM and 5 μM for 24 h. Colony numbers were counted after fixing and staining the cells with crystal violet solution (Gram's crystal violet, Merck). All statistical studies were carried out using GraphPad Prism 8.0.

III.2.7.5. Wound Healing Assay

To assess the effect of **RFC** on the migration potential of MCF- 7 cells the wound healing assay was performed for which MCF-7 cells were seeded in a sterile 6 well-plate at a high density of 10⁸ cell/well in a serum free media in order to minimize the cellular proliferation. Cells were maintained till it was about 90% confluent. A sterile 200 μl tip was used to make a scratch in the cell monolayer in each well ultimately forming a wound and subsequently washed with PBS. The cells were thereafter treated with solution of **RFC** diluted in MEM. Images were captured after every 24 h in a phase contrast microscope. The scratch area was estimated by using the Wound Healing Tool in ImageJ software with respect to the relative area of wound closure with respect to the control group. All statistical analyses were performed using Graph Pad Prism8.0.

III.2.7.6. Nuclear Fragmentation Assay

The Nuclear fragmentation assay was performed to analyze the morphological changes in the nucleus of the cancer cells due to induction of apoptosis by cytotoxicity of the drug, **RFC**.

MCF-7 cells were seeded into sterile 6-well plates with coverslips placed in each well at a density of 2×10^4 cells/well, followed by treatment with **RFC** after 24 h at a concentration of 2.5 μM and 5 μM for the next 24 h. On next day the cells were washed with PBS and fixed with a 4% Paraformaldehyde solution. Incubation was carried out for 30 min upon adding Hoechst 33258 (10 μM) in the dark and observation of the morphological changes in the nuclei was made using Fluorescent Microscope (Olympus) with CellSens software.

III.2.7.7. Western Blot analysis of Apoptotic markers

The MCF-7 cells were treated with **RFC** (5 μM) drug for 24 h. Extraction of protein was performed using RIPA buffer with added PMSF as the protease inhibitor. Proteins were separated (60 μg of total) using SDS-PAGE followed by transfer to a PVDF membrane. Blocking of membranes was done using 5% skimmed milk-TBST solution followed by incubation with primary antibodies: monoclonal rabbit BAX, BAD, BAK, PUMA (Cell Signaling CST, Danvers, MA, USA), and β -actin (Santa Cruz Biotechnology, CA, USA); for secondary antibodies polyclonal anti-rabbit (Cell Signaling, Danvers, MA, USA); monoclonal mouse anti- β -actin (Santa Cruz Biotechnology, CA, USA) was used as the loading control. The membranes was washed (3 times) by TBST followed by the addition anti-rabbit secondary antibody conjugated to horseradish peroxidase or anti-mouse HRP secondary antibody (Santa Cruz Biotechnology, CA, USA) for 1 h at room temperature. Membranes were washed (3 times) and used for the detection of the antigen-antibody complexes (ECL detection reagent (Bio-Rad) on ChemiDoc XRS+ (Bio-Rad).

III.2.7.8. Growth inhibition analysis on Tumor spheroid (3D) model

Analysis of growth inhibition was performed on a Multicellular 3D tumor spheroid model using MCF-7 cells in a liquid overlay method. Cells were seeded at 3000-5000 cells/ml in 35 mm plates pre-coated with 1% Agarose (wt./volume) and incubated with 5% humidified CO₂ incubator and regularly checked for spheroid formation followed by the treatment with the two

selected doses of **RFC** was given and the change in the morphology and size of the spheroids were noted up to 8 days. Images were taken in bright field in an inverted microscope (Olympus). All statistical studies were carried out using GraphPad Prism 8.0.

III.3. Results and discussion

III.3.1. The structure of RFC

The reaction between rhodamine-ethyl amine (**REN**) and 3-formyl chromone has isolated a novel rhodamine-based Schiff base, **RFC** (Scheme III.a). The ESI-MS spectrum of **RFC** shows

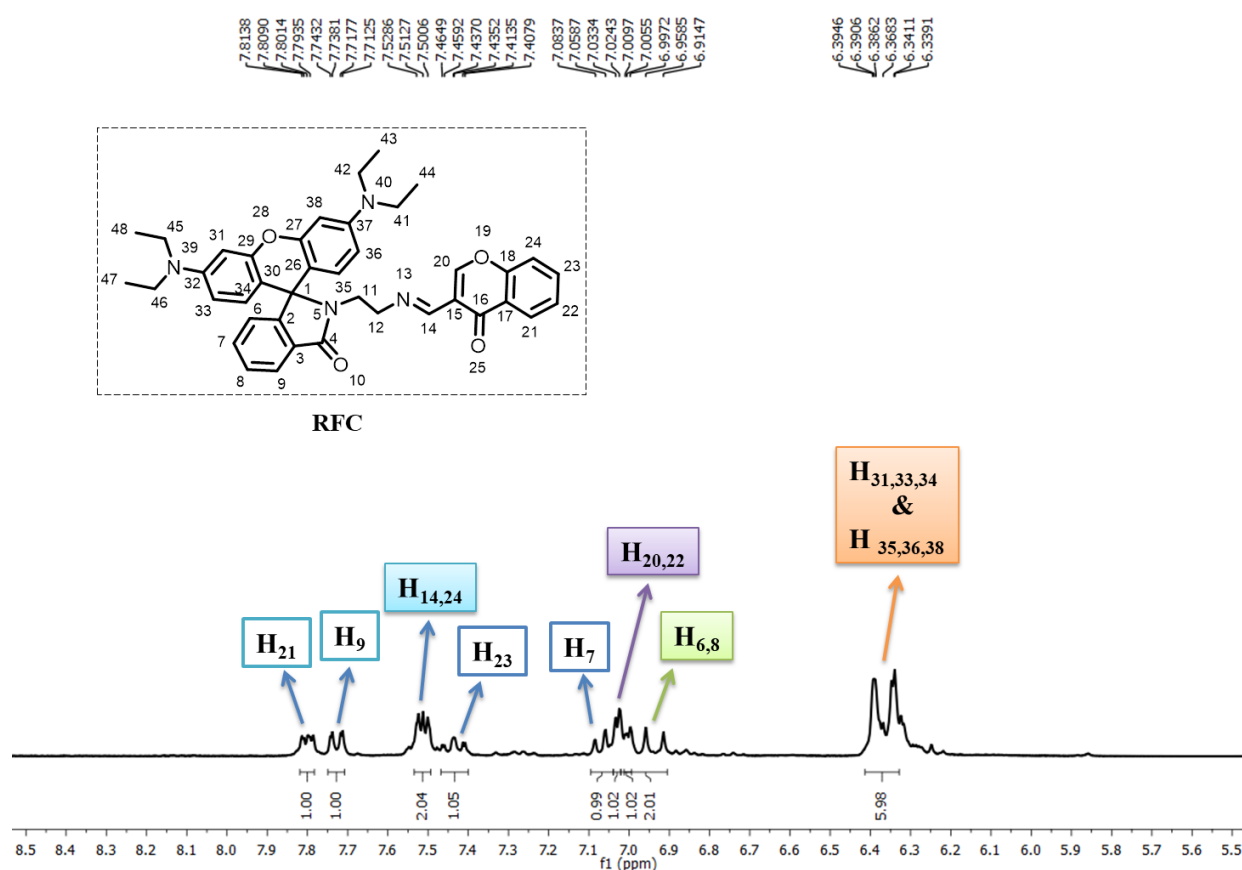


Fig.III.5. 1H NMR spectrum of **RFC** with characteristic region expansion.

a molecular ion peak at 641.35, which is matched with the calculated value (m/z , $[M+H]^+$) 641.31. The IR spectrum of **RFC** shows the existence of $-C-H$ (2929 cm^{-1}), $-C=O$ (1688 cm^{-1}), $-C=N$ (1611 cm^{-1}) functional groups. The NMR spectrum (**Fig.III.4** and **Fig.III.5**) shows

two most downfield doublet signals are assigned to H_{21} (7.81 ppm) and H_9 (7.73 ppm) protons adjacent to C=O functions in chromone and Rhodamine, respectively. Unambiguous assignment to all the Hs is difficult due to the overlapping of signals. The imine H ($-N=CH_{14}$) appears at 7.51 ppm which is combined with H_{34} (7.52 ppm) of the Rhodamine motif. The $N-CH_2-CH_3$ signals in NMR spectrum appear as overlapped signal at 3.3 ppm while $=N-CH_2-CH_2-$ protons show resonance at 3.18-3.27 ppm. Other aromatic protons resonate at common aromatic region of the spectrum (**Fig.III.4**).

III.3.2. Absorption and Emission spectral behaviour

The probe, **RFC** shows an intense absorption band at 350 nm (**Fig.III.6**) in methanol-water (99:1, v/v; HEPES buffer, pH, 7.2) which may correspond to $\pi-\pi^*$ transition; and on the

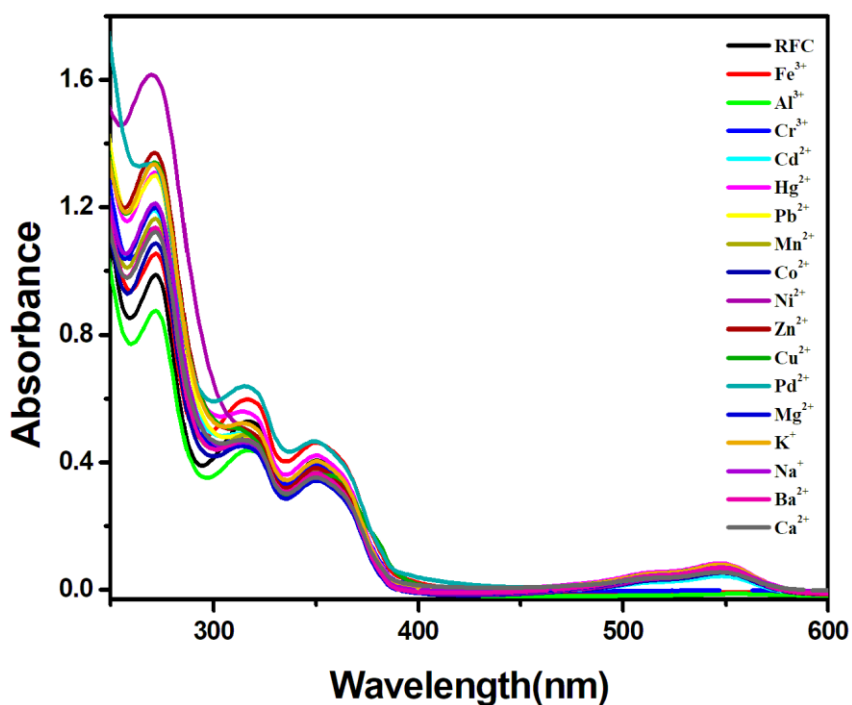


Fig.III.6. UV-vis absorption spectra of **RFC** with different metal ions in methanol-water (99:1, v/v) of pH, 7.2 (HEPES buffer).

addition of various cations (Pb^{2+} , Pd^{2+} , Mn^{2+} , Cd^{2+} , Cu^{2+} , Ba^{2+} , Mg^{2+} , Zn^{2+} , Na^+ , Hg^{2+} , K^+ , Ca^{2+} , Co^{2+} , Ni^{2+} , Ru^{3+} , Au^{3+} , In^{3+} , La^{3+} , Sm^{3+} , Gd^{3+} , Eu^{3+} , Dy^{3+} , Tb^{3+} , In^{3+}) in methanol-water

(99:1, v/v; HEPES buffer, pH, 7.2) (**Fig.III.6**) to **RFC** solution do not show any significant change either in intensity or shifting of absorption band. Most significant observation in the spectral feature is because of the addition of Al^{3+} , Cr^{3+} and Fe^{3+} solutions to **RFC**. The probe, **RFC** shows very intense absorption at 350 nm and a weak absorption with a double hump feature at 547 nm and 513 nm; upon gradual addition of Fe^{3+} (**Fig.III.7**)/ Al^{3+} (**Fig.III.8a**)/ Cr^{3+} (**Fig.III.8b**) the absorption intensity gradually increases at 350 nm and decreases at 547 nm and 513 nm in methanol-water (99:1, v/v; HEPES buffer, pH, 7.2) solution. This implies that **RFC** interacts with these three ions (Fe^{3+} , Al^{3+} , Cr^{3+}) while other ions remain indifferent. On irradiation, the **RFC** solution in UV chamber does not show noteworthy emission, while the addition of Al^{3+} , Cr^{3+} and Fe^{3+} (**Fig.III.9**) turns strong pink color and other cations (Pb^{2+} , Pd^{2+} , Mn^{2+} , Cd^{2+} , Cu^{2+} , Ba^{2+} , Mg^{2+} , Zn^{2+} , Na^{+} , Hg^{2+} , K^{+} , Ca^{2+} , Co^{2+} , Ni^{2+} , Ru^{3+} , Au^{3+} , In^{3+} , La^{3+} , Sm^{3+} , Gd^{3+} , Eu^{3+} , Dy^{3+} , Tb^{3+} , In^{3+}) do not change the original colour of free **RFC**.

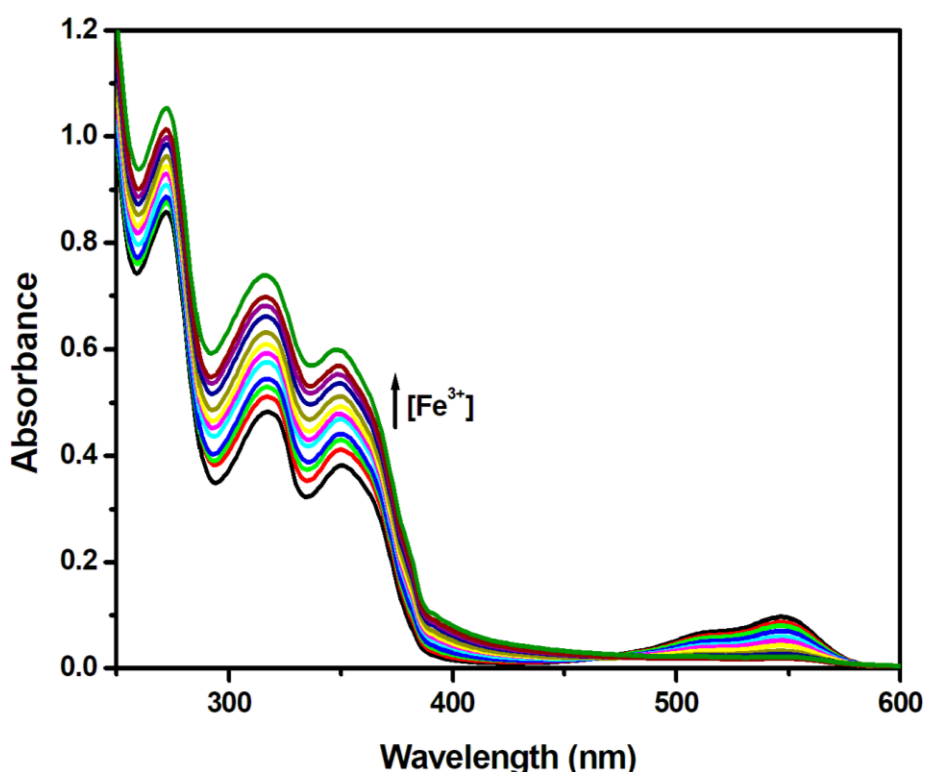


Fig.III.7. UV–vis absorption spectra of **RFC** with increasing concentration of Fe^{3+} in methanol-water (99:1, v/v) of pH, 7.2 (HEPES buffer).

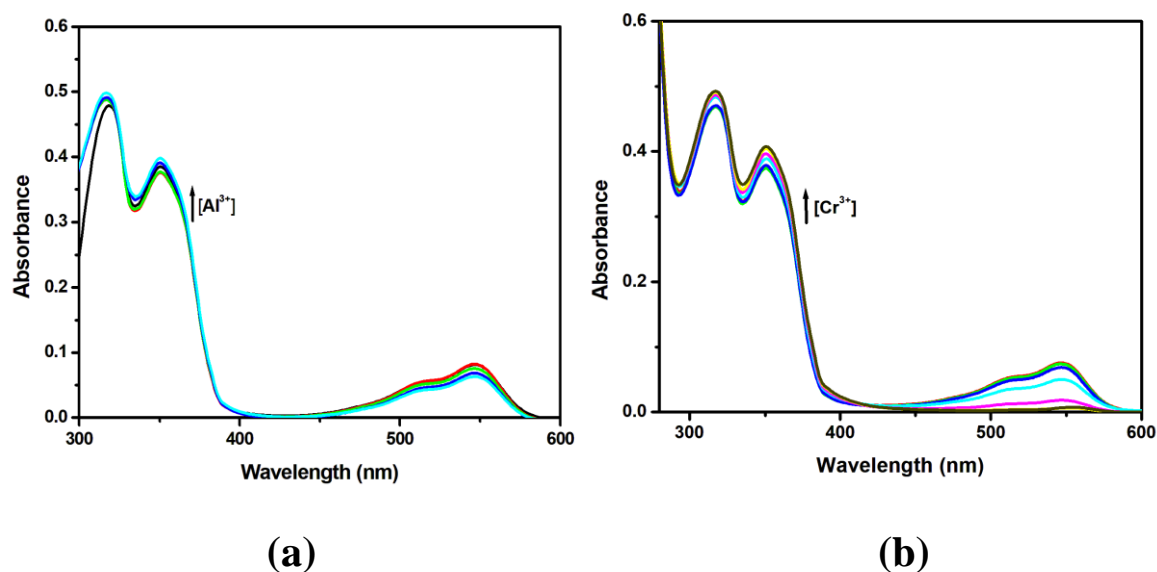


Fig.III.8. UV-vis absorption spectra of **RFC** with increasing concentration of (a) Al^{3+} and (b) Cr^{3+} in methanol-water (99:1, v/v) of pH, 7.2 (HEPES buffer).

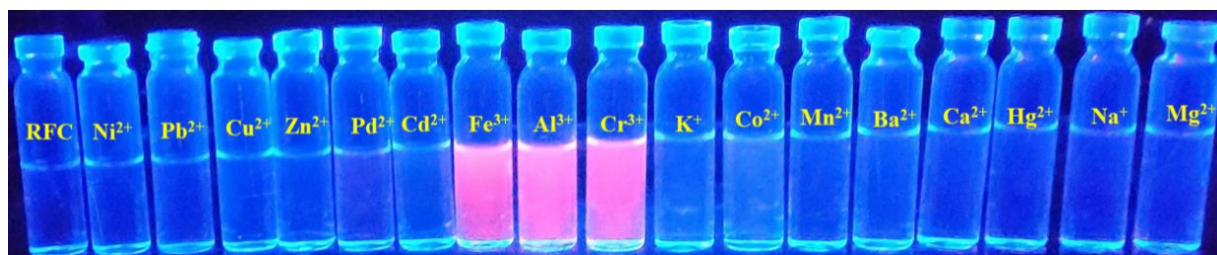


Fig.III.9. Vial image in UV chamber of the probe **RFC** in presence of different cations in methanol-water (99:1 v/v; HEPES buffer, pH, 7.2)

The spectroscopic investigation also shows that **RFC** does not show any notable emission band, nevertheless in existence of Fe^{3+} , Al^{3+} and Cr^{3+} ions a highly intense emission band at 583 nm (**Fig.III.10**) with 350 fold (Fe^{3+}), 250 fold (Al^{3+}) and 220 fold (Cr^{3+}) in methanol-water (99:1,v/v; HEPES buffer, pH, 7.2) medium.

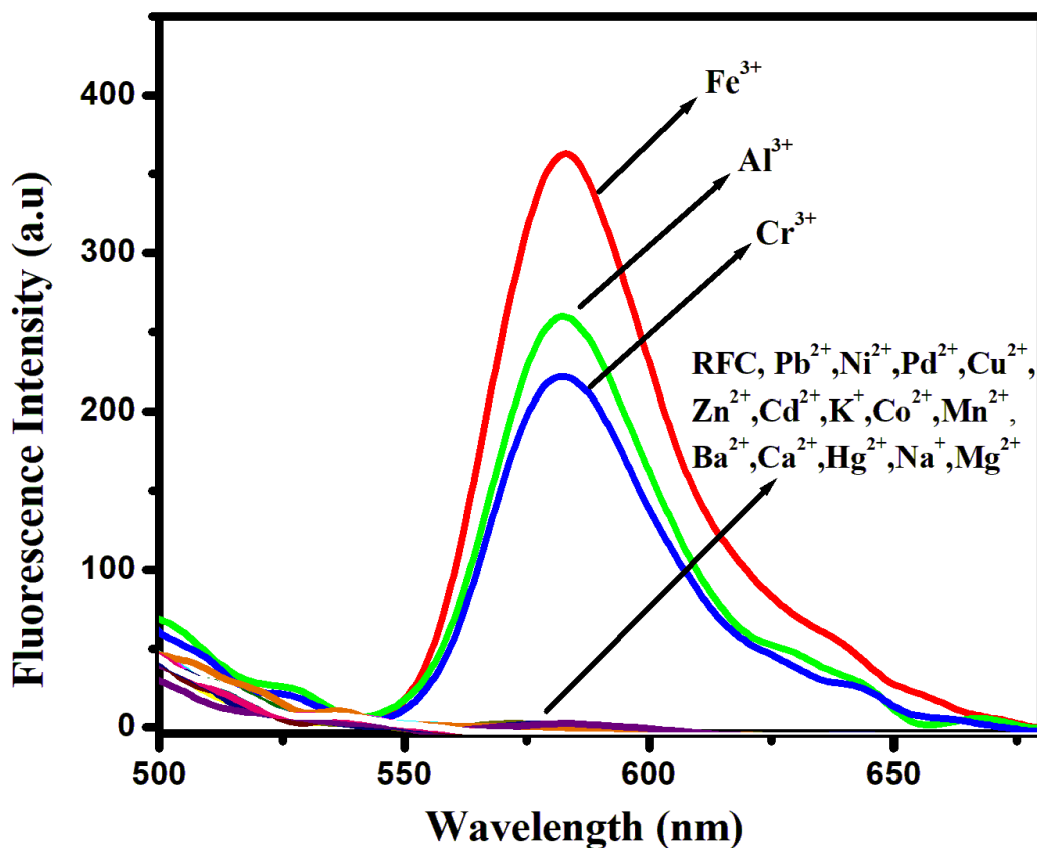


Fig.III.10. Emission spectra of the probe **RFC** in methanol-water (99:1, v/v; HEPES buffer, pH, 7.2) in presence of various metal ions.

The emission spectra of **RFC** in presence of cations (Pd^{2+} , Mn^{2+} , Cd^{2+} , Cu^{2+} , Ba^{2+} , Mg^{2+} , Zn^{2+} , Na^+ , K^+ , Ca^{2+} , Hg^{2+} , Ni^{2+} , Co^{2+} , Pb^{2+} , Ru^{3+} , Au^{3+} , In^{3+} , La^{3+} , Sm^{3+} , Gd^{3+} , Eu^{3+} , Dy^{3+} , Tb^{3+} , In^{3+}) have been recorded (**Fig.III.10**) and the spectra do not show distinguishable turn-on emission. The fluorescence spectra of **RFC** in presence of lanthanides and other different trivalent metal ions (Ru^{3+} , Au^{3+} , In^{3+} , La^{3+} , Sm^{3+} , Gd^{3+} , Eu^{3+} , Dy^{3+} , Tb^{3+} , In^{3+}) have been experimentally verified (**Fig.III.11**) but the resulting emission spectra do not show distinguishable turn-on emission.

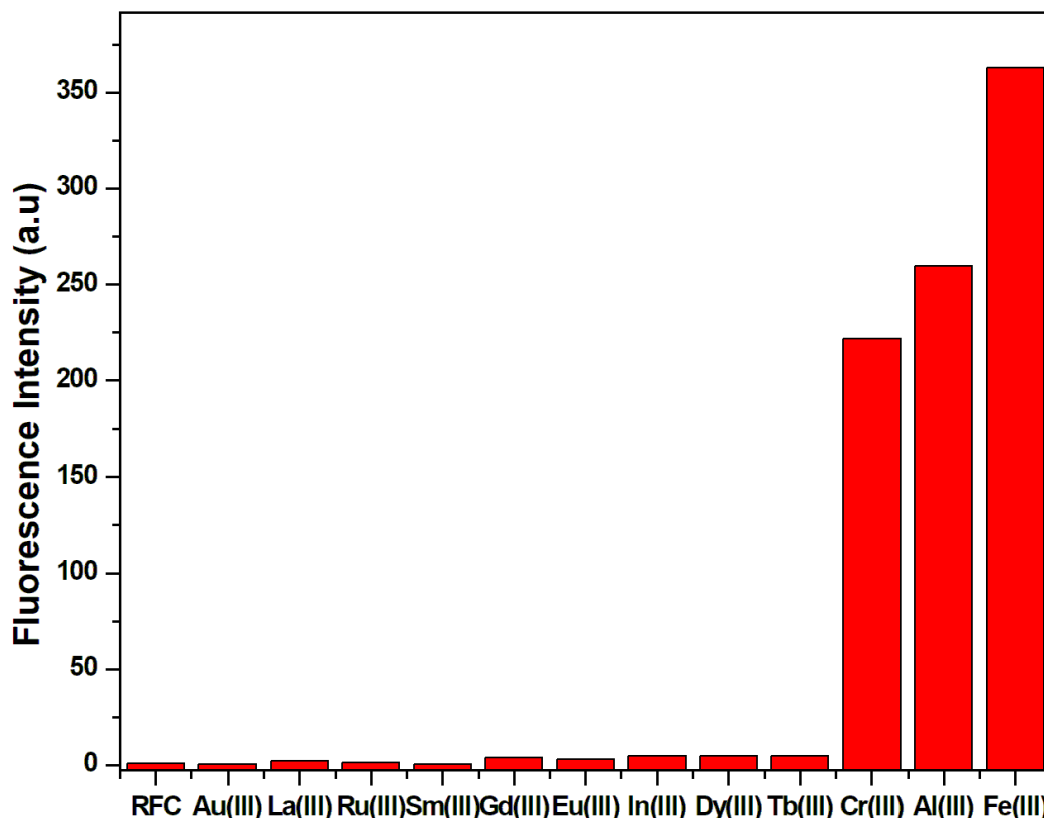


Fig.III.11. Fluorescence response profile of the probe **RFC** with trivalent lanthanides and other trivalent cations in methanol-water (99:1, v/v; HEPES buffer, pH, 7.2).

On the addition of solution containing $Fe^{3+}/Al^{3+}/Cr^{3+}$, the emission intensity of **RFC** at 583 nm increases and becomes saturated at a 1:1 stoichiometric ratio of **RFC** and metal ions (Fe^{3+} , Al^{3+} , Cr^{3+}) in methanol-water solution (99:1,v/v; HEPES buffer, pH, 7.2) (Fe^{3+} (**Fig.III.12**), Al^{3+} (**Fig.III.13**) and Cr^{3+} (**Fig.III.14**)).

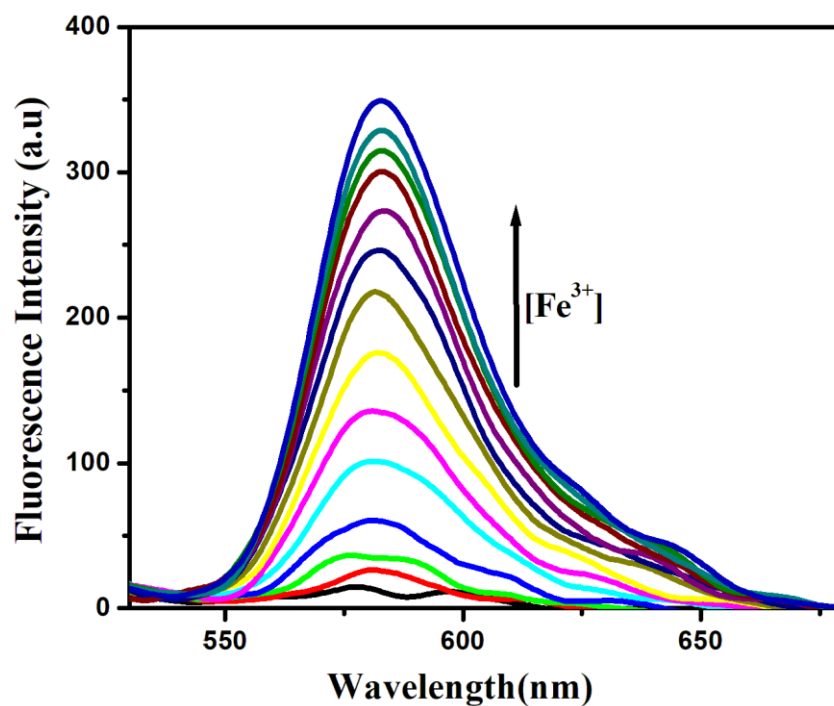


Fig.III.12. Fluorescence spectra of the probe **RFC** (25 μ M) with incremental addition of Fe^{3+} (3 μ L each time) in methanol-water (99:1, v/v; HEPES buffer, pH, 7.2) in presence of different cations.

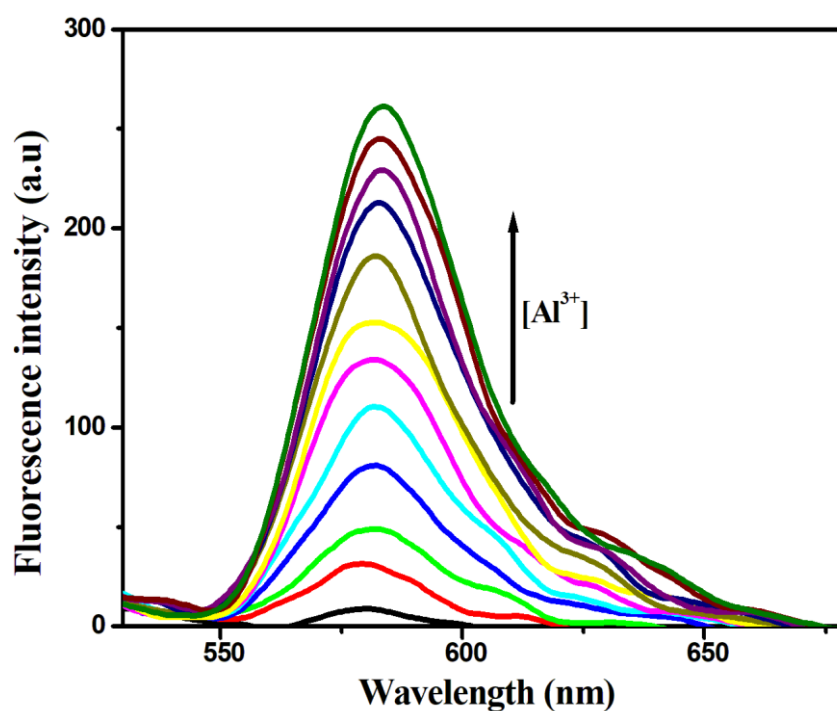


Fig.III.13. Fluorescence spectra of **RFC** (25 μ M) with increasing concentration of Al^{3+} (3 μ L each time) in methanol-water (99:1, v/v) of pH, 7.2 (HEPES buffer).

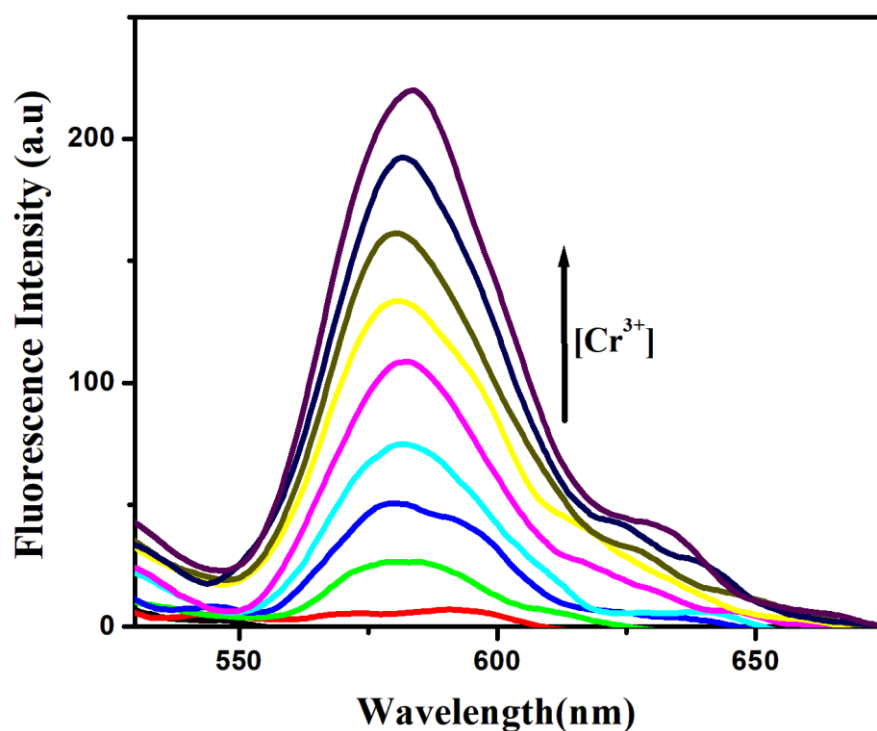


Fig.III.14. Fluorescence spectra of **RFC** (25 μ M) with increasing concentration of Cr^{3+} (3 μ L each time) in methanol-water (99:1, v/v) of pH, 7.2 (HEPES buffer).

The Fluorescence selectivity profile of **RFC** with Fe^{3+} (**Fig.III.15**), Al^{3+} (**Fig.III.16**) and Cr^{3+} (**Fig.III.17**) ions in the existence of competing cations (Pb^{2+} , Pd^{2+} , Mn^{2+} , Cd^{2+} , Cu^{2+} , Ba^{2+} , Mg^{2+} , Zn^{2+} , Na^+ , Hg^{2+} , K^+ , Ca^{2+} , Co^{2+} , Ni^{2+} , Ru^{3+} , Au^{3+} , In^{3+} , La^{3+} , Sm^{3+} , Gd^{3+} , Eu^{3+} , Dy^{3+} , Tb^{3+} , In^{3+}) has been examined and interference is noted.

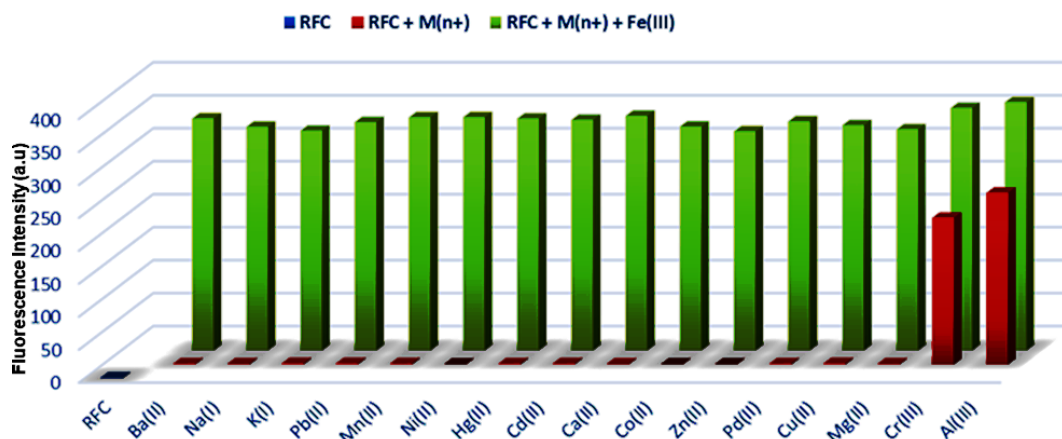


Fig.III.15. Fluorescence selectivity profile of **RFC** with Fe^{3+} in presence of competing cations in methanol-water (99:1, v/v; HEPES buffer, pH, 7.2)

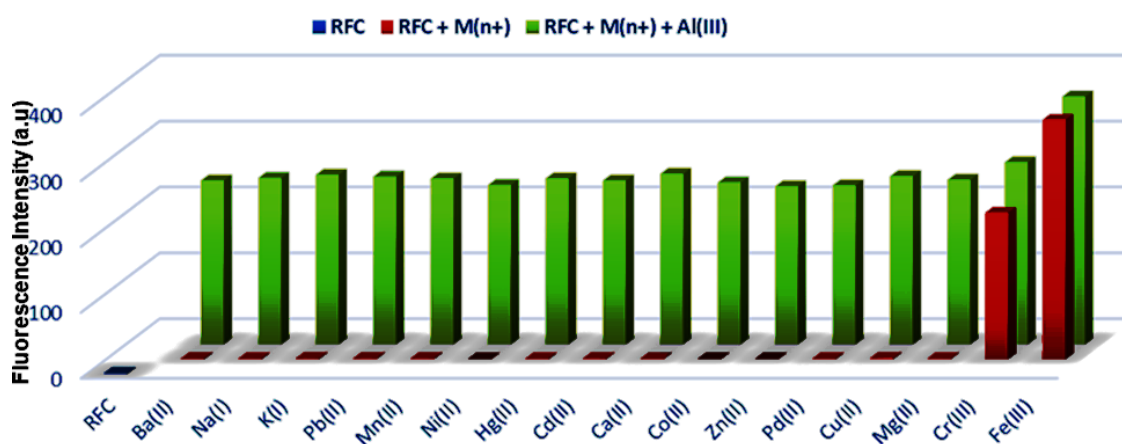


Fig.III.16. Fluorescence selectivity profile of **RFC** with Al^{3+} in presence of competing metal ions in methanol- water (99:1, v/v; HEPES buffer, pH, 7.2)

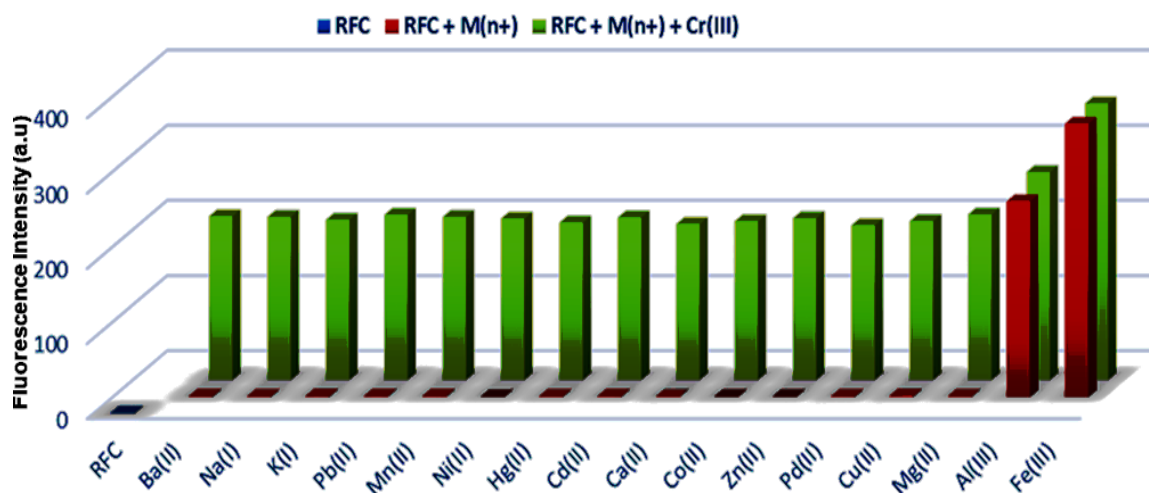


Fig.III.17. Fluorescence selectivity profile of **RFC** with Cr^{3+} in presence of competing metal ions in methanol-water (99:1, v/v; HEPES buffer, pH, 7.2)

The quantum yield of **RFC** is very low (Φ , 0.0021) which is increased to 0.66 (**RFC**+ Fe^{3+}), 0.48 (**RFC**+ Cr^{3+}), 0.39 (**RFC**+ Al^{3+}) respectively.

The limit of detection (LOD) has been measured for the recognition of experimental cations (Cr^{3+} , Al^{3+} and Fe^{3+}) by $3\sigma/M$ methods and the observed values are 0.0051 ppm (Fe^{3+}) (**Fig.III.18**), 0.0029 ppm (Al^{3+}) (**Fig.III.19a**) and 0.0052 ppm (Cr^{3+}) (**Fig.III.19b**) below the WHO recommended threshold value in drinking water (Cr^{3+} , 0.05 ppm; Fe^{3+} , 0.3 ppm; Al^{3+} , 0.2 ppm).

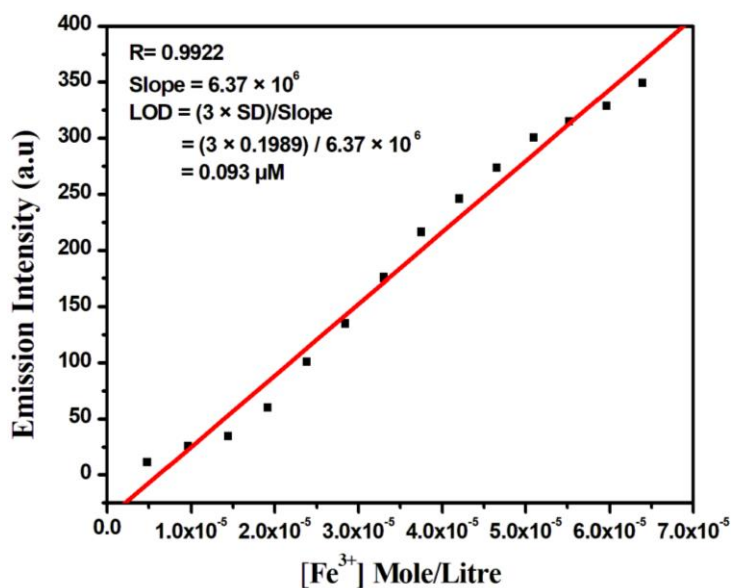


Fig.III.18. Evaluation of LOD of Fe^{3+} by **RFC** in methanol-water (99:1, v/v) of pH, 7.2 (HEPES buffer) using 3σ method.

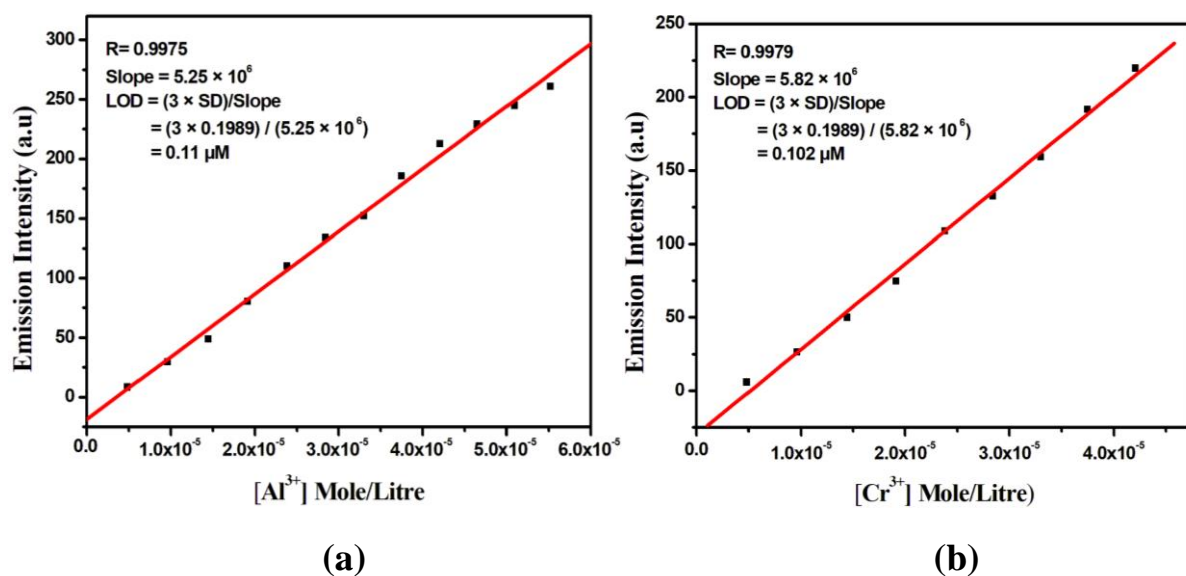


Fig.III.19. Evaluation of LOD of (a) Al^{3+} (b) Cr^{3+} by **RFC** in methanol-water (99:1, v/v) of pH, 7.2 (HEPES buffer) using 3σ method.

The binding constant (K_d) of the probe **RFC** towards experimental cations (Al^{3+} , Cr^{3+} , Fe^{3+}) have been determined from the Benesi-Hildebrand plot, and the observed values are $5.81 \times 10^3 M^{-1}$ (Fe^{3+}) (**Fig.III.20**), $5.82 \times 10^3 M^{-1}$ (Al^{3+}) (**Fig.III.21a**) and $4.57 \times 10^3 M^{-1}$ (Cr^{3+}) (**Fig.III.21b**).

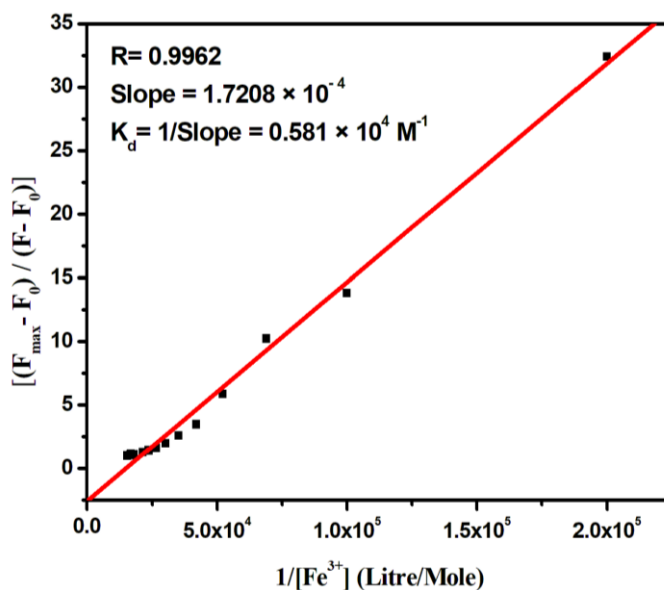


Fig.III.20. Benesi-Hildebrand plot of the probe **RFC** in presence of Fe^{3+} in methanol-water (99:1, v/v) of pH, 7.2 (HEPES buffer)

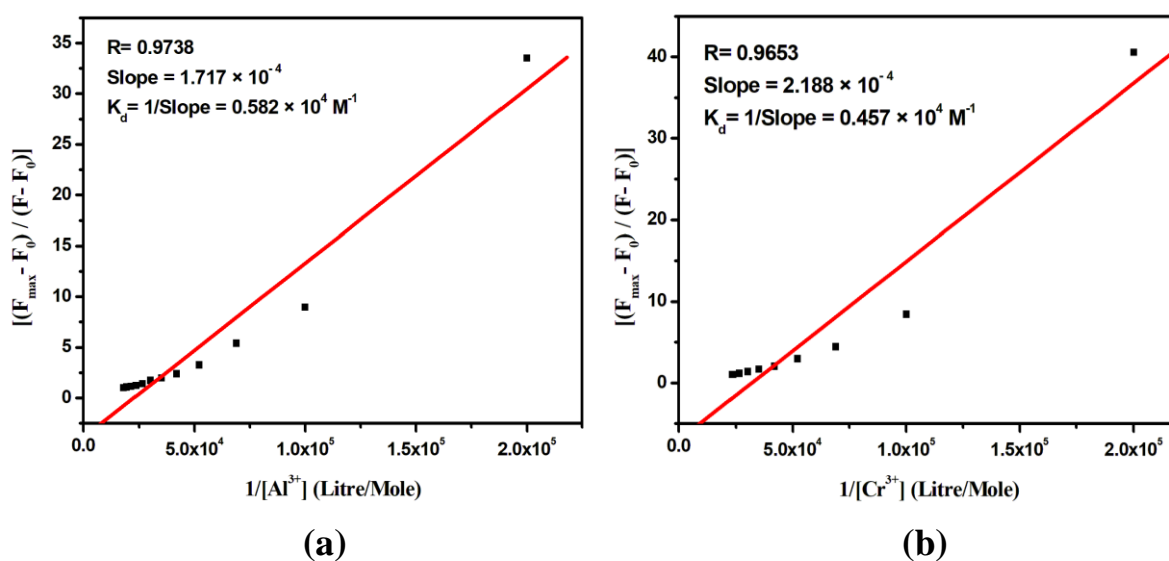


Fig.III.21. Benesi-Hildebrand plot of the probe **RFC** in presence of (a) Al^{3+} and (b) Cr^{3+} in methanol-water (99:1, v/v) of pH, 7.2 (HEPES buffer)

The stoichiometric study of **RFC** towards the cations (Fe^{3+} , Al^{3+} and Cr^{3+}) has been studied using Job's plot (**Fig.III.22**, **Fig.III.23a**, and **Fig.III.23b**) by fluorometric method which has established 1:1 stoichiometric binding between **RFC** and trivalent cations (Cr^{3+} , Fe^{3+} and Al^{3+}).

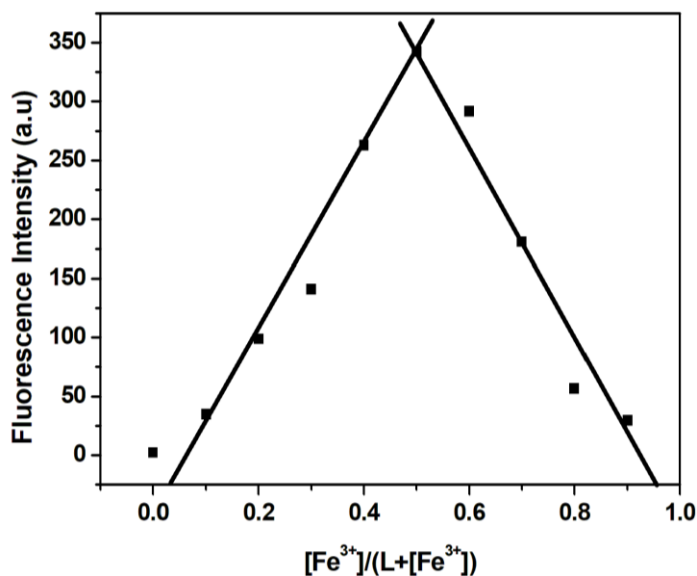


Fig.III.22. Job's plot of the probe **RFC** with Fe^{3+} in methanol-water (99:1, v/v) of pH, 7.2 (HEPES buffer).

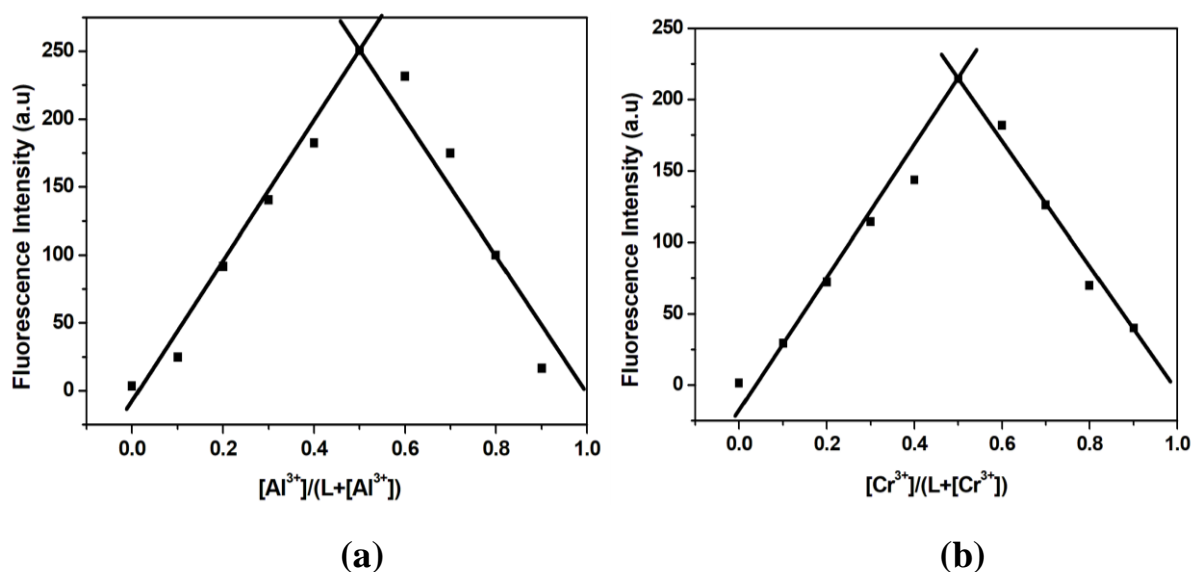


Fig.III.23. Job's plot of the probe **RFC** in presence of (a) Al^{3+} and (b) Cr^{3+} in methanol-water (99:1, v/v) of pH, 7.2 (HEPES buffer).

The Time-resolved fluorescence measurement determines the lifetime of free **RFC** (τ , 0.73 ns) which is lower than that of complex mixture, **RFC**+ $Fe^{3+}/Al^{3+}/Cr^{3+}$ (τ , 0.97 ns, **RFC** + Fe^{3+}), (τ , 1.109 ns, **RFC** + Al^{3+}), (τ , 1.037 ns, **RFC** + Cr^{3+}) (**Fig.III.24**) which also implies the overlapping of participating functions of M^{3+} and **RFC**.

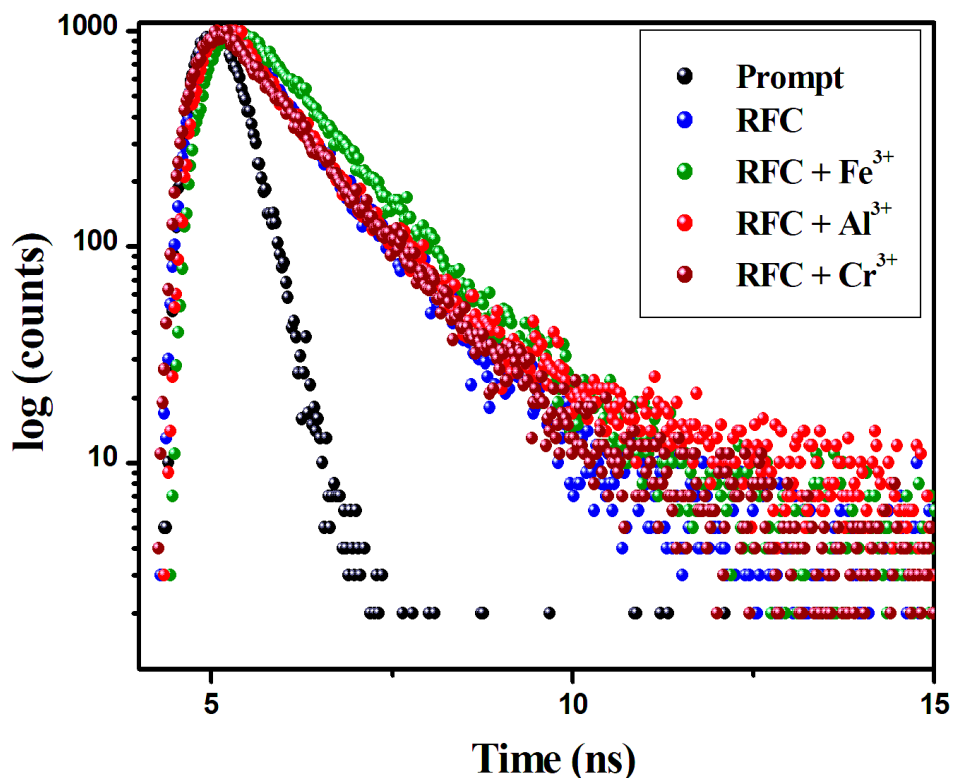


Fig.III.24. Fluorescence lifetime spectra of **RFC** and **RFC** in presence of Fe^{3+} , Al^{3+} and Cr^{3+} in methanol-water (99:1, v/v; HEPES buffer, pH, 7.2)

Spectrophotometric experiments of **RFC** and **RFC+ Fe^{3+} / Al^{3+} / Cr^{3+}** were carried out in the pH range 2-11 (**Fig.III.25-27**). It is observed that no spirolactam ring-opening of **RFC** takes place for pH > 3.0 and hence no emission is recorded. Upon addition of the cations (Fe^{3+} , Al^{3+} and, Cr^{3+}) the emission intensity slowly decreases from pH 2 to 7 but at pH > 8 the emission intensity of (**RFC + M^{3+}**) ($M = Fe^{3+}$, Al^{3+} , Cr^{3+}) falls significantly which is owing to the precipitation of corresponding metal hydroxides.

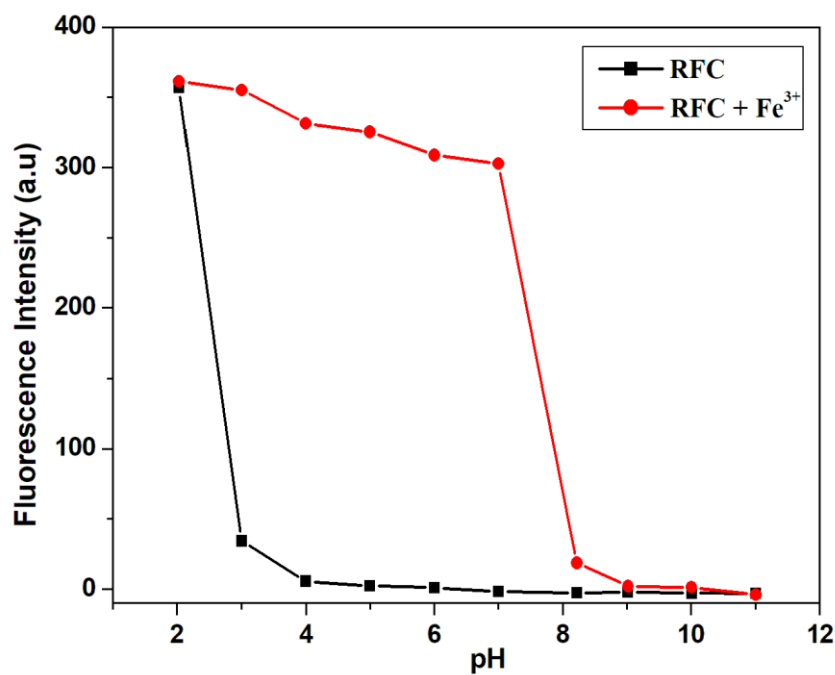


Fig.III.25. Effect of pH on RFC and (RFC + Fe^{3+}).

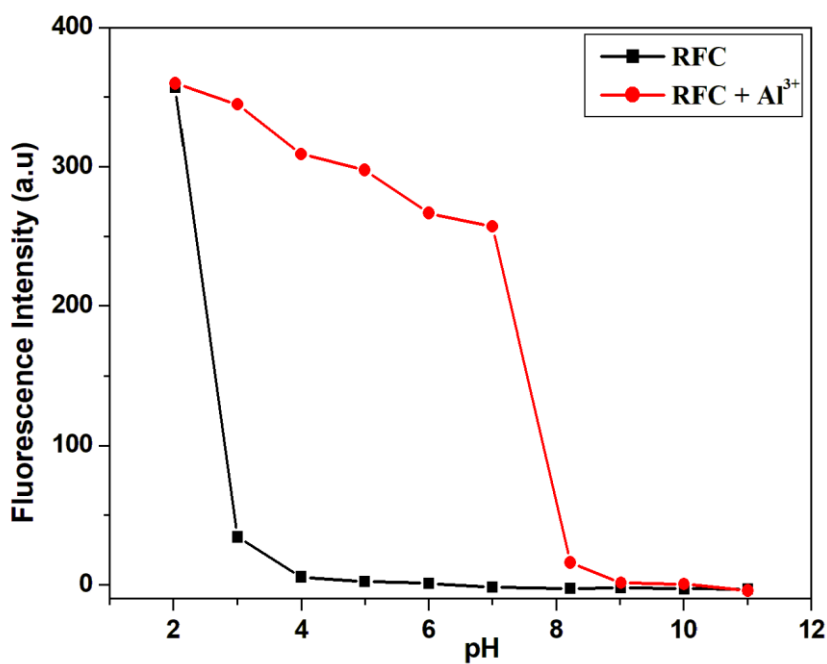


Fig.III.26. Effect of pH on RFC and (RFC + Al^{3+}).

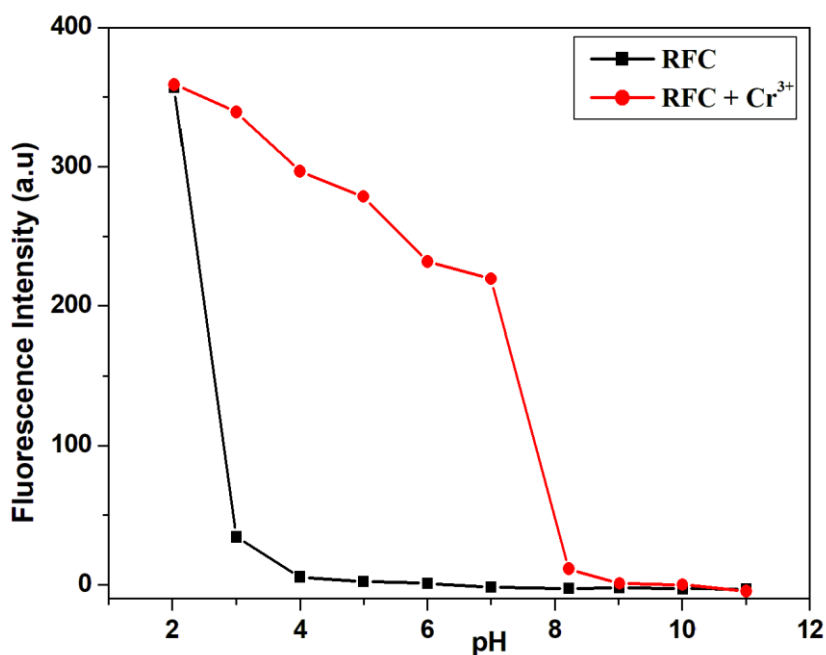
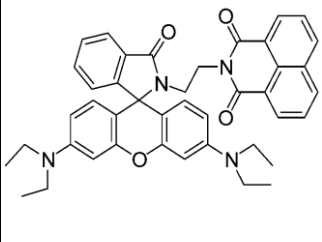
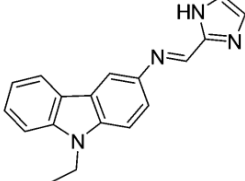
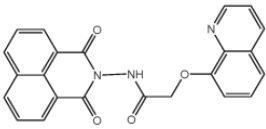
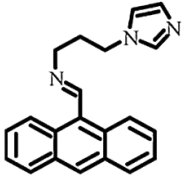
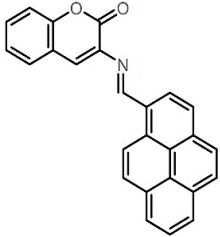
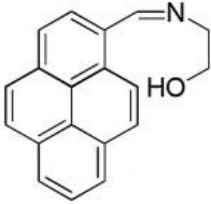
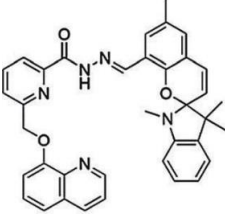
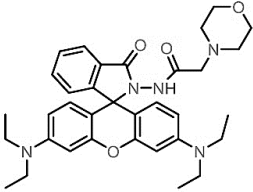
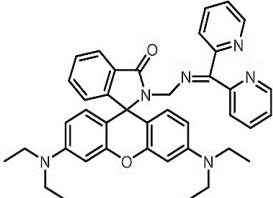
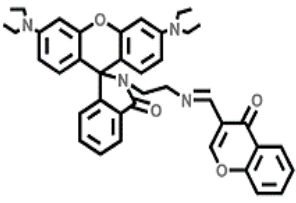


Fig. III.27. Effect of pH on RFC and (RFC + Cr³⁺).

The probe shows efficient selectivity towards Al^{3+} , Cr^{3+} and Fe^{3+} and the recently published results (Table III.1) have been compared and it is found that the selectivity performance of the probe, RFC, is the highest sensitive and the detection limit is the lowest.

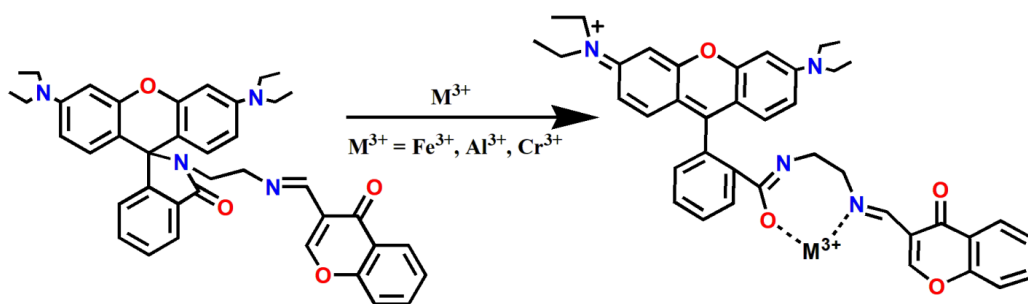
Table III.1. Correlation table of some parameters of some recently published related research works

Probe	Solvent	LOD	$K_d(M^{-1})$	Reference
	CH ₃ OH–H ₂ O (6:4, v/v)	1.74 nM (Al^{3+}) 2.36 μ M (Cr^{3+}) 2.90 μ M (Fe^{3+})	$1 \times 10^4 M^{-1}$ (Al^{3+}) $2.6 \times 10^2 M^{-1}$ (Cr^{3+}) $1.2 \times 10^2 M^{-1}$ (Fe^{3+})	[44]
	THF – H ₂ O (8:2) mixture	0.36 nM (Cr^{3+}) 0.38 nM (Fe^{3+}) 0.38 nM (Al^{3+})	Not determined	[45]

Probe	Solvent	LOD	$K_d(M^{-1})$	Reference
	CH ₃ CN–HEPES buffer solution (40/60, v/v, pH = 7.4)	25 μ M (Cr^{3+}) 23 μ M (Al^{3+}) 20 μ M (Fe^{3+})	$1.08 \times 10^4 M^{-1}$ (Fe^{3+}) $8.7 \times 10^3 M^{-1}$ (Al^{3+}) $5.6 \times 10^3 M^{-1}$ (Cr^{3+})	[46]
	CH ₃ OH–H ₂ O (1:1, v/v)	1.6 μ M (Al^{3+}) 2.66 μ M (Cr^{3+}) 0.799 μ M (Fe^{3+})	Not determined	[47]
	MeOH/H ₂ O(6:4, v/v, pH=7.4, 10mM HEPESbuffer)	0.79 nM (Al^{3+}) 1.15 μ M (Cr^{3+}) 1.28 μ M (Fe^{3+})	$7.3 \times 10^4 M^{-1}$ (Al^{3+}) $2.8 \times 10^4 M^{-1}$ (Cr^{3+}) $1.1 \times 10^5 M^{-1}$ (Fe^{3+})	[48]
	CH ₃ CN	0.106 μ M (Fe^{3+}) 0.111 μ M (Cr^{3+}) 0.117 μ M (Al^{3+})	$2.25 \times 10^6 M^{-1}$ (Fe^{3+}) $2.24 \times 10^6 M^{-1}$ (Cr^{3+}) $2.26 \times 10^6 M^{-1}$ (Al^{3+})	[49]
	CH ₃ CN–HEPES buffer solution (1:1, pH = 7.4)	93 nM (Cr^{3+}) 32 nM (Al^{3+}) 90 nM (Fe^{3+})	Not determined	[50]
	CH ₃ OH/H ₂ O (8:2, v/v, Tris 10 mM, pH 7.4)	2.7 mM (Al^{3+}) 3.5 mM (Cr^{3+}) 1.9 mM (Fe^{3+})	$3.3 \times 10^4 M^{-1}$ (Al^{3+}) $3.7 \times 10^4 M^{-1}$ (Cr^{3+}) $4.3 \times 10^4 M^{-1}$ (Fe^{3+})	[51]
	EtOH/H ₂ O (1:1, v/v)	1.17 μ M (Al^{3+}), 2.50 μ M (Fe^{3+}) 3.16 μ M (Cr^{3+})	$1.42 \times 10^3 M^{-1}$ (Fe^{3+}), $3.88 \times 10^3 M^{-1}$ (Al^{3+}) $9.16 \times 10^3 M^{-1}$ (Cr^{3+}).	[52]
	Methanol-water (99:1, v/v; HEPES buffer, pH, 7.2)	0.093 μ M (Fe^{3+}) 0.11 μ M (Al^{3+}) 0.10 μ M (Cr^{3+})	$5.81 \times 10^3 M^{-1}$ (Fe^{3+}) $5.82 \times 10^3 M^{-1}$ (Al^{3+}) $4.57 \times 10^3 M^{-1}$ (Cr^{3+})	This work

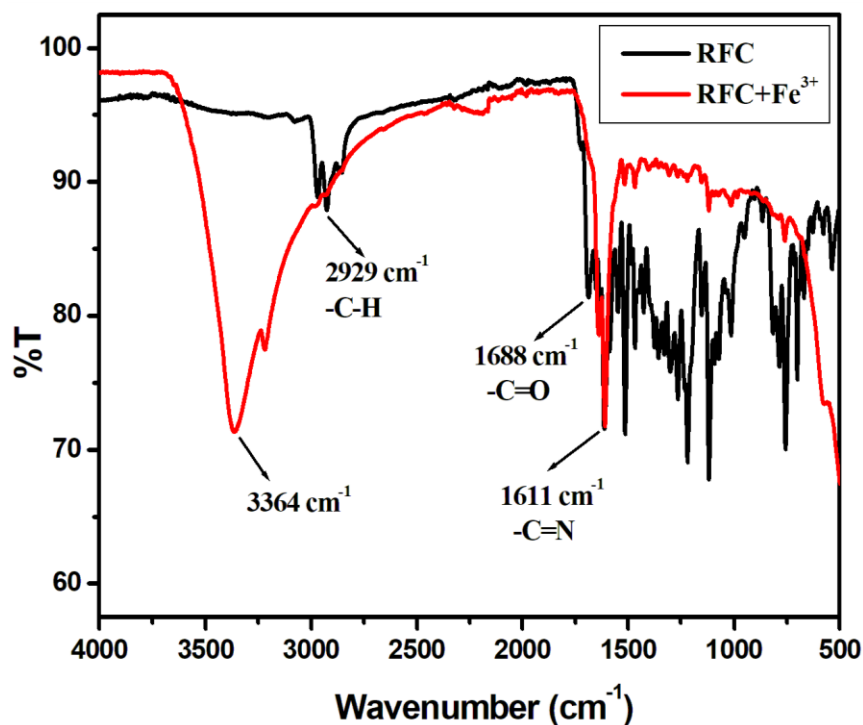
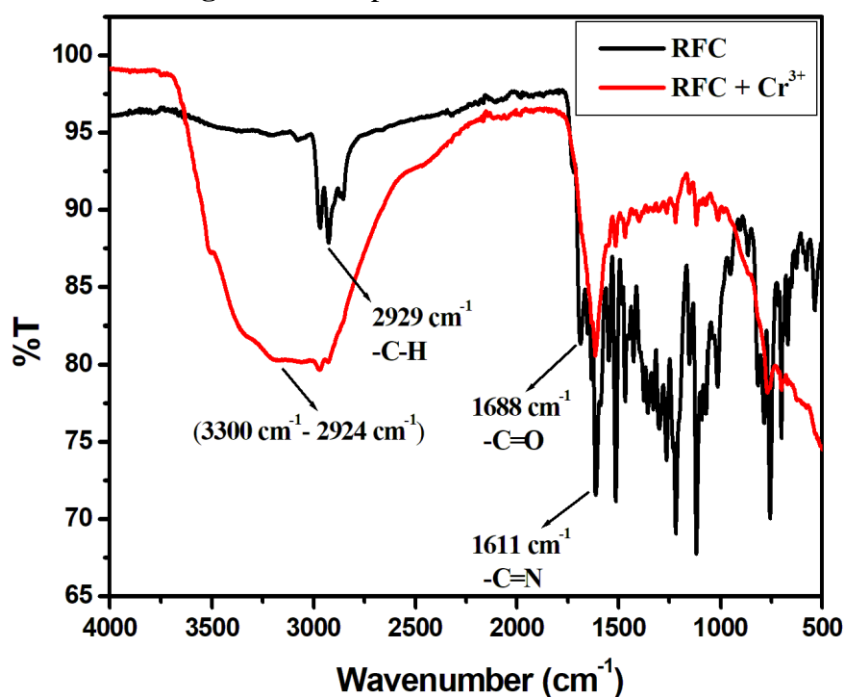
III.3.3. Mechanism of sensing of Fe^{3+} , Al^{3+} , and Cr^{3+} by RFC

Rhodamine derivatives, in general, change their colour on the cleavage of spirolactam ring. On changing pH or interaction with specific metal ion(s) with available donor N/O centres may develop strain on the spirolactam ring which leads to cleavage followed by chelation and concomitant colour change. After the cleavage of the spirolactam ring the donor atoms (O, N) come from amidic moiety may initiate noncovalent interaction (Scheme III.b) with trivalent cations (Fe^{3+} , Al^{3+} , and Cr^{3+}).



Scheme III.b. The probable interacting procedure among the probe **RFC** and **[RFC + M^{3+}]** ($M^{3+} = Fe^{3+}$, Al^{3+} and, Cr^{3+}).

The IR spectroscopic studies of **RFC** and its metal coordinated system have revealed that the metal ions are chelated through O, N donors of the opened form of the probe. This has been supported by the disappearance of a peak at 1688 cm^{-1} ($\nu C=O$ of spirolactam ring) (**Fig.III.28** & **Fig.III.29**).

Fig.III.28. IR spectrum of RFC + Fe^{3+} Fig.III.29. IR spectrum of RFC + Cr^{3+}

The 1H -NMR titration of the probe, **RFC** with M^{3+} ions (Cr^{3+} , Al^{3+} , Fe^{3+}) shows the broadening of the proton signal; such as, two doublets of doublets at 7.81 (H_{21}) and 7.73 (H_9) ppm in chromone and Rhodamine unit respectively of **RFC** were broadened after adding 0.5 equiv.

Fe^{3+} in DMSO- d_6 . Upon addition of 1.0 equiv. Fe^{3+} both these proton signals (H_{21} and H_9) merge to a broad singlet (**Fig.III.30**). In the same way, the peaks at the region 6.2-7.6 ppm were also broadened at large extent. The same observations were also noticed in the case of Al^{3+} and Cr^{3+} ions as well (**Fig.III.31 & Fig.III.32**). The NMR broadening may also be due to the paramagnetic expansion impact of Fe^{3+} and Cr^{3+} complexation along with the ring-opening effect of the spirolactam ring. Therefore, the result supports the selective metal ions induced spirolactam ring opening of the probe **RFC** and the formation complexes which enriches the concept of ring opening enhancement of emission intensity (**Scheme III.b**).

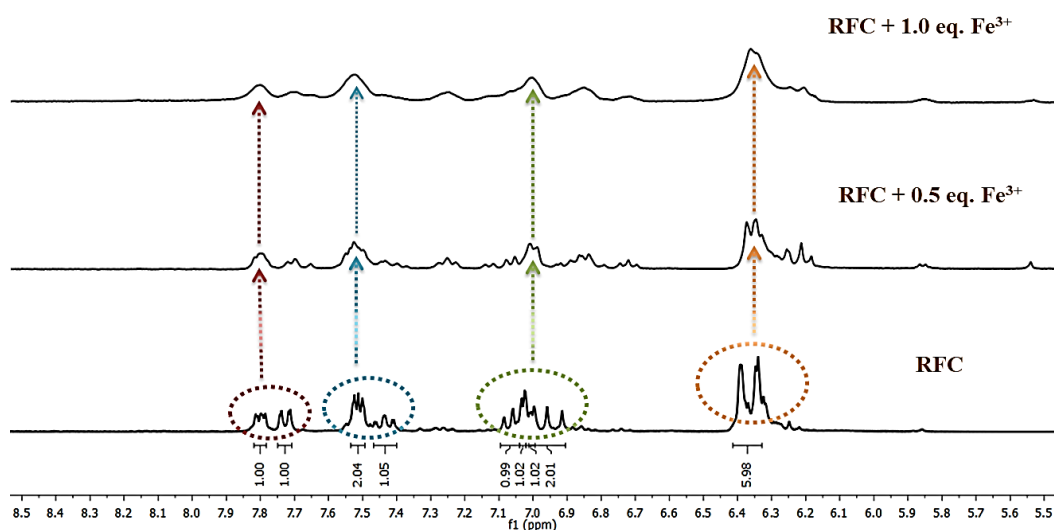


Fig.III.30. NMR titration of **RFC** in presence of Fe^{3+}

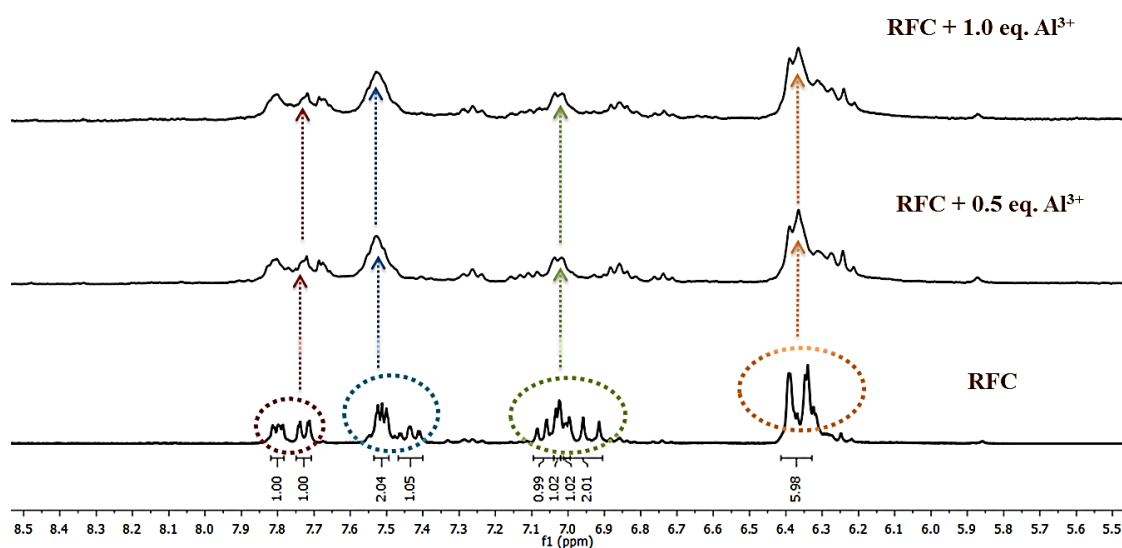


Fig.III.31. NMR titration of **RFC** in presence of Al^{3+} .

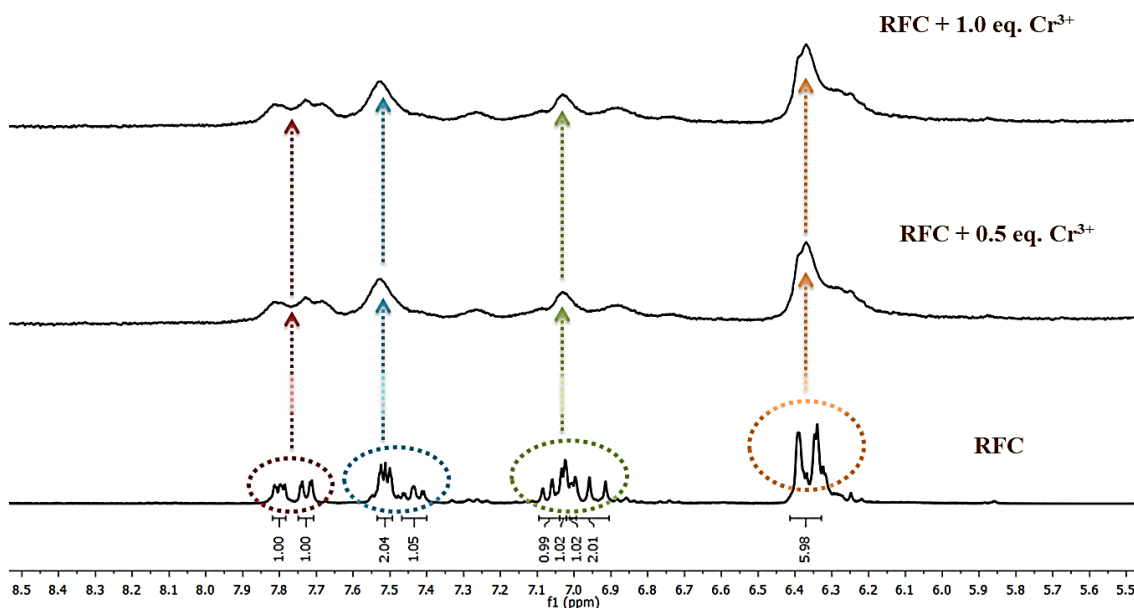


Fig.III.32. NMR titration of RFC in presence of Cr^{3+} .

The complexation also supported by the significant peaks in Mass spectrum of the complex ion, which is found at $m/z = 274.2764$ (calculated for $FeC_{44}H_{56}N_4O_8 = 274.7810$) (**Fig.III.33**) assignable to $[Fe(L)(C_2H_5OH)_2(H_2O)_2]^{3+}$ ion., $m/z = 837.1642$ (calculated for $C_{42}H_{46}AlN_6O_{11} = 837.30$) (**Fig.III.34**) assignable to $[Al(L)(NO_3)_2(C_2H_5OH)]^+$ ion and $m/z = 243.1517$ (calculated for $CrC_{40}H_{44}N_4O_6 = 242.7550$) (**Fig.III.35**) assignable to $[Cr(L)(H_2O)_2]^{3+}$ ion.

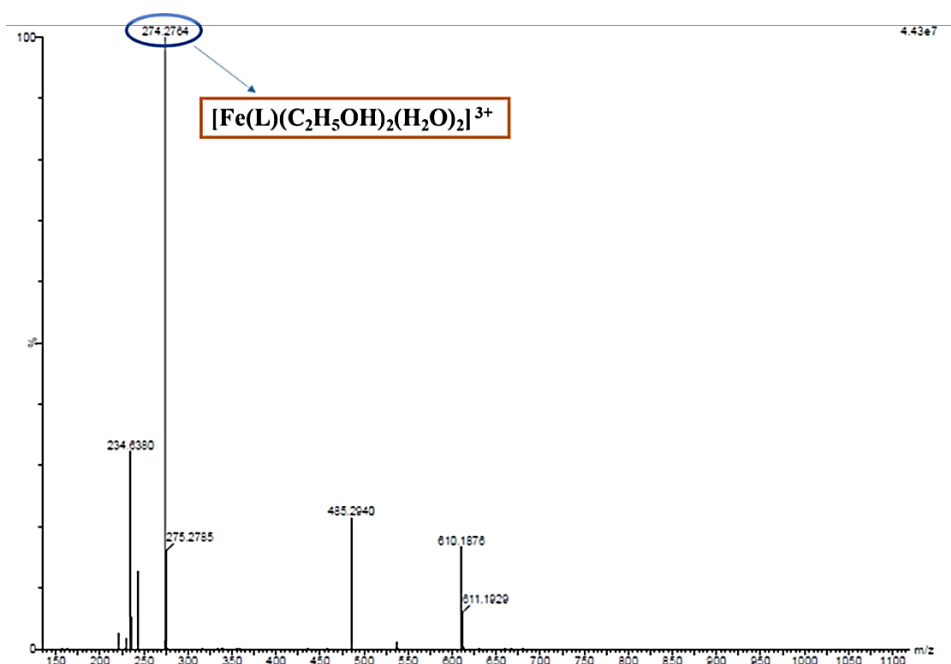


Fig.III.33. Mass spectrum of $[Fe(L)(C_2H_5OH)_2(H_2O)_2]^{3+}$ complex ion.

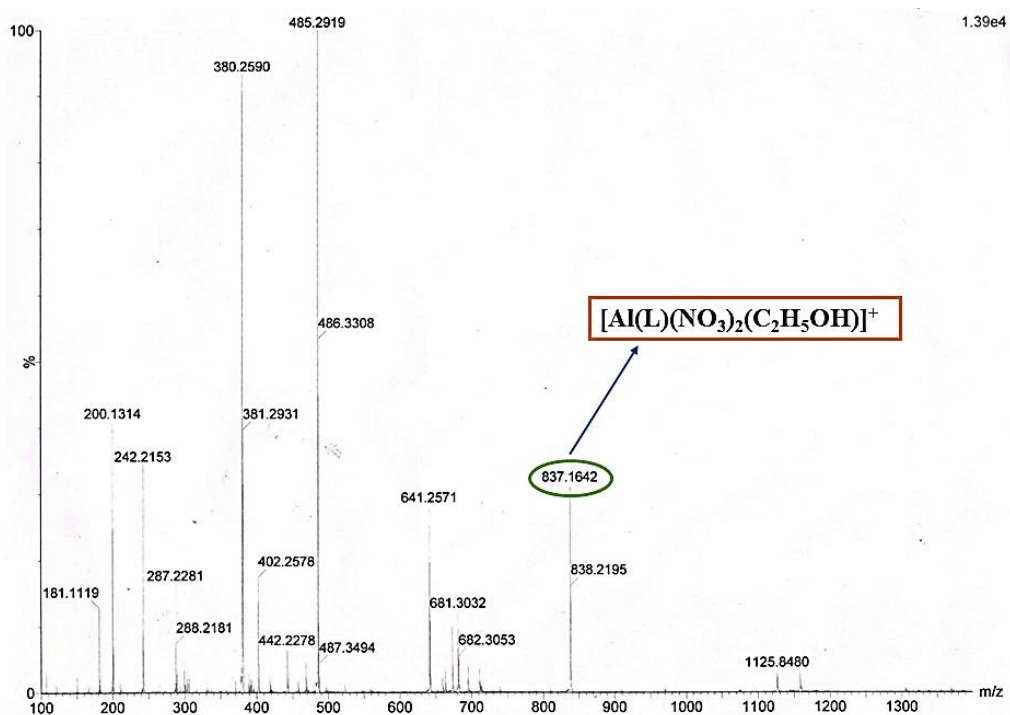


Fig.III.34. Mass spectrum of $[Al(L)(NO_3)_2(C_2H_5OH)]^+$ complex ion.

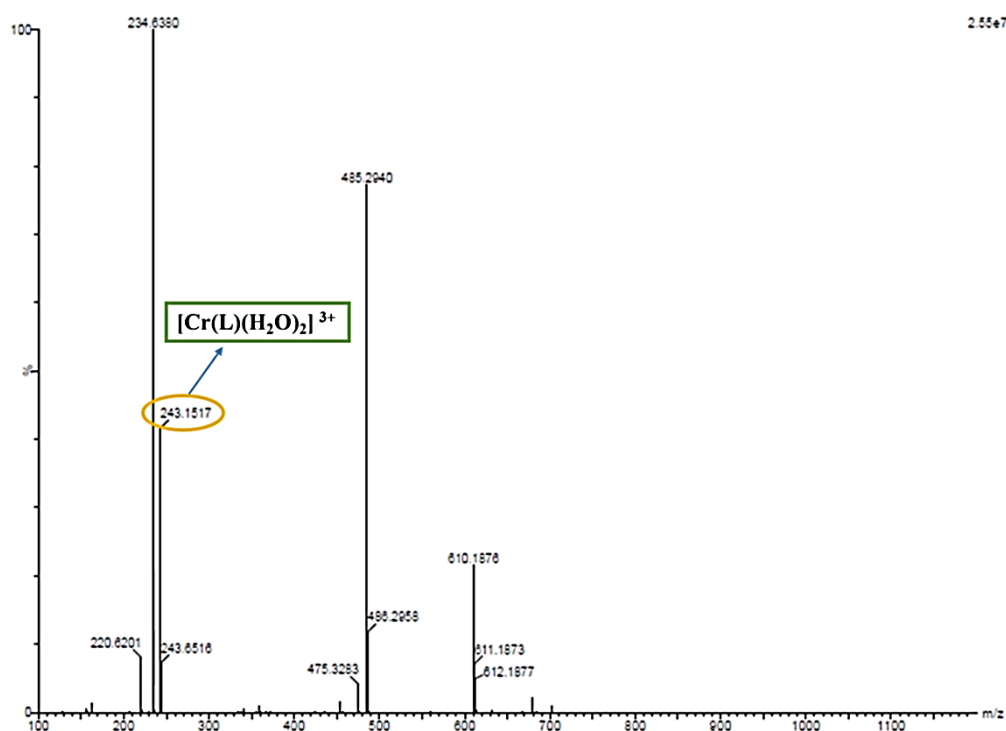


Fig.III.35. Mass spectrum of $[Cr(L)(H_2O)_2]^{3+}$ complex ion.

Reversibility and recyclability are considered the most noticeable sustainable parameters in the Green Engineering and Technology [53]. The CHEF-induced emission of probe on the introduction of Fe^{3+} and its instantaneous quenching in the addition of CN^- can be repeated up to 5 cycles (**Fig.III.36**) upon addition of Fe^{3+} in (99:1, v/v; HEPES buffer, pH, 7.2) medium.

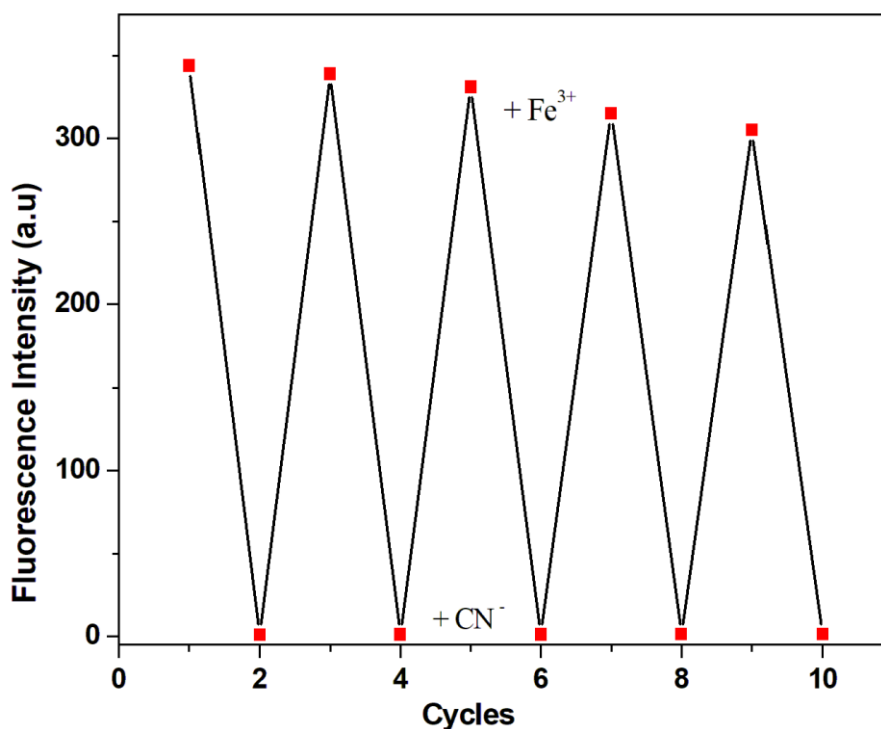


Fig.III.36. Reversible response cycles of **RFC** after the addition of Fe^{3+} along with CN^-

Established on the basis of switchable fluorescence features of the probe **RFC** towards Fe^{3+} , an INHIBIT logic gate (**Fig.III.37**) can be created with the two input signals of Fe^{3+} and CN^- and the fluorescence intensity at 583 nm as the output signal. In this case the turn on emission can be represented as 1, on the other hand the quenched state can be signified as 0. The corresponding truth table (**Fig.III.37**) was created for the given logical circuit; the output is denoted as 1 when it results in the increment of emission [54].

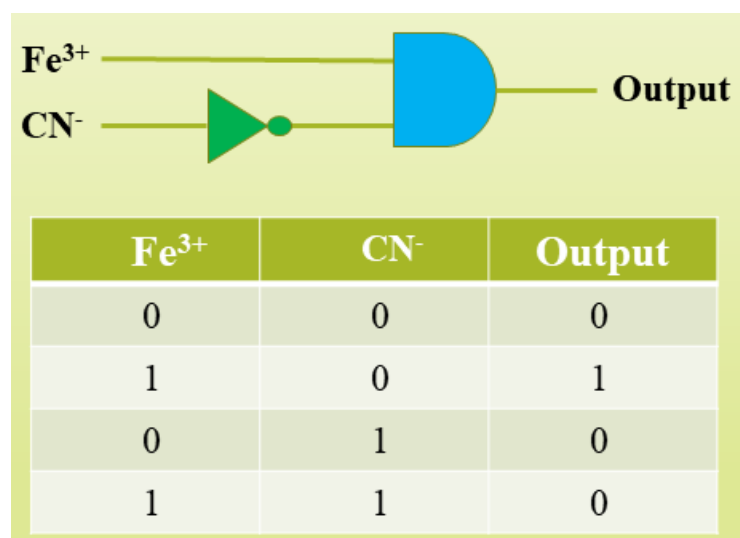


Fig.III.37. General representation of an INHIBIT logic gate and truth table for two inputs: Fe^{3+} and CN^- and single output at 583 nm.

The time-dependent fluorescence spectra of the probe **RFC** upon exposure to UV light at $\lambda_{ex} = 366$ nm for 180 min have been studied (**Fig.III.38**). The observation reveals good photostability of the probe **RFC**.

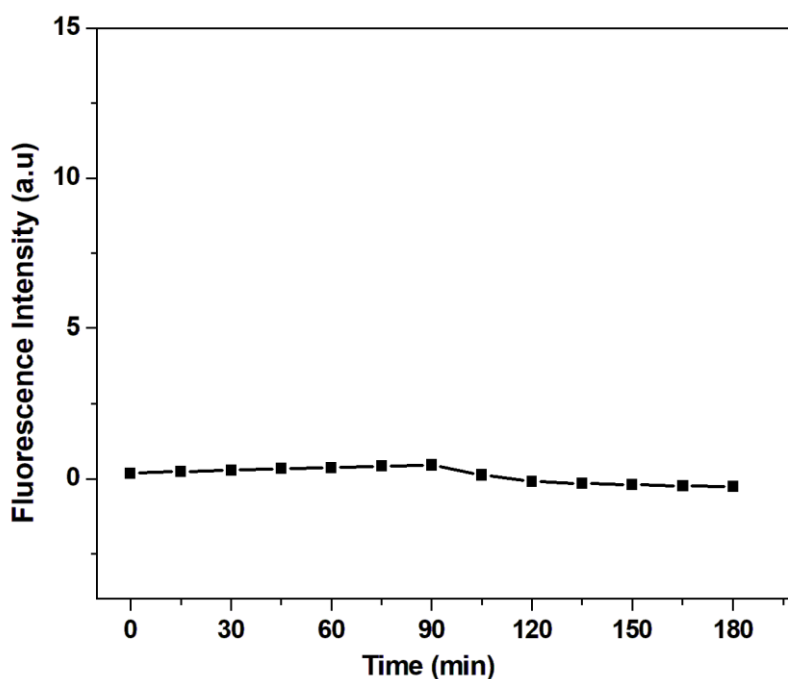


Fig.III.38. Change in Time-dependent fluorescence intensity of the probe **RFC** upon exposed to UV light ($\lambda_{ex} = 366$ nm) for 180 min.

III.3.4. Fluorescence Imaging

The application of the probe, **RFC** as chemosensor was examined by treatment of the compound (**RFC**) in the presence of three metal salts Cr^{3+} , Al^{3+} , and Fe^{3+} on MCF-7 cell line and has been compared with WI-38 normal cell line. In the presence of the salt and the **RFC** bright red fluorescence was observed as opposed to the absence of fluorescence in the case of control and only **RFC** (**Fig.III.39**). This helps to speculate the fact that the compound **RFC** probe has good potential as a chemosensor molecule.

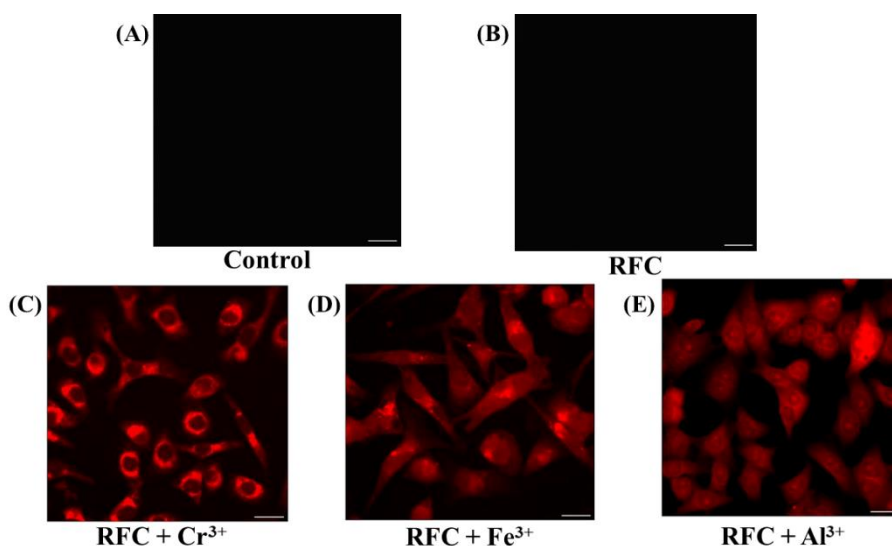


Fig.III.39. The chemosensing application of **RFC** in the presence of three metal salts of $FeCl_3 \cdot 6H_2O$, $Al(NO_3)_3 \cdot 9H_2O$, and $CrCl_3 \cdot 6H_2O$ on the MCF-7 cell line. A bright red fluorescence was observed (C-E) for **RFC**+ M^{3+} as opposed to the absence of fluorescence in the case of control and only **RFC** (A-B). Images have been captured in 40X magnification in the TRITC filter. The scale bar corresponds to 20 μm .

III.3.5. Cell Cytotoxicity

The cytotoxicity analysis was performed on the MCF-7 and WI-38 cell lines using 3-(4, 5-dimethylthiazol-2-yl)-2, 5-diphenyltetrazolium bromide (MTT). In 96 well plates the cells

were seeded and then **RFC** probe was added in the variable concentration range (100 μ M to 1.62 μ M) for 24 h. The proliferation of MCF-7 breast cancer cells was inhibited while it does not exhibit significant cytotoxicity on WI-38 normal lung fibroblast cells and the IC_{50} of the RFC probe on MCF-7 and WI-38 cells were calculated to be 2.53 and 393.7 μ M respectively (**Fig.III.40**) using compusyn software.

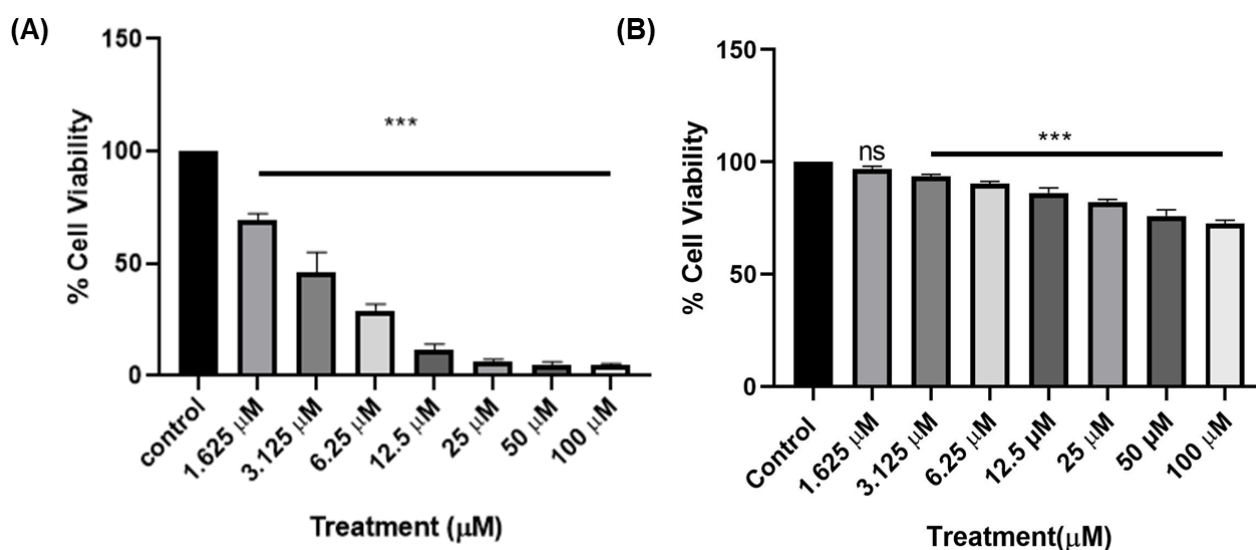


Fig.III.40. Cell viability of **RFC** probe on (A) MCF-7 cells and (B) WI-38 cells at various concentrations. The error bars correspond to the standard error of the value after performing the experiment in triplicates. (n=3) (Two-way ANOVA, *** $p < 0.001$).

III.3.6. Colony Formation Assay

For investigating the effect of **RFC** on MCF-7 cells, Colony Formation Assay was performed. For this MCF-7 cells were seeded in 6 well for 24 h followed by treatment with two doses (2.5 μ M and 5 μ M) of the probe **RFC**. After 24 h of treatment, the colony size, as well as their numbers, was visibly diminished in both the concentrations which again proved the anticancer property of **RFC** (**Fig.III.41**).

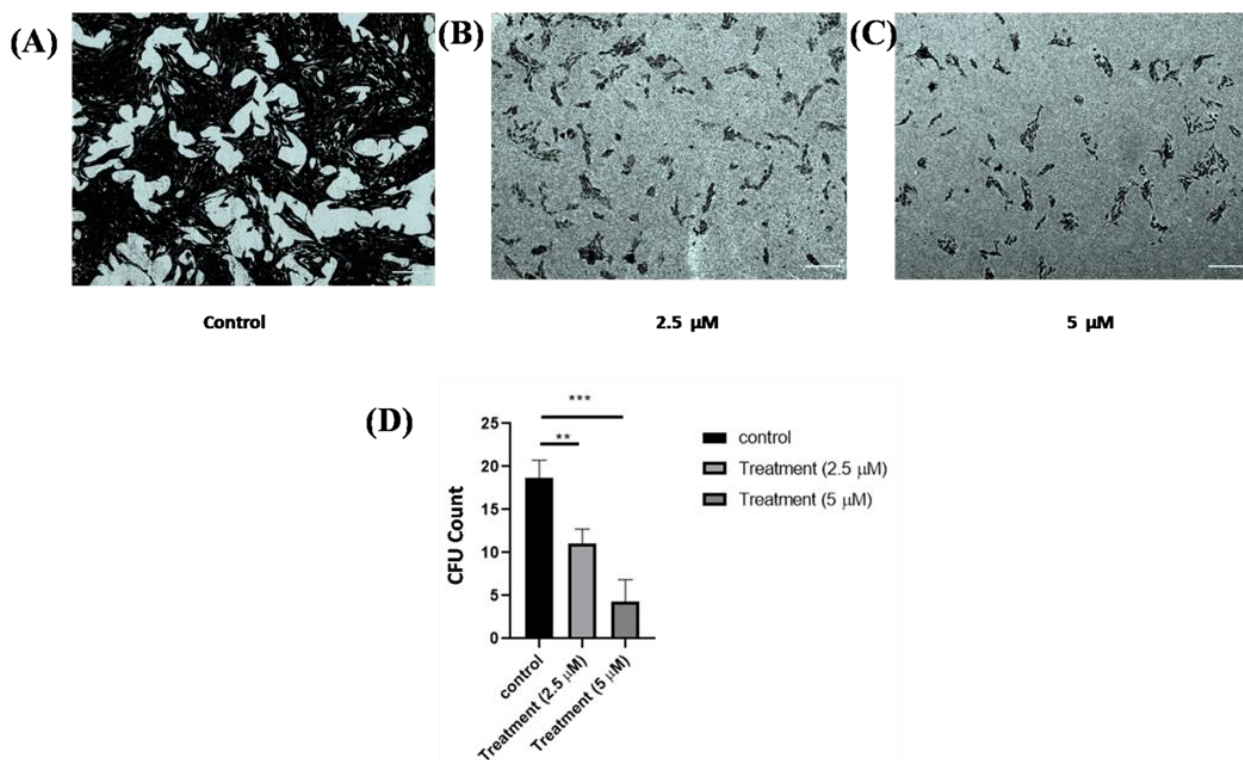


Fig.III.41. Colony formation assay performed in MCF-7 cells treated with 2.5 μ M and 5 μ M of **RFC**. (A-C) Significant inhibition of colony formation and development is observed in **RFC** treated MCF-7 cells as compared to untreated control. Scale bar corresponds to 100 μ m; (D) Graph showing reduction in number of colonies on treatment as compared to untreated control. The error bars correspond to standard error of the value after performing the experiment in triplicates. (n=3) (Two-way ANOVA, ** p< 0.05 *** p<0.001).

III.3.7. Wound Healing Assay

The inhibitory effect of the **RFC** probe on the migration potential of the MCF-7 cells was thereafter assessed by its ability to inhibit the curing of the wound. For this analysis the wound healing (Scratch) assay was performed, whereby MCF-7 cells were seeded in sterile 6 well plates and after 24 h of incubation a scratch was prepared using a 200 μ l micro tip. After treatment with 2.5 μ M and 5 μ M of **RFC** for 24 h, it was observed that the rate of cell migration, as well as invasion, decreased and eventually, after 48 h of treatment, **RFC** was found to

significantly inhibit the closure of wounds in proportion with the dose of treatment in MCF-7 cells as compared to control (**Fig.III.42**).

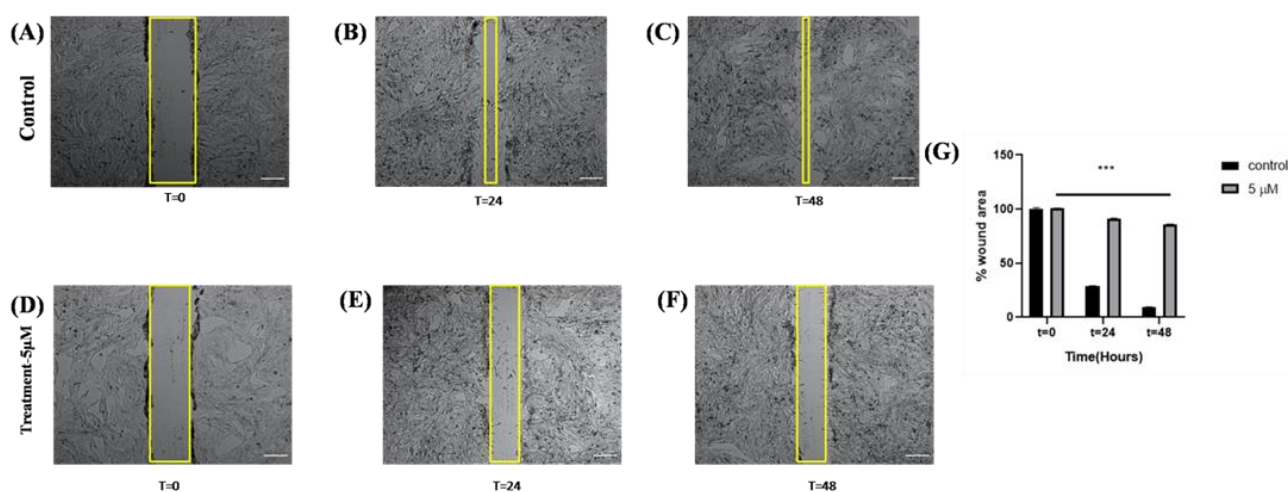


Fig.III.42. Wound healing assay carried out in MCF-7 cells treated with 5 μM **RFC** probe.

(A-F) Significant inhibition of the closure of the wound is observed in treated cells as compared to the untreated control. The scale bar corresponds to 100 μm. (G) Graph showing reduction in wound healing area on treatment with **RFC** as compared to untreated control where the wound almost completely closes at 48 h. The error bars correspond to the standard error of the value after performing the experiment in triplicates. (n=3) (Two-way ANOVA, *** p<0.001).

III.3.8. Nuclear Fragmentation Assay:

Following treatment of 24 h on MCF-7 cells, observation was done for investigating changes in nuclear morphology under a Fluorescence microscope (Olympus). Uneven staining of Hoechst 33258 in the nuclei and apoptotic morphology with gradual nuclear fragmentation was observed in **RFC** treated MCF-7 cells whereas the cells in the control showed uniform staining and normal nucleus without any type of condensation and fragmentation. This speculates that **RFC** contains the potential of inducing apoptosis in MCF-7 cells (**Fig.III.43**).

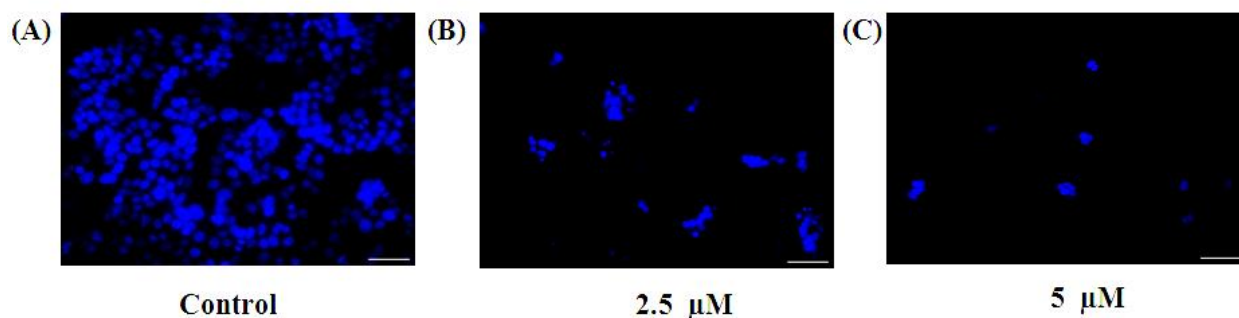


Fig.III.43. DNA fragmentation assay using Hoechst 33258 dye on MCF -7 cells after treatment with 2.5 & 5 μ M **RFC**. The cell nuclei in the control are mostly unlike the treatment groups where the nucleus has undergone fragmentation and shrinkage with the increase in the dose of treatment. The images have been captured in the DAPI channel at 40X magnification Scale bar corresponds to 20 μ m.

III.3.9. Western Blot Analysis

Western Blot analysis was carried out to examine the apoptotic markers on the MCF-7 cell line after treatment with 5 μ M **RFC**. The expression of all the pro-apoptotic markers has promisingly increased after treatment with respect to the control (**Fig.III.44**). The expression band intensity was normalized to that of Beta-actin used as the loading control. The increase in the expression of the pro-apoptotic markers with respect to control in the treatment group indicates that the compound **RFC** possesses apoptosis-inducing potential, which also helps to get a better insight into the anticancer potential of a compound by inducing apoptosis in MCF-7 breast cancer cell line.

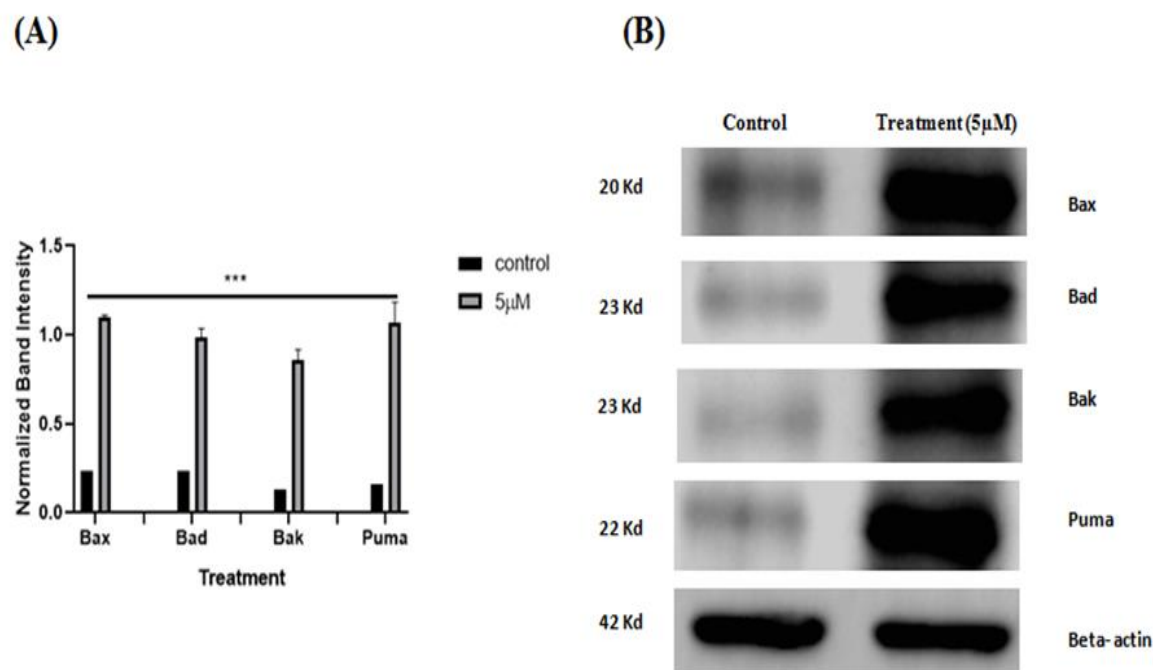


Fig.III.44. Western Blot analysis was carried out to examine the apoptotic markers on the MCF-7 cell line after treatment with 5 μ M **RFC**. The expression of all the proapoptotic markers has promisingly increased after treatment with respect to the control. The expression band intensity was normalized to that of Beta-actin used as the loading control. The error bars correspond to the standard error of the value after performing the experiment in triplicates. (n=3) (Two-way ANOVA, *** $p < 0.001$).

III.3.10. Growth Inhibition Analysis in Tumor Spheroid Model

The growth inhibition assay on the Tumor spheroid model was performed to understand the anticancer effect of **RFC** in the 3D tumor model as it is closer to the complex tumor microenvironment as well as to know the effect of the compound on Cancer stem cell population which is responsible for spheroid formation under low attachment conditions. A significant amount of shrinkage in the MCF-7 mammospheres was noticed in the **RFC** treated group as compared to the untreated (control) group where an increase in the volume of the

mammospheres with an increasing number of days was observed (**Fig.III.45**). This shows that **RFC** inhibits breast cancer MCF-7 cells in both 2D and 3D tumor models.

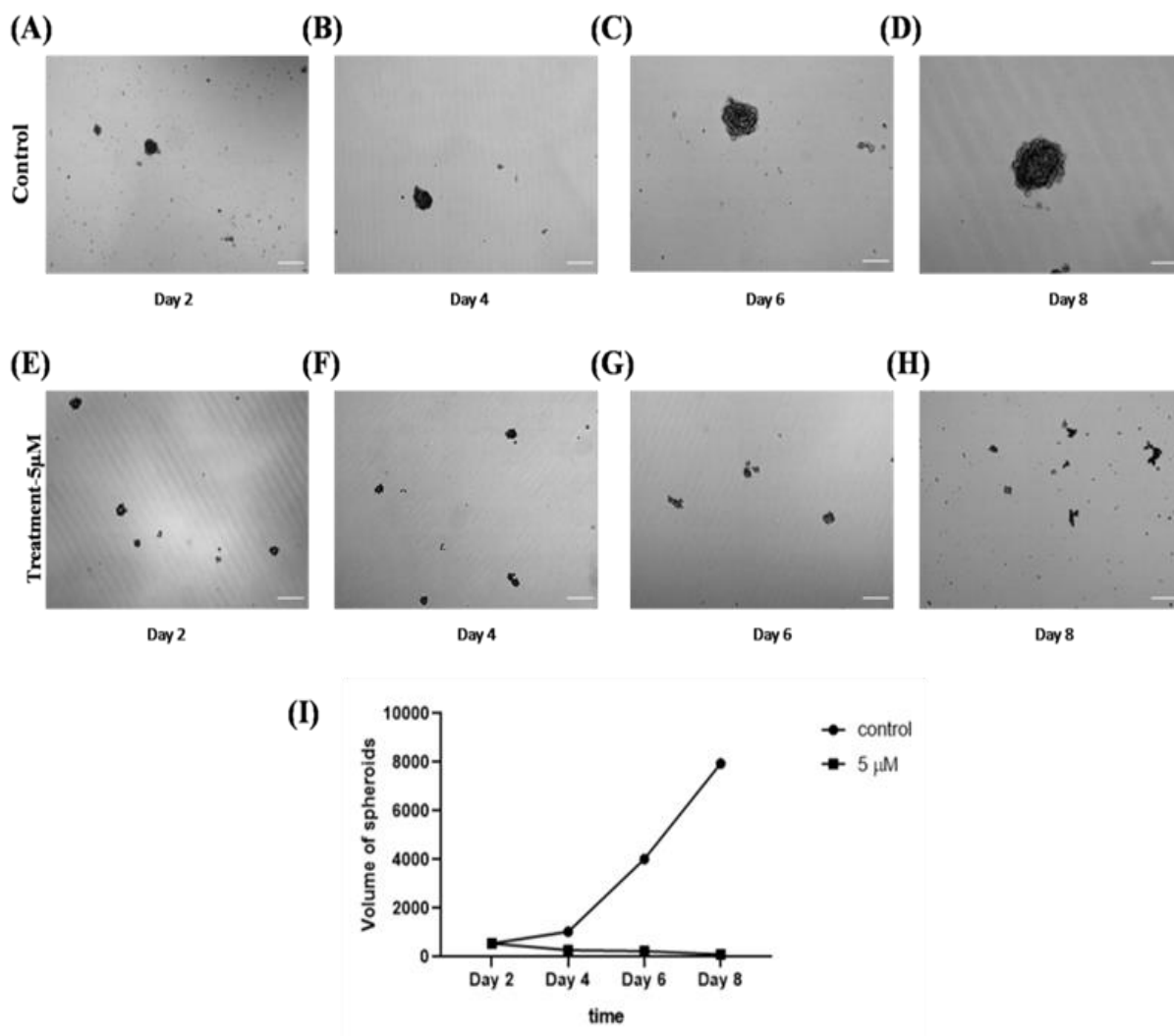


Fig.III.45. Spheroid Growth inhibition assay performed in MCF-7 cells after treatment with 5 μ M **RFC**. (A-H) Inhibition in the growth of mammospheres is observed on treatment with 5 μ M **RFC** as compared to untreated mammospheres where uninhibited growth of the spheroid occurs. Scale bar corresponds to 100 μ m. (I) Graphical representation of the spheroid growth inhibition compared to untreated control up to 8 days. The error bars correspond to standard error of the value after performing the experiment in triplicates. (n=3) (Two-way ANOVA, *** $p < 0.001$).

III.4. Conclusion

A probe consisting of two fluorogenic units, Rhodamine and chromone, are attached through C=N- to make a Schiff base (**RFC**) which exhibits efficient 'turn on' fluorescent emission towards Al^{3+} , Cr^{3+} and Fe^{3+} ions in existence of different competitive metal ions. Therefore, the material may be employed for the fabrication of a detection device. The probe shows selective efficiency to three Analytical Group III metal ions and the limit of detection (0.0051 ppm (Fe^{3+}), 0.0029 ppm (Al^{3+}) and 0.0052 ppm (Cr^{3+})) which is much below the WHO recommended data. The probe has excellent anticancer activity against MFC-7 (breast cancer) (IC_{50} , 2.53 μ M) on comparing with normal cell line, WI-38 (IC_{50} , 393.7 μ M). So, the molecule has multi-functional properties and it may be an exquisite material in view of the technological and biological field.

III.5. References:

- [1]. T. Rasheed, F. Nabeel, M. Adeel, K. Rizwan, M. Bilal, H.M.N. Iqbal, *J. Mol. Liq.*, 292 (2019) 111425.
- [2]. T. Rasheed, F. Nabeel, *Coord. Chem. Rev.*, 401 (2019) 213065.
- [3]. X. Zhao, S. Wang, L. Zhang, S. Liu, G. Yuan, *Inorg. Chem.*, 58 (2019) 2444.
- [4]. Y. Chen, Y. Bai, Z. Han, W. He, Z. Guo, *Chem. Soc. Rev.*, 44 (2015) 4517-4546.
- [5]. Z. Yuan, A.H. Younes, J.R. Allen, M.W. Davidson, L.J. Zhu, *J. Org. Chem.*, 80 (2015) 5600.
- [6]. Z. Li, Q. Hu, C. Li, J. Dou, J. Cao, W. Chen, Q. Zhu, *Tetrahedron Lett.*, 55 (2014) 1258.
- [7]. B. Dutta, S. Dey, K. Pal, S. Bera, S. Naaz, K. Jana, C. Sinha, M.H. Mir, *New J. Chem.*, 44 (2020) 13163.
- [8]. S. Goswami, A.K. Das, A.K. Maity, A. Manna, K. Aich, S. Maity, P. Saha, T. K. Mandal, *Dalton Trans.*, 43 (2014) 231.

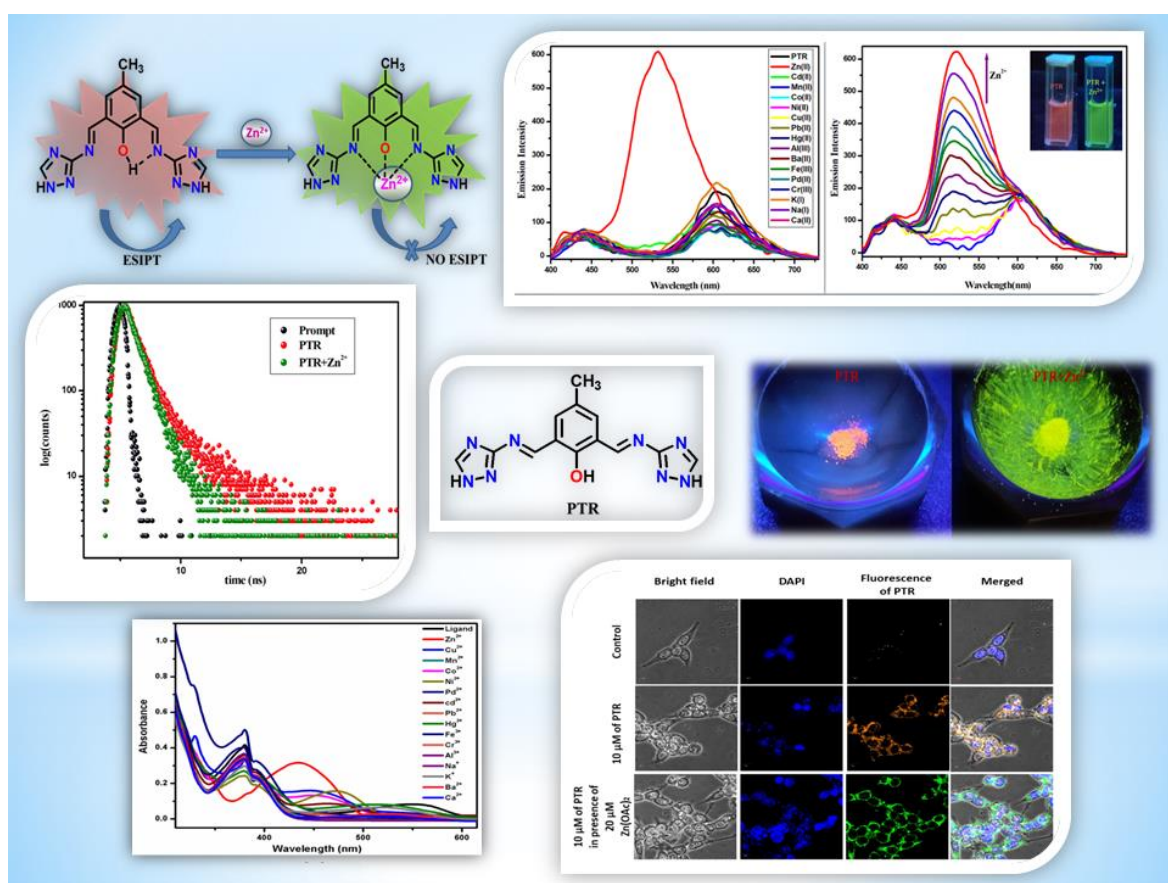
- [9]. S. Fakhri, M. Podinovskaia, X. Kong, H.L. Collins, U.E. Schaible, R.C. Hider, *J. Med. Chem.*, 51 (2008) 4539-4552.
- [10]. S. Hou, Z. Qu, K. Zhong, Y. Bian, L. Tang, *Tetrahedron Lett.*, 57 (2016) 2616.
- [11]. S. Paul, S. Maity, S. Halder, B. Dutta, S. Jana, K. Jana, C. Sinha, *Dalton Trans.*, 51 (2022) 3198.
- [12]. A.K. Adak, B. Dutta, S.A. Ali, K. Pal, K. Jana, S. Samanta, C. Sinha, *J. Indian Chem. Soc.*, 98 (2021) 100085.
- [13]. B. Dutta, R. Jana, A.K. Bhanja, P.P. Ray, C. Sinha, M.H. Mir, *Inorg. Chem.*, 58 (2019) 2686.
- [14]. R. Azadbakht, H. Veisi, H. Mohamadvand, J. Khanabadi, *Spectrochim. Acta, Part A.*, 145 (2015) 575.
- [15]. S. Zhan, H. Xu, D. Zhang, B. Xia, X. Zhan, L. Wang, J. Lv, P. Zhou, *Biosens. Bioelectron.*, 72 (2015) 95.
- [16]. L. Zhu, A.H. Younes, Z. Yuan, R.J. Clark, *J. Photochem. Photobiol., A.* 311 (2015) 1.
- [17]. L. Zhu, Z. Yuan, J.T. Simmons, K. Sreenath, *RSC Adv.*, 4 (2014) 20398.
- [18]. M.B. Maity, B. Dutta, A. Rahaman, N. Sahu, D.P. Mandal, S. Bhattacharjee, C. Sinha, *J. Mol. Struct.*, 1250 (2022) 131870.
- [19]. A.K. Adak, B. Dutta, S.K. Manna, C. Sinha, *ACS omega.*, 4 (2019) 18987.
- [20]. R. Purkait, C. Sinha, *New J. Chem.*, 43 (2019) 9815.
- [21]. G. Berthon, *Coord. Chem. Rev.*, 149 (1996) 241.
- [22]. P. Wang, J. Wu, L. Liu, P. Zhou, Y. Ge, D. Liu, W. Liu, Y. Tang, *Dalton Trans.*, 44 (2015) 18057.
- [23]. M. Wang, F. Wang, Y. Wang, W. Zhang, X. Chen, *Dyes Pigm.*, 120 (2015) 307.
- [24]. B. Das, A. Ghosh, D.P. Dorairaj, M. Dolai, R. Karvembu, S. Mabhai, H. Im, S. Dey, A. Jana, A. Misra, *J. Mol. Liq.*, 354 (2022) 118824.
- [25]. T. Liu, Q. Huang, W. Wu, T. Ren, J. Zhang, *Opt. Mater.* 130 (2022) 112568.
- [26]. S.-L. Yao, Y.-C. Xiong, X.-M. Tian, S.-J. Liu, H. Xu, T.-F. Zheng, J.-L. Chen, H.-R. Wen, *CrystEngComm.*, 23 (2021) 1898-1905.

- [27]. R.S. Eisenstein, *Annu. Rev. Nutr.*, 20 (2000) 627.
- [28]. T.A. Rouault, *Nat. Chem. Biol.*, 2 (2006) 406-414.
- [29]. D.J. Bonda, H.G. Lee, J.A. Blair, X. Zhu, G. Perry, M.A. Smith, *Metallomics*, 3 (2011) 267.
- [30]. X. Chen, X.Y. Shen, E. Guan, Y. Liu, A. Qin, J.Z. Sun, B.Z. Tang, *Chem. Commun.*, 49 (2013) 1503.
- [31]. J.B. Vincent, *Nutr. Rev.*, 58 (2000) 67.
- [32]. T. Han, X. Feng, B. Tong, J. Shi, L. Chen, J. Zhi, Y. Dong, *Chem. Commun.*, 48 (2012) 416.
- [33]. Z. Zhang, S. Lu, C. Sha, D. Xu, *Sens. Actuators B: Chem.*, 208 (2015) 258.
- [34]. A.K. Singh, V.K. Gupta, B. Gupta, *Anal. Chim. Acta*, 585 (2007) 171.
- [35]. M. Sperling, S. Xu, B. Welz, *Anal. Chem.*, 64 (1992) 3101.
- [36]. Q. Yan, Y. Wang, Z. Wang, G. Zhang, D. Shi, H. Xu, *Spectrochim. Acta A Mol. Biomol. Spectrosc.*, 279 (2022) 121384.
- [37]. Y. Chen, G. Xian, H. Yan, Y. Wang, Y. Li, J. Lu, H. Xu, J. Tao, S. Wang, *J. Solid State Chem.*, 296 (2021) 121952.
- [38]. L. Sun, X. Wang, J. Shi, S. Yang, L. Xu, *Spectrochim. Acta A Mol. Biomol. Spectrosc.*, 249 (2021) 119303.
- [39]. X. M. Li, R. R. Zhao, Y. Yang, X.W. Lv, Y. L. Wei, R. Tan, J. F. Zhang, Y. Zhou, *Chin Chem Lett.*, 28 (2017) 1258.
- [40]. J. Xue, L.-M. Tian, Z.-Y. Yang, *J. Photochem. Photobiol. A: Chem.*, 369 (2019) 77.
- [41]. G. A. Crosby, J. N. Demas, *J. Phys. Chem.*, 75 (1971) 991.
- [42]. C.S. Choi, M.K. Kim, K.S. Jeon, K.H. Lee., *J. Lumin.*, 109 (2004) 121
- [43]. C. Wende, N. Kulak, *Chem. Commun.*, 51 (2015) 12395.
- [44]. S. Paul, A. Manna, S. Goswami., *Dalton Trans.*, 44 (2015) 11805.
- [45]. M. Venkateswarulu, T. Mukherjee, S. Mukherjee, R. R. Koner., *Dalton Trans.*, 43 (2014) 5269.
- [46]. S. Goswami, K. Aich, A. K. Das, A. Manna, S. Das., *RSC Adv.*, 3 (2013) 2412.

- [47]. S. Samanta, S. Goswami, A. Ramesh, G. Das., *Sens. Actuators B: Chem.*, 194 (2014) 120.
- [48]. S Mahata, G. Janani, B. B. Mandal, V. Manivannan., *J. Photochem. Photobiol. A: Chem.*, 417 (2021) 113340.
- [49]. T. Simon, M. Shellaiah, V. Srinivasadesikan, C. C. Lin, F. H. Ko, K. W. Sun, M. C. Lin, *Sens. Actuators B: Chem.*, 231 (2016) 18.
- [50]. S. Goswami, K. Aich, S. Das, A. K. Das, D. Sarkar, S. Panja, T. K. Mondal, S. Mukhopadhyay, *Chem. Commun.*, 49 (2013) 10739.
- [51]. S. Hou, Z. Qu, K. Zhong, Y. Bian, L. Tang, *Tetrahedron Lett.*, 57 (2016) 2616.
- [52]. H. Kilic, E. Bozkurt, *J. Photochem, Photobiol. A: Chem.*, 363 (2018) 23.
- [53]. S. Paul, S. Dey, K. Pal, S. Maity, K. Jana, C. Sinha, *ChemistrySelect*. 5 (2020) 15233.
- [54]. S. Dey, R. Purkait, K. Pal, K. Jana, C. Sinha., *ACS Omega*, 4 (2019) 8451.

Chapter IV

Use of Diformyl-triazolo Schiff base for Zn²⁺ Sensing and intracellular Live Cell Imaging



CHAPTER IV

Abstract

A diformylphenol Schiff base of triazole-amine, 4-Methyl-2, 6-bis-[(1H-[1,2,4] triazol-3-ylimino)-methyl]-phenol (**PTR**) has been synthesized and characterised by spectroscopic data (ESI-MS, UV-Vis, FT-IR, NMR spectra). The probe, **PTR**, emits at 610 nm upon excitation at 380 nm and the emission is strongly intensified on interacting with Zn^{2+} ion in DMSO-water (99:1,v/v; HEPES buffer, pH, 7.2) solution even in presence of fifteen other cations (Cu^{2+} , Mn^{2+} , Co^{2+} , Ni^{2+} , Pd^{2+} , Cd^{2+} , Pb^{2+} , Hg^{2+} , Fe^{3+} , Cr^{3+} , Al^{3+} , Na^+ , K^+ , Ba^{2+} , Ca^{2+}) and the emission band has been shifted to 530 nm. The limit of detection of Zn^{2+} , 0.30 μM is much lower than WHO recommended value (76 μM). The binding constant (K_d) is $4.2585 \times 10^4 \text{ M}^{-1}$. Selective and sensitive chemosensing behaviour of **PTR** to Zn^{2+} has been explained by switching off ESIPT quenching of the keto-enol tautomerisation of the probe along with the chelation enhancement of fluorescence (CHEF) by binding with Zn^{2+} . The Job's plot and NMR titration have been extended to measure the 1:1 molar composition [**PTR**+ Zn^{2+}]. The energy calculation by the DFT computation of keto and enol isomers supports easy tautomerisation and helps ESIPT quenching by proton transfer. Intracellular Zn^{2+} ions in living cells of HEK293 (PBS: Phosphate Buffer Saline, pH-7.2) have also been identified by the probe, **PTR**, using fluorescence microscopic imaging technique.

IV.1. Introduction

Zinc is a useful element in the progress of civilization since ancient times. Zn (II) is second most abundant micronutrient (1st is Iron) and plays a vital role in the growth and development of the human body. It regulates neural signal transmission [1], immune function [2], mammalian reproduction and others [3–5]. The deficiency of Zn^{2+} ions cause severe harmful effect on eye, skin and the excessive presence of it causes Parkinson's [6-8], Alzheimer's [9-10] and many other diseases. Although Zn^{2+} (d^{10}) is redox innocent but its structural integrity, cooperation to other ions, structural flexibility, easy participation in substitution reaction etc. contributes key function towards large number of enzyme catalyses [11,12]. Therefore, the analytical detection of Zinc is an important task for sustainable health maintenance planning. There are several quantitative techniques such as gravimetric, volumetric, electroanalytical, spectroscopic etc. The simplest, easiest, selective and sensitive method of ion/molecule detection is the fluorometric method [13-17]. Several probes are reported for the detection of Zn^{2+} ion [18-24], and the working principle involves different mechanism [25-40] like CHEF, FRET, ICT, for enhancement of emission.

Last several years, the research endeavour from our group is focused on the design of fluorogenic sensors to improve quality of emission and simplify the measurement protocol [41-50]. In this work, we have designed a Schiff base probe, 4-Methyl-2, 6-bis-[(1H-[1,2,4] triazol-3-ylimino)-methyl]-phenol (**PTR**), from 4-methyl-2, 6-diformylphenol and 3-amino-1, 2, 4-triazole which detects selectively Zn^{2+} ion both in solution and solid phase by colorimetric and fluorometric routes. The fluorometric measurement in solution phase is carried out in DMSO-water (99:1, v/v; HEPES buffer, pH, 7.2) due to sparing solubility of the probe, **PTR**, in aqueous medium and the plausible mechanism is explained by switching off ESIPT of the probe and the chelation enhancement of fluorescence (CHEF) on selective binding with Zn^{2+} ion. The

limit of detection is 0.30 μM towards Zn²⁺ ion and the emission does not perturb even in presence of many competitive ions. Intracellular Zn²⁺ ions in living cells of HEK293 cell line is also identified by the fluorescence imaging of **PTR** and it shows a significant effect on the cell lines.

IV.2. Experimental Section

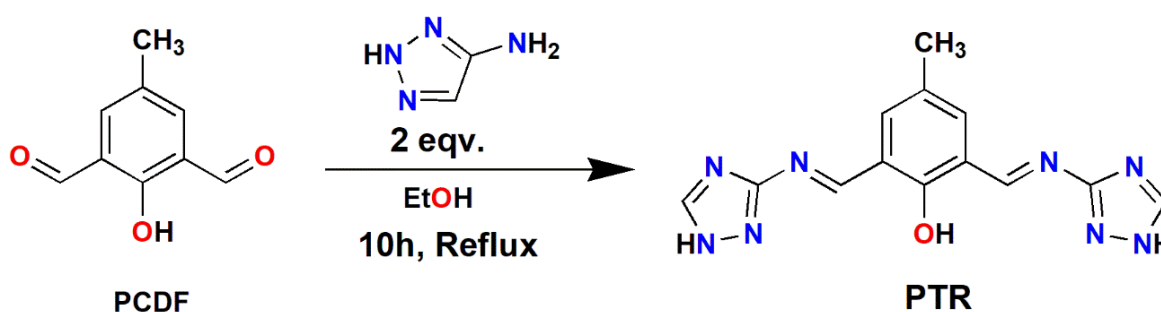
IV.2.1. Chemicals and testing equipment

All the required chemicals including 3-Amino-1, 2, 4-triazole and solvents were purchased from the local commercial source and 4-methyl-2, 6-diformylphenol (PCDF) was synthesized from *p*-cresol. HEK293 (human embryonic kidney) cell line (NCCS Pune, India) used in this work. Penicillin streptomycin neomycin (PSN) antibiotic, fetal bovine serum (FBS), trypsin, di-sodium ethylene diamine tetraacetic acid (Na₂EDTA) and Dulbecco's Modified Eagle Medium (DMEM) were collected from Gibco BRL (Grand Island, NY, USA). Tissue culture plastic wares (NUNC, Roskilde, Denmark) and 3-(4, 5-dimethylthiazol- 2-yl)-2, 5-diphenyltetrazolium bromide (MTT) (SRL, India) were used in this research.

Perkin Elmer Lambda 25 spectrophotometer was used to record the UV-Visible spectroscopy data. Fluorescence was measured by the Perkin Elmer LS55 fluorescence spectrophotometer with the slit 10/10 and excitation wavelength of 380 nm. Perkin Elmer RX-1 spectrophotometer (4000–400 cm⁻¹) was used to collect the IR data. NMR spectra was recorded from the Bruker 300 MHz NMR spectrometer with TMS as internal standard in DMSO-d₆ and the mass spectrum data was collected from water ESI-MS model XEVO-G2QTOF#YCA351 spectrometer. Life time values were evaluated using the Horiba Jobin Yvon fluorescence spectrophotometer. Gaussian 09W was used to calculate the band gap electronic transition, transition state etc.

IV.2.2. Synthesis of PTR

4-Methyl-2,6-diformylphenol (PCDF) was synthesized by slight modification of the published procedure [51]. To ethanol solution (10 ml) of PCDF (1 mmol, 0.164 g) a solution of 3-amino-1,2,4-triazole (0.168 g, 2 mmol) was added followed by the addition of two drops of acetic acid stirred the solution for 10 min and then the resulting solution was refluxed for 10 h. The solution was then cooled to room temperature and evaporated in air to dryness (**Scheme IV.a**). A yellowish orange coloured solid was collected and washed with hot hexane solution. After that the crude product was vacuum-dried to obtain the yellowish orange solid **PTR** (0.189 g, yield 64%).



Scheme IV.a. Synthetic route of Schiff base **PTR** using 4-methyl-2,6-diformyl phenol (PCDF) and 3-Amino-1,2,4-triazole.

ESI-MS spectrum of **PTR** : Calcd for C₁₃H₁₂N₈O [M+Na]⁺ 319.10 ; found 319.04 (**Fig.IV.1**); IR data, $\bar{\nu}$ (cm⁻¹) 3116 ν (O-H), 2923 ν (N-H), 2774 ν (C-H) 1621 ν (C=N), 1156 ν (C-O) (**Fig.IV.2**); ¹H NMR spectrum (d₆-DMSO, 300MHz) (ppm) δ : 14.34 (s, 2H), 13.74 (s, 1H), 9.52 (s, 2H), 8.59 (s, 2H), 7.95 (s, 2H), 2.37 (s, 3H) (**Fig.IV.3**). ¹³C NMR spectrum (d₆-DMSO, 75 MHz) δ (ppm):165, 161, 140, 137, 129, 123, 120, 20 (**Fig.IV.4**).

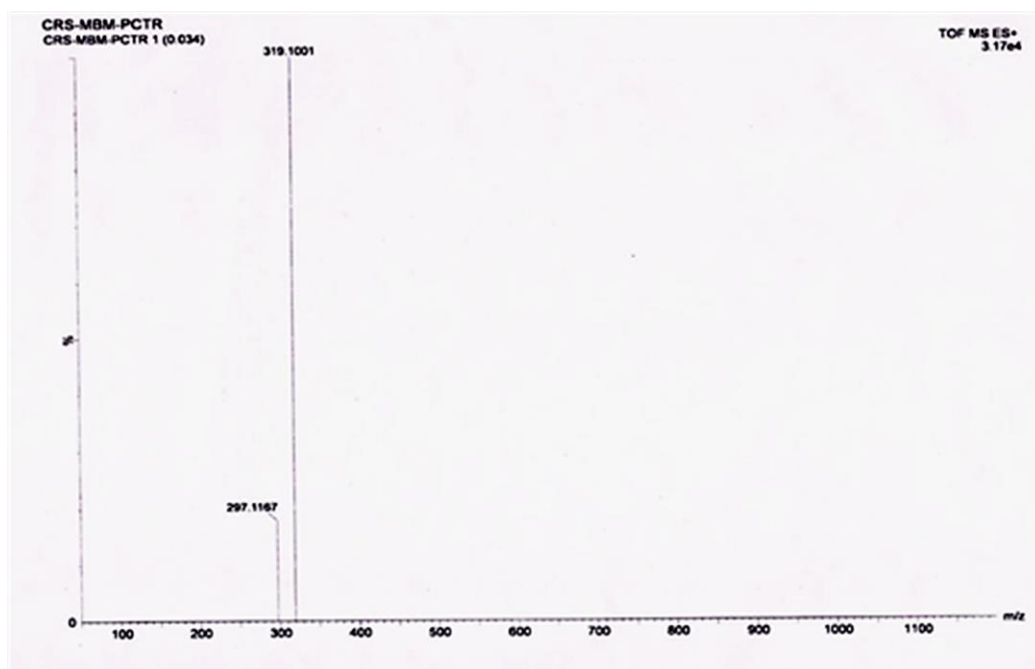


Fig.IV.1. Mass spectrum of the probe PTR.

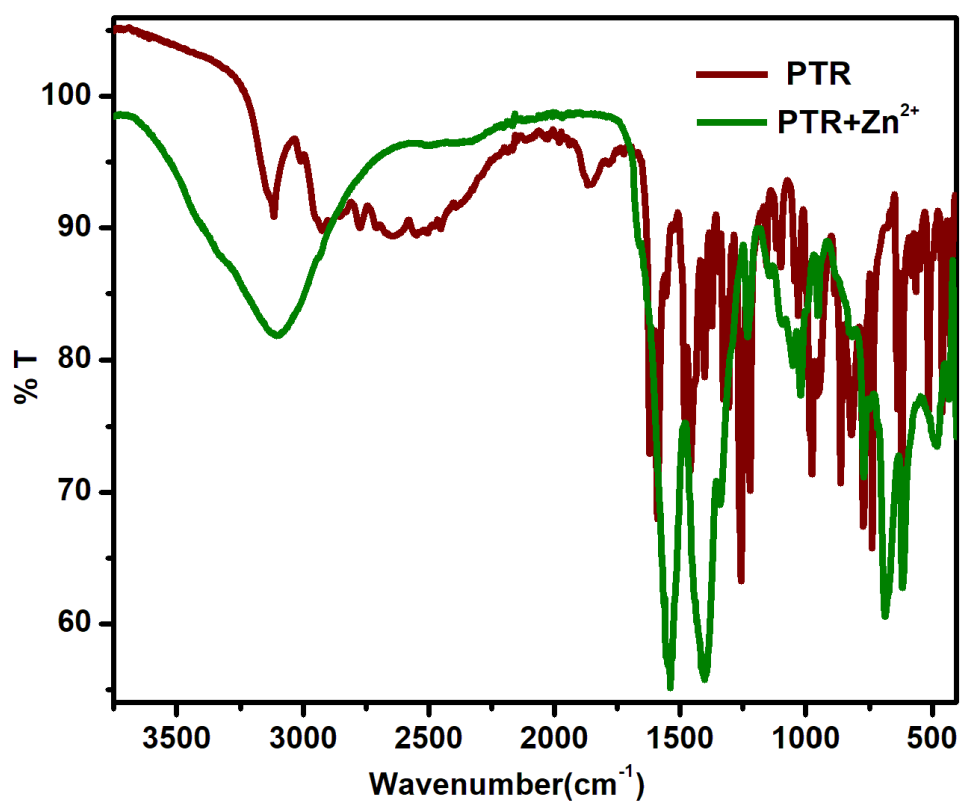


Fig.IV.2. IR spectra of PTR and PTR+ Zn^{2+} .

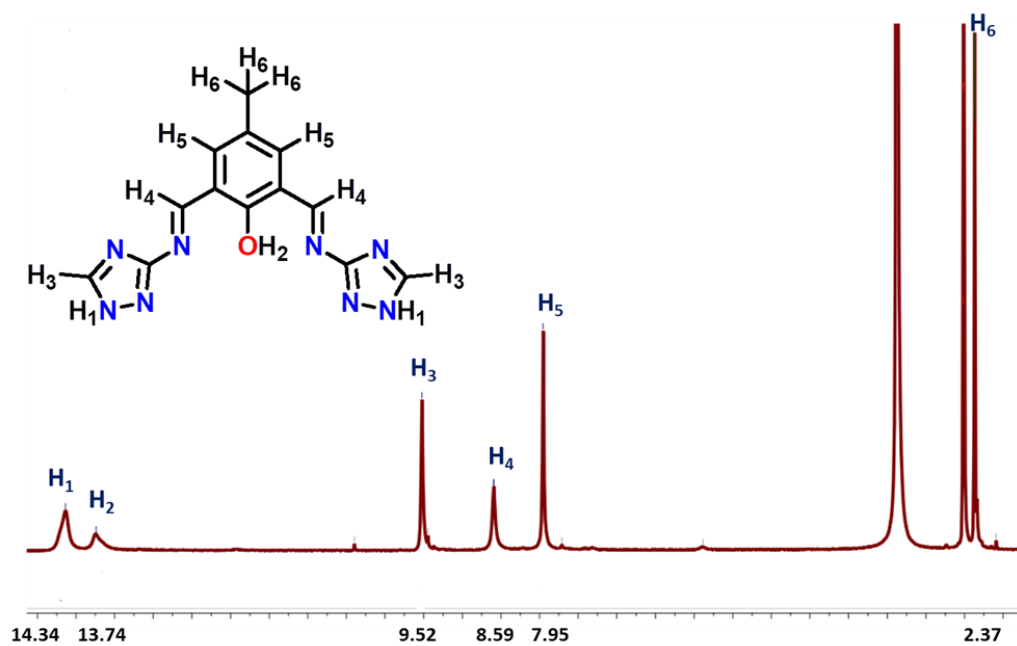


Fig.IV.3. ¹H NMR (300 MHz) spectra of probe PTR in d₆-DMSO.

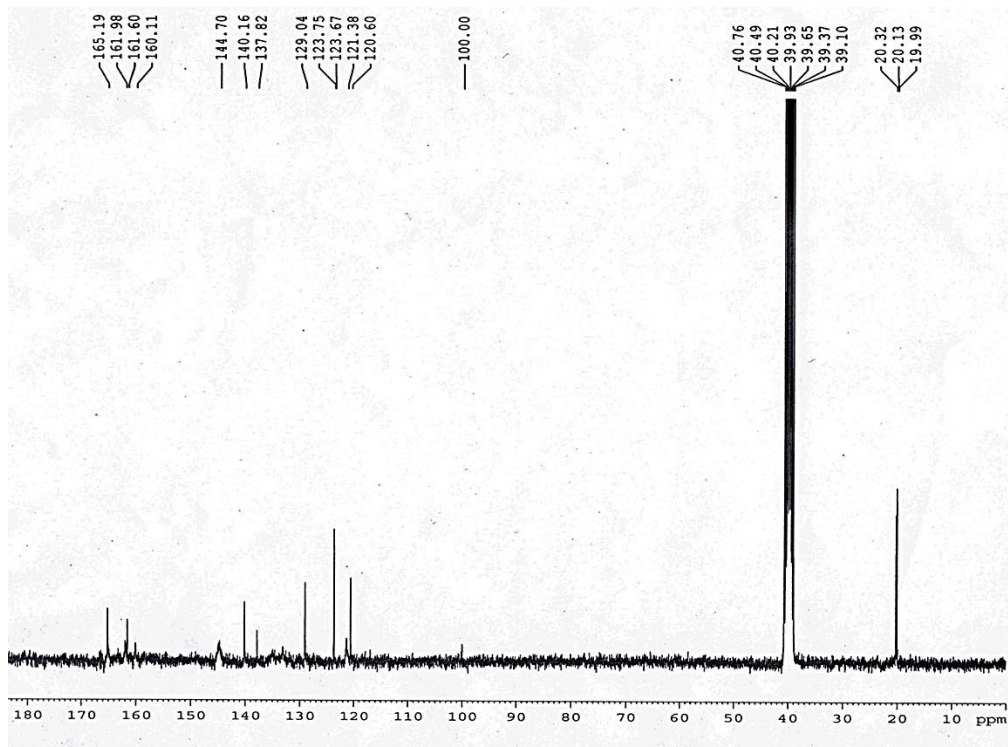


Fig.IV.4. ¹³C NMR (75 MHz) spectra of the probe PTR in d₆-DMSO.

IV.2.3. Sensing Experiment

The stock solution of **PTR** (10^{-3} M) was prepared in DMSO and the solution was diluted with DMSO-water in (99:1, v/v; HEPES buffer, pH, 7.2) to make solution of strength 25 μ M and this solution was used in the entire fluorescence and UV-visible spectroscopic experiments. The metal salts such as: $FeCl_3 \cdot 6H_2O$, $Al(NO_3)_3 \cdot 9H_2O$, $CrCl_3 \cdot 6H_2O$, $NiCl_2 \cdot 6H_2O$, $Cd(OAc)_2 \cdot 2H_2O$, $CaCl_2 \cdot 6H_2O$, $Zn(OAc)_2 \cdot 2H_2O$, $Hg(OAc)_2$, $Cu(OAc)_2 \cdot H_2O$, $NaCl$, $Co(NO_3)_2 \cdot 6H_2O$, $PdCl_2$, $Pb(NO_3)_2$, $MnCl_2 \cdot 4H_2O$, $BaCl_2 \cdot 2H_2O$, KBr were used for experiment in MilliQ water. The stock solution (1×10^{-3} M) of different metal ions were prepared and was used in the entire fluorescence and UV-visible spectroscopic experiments. The excitation wavelength was 380 nm. For the spectral titration of **PTR** probe, the Zn^{2+} solution (3 μ L added Zn^{2+} in every step) was added and the emission wavelength and intensity were recorded. The interference effect of different metal ions towards the sensing of Zn^{2+} by **PTR** probe were assessed by the bar plot. The composition of the **PTR-Zn²⁺** was assessed by Job's plot. Limit of detection (LOD) was evaluated by the $3\sigma/M$ method (M is the slope and σ is standard deviation). Effect of pH (2-12) on emission of **PTR** and **PTR-Zn²⁺** was examined. Binding constant (K_d) was calculated using the Benesi-Hildebrand plot $1/\Delta I = 1/\Delta I_{max} + (1/K_a[C])(1/\Delta I_{max})$. Herein, $\Delta I = I - I_0$ and $\Delta I_{max} = I_{max} - I_0$, where I_0 , I and I_{max} are the fluorescence intensities of probe **PTR** measured in the absence of Zn^{2+} , at an intermediate Zn^{2+} concentration and at a concentration of complete saturation, respectively. Binding constant is K_d and concentration of Zn^{2+} denoted by $[C]$. K_d value calculated from the slope and intercept of $\{1 / (I - I_0)\}$ against $1/[C]$ plot. The mass spectra of mixture of **PTR+Zn²⁺** was examined to assess the composition of the emissive complex.

IV.2.4. MTT assay

The cell viability was checked by MTT assay technique [52]. The HEK293 cells were placed in 96 well plates and treated with different concentrations (0, 10, 20, 30, 40, 50, 60, 70, 80, 90

and 100 μ M) of **PTR** for 24 h. Four hours after the addition of MTT, formazan was solubilised with acidic isopropanol and the absorbance of the solution was measured at 595 nm using ELISA (enzyme-linked immunosorbent assay) reader. The DMSO treated data was also taken and subtracted from the PTR treated optical density value.

IV.2.5. Confocal Microscopy

Intracellular Zn^{2+} ions in HEK293 could not be detected unless the probe, **PTR** [53] was added. To Zn^{2+} solution (20 μ M) in HEPES buffer (pH, 7.4) of HEK293 cell lines the incubation was allowed for 45 min and then washed with buffer of pH 7.4 and mounted on a grease free glass slide by adding paraformaldehyde (4% solution) as fixative agent. The confocal laser-scanning microscope (FV 10i, Olympus, Japan) was used for cell imaging before and after addition of **PTR** (10 μ M) in the buffer medium.

IV.2.6. Statistical analysis

OriginPro version 8.0, a statistical software, was used for the data analysis. The statistical significance values were evaluated through one-way ANOVA analysis. The critical significance level was set at $p < 0.05$. The values were represented as mean values with their standard errors (mean \pm SEM).

IV.3. Results and discussion

IV.3.1. Absorption and Emission Spectroscopic Measurements

The probe, **PTR** responses prominently in the UV-Visible spectrophotometric measurement in DMSO-water (99:1, v/v; HEPES buffer, pH, 7.2) medium with two bands at 380 nm and 550 nm. Upon addition of aqueous solution of different cations (Cu^{2+} , Zn^{2+} , Mn^{2+} , Co^{2+} , Ni^{2+} , Pd^{2+} , Cd^{2+} , Pb^{2+} , Hg^{2+} , Fe^{3+} , Cr^{3+} , Al^{3+} , Na^{+} , K^{+} , Ba^{2+} , Ca^{2+}) no significant absorption change either in naked eye or in spectral behaviour is noted other than Zn^{2+} ion. Appearance of a new band

absorption peak at 435 nm (**Fig.IV.5**) upon addition of Zn^{2+} ion proves high specificity and selectivity to it.

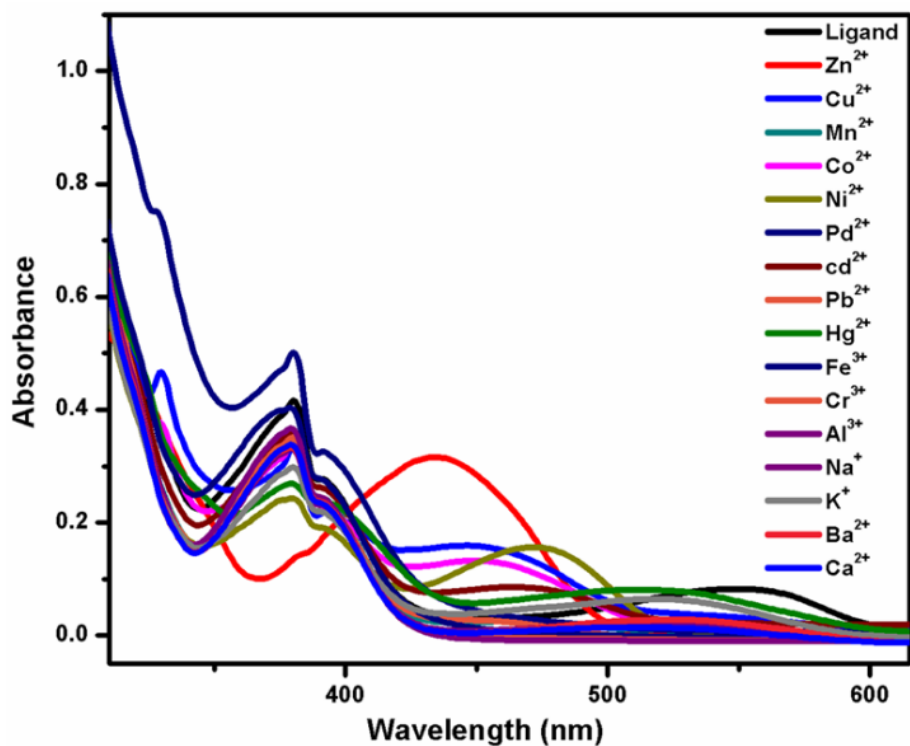


Fig.IV.5. UV-vis absorption spectra of **PTR** (25 μ M) with various cations in DMSO-water (99:1, v/v; HEPES buffer, pH, 7.2) medium.

The UV-vis spectroscopic titration of the probe, **PTR** was carried out upon incremental (3 μ L of Zn^{2+} in every time) addition of Zn^{2+} ion in DMSO-water (99:1, v/v; HEPES buffer, pH, 7.2). The observation shows a decrease in absorbance intensity at 380 nm and increase the same at 435 nm (**Fig.IV.6**) which indicates the interaction of **PTR** with the Zn^{2+} ion.

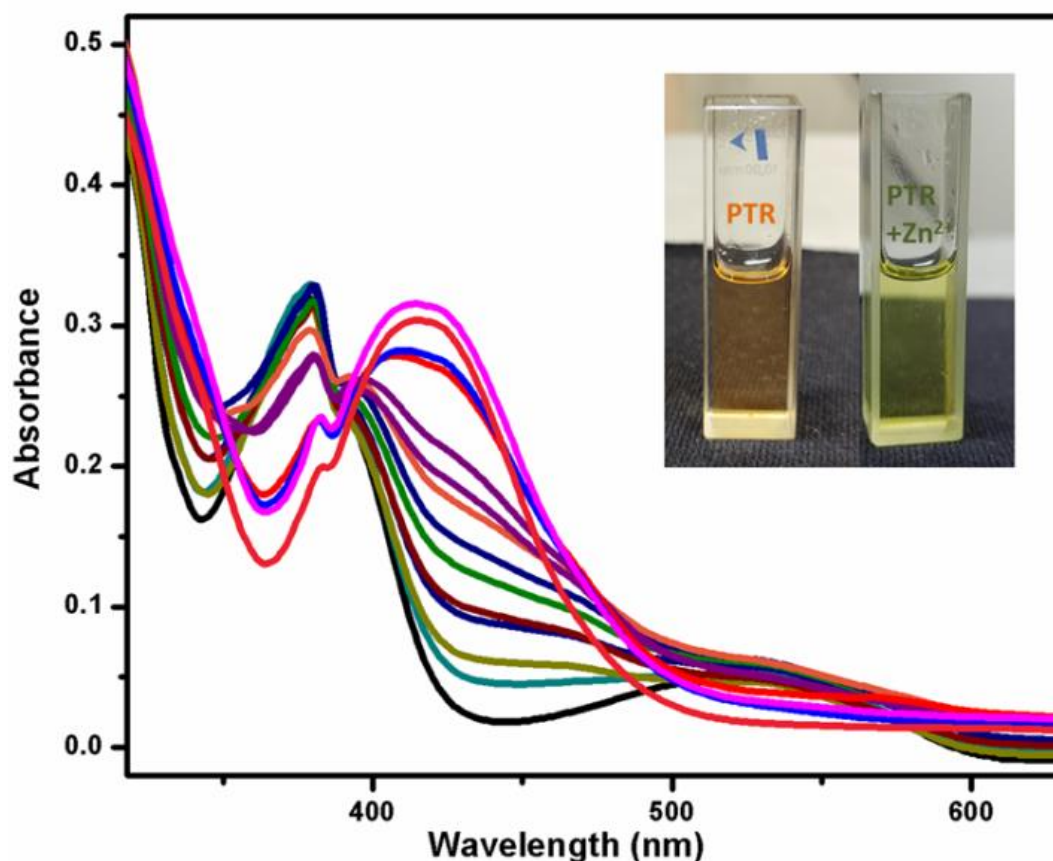


Fig.IV.6. UV-vis titration of **PTR** (25 μM) upon incremental (3 μL of Zn^{2+} in every time) addition of Zn^{2+} ion in DMSO-water (99:1, v/v; HEPES buffer, pH, 7.2) medium.

The specific reaction of Zn^{2+} with the **PTR** was also examined using the fluorescence spectra on exciting at 380 nm. The probe **PTR** exhibits main emission at 610 nm with a weak band at 440 nm. In the presence of Zn^{2+} the emission intensity at 610 nm is shifted to the shorter wavelength, 530 nm, with the significant enhancement of emission intensity (**Fig.IV.7**) but in presence of other metal ions (like Na^+ , K^+ , Ca^{2+} , Ba^{2+} , Fe^{3+} , Cr^{3+} , Al^{3+} , Mn^{2+} , Co^{2+} , Ni^{2+} , Cu^{2+} , Cd^{2+} , Hg^{2+} , Pd^{2+} , Pb^{2+}) no such change in emission intensity is noted.

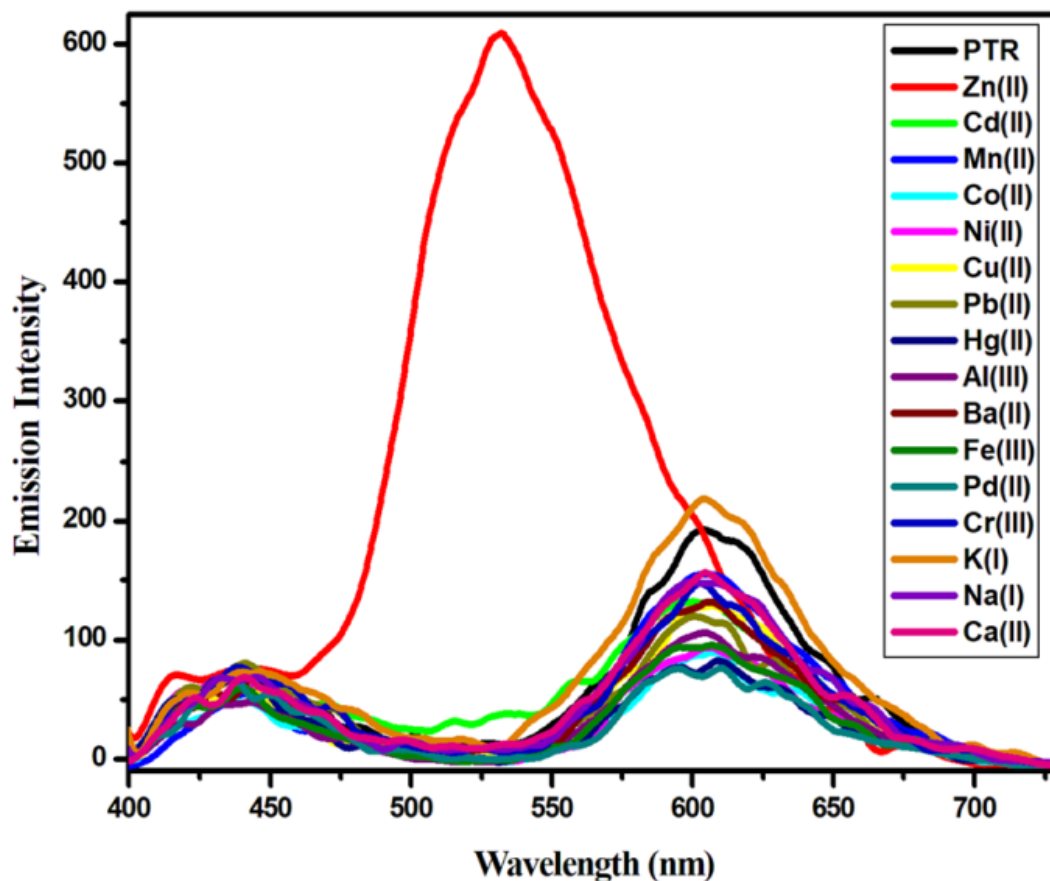


Fig.IV.7. Emission spectra of the probe **PTR** (25 μ M) in presence of different metal ions upon excitation at 380 nm in DMSO-water (99:1, v/v; HEPES buffer, pH, 7.2) medium.

The fluorescence titration of **PTR** with incremental addition (3 μ L Zn^{2+} in every time) of Zn^{2+} has been carried out. The emission intensity gradually increases with the blue shifting (**Fig.IV.8**) of emission wavelength.

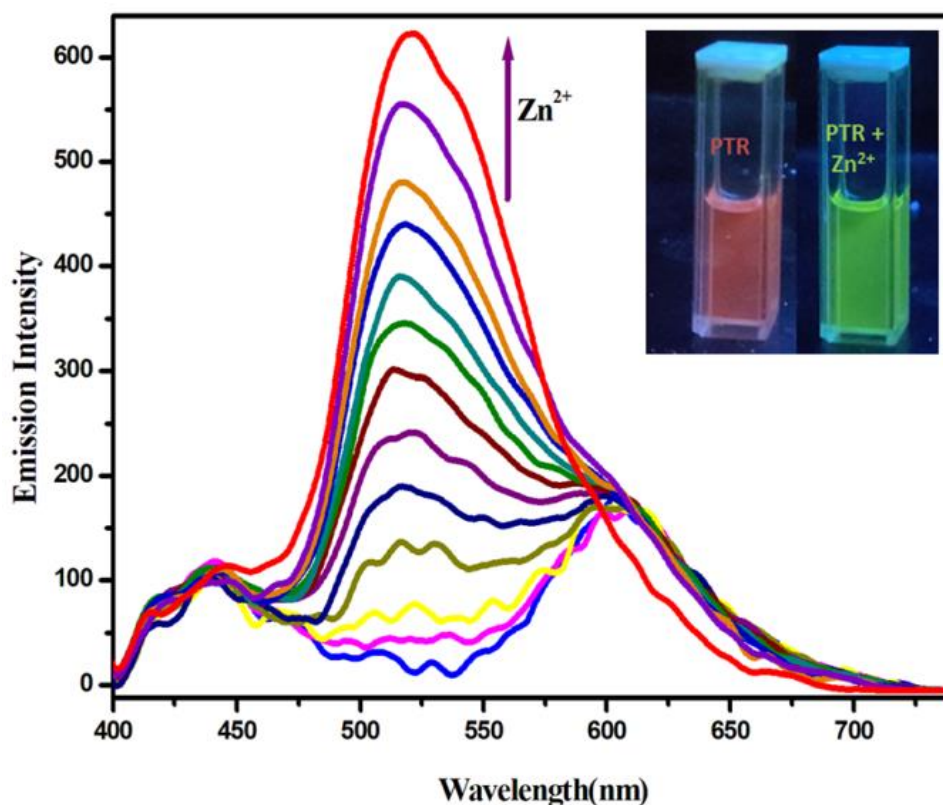


Fig.IV.8. Fluorescence titration of PTR (25 μM) upon incremental (3 μL of Zn^{2+} in every time) addition of Zn^{2+} ion and excitation is performed at 380 nm in DMSO-water (99:1, v/v; HEPES buffer, pH, 7.2) medium.

The Limit of detection (LOD) value has been evaluated by using $3\sigma/M$ method (σ : standard deviation) = 4.101 and M (slope) = 3.533×10^7 in DMSO-water (99:1, v/v; HEPES buffer, pH, 7.2)) and it is 0.30 μM (**Fig.IV.9**) which is much lower than the WHO recommended threshold value (76 μM) of Zn^{2+} ion in drinking water.

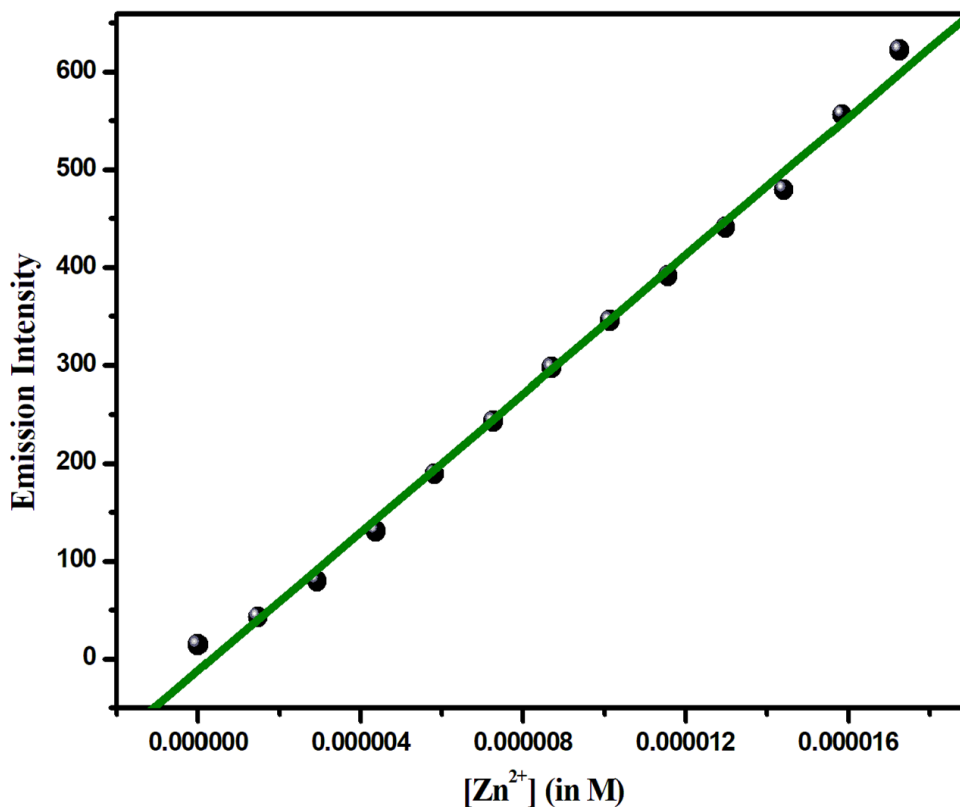


Fig.IV.9. Limit of detection (LOD) plot of Zn^{2+} binding with **PTR** in DMSO-water (99:1, v/v; HEPES buffer, pH, 7.2)

The effect of acidity (pH, 2-11) was examined on the emission intensity of **PTR** and **PTR+Zn²⁺** complex (**Fig.IV.10**). At pH 7 the probe, **PTR** shows high emission intensity but upon lowering the pH (6 to 2) the emission intensity of the probe gradually decreases. In the alkaline range (8 to 11) emission intensity also decreases after that the intensity slightly increase. The fluorescence sensing efficiency of the probe towards Zn^{2+} is found better at the pH range 6 to 8 (**Fig.IV.10**).

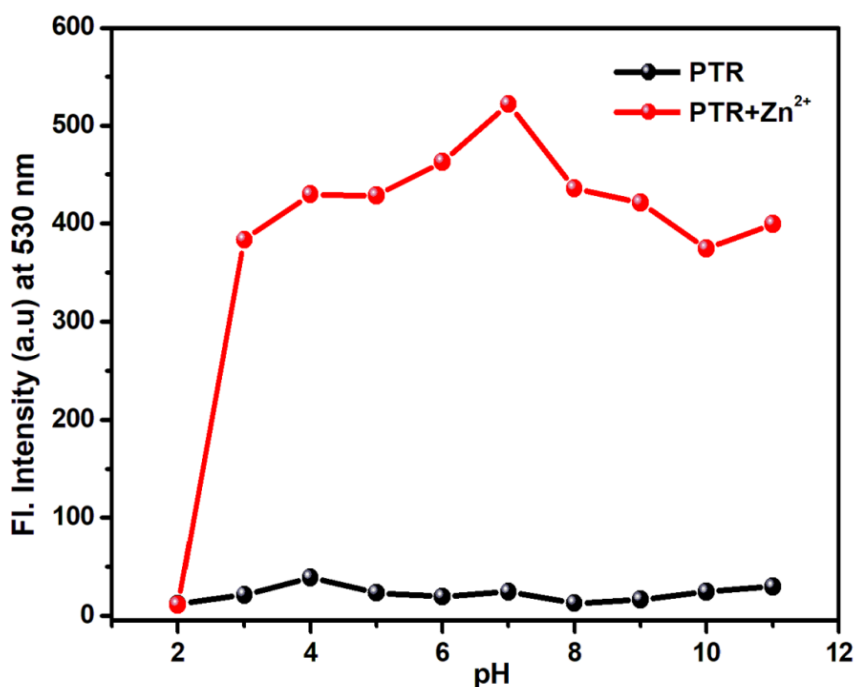
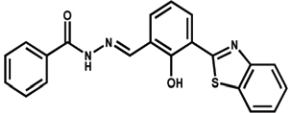
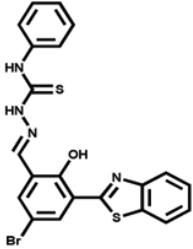
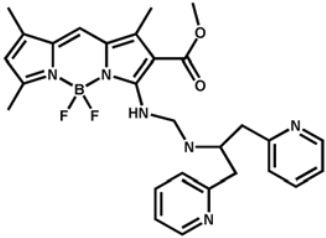
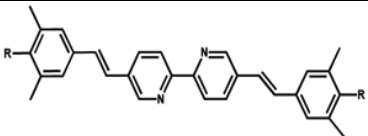
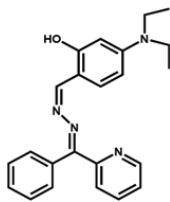
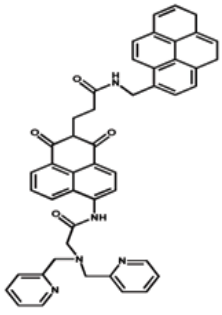
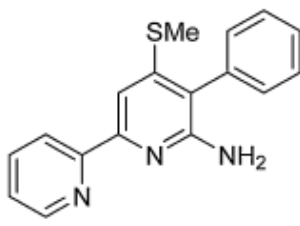
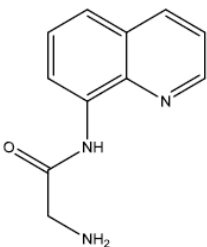
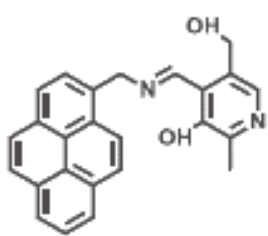
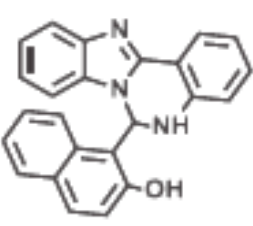


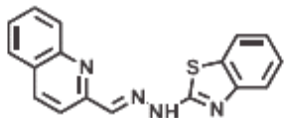
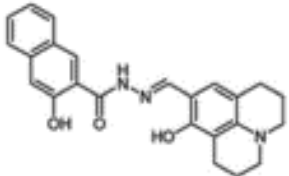
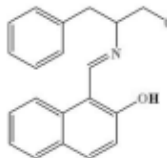
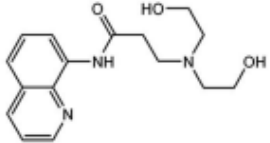
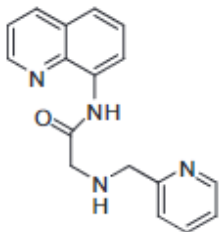
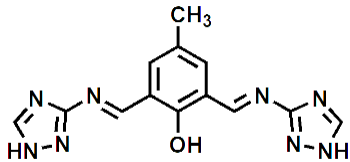
Fig.IV.10. Change in emission intensity of **PTR** and Zn²⁺-PTR complex with different pH value.

The probe, **PTR** shows a significant detecting ability compared to some recently published articles (**Table IV.1**).

Table IV.1. Correlation table of different parameters of some recently published work.

Probe	Solvent	LOD (M)	Reference
	MeOH : H ₂ O (1 : 1, v/v, 10 mM HEPES buffer, pH = 7.2)	1.6×10^{-7}	[54]
	MeOH:H ₂ O (3 : 2, v/v, 25 mM HEPES buffer, pH = 7.4)	3.77×10^{-8}	[55]
	CH ₃ CN : H ₂ O (1 : 1, v/v, 0.02 M HEPES, pH = 7)	No data	[56]

Probe	Solvent	LOD (M)	Reference
	MeOH : H ₂ O (1 : 1, v/v, 50 mM HEPES buffer, pH = 7.4)	$\sim 5 \times 10^{-8}$	[57]
	CH ₃ CN : H ₂ O (1/1, v/v, 10 mM HEPES buffer, pH = 7.4)	No data	[58]
	MSO : H ₂ O (1 : 9, v/v, 10 mM HEPES buffer, pH = 7.4)	1.05×10^{-8}	[59]
	HEPES buffer (100 mM, 5% DMSO, pH = 7.4).	5.0×10^{-6} M	[60]
	Tris-HCl aqueous buffer pH 7.4 solution containing methanol (1% v/v)	1.6×10^{-6} M	[61]
	50 μL H ₂ O, 1950 μL DMSO	2.34×10^{-6} M	[62]
	CH ₃ OH/H ₂ O (8: 2 v/v)	5.59×10^{-6} M	[63]

Probe	Solvent	LOD (M)	Reference
	EtOH/HEPES (4: 1 v/v)	2.23 x 10 ⁻⁶ M	[64]
	bis-tris buffer– DMF (1 : 1, v/v, 10mM, pH 7.0) Solution	3.3 x 10 ⁻⁶ M	[65]
	10 mM HEPES aqueous buffer– CH3OH (3 : 2, v/v)	10 x 10 ⁻⁶ M	[66]
	bis-tris buffer solution (10mM, pH 7.0)	4.48 x 10 ⁻⁶ M	[67]
	HEPES buffer (20 mM, pH 7.4)	3.2 x 10 ⁻⁶ M	[68]
	DMSO-water (99:1,v/v; HEPES buffer, pH, 7.2)	3 x 10 ⁻⁷	This work

The stability of the probe **PTR** and **PTR+Zn²⁺** complex in excited state were evaluated by using the life time plot at 380 nm and 435 nm excitation wavelength, respectively. The result shows that the life time of **PTR** (1.08 ns) is slightly longer than **PTR+Zn²⁺** (0.97 ns) (**Fig.IV.11**).

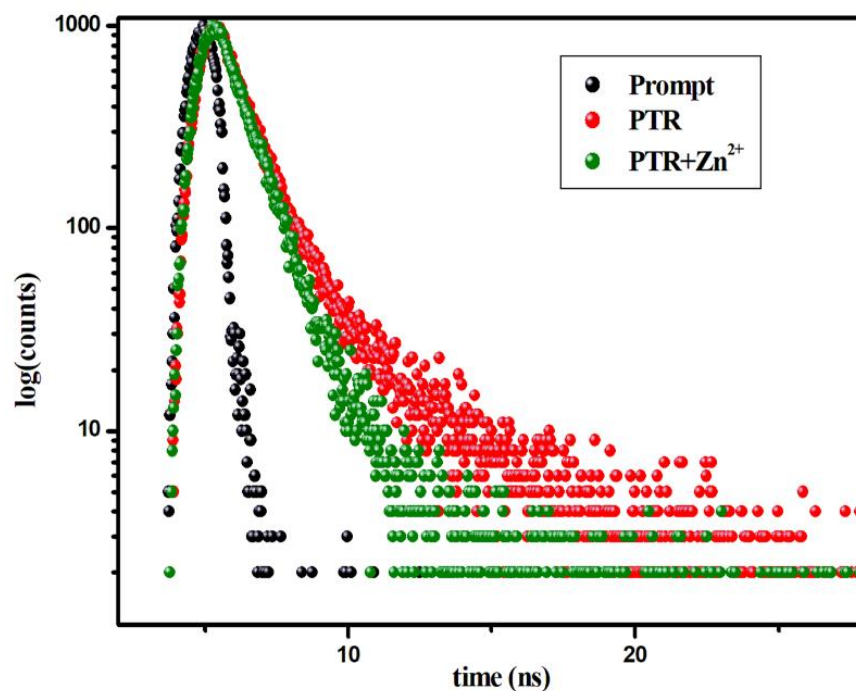


Fig.IV.11. The life time plot for the probe PTR and PTR with the addition of Zn^{2+} in DMSO-water (99:1,v/v; HEPES buffer, pH, 7.2).

IV.3.2. Solid state study

The probe, **PTR** is grinded with $Zn(OAc)_2$ to prepare PTR- Zn^{2+} complex in solid state. After the grinding the colour of the probe changes from orange to green in naked eye as well as in UV chamber (**Fig.IV.12**).

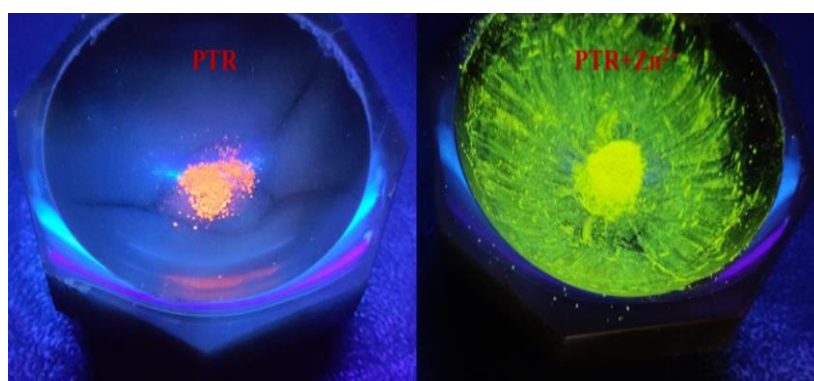


Fig.IV.12. The solid state colour change in UV chamber of the probe **PTR** after the grinding with $Zn(OAc)_2$.

In the solid state, the probe, **PTR** shows an orange emission at 610 nm and it exhibits green emission at 520 nm in presence of Zn^{2+} . This significant and distinguishable solid-state emission (**Fig.IV.13**) of the probe **PTR** and the **PTR- Zn^{2+}** complex makes the probe more effective towards the detection of Zn^{2+} ion in naked eye.

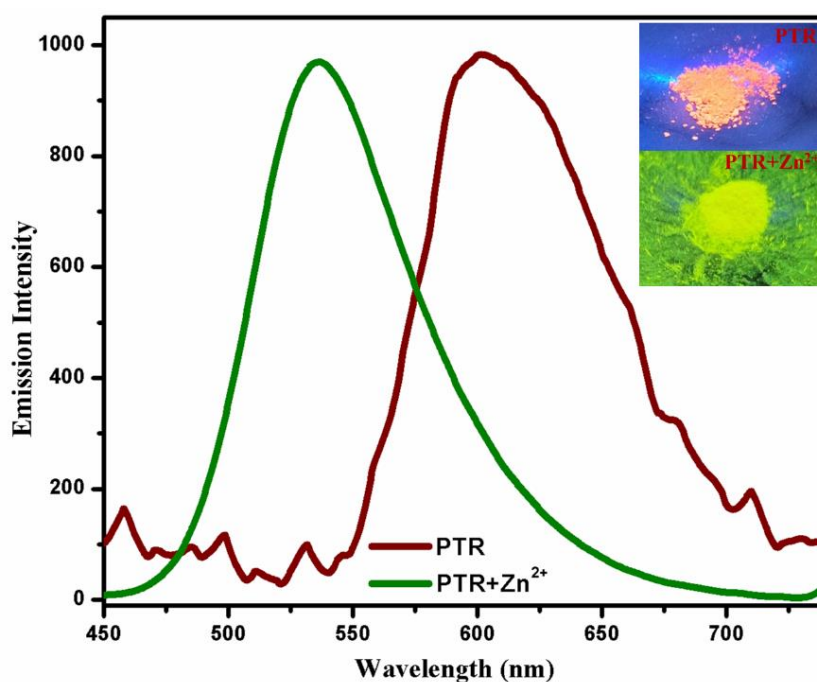
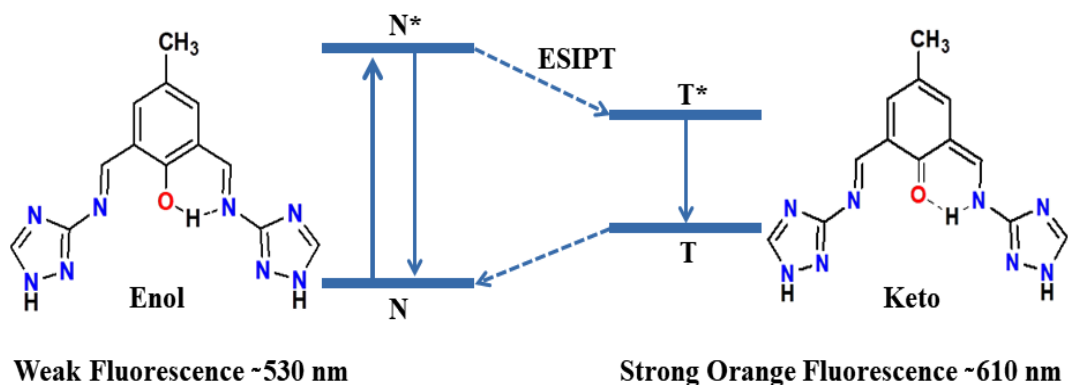


Fig.IV.13. The solid state emission spectra of the probe **PTR** and **PTR + Zn^{2+}** complex.

The addition of Zn^{2+} ion to the solution of probe, **PTR** changes the colour from orange to green (**Fig.IV.8**). The blue shifting of band (610 nm \rightarrow 530 nm) may be explained on considering the switching off the ESIPT process between keto and enol isomers of **PTR** (**Scheme IV.b**) and also enhancement due to CHEF process via chelation with Zn^{2+} . Upon excitation of the probe, **PTR** at 380 nm the weak emission at 440 nm shows normal stokes shift (60 nm) and strong emission at 610 nm shows larger stokes shift (230 nm) which clearly supports the ESIPT mechanism [69,70]. On addition of Zn^{2+} to the solution of **PTR** the emission intensity is enhanced and has shifted to 530 nm which is assumed that the emission arises from enol group because enol may form complex on deprotonation of -OH group. Rigidity of the probe has been

increased due to the formation of **PTR- Zn^{2+}** complex which can be explained by the chelation-enhancement of fluorescence (CHEF) mechanism.



Scheme IV.b. ES IPT mechanism of quenching of the probe, **PTR**.

The interference study in presence of different competitive metal ion has been examined (**Fig.IV.14**) in presence of Zn^{2+} ion. It can be shown that no such metal ion interferes to the Zn^{2+} ion sensing.

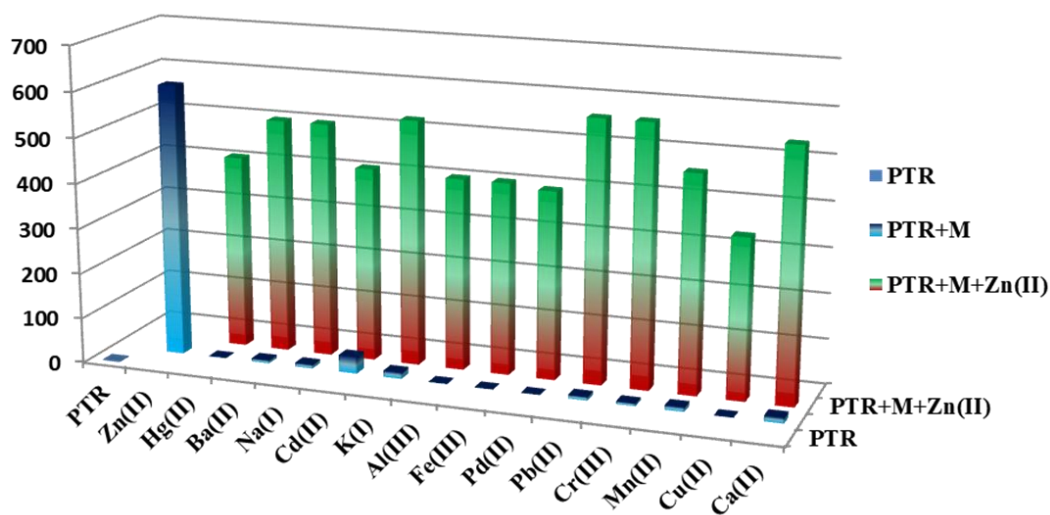


Fig.IV.14. Competitive study of **PTR** towards Zn^{2+} ion sensing in presence of different metal ions in DMSO-water (99:1, v/v; HEPES buffer, pH, 7.2)

IV.3.3. Binding mechanism of PTR towards Zn^{2+}

The stoichiometry of complexation between probe, **PTR** and Zn^{2+} has been examined by Job's plot (**Fig.IV.15**) and the result shows the 1:1 molar stoichiometry between the probe **PTR** and Zn^{2+} ion.

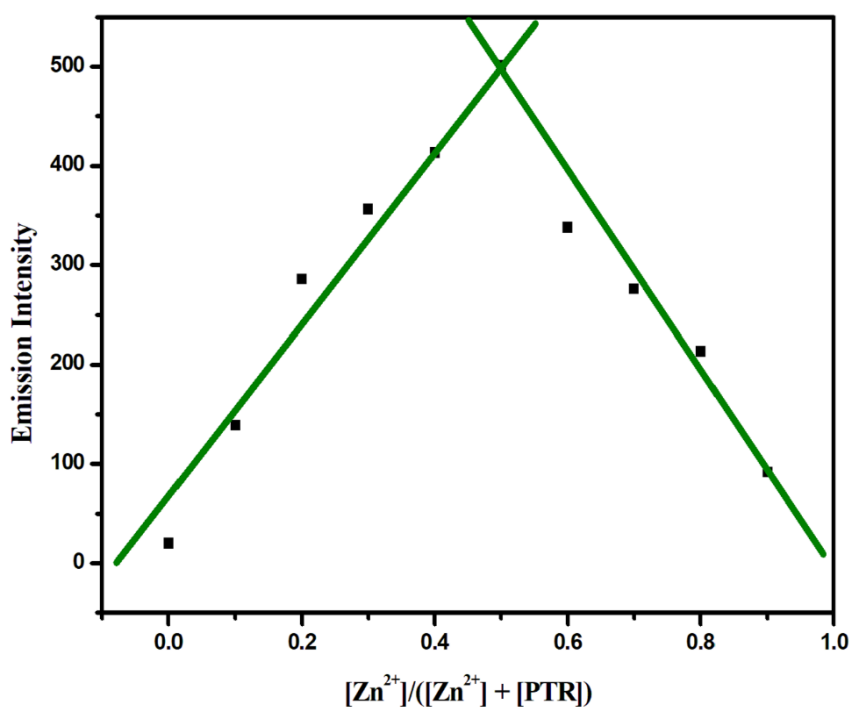


Fig.IV.15. Job's plot of the probe **PTR** binding with Zn^{2+} in DMSO-water (99:1, v/v; HEPES buffer, pH, 7.2)

The mass spectrum of **PTR** in presence Zn^{2+} ion also supports the composition. The calculated mass is $[PTR+Zn^{2+}+Na]^+ = 413.04$ and observed mass is 412.93 (**Fig.IV.16**); which supports the composition of the complex as $[Zn (PTR)(OCH_3)]$ (where **PTR** = discussed probe).

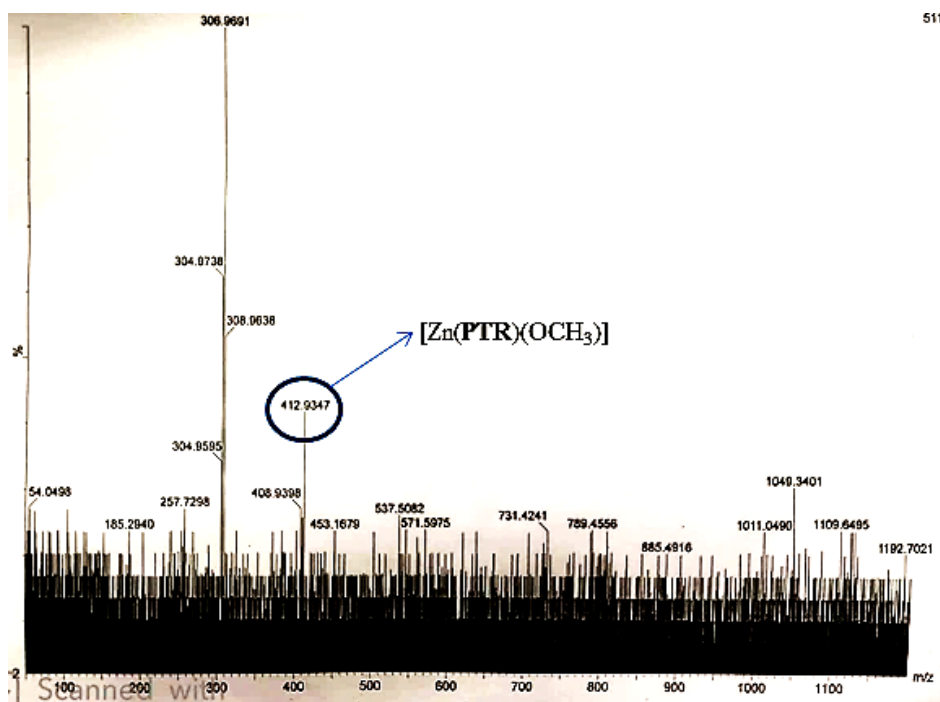


Fig.IV.16. Mass spectrum of $[Zn(PTR)(OCH_3)]$ complex.

Binding constant value ($4.2585 \times 10^4 M^{-1}$) was calculated using the Benesi-Hildebrand plot (Fig.IV.17).

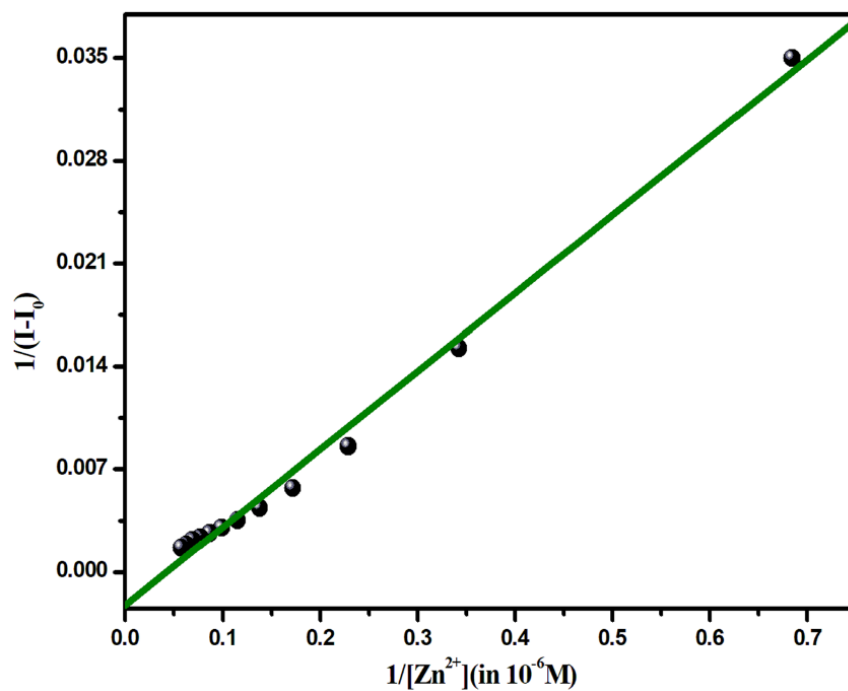


Fig.IV.17. Benesi-Hildebrand plot of PTR in presence of Zn^{2+} in DMSO-water (99:1, v/v; HEPES buffer, pH, 7.2).

The Binding mechanism of Zn^{2+} with the probe **PTR** was supported by 1H NMR spectral titration. In the 1H NMR spectrum of the probe **PTR**; phenolic $-OH$ (H2) and $-NH$ (H1) peaks appear at 13.74 and 14.34 ppm, respectively. The peak for imine proton ($CH=N$) (H4) appears at 8.59 ppm. Triazole proton (H3) and aromatic proton (H5) peaks appear at 9.52 and 7.95 ppm, respectively. In the **PTR**+ Zn^{2+} complex phenolic $-OH$ signal (H2) was disappeared and NH peak (H1) has been shifted to 11.94 ppm (**Fig.IV.18**). The broadening of imine protons (H4) and shifting to more shielding zone (8.59 \rightarrow 8.50 ppm) are observed for complex, PTR- Zn^{2+} . All other peaks either remain unperturbed or shifted slightly to upfield region. A new peak arises at 1.92 ppm that is signature to the binding of $-OCH_3$ with Zn^{2+} . The above discussion has concluded that the phenolic $-OH$, imine protons and imine nitrogen are involved in the formation of the Zn^{2+} -complex.

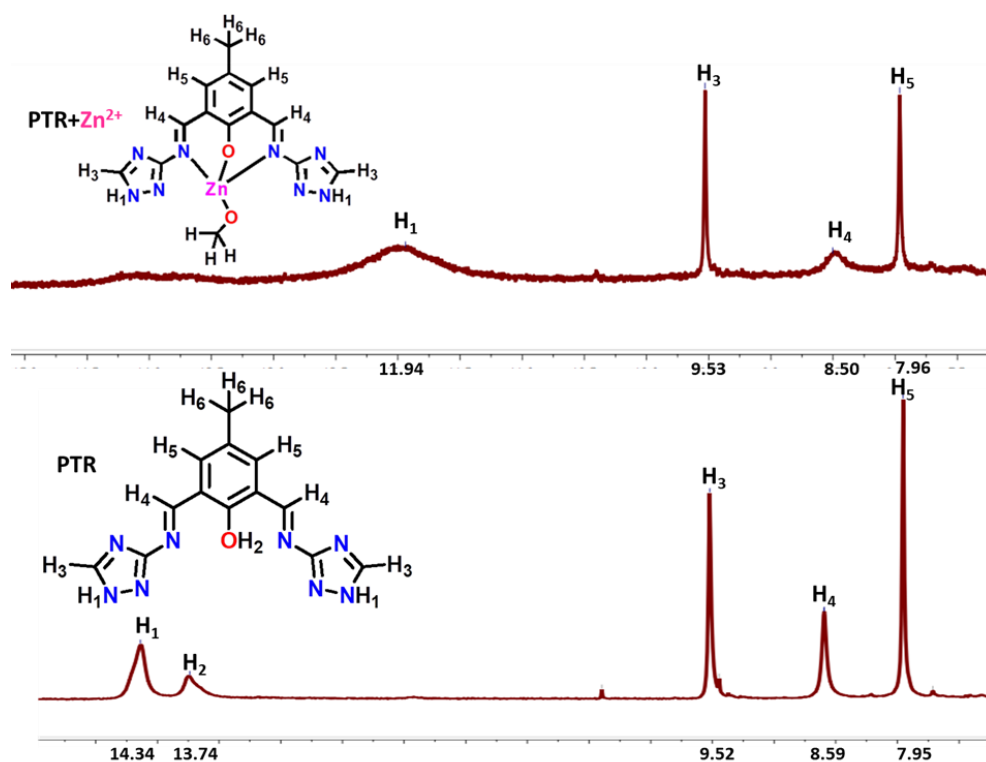
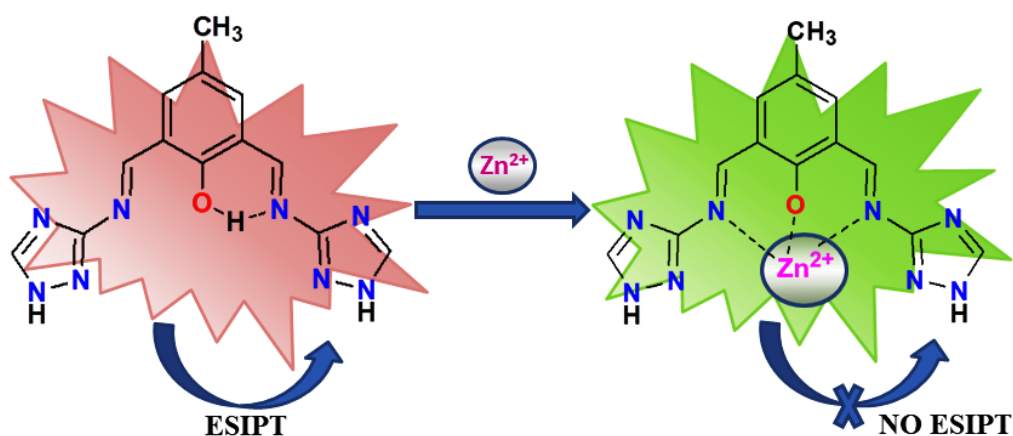


Fig.IV.18. The 1H NMR (300 MHz, d_6 -DMSO) titration spectra of **PTR** in presence of Zn^{2+} ion.

In the probe **PTR**, IR band appear at 3116 (O-H), 2923 (N-H), 2774 (C-H) and 1621 (C=N) cm^{-1} . In the Zn^{2+} -**PTR** complex, O-H band (3116 cm^{-1}) is eliminated whereas other peaks of N-H and C=N shifted to different region in the IR spectrum which indicates the binding of Zn^{2+} with **PTR** through phenolic - O and imine - N (**Scheme IV.c**).



Scheme IV.c. The sensing mechanism of probe **PTR** in presence of Zn^{2+} ion.

The sensing mechanism of the probe **PTR** towards the Zn^{2+} ion has also been assessed by the DFT calculation. The energy optimized forms of **PTR** is flat form with dihedral angle 179.91° (C2, C9, N16, C17)/ (C6, N10, C21, C22) and bond length 1.303 Å (C9, N16)/ (N10, C21). Theoretical calculation of Zn^{2+} -**PTR** complex is carried out considering the 1:1 stoichiometry as approved the spectroscopic results. The distorted tetrahedral Zn^{2+} -**PTR** complex is formed with the dihedral angles are 172.96° (C2, C9, N17, C18), 173.56° (C5, C10, N22, C23) and bond distances are 1.326 (C10, N22), 1.329 (C9, N17) Å. The TD-SCF calculation protocol helps to evaluate the transition energy and oscillator strengths of **PTR** (**Table IV.2**, **Table IV.4**) and **PTR- Zn^{2+}** complex (**Table IV.3**, **Table IV.5**).

Table IV.2. DFT table of PTR

Excitation Energy (eV)	Wavelength Exp.(nm)	Wavelength Thro.(nm)	Oscillation frequency (f)	Key Transitions	Nature of Transitions
4.4521	288.30	278.48	0.6838	(38%) HOMO-2 →LUMO+1	ILCT
3.0937	379.71	400.76	0.2312	(48%) HOMO→LUMO	ILCT

ILCT: Intra ligand charge transfer transition.

Table IV.3. DFT table of PTR+Zn²⁺

Excitation Energy (eV)	Wavelength Exp.(nm)	Wavelength Thro.(nm)	Oscillation frequency (f)	Key Transitions	Nature of Transitions
4.1693	298.96	297.37	0.0061	(49%) HOMO-1 →LUMO+3	ILCT
4.1038	298.96	302.12	0.2554	(28%) HOMO-4 →LUMO	ILCT
2.6600	433.88	466.11	0.1456	(34%) HOMO-2 →LUMO	ILCT

ILCT: Intra ligand charge transfer transition.

Table IV.4: Selected MO's of PTR with their corresponding energy value.

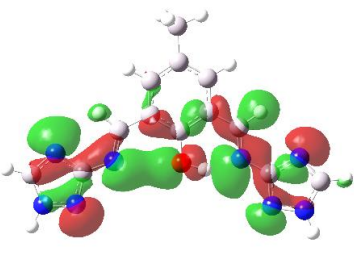
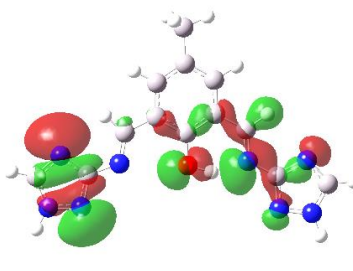
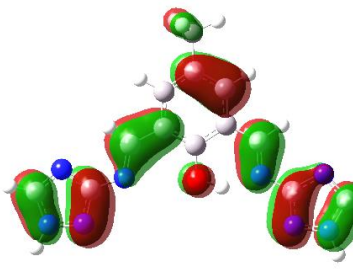
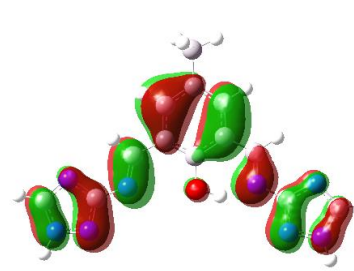
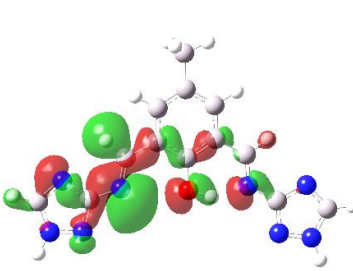
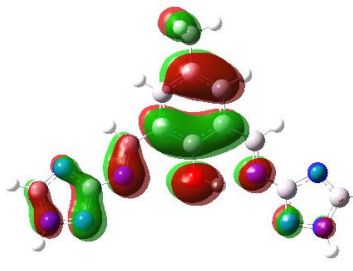
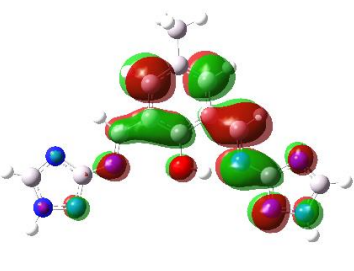
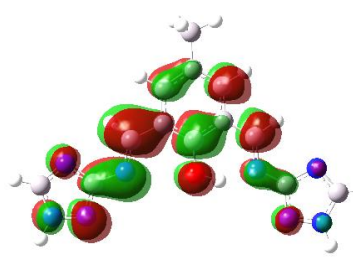
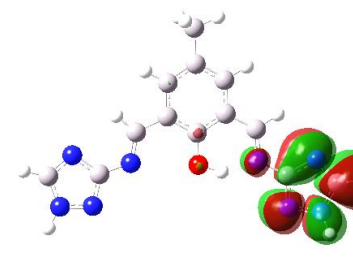
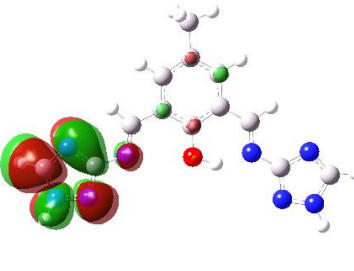
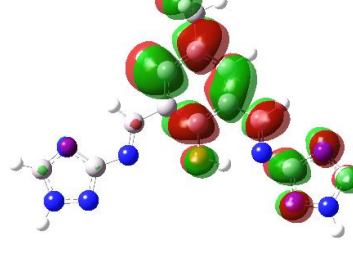
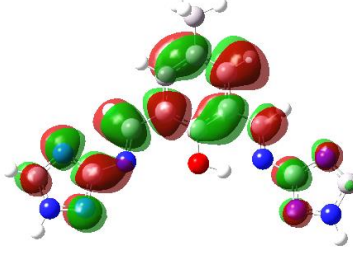
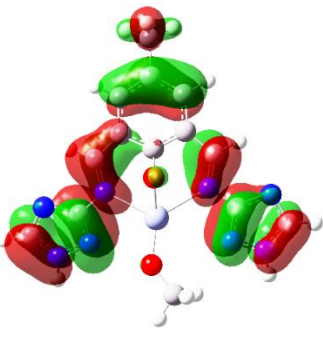
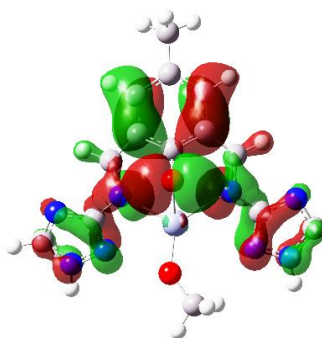
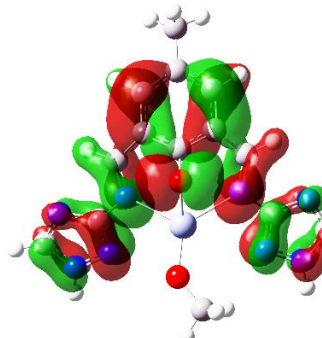
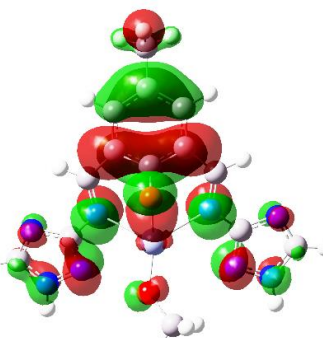
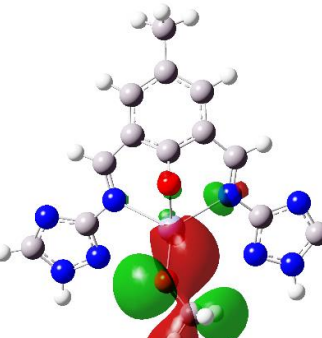
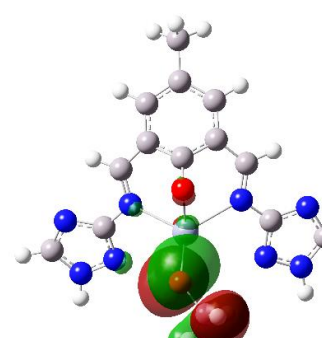
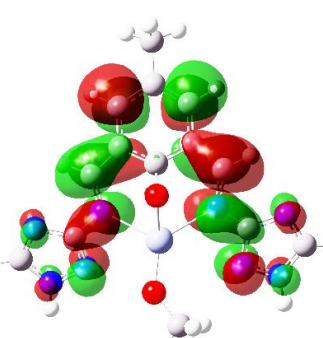
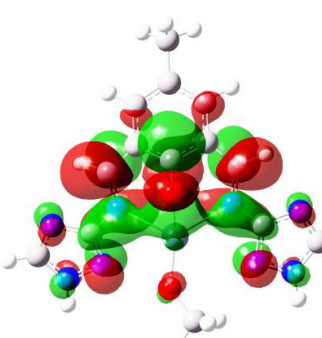
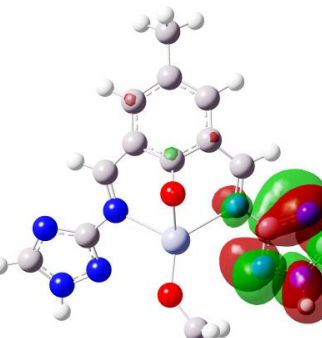
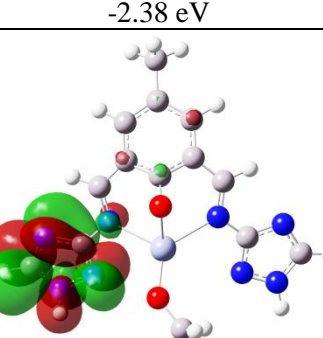
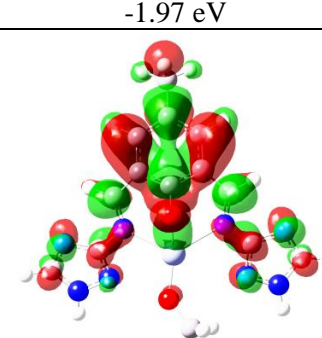
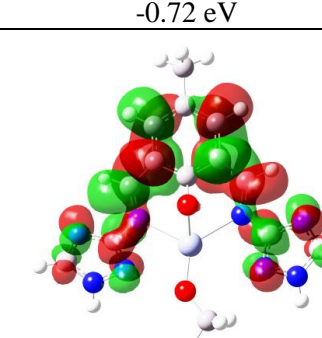
		
HOMO-5 -7.58 eV	HOMO-4 -7.47 eV	HOMO-3 -7.34 eV
		
HOMO-2 -6.42 eV	HOMO-1 -6.38 eV	HOMO -5.82 eV
		
LUMO -2.24 eV	LUMO+1 -1.54 eV	LUMO+2 -0.66 eV
		
LUMO+3 -0.22 eV	LUMO+4 0.36 eV	LUMO+5 0.73 eV

Table IV.5: Selected MO's of PTR+ Zn^{2+} with their corresponding energy value.

		
HOMO-5 -7.52 eV	HOMO-4 -6.88 eV	HOMO-3 -6.36 eV
		
HOMO-2 -5.54 eV	HOMO-1 -5.29 eV	HOMO -5.01 eV
		
LUMO -2.38 eV	LUMO+1 -1.97 eV	LUMO+2 -0.72 eV
		
LUMO+3 -0.52 eV	LUMO+4 0.03eV	LUMO+5 0.46 eV

The HOMO→LUMO transition is determined from the MO contribution of **PTR**; the result shows that the electron density of HOMO is mainly localised on PCDF (4-methyl-2, 6-diformylphenol) moiety (75%) and one triazole moiety (25%) whereas electron density of LUMO is localised in PCDF motif (67%) and triazole moiety (33%). In the complex (Zn^{2+} -**PTR**) electron density of HOMO is mainly localised in the Zn-OCH₃ moiety (99%) and electron density of LUMO is localised in triazole (69%) and PCDF moiety (31%). Theoretical electronic transitions are comparable with the UV-vis experimental results of **PTR** and **PTR-Zn²⁺** complex (**Table IV.4**, **Table IV.5**). Upon addition of Zn^{2+} to the probe **PTR**, the HOMO energy is increased and the LUMO energy is decreased (**Fig.IV.19**). The energy gap between HOMO-LUMO is decreased as a result the absorption bands of probe were shifted (288 → 298 and 380 → 434 nm) to longer wavelength. The proton movement has been assessed by the Transition State (TS) (**Fig.IV.20**). In the transition state (TS) the shifting of proton from N to O atom takes place as a result of enol and keto forms. The TS containing one imaginary negative frequency = -1122.62, on the other hand enol form has positive frequency = 27.87, and keto form has positive frequency = 22.62.

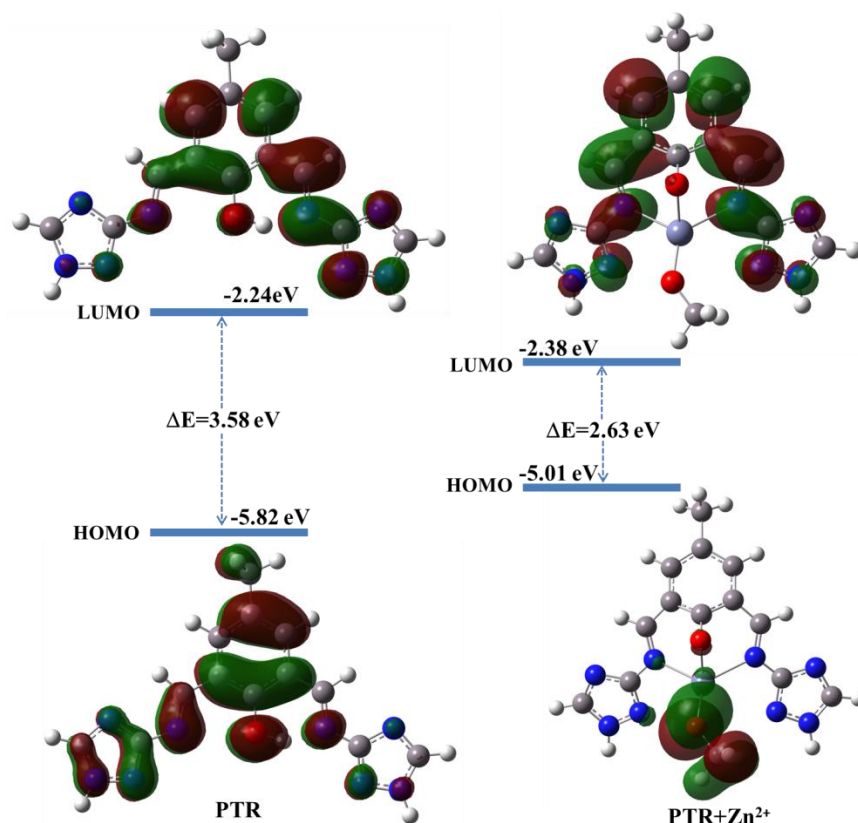


Fig.IV.19. The correlation between the HOMO–LUMO energy gap of **PTR** and **PTR-Zn²⁺** complex.

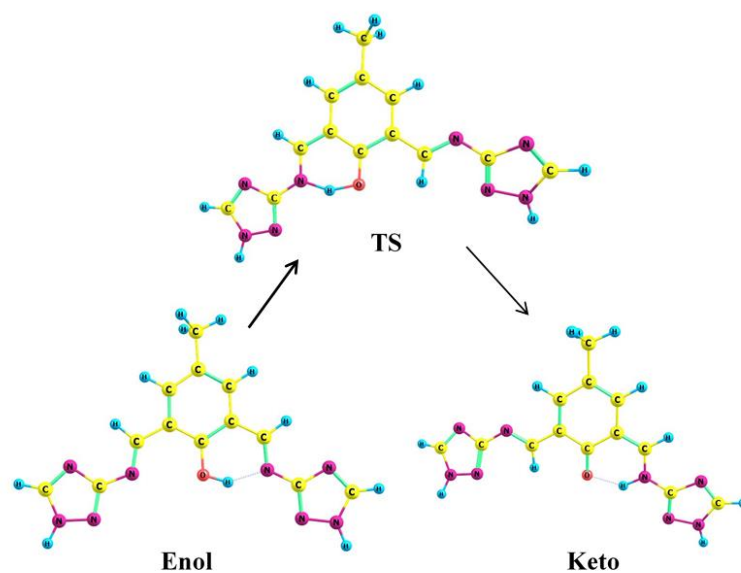


Fig.IV.20. The Transition State (TS) diagram of the probe **PTR** in its keto and enol form.

IV.3.4. Biological study

The MTT assay of **PTR** probe was examined followed by the cytotoxicity study in HEK293 cell line (PBS Phosphate Buffer Saline, pH-7.4). The experiment shows a clear transparent solution of 100 μ M **PTR** and the solution has been prepared to check the cytotoxicity via MTT assay. For each group, DMSO control also taken. In this experiment maximum 4% v/v DMSO was used. The available reports [71,72] also confirmed that DMSO can be used up to 10% v/v for human peripheral blood mononuclear cells (PBMC) and HEK293 cell line without any toxicity. The MTT data (**Fig.IV.21**) suggested that no cellular toxicity was observed upto 20 μ M of **PTR** concentration. So, 10 μ M concentration of **PTR** was selected for cellular imaging. After that the fluorescence imaging of intracellular Zn^{2+} ions in HEK293 cell line in PBS buffer of pH 7.2 was examined by adding the **PTR** probe (**Fig.IV.22**). The DMSO control was also taken to check the DMSO cytotoxicity. For the maximum concentration of **PTR** treatment (100 μ M), 9 μ l DMSO was added in 100 μ l of DMEM media. In case of 10 and 20 μ M treatment few drops of DMSO was added. Furthermore, the DMSO control data were deducted from the **PTR** treatment panel in each case. It has been visualized that in presence of only **PTR** there is a yellowish orange emission in cellular cytoskeleton at 10 μ M of **PTR** concentration, whereas in **PTR** untreated cells there was no emission. Upon addition of $Zn(OAc)_2$ (20 μ M) to HEK293, the fluorescence emission has changed to green colour in presence of **PTR** (20 μ M). DAPI was used as nuclear stainer, which shows blue emission. This microscopic images of HEK293 have confirmed that **PTR** has great in vitro potential as a Zn^{2+} ion sensor.

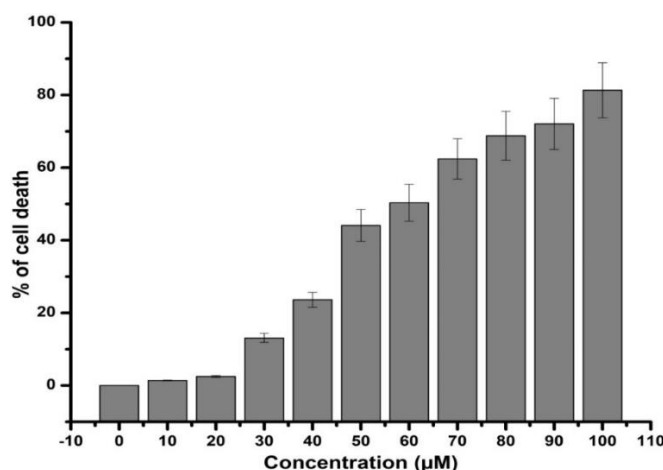


Fig.IV.21. The cell viability test using MTT assay upon adding **PTR**

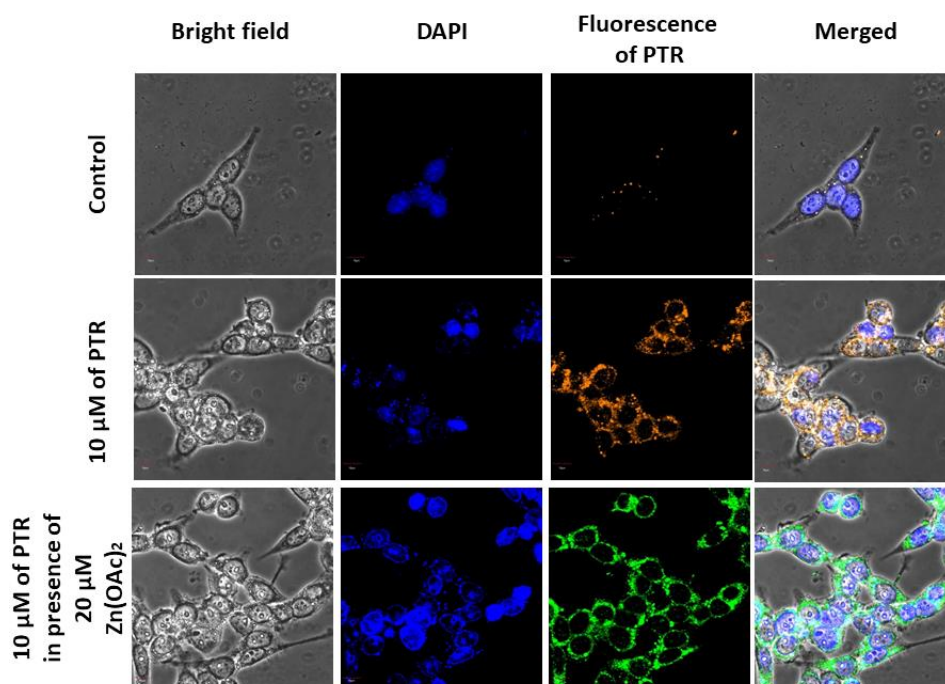


Fig.IV.22. Confocal microscopy images of HEK293 cells in presence of only **PTR** and **PTR+ Zn(OAc)₂**, where DAPI was used as nuclear stainer. Scale bar is 10 μm .

IV.4. Conclusion

A new probe, triazole Schiff base of diformyl phenol, **PTR**, is spectroscopically characterised and shows selective and specific recognition to Zn^{2+} even in presence of large number of other cations. The detection limit is much below the WHO recommended value of Zn^{2+} (LOD, 0.30

μM; WHO limit, 76 μM). The probable binding between **PTR** and Zn²⁺ is examined by ESI-MS analysis, Job's experiment, ¹H NMR titrations and DFT computational study and the sensing mechanism is established by the suppression of excited state intramolecular proton transfer (ESIPT) pathway followed by CHEF process. The probe shows excellent cell imaging of intracellular Zn²⁺ ion which can be confirmed by microscopic imaging of HEK293 cell line.

IV.5. References:

- [1]. H. Haase, L. Rink, *BioMetals*, 20 (2007) 579.
- [2]. A. Czyżowska, B. Dyba, E. R. Szydło, A. Barbasz, *J. Appl. Toxicol.*, 419 (2021) 458.
- [3]. M. D. Pluth, E. Tomat, S. J. Lippard, *Annu. Rev. Biochem.*, 80 (2011) 333.
- [4]. A. R. Kay, K. Toth, *Sci. Signaling*, 1 (2008) re3.
- [5]. S. L. Sensi, P. Paoletti, A. I. Bush, I. Sekler, *Nat. Rev. Neurosci.*, 10 (2009) 780.
- [6]. A. B. D. Santos, M. A. Bezerra, M. E. Rocha, G. E. Barreto, K. A. Kohlmeier, *J. Neural Transm.*, 126 (2019) 1291.
- [7]. J. Baesler, J. F. Kopp, G. Pohl, M. Aschner, H. Haase, T. Schwerdtle, J. Bornhorst, *J. Trace Elem. Med. Biol.*, 55 (2019) 44.
- [8]. V. Kumar, D. Singh, B. K. Singh, S. Singh, N. Mittra, R. R. Jha, D. K. Patel, C. Singh, *Mol. Cell. Biochem.*, 444 (2017) 149.
- [9]. X. N. Wan, X. H. Sun, F. Cao, K. Wang, *J. Solid State Chem.*, 288 (2020) 121447.
- [10]. X. Zhang, M. Zhong, P. Zhao, X. Zhang, Y. Li, X. Wang, J. Sun, W. Lan, H. Sun, Z. Wang, H. Gao, *Biomater. Sci.*, 7 (2019) 5197.
- [11]. M. Bangera, G. Gowda, S. R. Sagurthi, M. R. N. Murthya, *Acta Crystallogr., Sect. D: Struct. Biol.*, 75 (2019) 475.
- [12]. R. J. Borges, F. F. Cardoso, C. A. H. Fernandes, T. R. Dreyer, D. S. Moraes, R. S. Floriano, L. R. Simioni, M. R. M. Fontes, *Biochim. Biophys. Acta, Gen. Subj.*, 1861 (2017) 3199.
- [13]. R. Feng, Y. Xu, H. Zhao, X. Duan, S. Sun, *Analyst*, 141 (2016) 3219.

- [14]. J. Wang, L. Lu, C. Wang, M. Wang, J. Ju, J. Zhu, T. Sun, *New J. Chem.*, 44 (2020) 15426.
- [15]. S. Maity, M. Shyamal, R. Maity, N. Mudi, P. Hazra, P. K. Giri, S. S. Samanta, S. Pyne, A. Misra, *Photochem. Photobiol. Sci.*, 19 (2020) 681.
- [16]. P. Wang, S. Wang, L. Chen, W. Wang, B. Wang, Y. Liao, *Spectrochim. Acta, Part A*, 240 (2020) 118549.
- [17]. S. Kim, H. Lee, H. So, H. Lee, K. T. Kim, C. Kim, *Spectrochim. Acta, Part A*, 228 (2020) 117787.
- [18]. L. Xue, G. Li, D. Zhu, Q. Liu, H. Jiang, *Inorg. Chem.*, 51 (2012) 10842.
- [19]. W. Li, B. Fang, M. Jin, Y. Tian, *Anal. Chem.*, 89 (2017) 2553.
- [20]. S. Gharami, K. Aich, L. Patra, T. K. Mondal, *New J. Chem.*, 42 (2018) 8646.
- [21]. S. A. Yoon, J. Lee, M. H. Lee, *Sens. Actuators, B*, 58 (2018) 50.
- [22]. S. Xia, J. Shen, J. Wang, H. Wang, M. Fang, H. Zhou, M. Tanasova, *Sens. Actuators, B*, 258 (2018) 1279.
- [23]. H. Diao, L. Guo, W. Liu, L. Feng, *Spectrochim. Acta, Part A*, 196 (2018) 274.
- [24]. S. Gharami, K. Aich, D. Sarkar, P. Ghosh, N. Murmu, T. K. Mondal, *New J. Chem.*, 43 (2019) 1857.
- [25]. Z. Li, G. Liu, C. Fan, S. Pu, *Anal. Bioanal. Chem.*, 413 (2021) 3281.
- [26]. W. Li, X. Hu, Q. Li, Y. Shi, X. Zhai, Y. Xu, Z. Li, X. Huang, X. Wang, J. Shi, X. Zou, S. Kang, *Food Chem.*, 320 (2020) 126623.
- [27]. B. Peng, M. Fan, J. Xu, Y. Guo, Y. Ma, M. Zhou, J. Bai, J. Wang, Y. Fang, *Microchim. Acta*, 187 (2020) 660.
- [28]. Y. J. Tong, J. X. Qi, A. M. Song, X. L. Zhong, W. Jiang, L. Zhang, R. P. Liang, J. D. Qiu, *Anal. Chim. Acta*, 1128 (2020) 11.
- [29]. W. J. Zhang, S. G. Liu, X. Y. Zhang, H. Q. Luo, N. B. Li, *Anal. Bioanal. Chem.*, 412 (2020) 4375.
- [30]. Z. Ye, L. Li, F. Zhao, Q. Yang, Y. Wang, K. Bohinc, X. Guo, *J. Mater. Sci.*, 55 (2020) 10168.

- [31]. T. V. Huynh, N. T. N. Anh, W. Darmanto, R. A. Doong, *Sens. Actuators, B*, 328 (2021) 129056.
- [32]. X. He, Q. Xie, J. Fan, C. Xu, W. Xu, Y. Li, F. Ding, H. Deng, H. Chen, J. Shen, *Dyes Pigm.*, 177 (2020) 108255.
- [33]. A. Das, S. Jana, A. Ghosh, *Cryst. Growth Des.*, 18 (2018) 2335.
- [34]. S. A. Yoon, J. Lee, M. H. Lee, *Sens. Actuators, B*, 58 (2018) 50.
- [35]. S. Xia, J. Shen, J. Wang, H. Wang, M. Fang, H. Zhou, M. Tanasova, *Sens. Actuators, B*, 258 (2018) 1279.
- [36]. H. Diao, L. Guo, W. Liu, L. Feng, *Spectrochim. Acta, Part A*, 196 (2018) 274.
- [37]. D. Wang, S. -J. Li, W. Cao, Z. Wang, Y. Ma, *ACS Omega*, 7 (2022) 18017.
- [38]. D. Yue, X. Zhang, Y. Tan, Z. Wang, Y. Zhang, *J. Lumin.*, 228 (2020) 117618.
- [39]. A. M. Song, Y. J. Tong, R. P. Liang, J. D. Qiu, *Microchem. J.*, 164 (2021) 106027.
- [40]. J. Liu, S. Wang, X. Wang, *J. Mater. Eng. Perform.*, 29 (2020) 5126.
- [41]. S. Paul, S. Maity, S. Halder, B. Dutta, S. Jana, K. Jana, C. Sinha, *Dalton Trans.*, 51 (2022) 3198.
- [42]. A. K. Bhanja, S. Mishra, K. D. Saha, C. Sinha, *Dalton Trans.*, 46 (2017) 9245.
- [43]. A. K. Adak, B. Dutta, B. Manna, C. Sinha, *ACS omega*, 4 (2019) 18987.
- [44]. R. Purkait, S. Dey, C. Sinha, *New J. Chem.*, 42 (2018) 16653.
- [45]. A. K. Adak, R. Purkait, S. K. Manna, B. C. Ghosh, S. Pathak, C. Sinha, *New J. Chem.*, 43 (2019) 3899.
- [46]. R. Purkait, A. D. Mahapatra, D. Chattopadhyay, C. Sinha, *Spectrochim. Acta Part A*, 207 (2019) 164.
- [47]. M. Baghayeri, A. Amiri, F. Karimabadi, S. D. Masi, B. Maleki, F. Adibian, A. R. Pourali, C. Malitesta, *J. Electroanal. Chem*, 888 (2021) 115059.
- [48]. F. Hajizadeh, F. M. Zonoz, S. Duval, B. Maleki, A. Amiri. *J. Mol. Struct.*, 1224 (2021) 129003.
- [49]. S. S. Ghasemi, M. Hadavifar, B. Maleki, E. Mohammadnia, *J. Water Process. Eng.*, 32 (2019) 100965.

- [50]. F. Laffafchi, M. Tajbakhsh, Y. Sarrafi, B. Maleki, M. Ghani, *Polycycl. Aromat. Compd.*, 43 (2023) 3240.
- [51]. C. Patra, A. K. Bhanja, C. Sen, D. Ojha, D. Chattopadhyay, A. Mahapatra, C. Sinha, *Sens. Actuators, B*, 228 (2016) 287.
- [52]. S. Mishra, K. Manna, U. Kayal, M. Saha, S. Chatterjee, D. Chandra, M. Hara, S. Datta, A. Bhaumik, K. D. Saha, *RSC Adv.*, 10 (2020) 23148.
- [53]. A. K. Bhanja, C. Patra, S. Mondal, S. Mishra, K. D. Saha, C. Sinha, *Sens. Actuators B.*, 252 (2017) 257.
- [54]. S. Gharami, K. Aich, D. Sarkar, P. Ghosh, N. Murmu, T. K. Mondal, *New J. Chem.*, 43 (2019) 1857.
- [55]. Q. Wu, L. Feng, J. B. Chao, Y. Wang, S. Shuang, *Analyst.*, 146 (2021) 4348.
- [56]. S. Xia, J. Shen, J. Wang, H. Wang, M. Fang, H. Zhou, M. Tanasova, *Sens. Actuators, B.*, 258 (2018) 1279.
- [57]. W. Li, B. Fang, M. Jin, Y. Tian, *Anal. Chem.*, 89 (2017) 2553.
- [58]. S. Gharami, K. Aich, L. Patra, T. K. Mondal, *New J. Chem.*, 42 (2018) 8646.
- [59]. S. A. Yoon, J. Lee, M. H. Lee, *Sens. Actuators, B.*, 58 (2018) 50.
- [60]. M. Hagimori, T. Temma, N. Mizuyama, T. Uto, Y. Yamaguchi, Y. Tominaga, T. Mukai H. Saji, *Sens. Actuators, B.*, 213 (2015) 45.
- [61]. K. Boonkitpatarakul, A. Smata, K. Kongnukool, S. Srisurichan, K. Chainok, M. Sukwattanasinitt, *J. Lumin.*, 198 (2018) 59.
- [62]. Y. Upadhyay, T. Anand, L. T. Babu, P. Paira, G. Crisponi, A. K. Sk, R. Kumar, S. K. Sahoo., *Dalton Trans.*, 47 (2018) 742.
- [63]. S. B. Roy, C. Prodhan, K. Chaudhuri, K. K. Rajak, *Photochem. Photobiol. Sci.*, 16 (2017) 1103.
- [64]. R. Singh, A. Gogoi, G. Das, *RSC advances.*, 6 (2016) 112246.
- [65]. G. J. Park, Y. J. Na, H. Y. Jo, S. A. Lee, A. R. Kim, I. Noh, C. Kim, *New J. Chem.*, 38 (2014) 2587.
- [66]. A. Hens, *RSC Adv.*, 5 (2015) 54352.

- [67]. Y. W. Choi, J. J. Lee, C. Kim, RSC Adv., 5 (2015) 60796.
- [68]. Y. Ma, F. Wang, S. Kambam, X. Chen, Sens. Actuators B: Chem., 188 (2013) 1116
- [69]. D. Udhayakumari, S. Saravanamoorthy, M. Ashok, S. Velmathi, Tet. Lett., 52 (2011) 4631.
- [70]. H. Zhuang, W. Shi, G. Zhao, Y. Yang, Y. Li. Spectrochim. Acta - A., 282 (2022) 121650.
- [71]. H. Kloverpris, A. Fomsgaard, A. Handley, J. Ackland, M. Sullivan, P. Goulder, J. Immunol. Meth., 356 (2010) 70-78.
- [72]. J. Lynch, J. Chung, Z. Huang, V. Pierce, N. S. Saunders, L. Niu, J. Neurosci. Meth., 350 (2021) 109058.

CHAPTER V

Abstract

Mercury (II) complexes, $[\text{Hg}(\text{p-NO}_2\text{aaiR})(\mu\text{-X})(\text{X})_2]$ (**2-4**) of p-NO₂-aaiR [1-Alkyl-2-(p-nitro-phenylazo) imidazole, (**1**), where R = -CH₃ (**1a**), -C₂H₅ (**1b**) and X = Cl (**2**), Br (**3**), I (**4**)] have been studied by spectral data. X-ray crystallography study in case of $[\text{Hg}(\text{p-NO}_2\text{aai-CH}_3)(\mu\text{-I})(\text{I})_2]$ (**4a**) has revealed the distorted dinuclear halobridge tetra-atomic puckered rhombohedral Hg(II) structure. The ligand, p-NO₂aaiR shows trans (E) - cis (Z) isomerisation both in free and coordination state in the complex on shocking UV light in the solution phase. The Z-to-E transformation is carried out by thermal treatment while photoisomerization is carried out very slowly on visible light absorption and $\phi_{\text{E} \rightarrow \text{Z}}$ (quantum yields for E-to-Z isomerisation) is higher for free ligand compare to the complex phase. The isomerisation rate shows the sequence, $[\text{Hg}(\text{p-NO}_2\text{ aaiR})(\mu\text{-I})(\text{I})_2]$ (**4**) < $[\text{Hg}(\text{p-NO}_2\text{ aaiR})(\mu\text{-Br})(\text{Br})_2]$ (**3**) < $[\text{Hg}(\text{p-NO}_2\text{aaiR})(\mu\text{-Cl})(\text{Cl})_2]$ (**2**) which is also the sequence of molecular mass of the complexes. The energy gap calculation of optimized structures by DFT (Density Functional Theory) also supports this conjecture.

V.1. Introduction

The structural change of some aromatic-azo compounds [1,2] by absorbing light has massive applications in the field of molecular machines [3], data storage,[4] bio-conjugates,[5] polymers towards optical stimuli-response,[6] nanomaterials [7,8] etc. Photochromism of 1-alkyl-2-(arylo) imidazole [9,10] and some of their complexes are published [11-14]. For detail investigation on the influence of substituent on the photoisomerisation, a nitro (-NO₂) functionalised azoimidazole, 1-alkyl-2-(*p*-nitro-phenylazo) imidazole, *p*-NO₂-aaiR (**1**) (R = -CH₃ (**1a**), -C₂H₅ (**1b**)) and its Hg (II) complexes are synthesized. The spectroscopic techniques are used for the characterisation of ligands and compounds. The single crystal X-ray structure determination is helpful for the establishment of structure of the complex [Hg(*p*-NO₂aai-CH₃)(μ -I)(I)]₂ only. The details structural parameters and role of secondary interactions in the molecular assembly are also investigated. This study reveals that the isomerisation process strongly depends on molecular construction. However, the isomerisation rates and quantum yields are compared between free ligand and coordination phase in the complex in presence of different halides. Theoretical study has been attempted to describe the light induced structural change. Therefore photo-responsive structural orientation of these types of free 'N=N' linkage can be paved the way towards the technology of molecular machine and optical mechanochemistry.

V.2. Experimental

V.2.1. Materials

1-Alkyl-2-(*p*-nitro-phenylazo) imidazoles (*p*-NO₂aaiR, **1**) were prepared as per the following literature procedure [15]. Mercury halides were acquired from Loba Chemicals, Bombay, India. Other chemicals were purchased from Aldrich.

V.2.2. Physical measurements

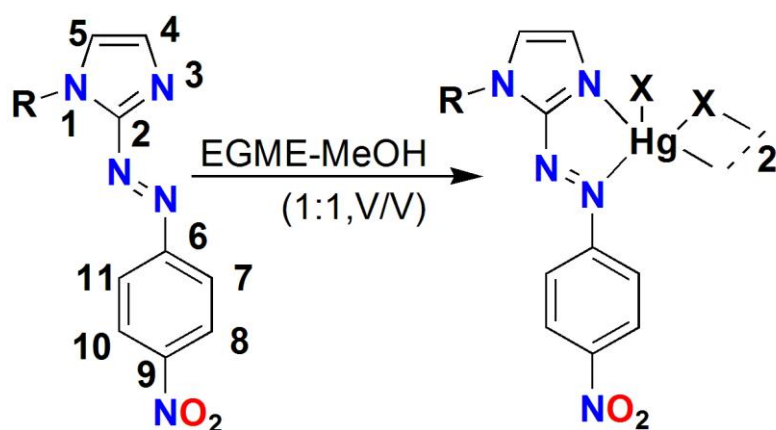
The Elemental (C, H, N) analysis carried out by Perkin-Elmer 2400 CHNS/O elemental analyzer. The UV-Vis spectra were recorded from Perkin Elmer Lambda 25 spectrophotometer. By using KBr pellets Perkin Elmer RX-1 FTIR collected IR spectra. The Perkin Elmer LS-55 spectrofluorimeter was used for photo excitation. The NMR spectra were taken from Bruker (AC) 300 MHz FTNMR spectrometer.

V.2.3. Synthesis of 1-Methyl-2-(*p*-nitrophenylazo) imidazole

To a dry THF solution (10 mL) of 2-(*p*-nitrophenylazo) imidazole (0.5 g, 2.7 mM) was added NaH (50% paraffin) (0.15 g) in small portions, and the resulting mixture was stirred in cold conditions with an ice bath for 30 min. Then the Methyl iodide (0.4 g, 2.8 mM) was added slowly for a period of 1 h and then allowed to warm for another 1 h. The solution so formed was evaporated to dryness, extracted with chloroform, and washed with NaOH solution and finally by distilled water. On slow evaporation in air, an orange crystalline product was obtained.

V.2.4. Synthesis of [Hg(*p*-NO₂ai-CH₃) (μ-I) (I)]₂ (4a)

Methanol (10 ml) was used to prepare solution of 1-methyl-2-(*p*-NO₂-phenylazo) imidazole (46.20 mg, 0.20 mmol) was added to ethyleneglycol monomethyl ether (EGME) solution (5 ml) of HgI₂ (90.88 mg, 0.20 mmol) and stirred (8 h) and filtered (**Scheme V.1**). The filtrate was allowed to evaporate slowly for a couple of weeks and needle shape; dark red colour crystals appeared (Yield, 63%). The structure of the complex so formed was established by the single crystal X-ray crystallography.



p -NO₂aai-CH₃ (**1a**), p -NO₂aai-C₂H₅ (**1b**), [Hg(p -NO₂aai-CH₃)(μ -Cl)(Cl)]₂ (**2a**), [Hg(p -NO₂aai-C₂H₅)(μ -Cl)(Cl)]₂ (**2b**) [Hg(p -NO₂aai-CH₃)(μ -Br)(Br)]₂ (**3a**), [Hg(p -NO₂aai-C₂H₅)(μ -Br)(Br)]₂ (**3b**) [Hg(p -NO₂aai-CH₃)(μ -I)(I)]₂ (**4a**), [Hg(p -NO₂aai-C₂H₅)(μ -I)(I)]₂ (**4b**)

Scheme V.a. Synthetic route of Hg (II)- halide complexes

V.2.5. General X-ray Crystallography

Red colour needle shaped crystal of size (0.112×0.101×0.090 mm³) was diffracted and data were collected using Bruker SMART APEX III Diffractometer using graphite-monochromated Mo-K α radiation (λ , 0.71073 Å). Data collection details were recorded in **Table V.1**. The least-squares refinement of all reflections within hkl range $-14 \leq h \leq 14$, $-9 \leq k \leq 9$, $-19 \leq l \leq 19$ were used for the calculation of unit cell parameters and crystal-orientation matrices. Lorentz and polarization effects [16] were used for intensity data on applying the condition $I > 2\sigma(I)$. Full matrix least-squares refinements on F^2 were performed *via* SAINT program using SHELXL-97 [17] with anisotropic displacement parameters for all non-hydrogen atoms.

V.2.6. Spectrophotometric measurements

PerkinElmer Lambda 25 UV/VIS Spectrophotometer used to collect absorption spectra at 298 K using Peltier thermostat. The source light was Xenon lamp in the Perkin Elmer LS 55

spectrofluorimeter. The extrapolation of the absorption spectra of a *cis*-rich mixture calculated the absorption spectra of the *cis* (*Z*) isomers and the composition was assumed from ¹H NMR integration. The equation, $v = (\Phi I^0 / V) (1 - 10^{-Abs})$ (I^0 , the photon flux; V , the volume of the solution; Abs , the initial absorbance at the irradiation wavelength) was used to calculate quantum yields (Φ) by measuring initial *trans*-to-*cis* (*E*-to-*Z*) isomerization rates (v). Azobenzene ($\Phi = 0.11$ for π - π^* excitation) was used for the calculation of I^0 [18].

The isomerisation rates (*cis*-to-*trans*, *Z*-to-*E*) at constant temperatures (298-313 K) were obtained by measuring the absorption changes intermittently from a *cis*-rich isomer. The Arrhenius equation, $\ln k = \ln A - E_a/RT$, (k , the measured rate constant; R , the gas constant, and T , temperature) was used for the calculation of activation energy (E_a) and the frequency factor (A). Using $\Delta G^* = E_a - RT - T\Delta S^*$ and $\Delta S^* = [\ln A - 1 - \ln(k_B T/h)]/R$ (k_B , Boltzmann's constant; h , Plank's constant) the activation free energy (ΔG^*) and activation entropy (ΔS^*) were calculated.

V.2.7. Computational methods

To get theoretical insight, DFT was used in GAUSSIAN 09 (G09) program package [19] and was implemented for the compounds $[\text{Hg}(p\text{-NO}_2\text{aaiCH}_3)(\mu\text{-X})(\text{X})_2]$ ($\text{X} = \text{Cl}$ (**2a**), Br (**3a**), I (**4a**)). The basis function B3LYP [20] (for C, H, N, O, Cl) and LanL2DZ [21-23] (for Hg, Br and I) were used. The vibrational frequency calculation had been achieved with the designed complexes; and the optimized molecular geometries at the local minima were ensured that and the only positive Eigen values were taken for grand. The coordinates from single crystal X-ray structure was used in the calculation. The experimental spectra are analysed using time dependent DFT (TD-DFT) calculations. Virtual transitions in DMF medium following the conductor-like polarizable continuum model were assigned to the lowest 25 singlet – singlet

transition and TD-DFT calculation results were comparable. GaussSum [24] was used for fractional contribution measurements.

V.3. Results and discussion

The ligands, *p*-NO₂aiiR (**1**), [R = -CH₃ (**1a**), -C₂H₅ (**1b**); {*p*-NO₂-aiiR=1-Alkyl-2-(*p*-nitrophenylazo) imidazole}], were prepared by literature process [15]. The complexes [Hg(*p*-NO₂aiiR) (μ-X)X]₂ [X= Cl, Br and I] (**2-4**) were synthesized by the reaction of *p*-NO₂aiiR (in MeOH) and HgX₂ (in EGME) (**Scheme V.a**). The structural analysis revealed that the single crystal of iodo-bridged mercury complex orients such a way that can participate in discussed photophysical property. In the following analysis the dependency of molecular construction in photochromism is highly correlated.

V.3.1. The X-Ray crystal structure of [Hg(*p*-NO₂aii-CH₃)(μ-I)(I)]₂ (**4a**)

The structure of [Hg(*p*-NO₂aii-CH₃) (μ-I)(I)]₂ (**4a**), crystal system, monoclinic; space group, P2₁/c; Z, 4) is shown in **Table V.1** and also the bond lengths and bond angles are given in **Table V.2**. The unit structure consists of dinuclear iodo-bridged Hg₂I₂ fragment (**Fig.V.1**).

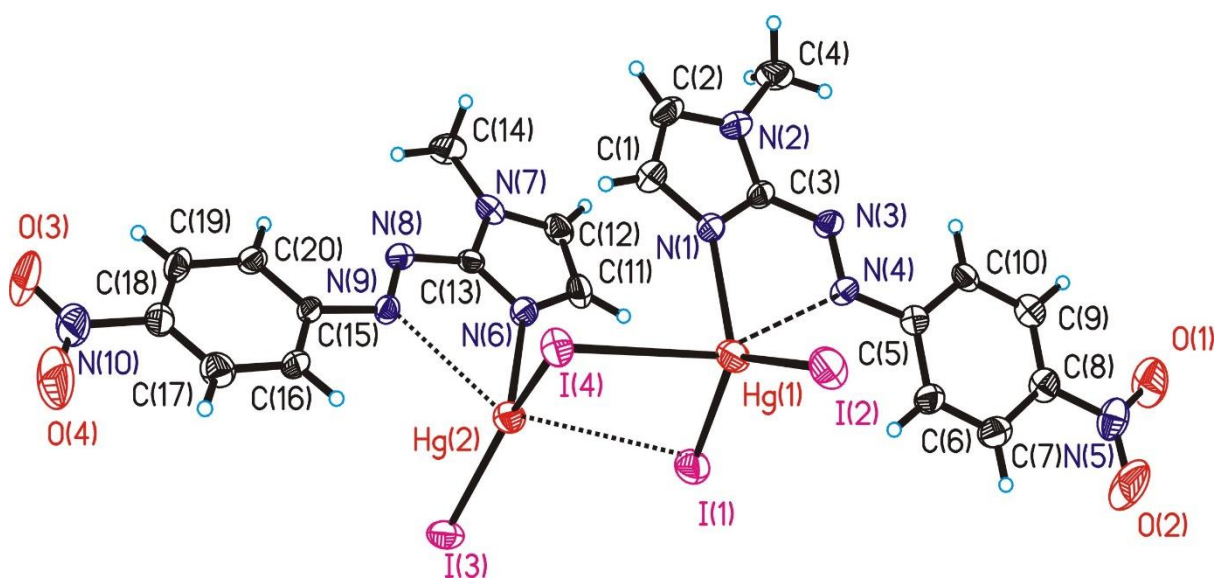


Fig.V.1. Asymmetric unit of compound [Hg(*p*-NO₂aii-CH₃)(μ-I)(I)]₂ (**4a**)

Table V.1. Summarized crystallographic data for [Hg(*p*-NO₂aiMe)(μ -I)(I)]₂ (**4a**)

Compound	[Hg(<i>p</i> -NO ₂ aiMe)(μ -I)(I)] ₂ (4a)
Empirical Formula	'C ₂₀ H ₁₈ I ₄ N ₁₀ O ₄ Hg ₂ '
Formula weight	1371.22
Temperature (K)	273(2) K
Crystal system	Monoclinic
Space group	'P 21/c'
Crystal size (mm) ³	0.42 X0.27 X0.19
a(Å)	7.8271(4)
b(Å)	18.8750(9)
c(Å)	22.0966(10)
α / ⁰	90
β / ⁰	94.032(2)
γ / ⁰	90
V(Å) ³	3256.4(3)
Z	4
μ (MoK α) (mm ⁻¹)	13.252
θ range	2.140-27.512
hkl range	-10<h<10; -24<k<24 ; -28<l<28
D _{calc} (mg m ⁻³)	2.797
Refine parameters	363
Total reflections	47075
Unique reflections	7466
R ₁ ^a [I > 2 σ (I)]	0.0502
wR ₂ ^b	0.1376
Goodness of fit	1.108

^aR = $\sum ||F_o| - |F_c| | / \sum |F_o|$. ^bwR₂ = $[\sum w(F_o^2 - F_c^2)^2 / \sum w(F_o^2)^2]^{1/2}$, $w = 1/[\sigma^2(F_o)^2 + (0.0778P)^2 + 9.4074P]$;

where P = $((F_o^2 + 2F_c^2) / 3)$.

Table V.2. Selected bond distances (Å) and angles (°) for [Hg (*p*-NO₂aa_i-CH₃)(μ-I)(I)]₂ (**4a**)

Bond distances (Å)		Bond angles (°)	
Hg(1)-I(1)	2.6736(10)	I(1)-Hg(1)-I(4)	95.67(3)
Hg(1)-I(2)	2.6639(11)	I(1)-Hg(2)-I(4)	92.20
Hg(1)-I(4)	3.2844(10)	N(1)-Hg(1)-N(4)	62.89
Hg(1)-N(1)	2.333(8)	N(6)-Hg(1)-N(9)	61.72
Hg(1)-N(4)	2.811	N(4)-Hg(1)-I(4)	151.71
Hg(2)-I(1)	3.449	I(1)-Hg(1)-I(2)	129.65
Hg(2)-I(3)	2.6194(9)	Hg(1)-I(4)-Hg(2)	85.37
Hg(2)-I(4)	2.6597(10)	Hg(1)-I(1)-Hg(2)	81.92
Hg(2)-N(6)	2.419(8)	I(3)-Hg(2)-I(4)	148.80
Hg(2)-N(9)	2.319		
N(4)-N(3)	1.260(11)		
N(8)-N(9)	1.232(11)		

* Symmetry: -x, -y, -z; ** Symmetry: 1-x, 2-y, 1-z

The ligand *p*-NO₂aa_iCH₃ is a N,N'-chelating ligand (N and N' refer to N(imidazolyl) and N(azo) donor centres) and a non-bridging I is appended from the axial position. The tetra-atomic puckered rhombohedral geometry of Hg₂I₂ bridge is exhibited by metric parameters: Hg(1)-I(1), 2.6736(10) Å; Hg(1)-I(4), 3.2844(10) Å (*symmetry: -x, -y, -z). The bond angles, I(1)-Hg(1)-I(2), 129.65°, I(1)-Hg-I(4), 92.20° (*symmetry, -x, -y, -z) support the distorted geometry [13]. The geometrical distortion around central metal ion is caused for the generation of small chelate angle (62.89°). The (Hg(1)-N(1), 2.333(8)Å) is shorter than (Hg(1)-N(4), 2.811Å), that implements the stronger interaction between Hg(II) to N(imidazolyl). The van der Waals radii of Hg(II) (1.55 Å) and N(sp²) (1.53 Å) suggest some sort of Hg----N(azo) interaction. The long Hg(1/2)-N(azo) distance promotes the molecules for activation by light followed by cleavage of the bond and rotation about -N=N- to govern photoisomerisation. The N=N distance (1.260(11) Å) is comparable with reported result (1.262(6) Å) [13,14]. Neighbouring molecules show π-π interactions with *p*-NO₂ phenyl and imidazolyl groups forming supramolecular

aggregation; the weak C-H- π secondary interactions between CH₂-H (imidazolyl) and aromatic rings *p*-NO₂ phenyl also play the pivotal to design the self-assembled molecular structure (**Fig.V.2**). This supramolecular aggregation may be inspired the exhibited molecular properties.

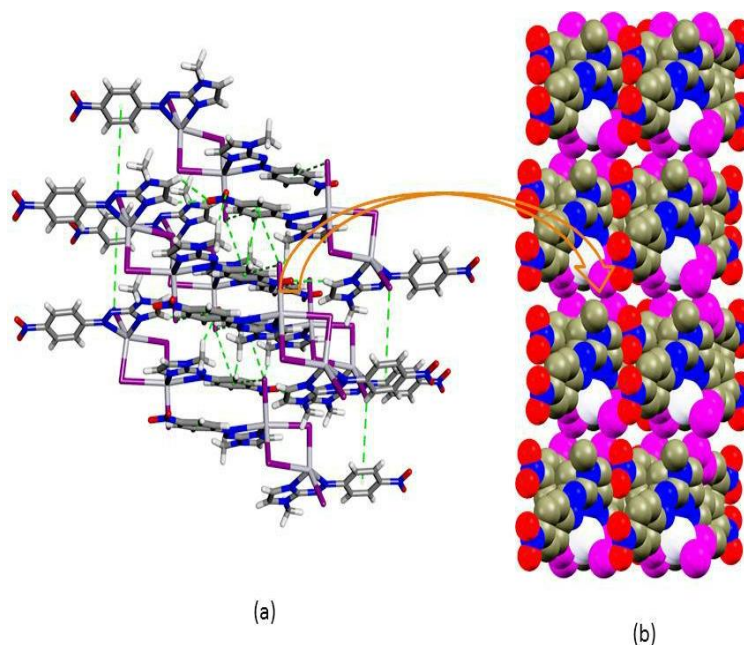
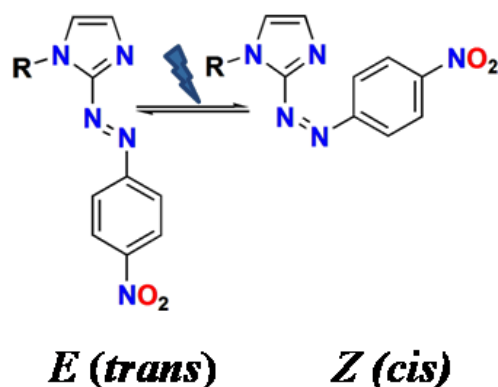


Fig.V.2. (a) Supramolecular interactions in Hg-compound; (b) Space fill view of supramolecular aggregated Hg-compound via different secondary interactions.

V.3.2. Spectrophotometric measurement of Photochromism



Scheme V.b. Isomerisation of 1-alkyl-2-(*p*-nitro-phenylazo) imidazole, *p*-NO₂aaIR, (**1**)

Light absorption in UV wavelength (λ_{max} , 364 nm) causes *trans*-(*E*-isomer) to *cis*-(*Z*-isomer) isomerisation (**Scheme V.b**). For free ligand methanol solution of ligand is used while the

complex is sparingly soluble in MeOH so DMF solution is used. The absorption at UV region is decreased ((**Fig.V.3** and **Fig.V.4**)) with following increase at the longer wavelength portion of the spectrum till a stationary state is reached. The *E*-to-*Z* transformation continues and becomes inaccessible at the *Z* molar ratio of ~ 65%. The continual spectral change is associated with isosbestic point (~340 nm).

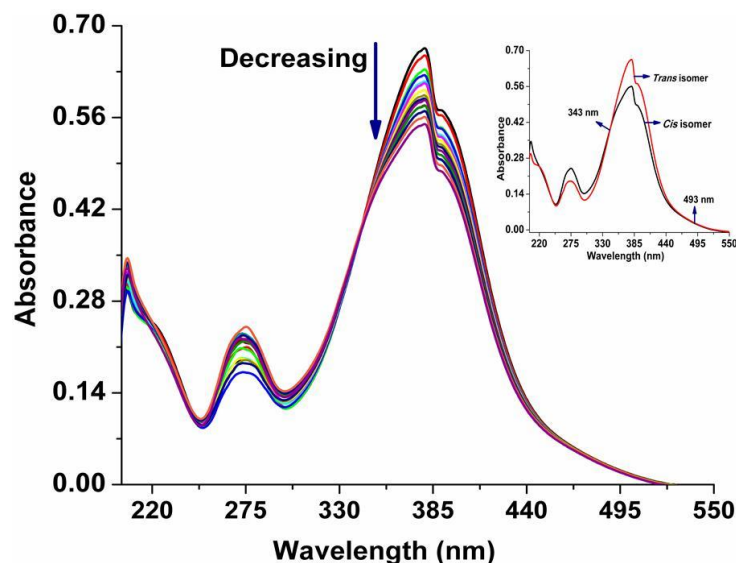


Fig.V.3. Evolution of absorption of *p*-NO₂aaiMe (**1a**) in MeOH upon irradiation at 364 nm at 3 min interval at 25°C.

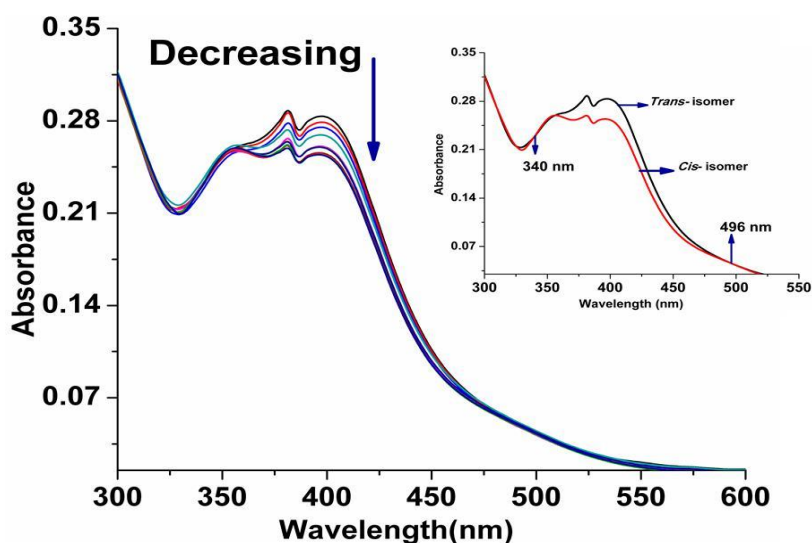


Fig.V.4. Evolution of absorption of [Hg(*p*-NO₂aai-CH₃)(μ -I)(I)]₂ (**4a**) in DMF upon irradiation at 368 nm at 5 min interval at 25°C.

Repetitive irradiation followed by spectral measurements of both the ligands and the complexes give an idea about little signal of dilapidation at least upto 15 cycles. The *E*-to-*Z* ($\Phi_{E \rightarrow Z}$) photoisomerisation for all the compounds has been quantitatively compared with their calculated rates and quantum yields (**Table V.3**). Data may be correlated with molar mass of the photochrome which suggest that increase in mass of the molecule decreases the rate and quantum yield.

Table V.3. Results of photochromism, rate of conversion and quantum yields upon UV light irradiation

Compds	λ_{π,π^*} (nm)	Isobestic point (nm)	Rate of E→Z conversion x 10 ⁸ (s ⁻¹)	$\phi_{E \rightarrow Z}$ conversion
(1a)	364	343, 493	5.010	0.221 ± 0.002
(1b)	365	343, 491	4.861	0.209 ± 0.006
(2a)	364	341,489	2.127	0.153± 0.002
(2b)	366	339,490	2.057	0.148± 0.003
(3a)	367	342,491	2.336	0.168± 0.002
(3b)	366	341,492	2.238	0.161± 0.001
(4a)	368	340,496	2.630	0.186± 0.002
(4b)	367	342,493	2.511	0.181± 0.003

Besides, the coordinated halide (Cl, Br, I) may have photo bleaching activity [25] and may grasp sizeable amount of energy from π - π^* excited state; I (iodo) has highest efficiency in this regard (having imbibing metallic character of I).

The spectral measurements of *cis* (*Z*) to *trans* (*E*) isomerisation of the compounds (**Fig.V.5**, **Fig.V.6**) at 298-313 K show linear relation with $1/T$ vs $-\ln(K/T)$ (Eyring plots) and the ΔS^* and ΔH^* are calculated (**Table V.4**, **Fig.V.7**) from the data. The E_a values of the complexes are

much lower than that of respective free ligand; this accounts the faster *Z*-to-*E* thermal isomerisation of the complex. The ΔS^* of the complexes are much lower than free ligands.

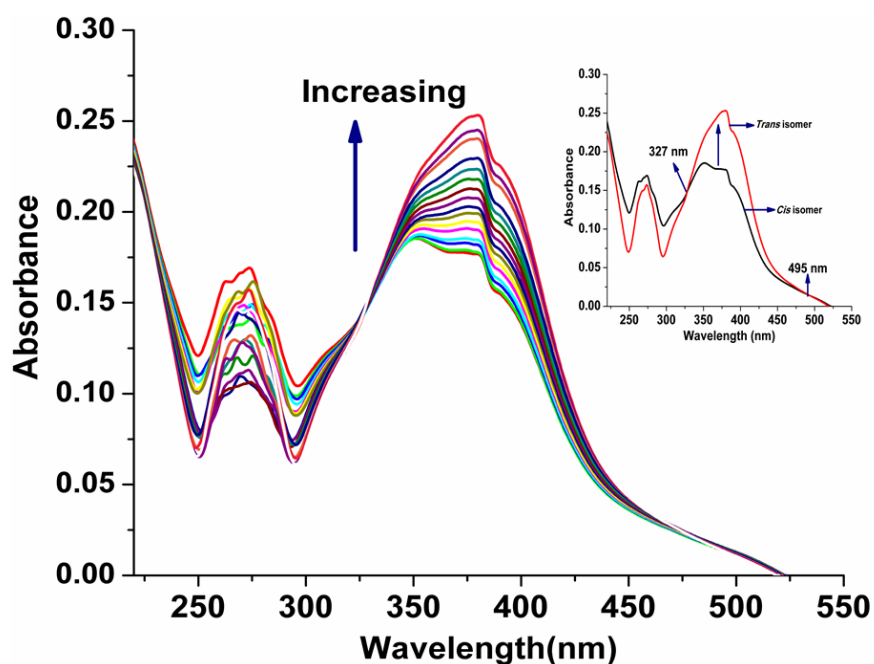


Fig.V.5. The thermal spectral changes of (*p*-NO₂aai-CH₃) (**1a**) in MeOH solution at 30°C.

Inset figure shows spectra of E (*Trans*) and Z (*Cis*) isomer.

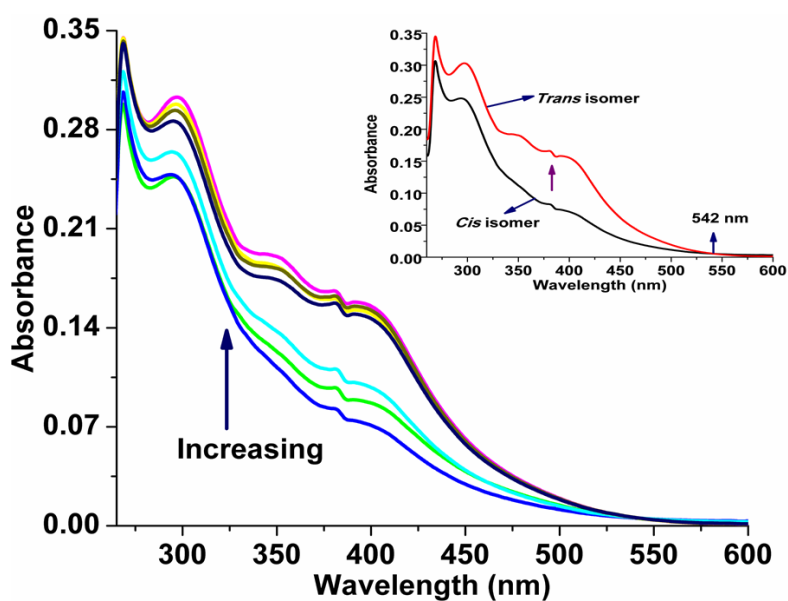


Fig.V.6. The thermal spectral changes of [Hg(*p*-NO₂aai-CH₃)(μ -I)(I)]₂ (**4a**) in DMF solution

at 30°C. Inset figure shows spectra of E (*Trans*) and Z (*Cis*) isomer.

Table V.4. Rate and activation parameters for Z (c) → E (t) thermal isomerisation

Compd	Temp (K)	Rate of thermal c→t conversion x 10 ⁴ (s ⁻¹)	E _a , kJ mol ⁻¹	ΔH* kJ mol ⁻¹	ΔS* J mol ⁻¹ K ⁻¹	ΔG* ^c kJ mol ⁻¹
(1a)	298	0.795	84.65	82.11	-48.14	96.82
	303	1.194				
	308	2.654				
	313	3.756				
(1b)	298	0.778	81.47	78.93	-58.61	96.84
	303	1.321				
	308	2.453				
(2a)	298	1.841	35.59	33.06	-205.60	96.40
	303	2.314				
	308	2.745				
(2b)	298	1.851	34.57	32.61	-206.98	95.84
	303	2.455				
	308	2.751				
(3a)	298	1.875	38.43	35.90	-195.28	95.56
	303	2.641				
	308	3.241				
(3b)	298	2.113	37.17	34.63	-199.11	95.46
	303	2.689				
	308	3.354				
(4a)	298	2.456	42.32	39.78	-180.44	94.90
	303	3.254				
	308	4.521				
(4b)	298	2.574	40.51	37.97	-186.20	94.85
	303	3.324				
	308	4.531				

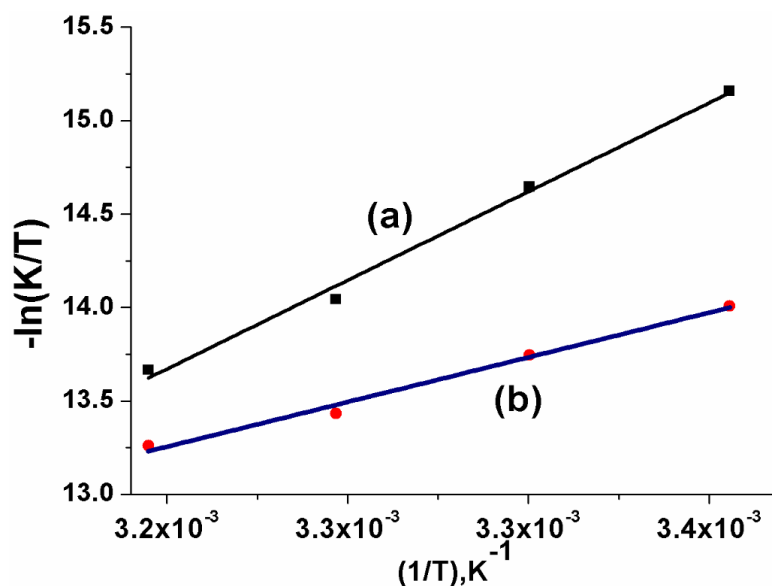


Fig.V.7. The Eyring plots of Z-to-E isomerisation: (a) *p*-NO₂aiMe (**1a**) and (b) [Hg(*p*-NO₂aiMe) (μ-I) (I)]₂ (**4a**) at 298-313 K.

V.3.3. Electronic structure and spectra

Using optimized molecular structures of [Hg(*p*-NO₂aiMe) (μ-X)(X)]₂ {X = Cl (**2a**), Br (**3a**), I (**4a**)} theoretical calculations are performed. From Gauss Sum calculation the energy values of molecular orbitals and fractional contributions of structural components are obtained. In **2a** the HOMO and HOMO-1 are degenerated (E_{HOMO} , -7.05 eV and $E_{\text{HOMO-1}}$, -7.10 eV) in which contribution of Cl is 97 % (**Table V.5**). The LUMO and LUMO+1 are closer in energy and have been constituted from the ligand side (E_{LUMO} , -4.42 eV and $E_{\text{LUMO+1}}$, -3.26 (eV). The HOMO-2 and lower MOs change both from energy and composition. Other unoccupied MOs appear at higher energy. In HOMO and HOMO-1 of **3a** Br covers 98 %. In **4a** the observation is comparable to **2a** and **3a** *i.e.*, the HOMO, HOMO-1 etc. have chief input (98%) from I. Therefore, theoretical measurements conclude about the major contributions of halogen atoms in major molecular orbitals.

Table V.5. Composition of MOs and their energies

Compound	[Hg(<i>p</i> -NO ₂ aaiCH ₃)(μ-Cl)(Cl)] ₂ (2a)			
MO	Energy	Cl	AZO	Hg
LUMO+5	-0.72	0	97	3
LUMO+4	-0.99	0	100	0
LUMO+3	-1.63	1	96	3
LUMO+2	-1.92	26	9	65
LUMO+1	-3.26	0	100	0
LUMO	-4.42	0	99	0
HOMO	-7.05	97	1	2
HOMO-1	-7.1	97	1	2
HOMO-2	-7.19	92	4	4
HOMO-3	-7.33	92	5	4
HOMO-4	-7.72	4	96	0
HOMO-5	-7.8	85	7	9
Compound	[Hg(<i>p</i> -NO ₂ aaiCH ₃)(μ-Br)(Br)] ₂ (3a)			
MO	Energy	Br	AZO	Hg
LUMO+5	-0.72	0	98	2
LUMO+4	-0.99	0	100	0
LUMO+3	-1.66	1	97	2
LUMO+2	-2.03	30	7	62
LUMO+1	-3.27	0	100	0
LUMO	-4.43	1	99	0
HOMO	-6.72	98	0	2
HOMO-1	-6.75	98	0	2
HOMO-2	-6.83	94	2	4
HOMO-3	-6.95	94	2	4
HOMO-4	-7.49	88	2	10
HOMO-5	-7.72	1	99	0
Compound	[Hg(<i>p</i> -NO ₂ aaiCH ₃)(μ-I)(I)] ₂ (4a)			
MO	Energy	I	AZO	Hg
LUMO+5	-0.7	0	98	2

LUMO+4	-0.98	0	100	0
LUMO+3	-1.67	0	80	1
LUMO+2	-2.08	35	98	60
LUMO+1	-3.26	0	100	0
LUMO	-4.42	1	100	0
HOMO	-6.38	98	1	1
HOMO-1	-6.42	98	0	1
HOMO-2	-6.47	95	0	4
HOMO-3	-6.57	95	2	4
HOMO-4	-7.17	88	1	11
HOMO-5	-7.69	2	1	1

UV light shocking is compulsory for photochromic process which implements that *trans*-isomer (E) is more stable than *cis*-isomer (Z). The UV radiation absorption involves $\pi \rightarrow \pi^*$ transition. Involvement of MLCT or XLCTs in the transition may associate with energy loss by energy transfer to the coordinated azoimidazole (via Hg-N(azo) bond cleavage) and hence is not sufficient to perform isomerisation.

Energy correlation diagram (**Fig.V.8**) shows the order of MOs of the complexes. The energies of the MOs show very close in **2a** and **3a** while **4a** differs significantly. The difference in energy ($\Delta E = E_{\text{LUMO}} - E_{\text{HOMO}}$) maintains the ordering $[\text{Hg}(p\text{-NO}_2\text{aaiMe})(\mu\text{-I})(\text{I})_2]$ (**4a**) (1.96 eV) < $[\text{Hg}(p\text{-NO}_2\text{aaiMe})(\mu\text{-Br})(\text{Br})_2]$ (**3a**) (2.29 eV) < $[\text{Hg}(p\text{-NO}_2\text{aaiMe})(\mu\text{-Cl})(\text{Cl})_2]$ (**2a**) (2.63 eV). It is observed a liner relation between ΔE versus rates of isomerisation and quantum yields (**Fig.V.9**). This is an indication of the straight forward relation between photophysical process and activation energy.

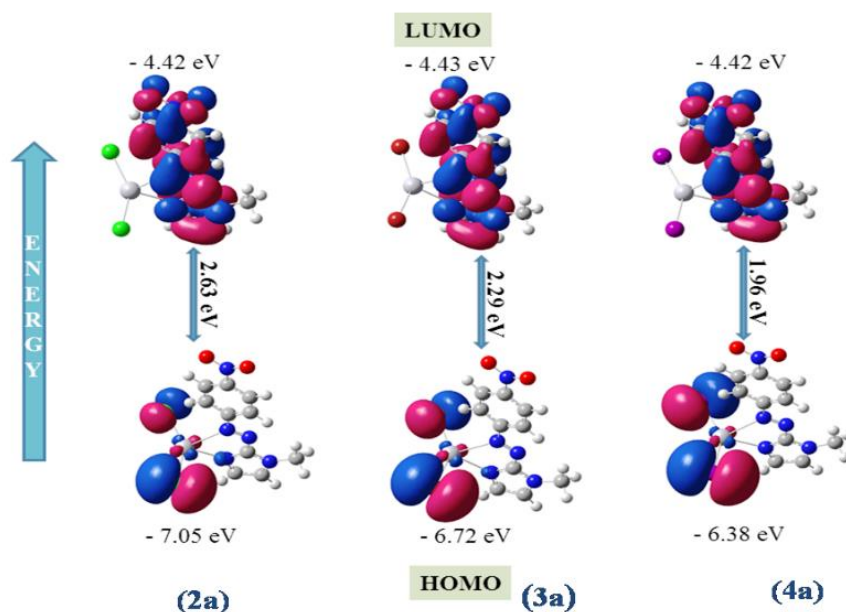


Fig.V.8. Correlation between HOMO (H) & LUMO (L) in terms of their energy of **2a**, **3a** and **4a**. Results obtained from DFT calculation of optimized geometries.

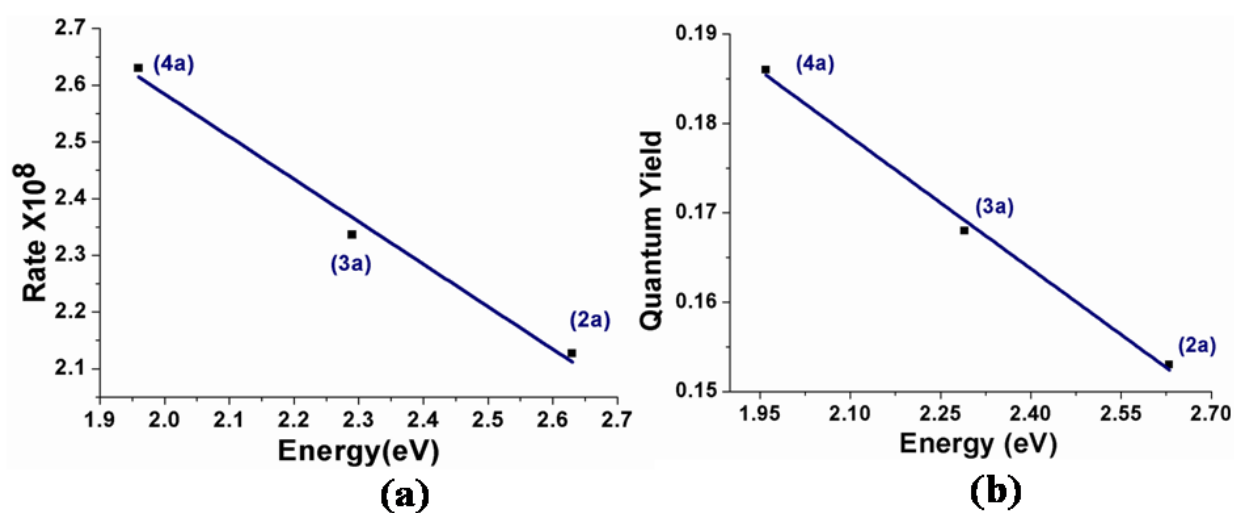


Fig.V.9. Correlation between (a) $\Delta E (= E_{LUMO} - E_{HOMO})$ vs rates of photoisomerisation and (b) $\Delta E (= E_{LUMO} - E_{HOMO})$ vs quantum yield

V.4. Conclusion

Hg(II)-halide complexes of 1-alkyl-2-(*p*-nitro-phenylazo)imidazoles, have been spectroscopically characterized and the structures has been confirmed in one case by single

crystal X-ray diffraction. UV light assisted photochromic behaviour of ligands and the complexes are checked. The rate and quantum yield of E-to-Z isomerisation of the complexes are less than that of free ligand data may be due to the higher rotor mass and volume that may be the regulating factors. DFT and TD-DFT calculations also support the experimental data of the rate and quantum yields.

V.5. References:

- [1]. A. D. W. Kennedy, I. Sandler, J. Andreasson, J. Ho, J. E. Beves, *Chem. Eur. J.*, 26 (2020) 1103-1110
- [2]. a) J. Otsuki, K. Suwa, K. K. Sarker, C. Sinha, *J. Phys. Chem. A*, 111 (2007) 1403-1409; (b) J. Otsuki, K. Suwa, K. Narutaki, C. Sinha, I. Yoshikawa, K. Araki, *J. Phys. Chem. A*, 109 (2005) 8064-8069.
- [3]. (a) A. Harada, *Acc. Chem. Res.*, 34 (2001) 456-464; (b) W. R. Browne, B. L. Feringa, *Nat. Nanotechnol.*, 1 (2006) 25-35; (c) M. Baroncini, S. Silvi, M. Venturi, A. Credi, *Angew. Chem. Int. Ed.*, 51 (2012) 4223-4226; (d) G. Ragazzon, M. Baroncini, S. Silvi, M. Venturi, A. Credi, *Nat. Nanotechnol.*, 10 (2014) 70-75; (e) S. Erbas-Cakmak, D. A. Leigh, C. T. McTernan, A. L. Nussbaumer, *Chem. Rev.*, 115 (2015) 10081-10206.
- [4]. Z. F. Liu, K. Hashimoto, A. Fujishima, *Nature*, 347 (1990) 658-660.
- [5]. (a) W. A. Velema, W. Szymanski, B. L. Feringa, *J. Am. Chem. Soc.*, 136 (2014) 2178-2191; (b) J. Broichhagen, J. A. Frank and D. Trauner, *Acc. Chem. Res.*, 48 (2015) 1947-1960; (c) Z. L. Pianowski, *Chem.- Eur. J.*, 25 (2019) 5128-5144.
- [6]. (a) A. Natansohn, P. Rochon, *Chem. Rev.*, 102 (2002) 4139-4176; (b) F. D. Jochum, P. Theato, *Chem. Soc. Rev.*, 42 (2013) 7468-7483; (c) K. Kumar, C. Knie, D. Bléger, M. A. Peletier, H. Friedrich, S. Hecht, D. J. Broer, M. G. Debije, A. P. H. J. Schenning, *Nat. Commun.*, 7 (2016) 11975; (d) O. S. Bushuyev, M. Aizawa, A. Shishido, C. J. Barrett, *Macromol. Rapid Commun.*, 39 (2018) 1700253; (e) G. Davidson-Rozenfeld, L. Stricker, J. Simke, M. Fadeev, M. Vázquez- González, B. J. Ravoo, I. Willner, *Polymer Chem.*, 10 (2019) 4106-4115.

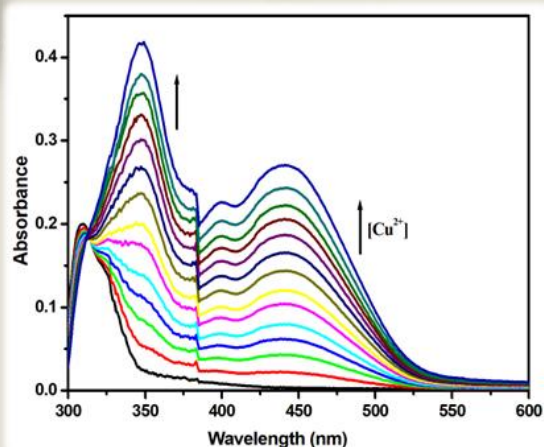
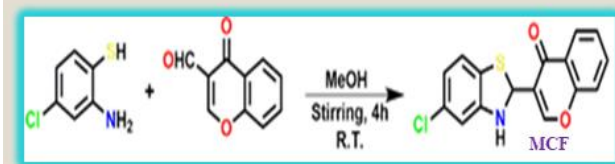
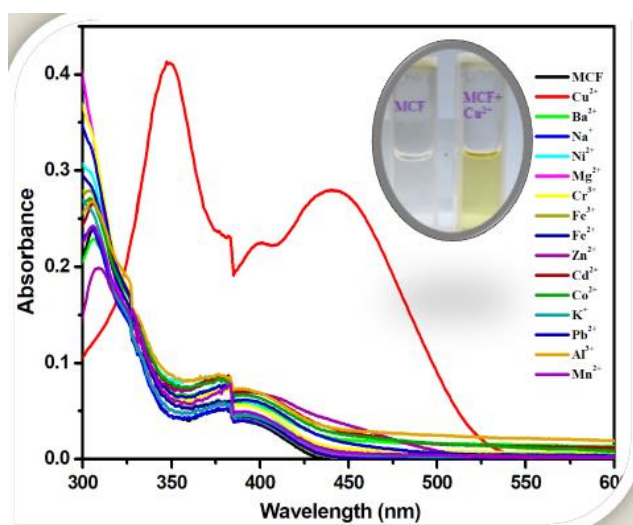
- [7]. (a) R. Klajn, J. F. Stoddart, B. A. Grzybowski, *Chem. Soc. Rev.*, 39 (2010) 2203-2237; (b) P. K. Kundu, D. Samanta, R. Leizrowice, B. Margulis, H. Zhao, M. Börner, T. Udayabhaskararao, D. Manna, R. Klajn, *Nat. Chem.*, 7 (2015) 646-652.
- [8]. (a) Y. Takashima, S. Hatanaka, M. Otsubo, M. Nakahata, T. Kakuta, A. Hashidzume, H. Yamaguchi, A. Harada, *Nat. Commun.*, 3 (2012) 1270; (b) S. Iamsaard, S. J. Aßhoff, B. Matt, T. Kudernac, J. J. L. M. Cornelissen, S. P. Fletcher, N. Katsonis, *Nat. Chem.*, 6 (2014) 229; (c) H. Nie, J. L. Self, A. S. Kuenstler, R. C. Hayward, J. Read de Alaniz, *Adv. Optical Mater.*, 7 (2019) 1900224.
- [9]. (a) P. Gayen, C. Sinha, *J. Lumin.*, 132 (2012) 2371; (b) P. Gayen, K. K. Sarker, C. Sinha, *Colloids Surf. A Physicochem. Eng. Asp.*, 429 (2013) 60; (c) P. Gayen, C. Sinha, *Spectrochim. Acta A*, 104 (2013) 477.
- [10]. U. Panda, S. Jana, B. K. Sarkar, C. Sinha, D. Mallick, *J. Indian Chem. Soc.*, 93 (2016) 613.
- [11]. K. K. Sarker, A. D. Jana, G. Mostafa, J.-S. Wu, T. -H. Lu, C. Sinha, *Inorg. Chim Acta*, 359 (2006) 4377.
- [12]. K. K. Sarker, D. Sardar, K. Suwa, J. Otsuki, C. Sinha, *Inorg. Chem.*, 46 (2007) 8291.
- [13]. K. K. Sarker, B.G. Chand.K. Suwa, J. Cheng, T. -H. Lu, J. Otsuki, C. Sinha, *Inorg Chem.*, 46 (2007) 670.
- [14]. P. Dutta, D. Mallick, S. Roy, E. L. torres, C. Sinha, *Inorg. Chim. Acta*, 423 (2014) 397.
- [15]. T. K. Misra, D. Das, C. Sinha, P. K. Ghosh, C. K. Pal, *Inorg. Chem.*, 37 (1998) 1672.
- [16]. SMART, SAINT, Bruker AXS Inc.: Madison, WI. 1998.
- [17]. G. M. Sheldrick, SHELXS 97, Program for the Solution of Crystal Structure, University of Gottingen, Germany, 1997.
- [18]. G. Zimmerman, L. Chow, U. Paik, *J. Am. Chem. Soc.*, 80 (1958) 3528.
- [19]. Gaussian 03, Revision C.02, M.J. Frisch; G.W. Trucks; H.B. Schlegel; G.E. Scuseria, M.A. Robb, J.R. Cheeseman, J.A. Montgomery, Jr.T. Vreven, K.N. Kudin, J.C. Burant, J.M. Millam, S.S. Iyengar; J. Tomas.; V. Barone; B. Mennucci; M. Cossi, G. Scalmani, N. Rega, G.A. Petersson, H. Nakatsuji, M. Hada, M. Ehara, K. Toyota, R.Fukud, J.Hasegawa, M. Ishida,T.Nakajima, Y. Honda, O.Kitao, H.Nakai, M. Klene, X. Li, J.E. Knox, H.P.Hratchian, J.B.Cross, V.Bakken, C. Adamo, J. Jaramillo, R. Gomperts,

R.E.Stratmann, O. Yazyev, A.J.Austin, P. Cammi, C. Pomelli, J.W.Ochterski, P.Y. Ayala, K.Morokuma, G.A.Voth, P.Salvador,J.J. Dannenberg, V.G.Zakrzewski, S.Dapprich, A.D.Daniels, M.C.Strain, O.Farkas, D.K. Malick, A.D.Rabuck, K.Raghavachari, J.B.Foresman, J.V. Ortiz, Q.Cui, A.G.Baboul, S.Clifford, J.Cioslowski, B.B.Stefanov, G.Liu, A.Liashenko, P.Piskorz, I.Komaromi, R.L.Martin, D. J. Fox, T. Keith, M.A.Al-Laham, C.Y.Peng, A. Nanayakkara, M. Challacombe, P.M.W. Gill, B. Johnson, W. Chen, M.W. Wong, C. Gonzalez, J. A. Pople, Gaussian, Inc., Wallingford CT 2004.

- [20]. B3LYP: A.D. Becke, J. Chem. Phys., 98 (1993) 5648.
- [21]. LanL2DZ: P.J. Hay, W. R. Wadt, J. Chem. Phys., 82 (1985) 270.
- [22]. W.R. Wadt, P.J. Hay, J. Chem. Phys., 82 (1985) 284.
- [23]. P.J. Hay, W. R. Wadt, J. Chem. Phys, 82 (1985) 299.
- [24]. N.M. O'Boyle, J.G. Vos, GaussSum 1.0; Dublin City, University: Dublin, Ireland 2005.
- [25]. A. T. Hutton, H. M. N. H. Irving, J. Chem. Soc. Dalton Trans., 11 (1982) 2299.

Chapter VI

Use of chromone based probe as colorimetric sensor for the detection of Cu^{2+} ion: design of test paper kit



CHAPTER VI

Abstract

A chromone-based molecule, 3-(5-chloro-2,3-dihydrobenzo[*d*]thiazol-2-yl)-4*H*-chromen-4-one (**MCF**) has been spectroscopically characterised (FT-IR, UV-Vis, ESI-MS, NMR) and has been used for the chromogenic selective recognition of Cu²⁺ ion in EtOH-H₂O (99:1, v/v) medium. The sensor shows excellent selectivity towards Cu²⁺ ion at very low limit of detection, 0.6 μM in presence of competitive ions which is much lower than the permissible limit (20 μM) in drinking water recommended by the World Health Organization (WHO). From the Job's plot it has been concluded that the probe **MCF** binds Cu²⁺ with 1:1 molar ratio. The binding constant ($4.9346 \times 10^4 \text{ M}^{-1}$) of **MCF** towards Cu (II) ion was determined by using the Benesi-Hildebrand equation. The naked eye change from colourless to yellowish brown of **MCF** solution upon addition of Cu²⁺ ion in presence of different competitive metal ions is very convincing and helps to design paper kits

VI.1. Introduction

Recognition of cations, anions and small molecular species are very essential towards the achievement of Sustainable Development Goals (**Chapter I**). The sensing is very useful for the different application in analytical chemistry as well as biological field. Being third most abundant and essential trace element, Copper can play a diverse role for the activity of biological system. The presence of excess quantity of copper can cause many diseases such as Wilson's disease [1,2], Parkinson's disease [3], Alzheimer's disease [4], Menkes syndrome [5,6] and the irregular intake of copper ions effects different human organs including kidney damage, gastrointestinal problems, diabetes, liver problems even extreme consumption of copper ion leads to life at risk [7].

The expansion of human civilisation demands a high production of different industrial chemical component, agricultural pesticide which can cause copper ion contamination. This copper ion accumulation leads to serious abnormalities of environment as well as human health [8-20]. Recently various types of chemical sensors have been synthesised for the detection of Cu²⁺ ion [21-24]. On this background, design of new sensor is focused to cultivate an easier technique by using low cost and less hazardous materials, which can show best selectivity and sensitivity towards analyte and may be handled even by a non-professional. Colorimetric method is superior over the other conventional method [25-29] because naked eye detection of an analyte is very easy and accessible within the laboratory settings. In recent times, various types of organic receptors have been synthesised and such receptors have been used to detect various species preferably cations [30-40] by colorimetric method. Chromone based chemosensors [41-44] recognise different ions at different structural backdrop and different conditions. Chromone based species have a great antioxidant nature therefore they play an

important role in pharmaceutical field. It has an immense utility in the field of antimicrobial, antifungal and anticancer studies [45–48].

In the present work, we have synthesized a novel chromone-based molecule, 3-(5-chloro-2,3-dihydrobenzo[*d*]thiazol-2-yl)-4*H*-chromen-4-one (**MCF**) and characterized by different spectroscopic techniques. This molecule shows selective, specific and sensitive colorimetric response towards Cu²⁺ ion in EtOH-H₂O (99:1, v/v) medium.

VI.2. Experimental Section

VI.2.1. Materials

3-Formylchromone, 2-amino-4-chlorobenzenethiol, all other reagents and solvents were of reagent grade and were purchased from Sigma-Aldrich, Spectrochem, SRL Chemical and Merck; were used in the experiment without further purification. All other chloride, nitrate, acetate and sulphate salt of different metals such as: NaCl, CrCl₃·6H₂O, FeCl₃·6H₂O, Al(NO₃)₃·9H₂O, NiCl₂·6H₂O, Cd(OAc)₂·2H₂O, [(NH₄)₂Fe(SO₄)₂(H₂O)₆] (Mohr's Salt), Zn(OAc)₂·2H₂O, Cu(NO₃)₂·3H₂O, Co(NO₃)₂·6H₂O, Pb(NO₃)₂, MnCl₂·4H₂O, BaCl₂·2H₂O, MgCl₂·6H₂O and KBr were used for experimental analysis.

VI.2.2. General Methods

Tetramethylsilane (TMS) served as the internal standard in ¹H-NMR spectra recorded on a 300 MHz (Bruker-DPX) in DMSO-d₆ solvents. ¹³C-NMR spectra were recorded on a 75 MHz (Bruker-DPX) instrument in DMSO-d₆ using same internal standard. HRMS (m/z) measurements were taken with an ESI method and a Q-Tof Micro mass spectrometer, respectively. A PerkinElmer FT-IR spectrum RX1 spectrometer was utilized to capture an infrared spectrum in KBr (4500-500 cm⁻¹). The elemental analyzer PerkinElmer 240C was used for the CHN analysis. Perkin Elmer Spectrofluorimeter model LS55 and Perkin Elmer

Spectrophotometer Lambda 25 were used, respectively, to record the measurements of the fluorescence and UV-vis spectra.

VI.2.3. Synthesis of the probe MCF

To methanol (10 mL) in a round bottom flask 3-formylchromone (174.2 mg, 1.0 mmol) was added followed by the dropwise addition of 2-amino-4-chlorobenzenethiol (159.6 mg, 1.0 mmol) in the same solvent and the mixture was stirred for 4 h (**Scheme VI.a**). White precipitate appeared during the course of the reaction and the solution was filtered off to obtain the desired product, 3-(5-chloro-2,3-dihydrobenzo[*d*]thiazol-2-yl)-4*H*-chromen-4-one (**MCF**). The product was dried and used for structural analysis without further purification; yield, 0.23 g (73%).



Scheme VI.a: Synthesis of 3-(5-chloro-2,3-dihydrobenzo[*d*]thiazol-2-yl)-4*H*-chromen-4-one (MCF)

Monoanalytical data the probe **MCF**: Elemental analysis (%) calculated for C₁₆H₁₀ClNO₂S: C, 60.86; H, 3.19; N, 4.44; found: C, 60.81; H, 3.17; N 4.46.

¹H NMR (300 MHz, DMSO-*d*⁶): δ 8.29 (s, 1H), 8.10 (d, *J* = 7.9 Hz, 1H), 7.84 (t, *J* = 8.3 Hz, 1H), 7.68 (d, *J* = 8.4 Hz, 1H), 7.53 (t, *J* = 7.4 Hz, 1H), 7.06 (d, *J* = 2.3 Hz, 1H), 7.00 (d, *J* = 8.04 Hz, 1H), 6.67 (d, *J* = 1.5 Hz, 1H), 6.61 (d, *J*₁ = 8.04 Hz, *J*₂ = 1.6 Hz, 1H), 6.39 (d, *J* = 2.6 Hz, 1H) (**Fig. VI.1**); ¹³C NMR (75 MHz, DMSO-*d*⁶): δ 176.12, 156.29, 153.84, 149.03, 134.99, 130.00, 126.12, 125.61, 125.23, 125.05, 123.30, 122.54, 118.95, 118.56, 109.43,

62.12 (**Fig.VI.2**). HRMS (ESI, m/z) calcd. for $\text{C}_{16}\text{H}_{11}\text{ClNO}_2\text{S}$ $[\text{M}+\text{H}]^+$: 316.0199; found: 315.9250 (**Fig.VI.3**); IR data: ν_{max} 3308, 1634, 1463, 1406, 1342 cm^{-1} (**Fig.VI.4**).

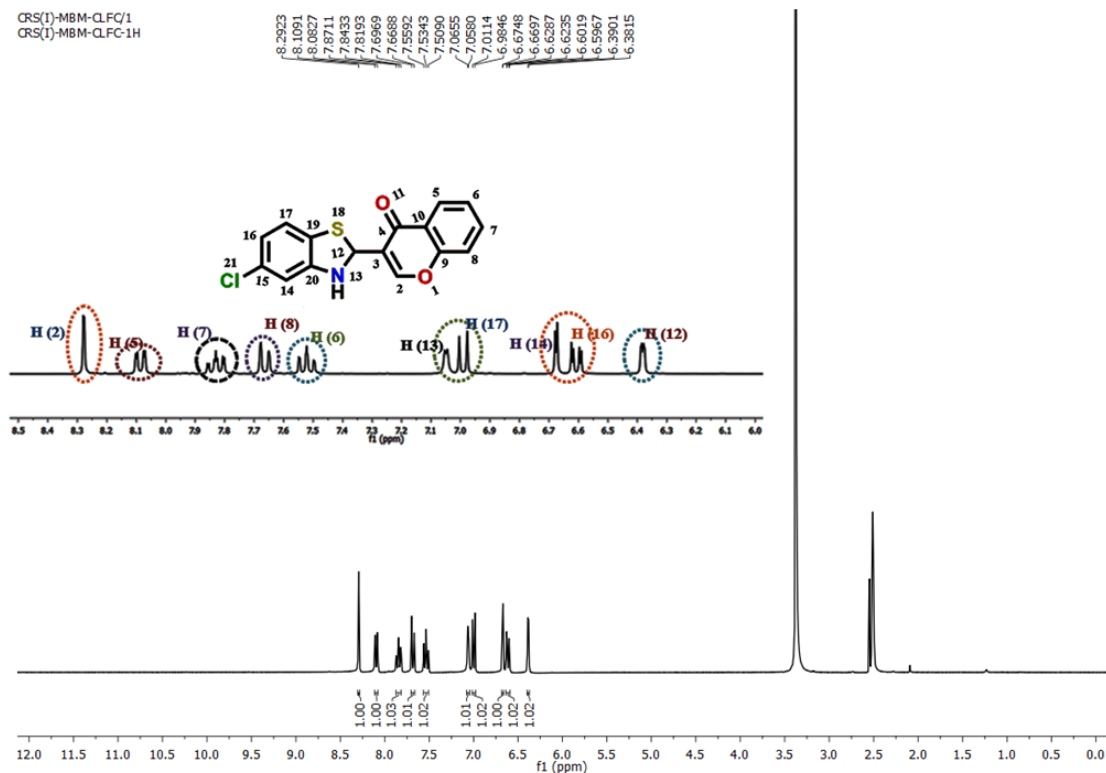


Fig.VI.1. ^1H NMR spectrum of MCF in DMSO-d_6 .

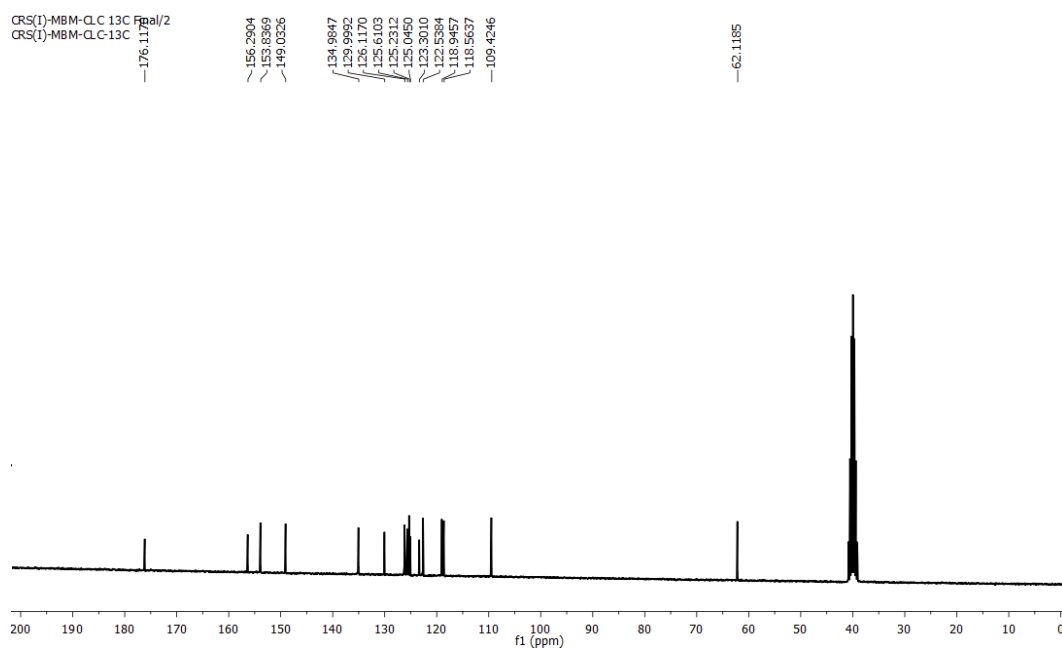


Fig.VI.2. ^{13}C NMR (75 MHz) spectra of the probe MCF in $\text{d}_6\text{-DMSO}$.

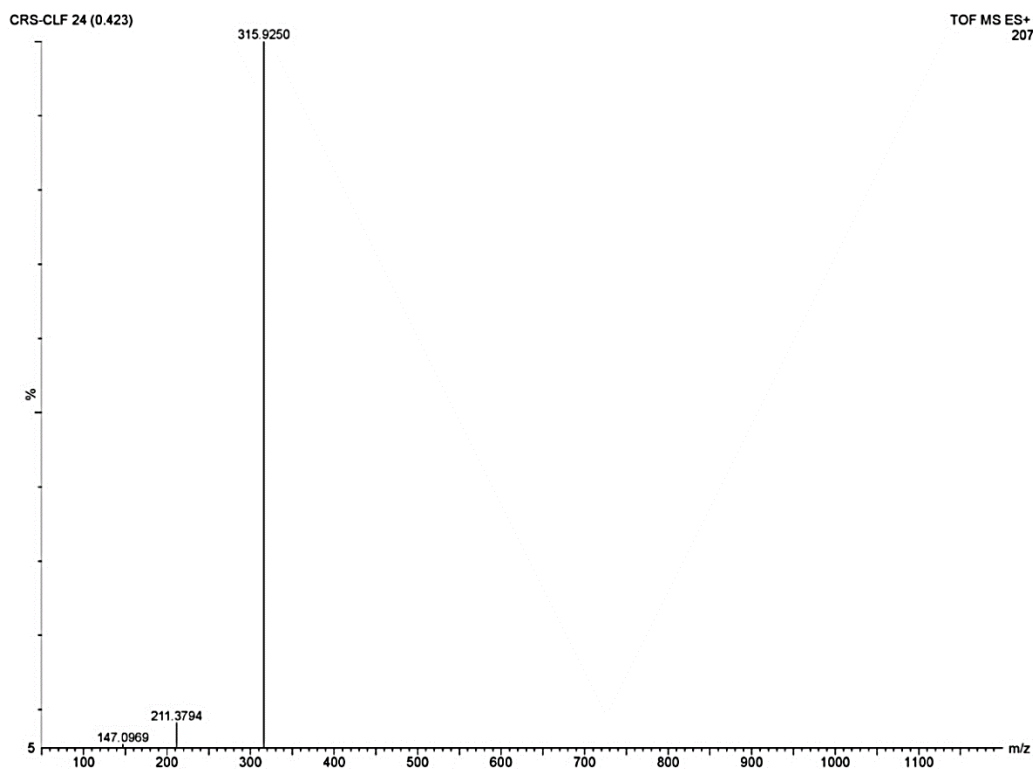


Fig.VI.3. Mass spectrum of the probe MCF.

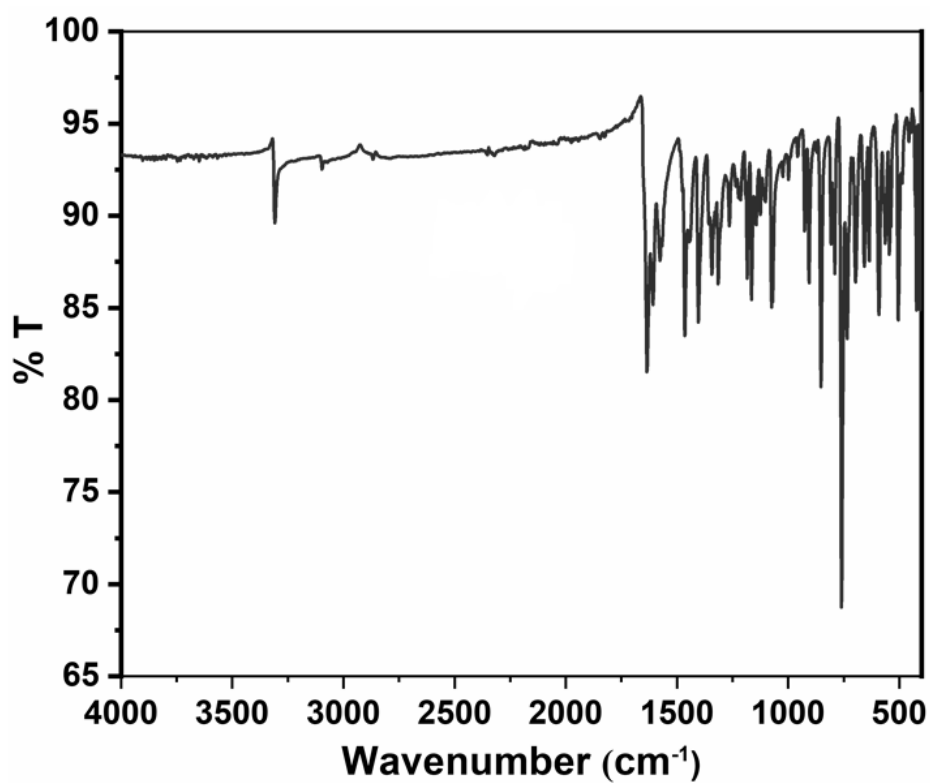


Fig.VI.4. IR spectra of the probe MCF.

VI.2.4. Preparation of experimental solution and test paper stripe

A solution of **MCF** (1×10^{-3} M) was prepared in ethanol and the solution of **MCF** was diluted to 25 μM with ethanol-water (99:1, v/v) solution and this solution was used in the entire UV-visible experiment. The stock solution (1×10^{-3} M) of different metal ions were prepared and this solution was used in the entire UV-visible experiment. The different metal ions sensing by the probe **MCF** were studied using UV-vis spectrophotometer in ethanol-water (99:1, v/v) medium at room temperature. For the preparation of paper stripe, a filter paper with the regular sizes were absorbed into the EtOH-H₂O (99:1, v/v) solution of **MCF** and then dried well in air. The dried test paper stripe containing **MCF** were then absorbed in methanolic solution of Cu(II) ion and dried very well in air about 4-5 min.

VI.3. Results and discussion

VI.3.1. UV-Vis spectroscopy measurements:

The free ligand **MCF** in EtOH-H₂O (99:1, v/v) exhibits absorption maxima centered at 306 nm and 382 nm (**Fig.VI.5**). The absorption maxima at 306 nm may be due to $\pi\text{-}\pi^*$ transition and the band at 382 nm may be due to $n\text{-}\pi^*$ transition [49]. Upon the addition of various metal ions, no such distinguishable change in absorption spectra takes place except for Cu^{2+} ions. Upon addition of 1.0 equiv. of Cu^{2+} ions to the solution of **MCF** two new absorption bands appeared at 348 nm and 441 nm. This spectrum shifts due to the complexation process pertains to intramolecular charge transfer (ICT) transition [50-52]. According to these findings, the probe **MCF** might be used as a naked-eye probe for Cu^{2+} because of its notable selectivity to the metal ion.

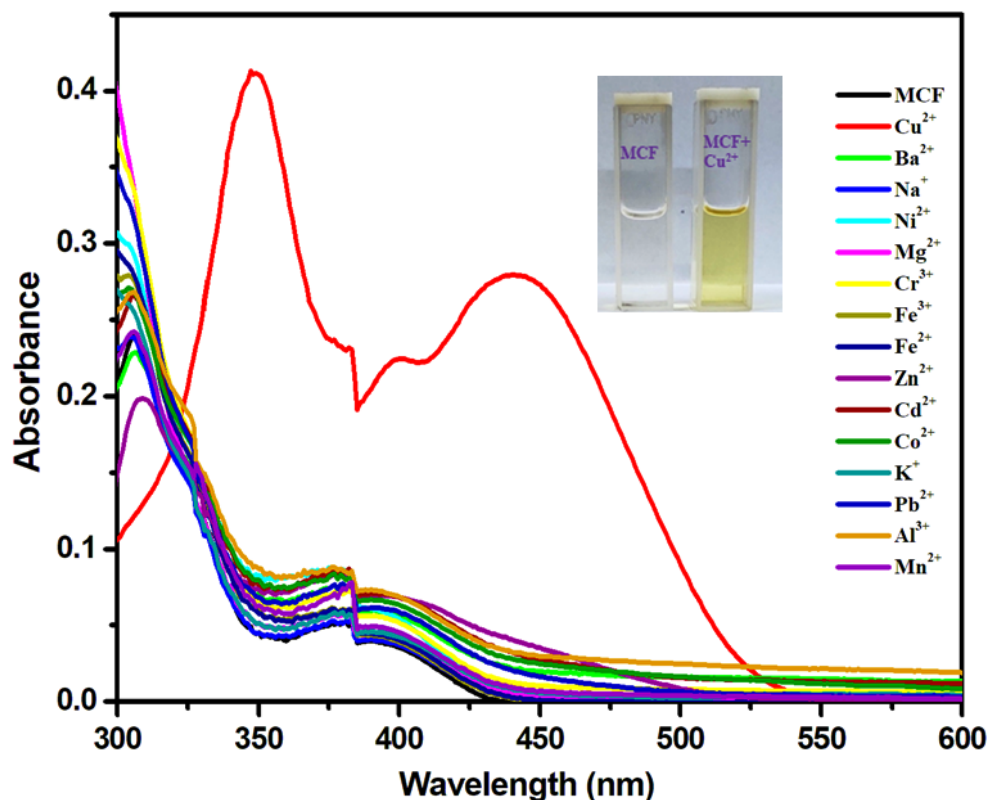


Fig.VI.5. UV–vis absorption spectra of **MCF** (25 μM) with various cations in ethanol/water (99:1, v/v) medium (a spike is due to instrumental parameter).

The UV-vis spectroscopic titration of the probe, **MCF** was carried out upon incremental (3 μL of Cu^{2+} in each time) addition of Cu^{2+} ions in ethanol/water (99:1, v/v) medium. The observation shows a gradual increase in absorbance intensity at 348 nm and 441 nm (**Fig.VI.6**) with a clear isobestic point at 313 nm this is due to the several vibronic transitions that occurred during the electronic transition. After the gradual addition of Cu^{2+} ions to the probe **MCF** the yellowish brown colour arises. These above observations indicate the interaction of **MCF** with the Cu^{2+} ions.

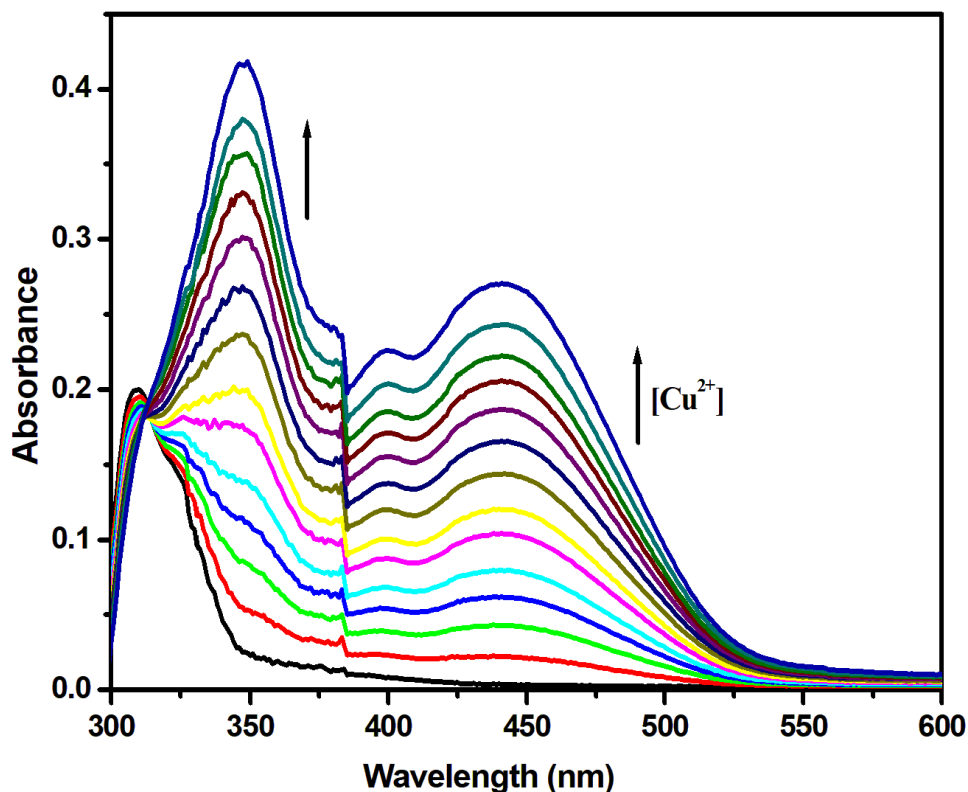


Fig.VI.6. UV-vis absorption spectra of MCF (25 μM) upon incremental (3 μL of Cu^{2+} in every time) addition of Cu^{2+} ions in ethanol/water (99:1, v/v) .

More importantly, a competitive study was carried out introducing Cu^{2+} to a solution of MCF in the presence of the various metal ions. This competitive study indicates that the other competitive metal ions did not significantly alter the absorption of MCF as shown in **Fig.VI.7**. This finding indicates that other competing metal ions have no discernible effect on probe's (MCF) ability to detect Cu^{2+} ions.

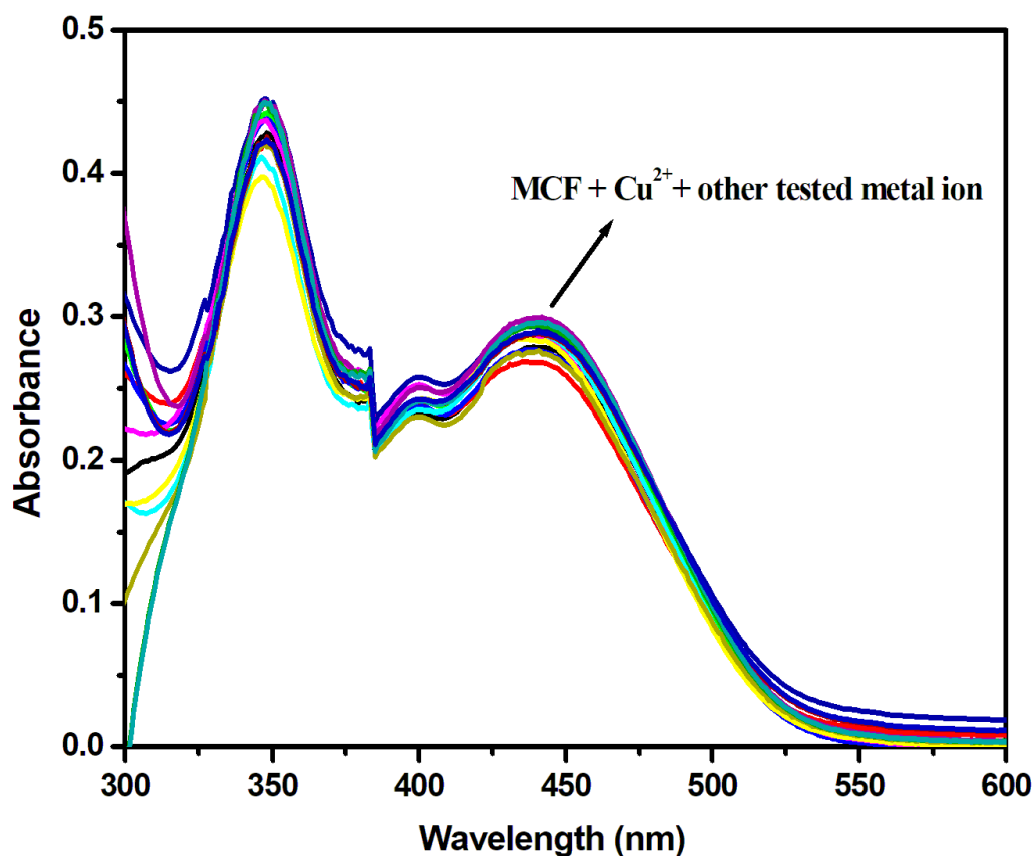


Fig.VI.7. Competitive study of **MCF** towards Cu^{2+} ion sensing in presence of different cations in ethanol-water (99:1, v/v) medium.

The association constant (K_a) has been determined literally from the titration profiles by interpreting $(A_{\text{max}}-A)/(A-A_0)$ vs $1/[\text{Cu}^{2+}]$. The $1/\text{slope}$ of the linear fit line was used to compute the K_a value in accordance with the Benesi-Hildebrand equation. From the Benesi-Hildebrand plot the association constant (K_a) evaluated as $4.9346 \times 10^4 \text{ M}^{-1}$ (**Fig.VI.8**). This association constant value proves the sufficient stability of the (**MCF**+ Cu^{2+}) complex.

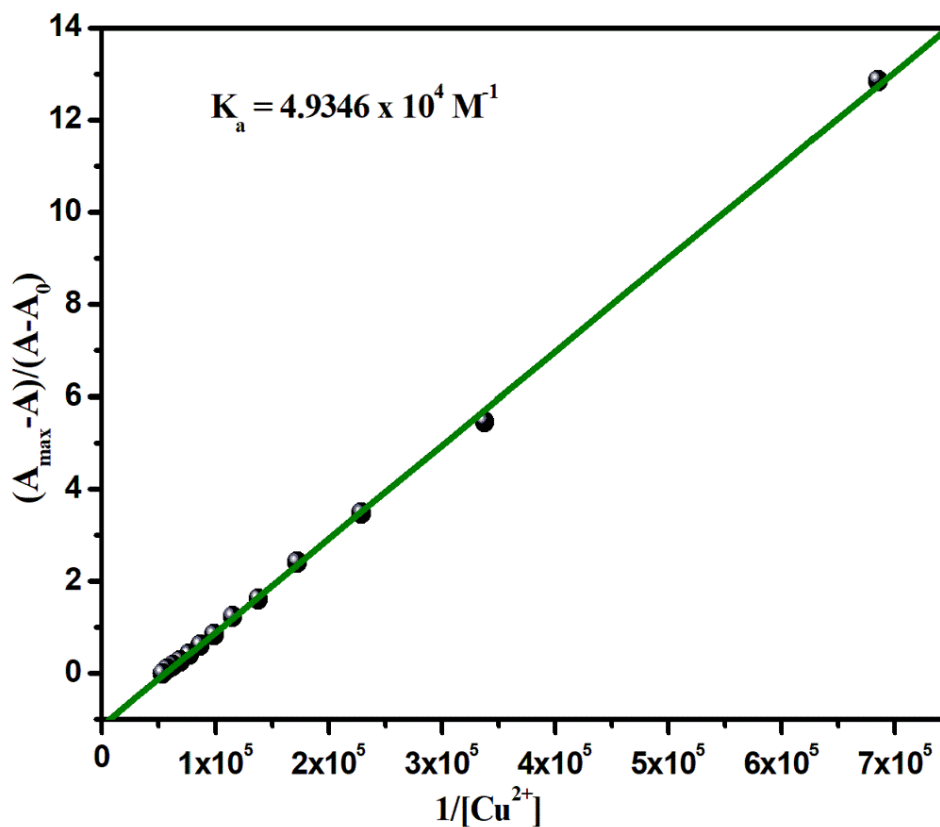


Fig.VI.8. Benesi-Hildebrand plot of **MCF** in presence of Cu^{2+} ions in ethanol/water (99:1, v/v) medium.

The stoichiometric study of **MCF** towards Cu^{2+} ions has been studied using Job's plot (**Fig.VI.9**) by colorimetric method which has established 1:1 stoichiometric binding between the probe **MCF** and Cu^{2+} ions.

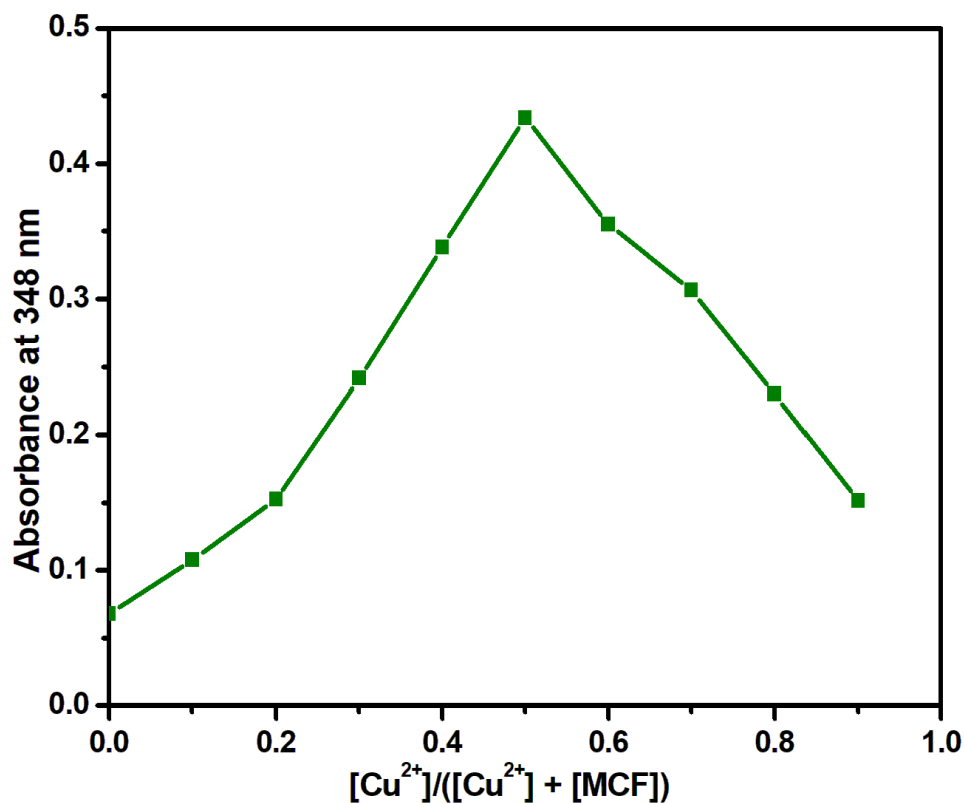


Fig.VI.9. Job's plot of the probe MCF with Cu^{2+} in ethanol-water (99:1, v/v) medium.

The Limit of detection (LOD) value has been evaluated by using $3\sigma/M$ method (σ : standard deviation and M: slope) in ethanol-water (99:1, v/v) medium and the LOD value observed as $0.6 \mu\text{M}$ (**Fig.VI.10**) which is much lower than the WHO recommended threshold value ($76 \mu\text{M}$) of Zn^{2+} ion in drinking water.

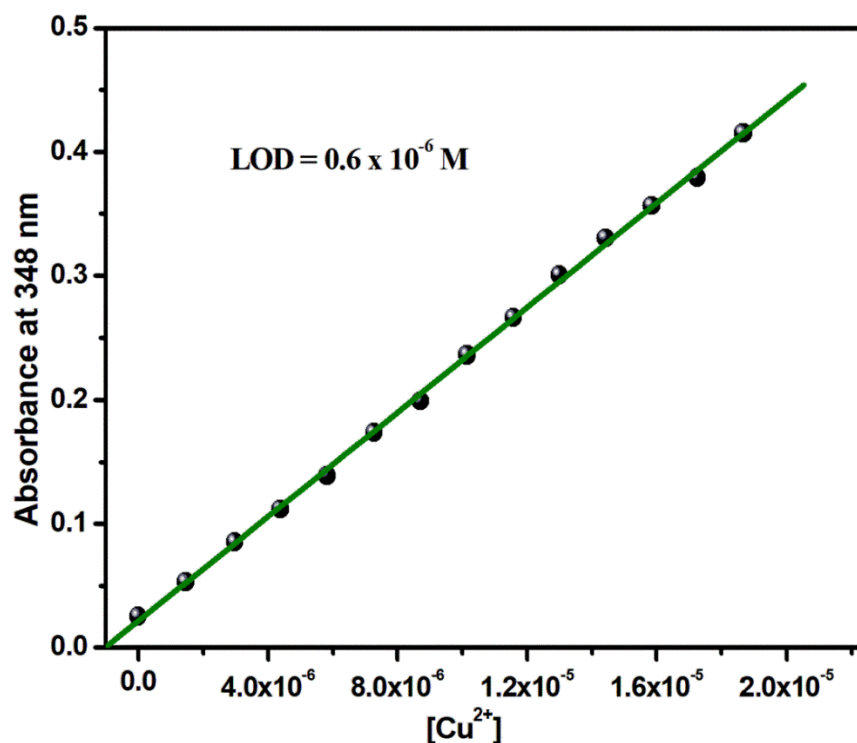


Fig.VI.10. Determination of LOD of Cu^{2+} ions by **MCF** in ethanol-water (99:1, v/v) medium using 3σ method.

VI.3.2. Effect of pH

For the detection of metal ions in practical applications, a compatible pH range is considered one of the most crucial aspects. The effect of pH on the spectral responses of **MCF** in the absence and presence of Cu^{2+} was studied with a pH range of 2 to 12. From the **Fig.VI.11**, it is observed that the pH from 2 to 7 did not alter the absorbance intensity of free **MCF** but after the pH 7 the absorbance intensity slightly increases upto pH 12. But upon the addition of Cu^{2+} ions to the probe **MCF** at a various pH range, the significant spectral and colour changes takes place. In case of the complex (**MCF**+ Cu^{2+}) the absorbance intensity gradually increases from pH 2 to 7 and after the pH 7 the absorbance intensity significantly decreases (**Fig.VI.11**) upto pH 12. Hence for the complex (**MCF**+ Cu^{2+}) the most intense and significant colour change

and absorption maxima observed at the pH 7. This result supports that the probe **MCF** can be used as a colorimetric probe for the recognition of Cu^{2+} ions in industrial and biological system.

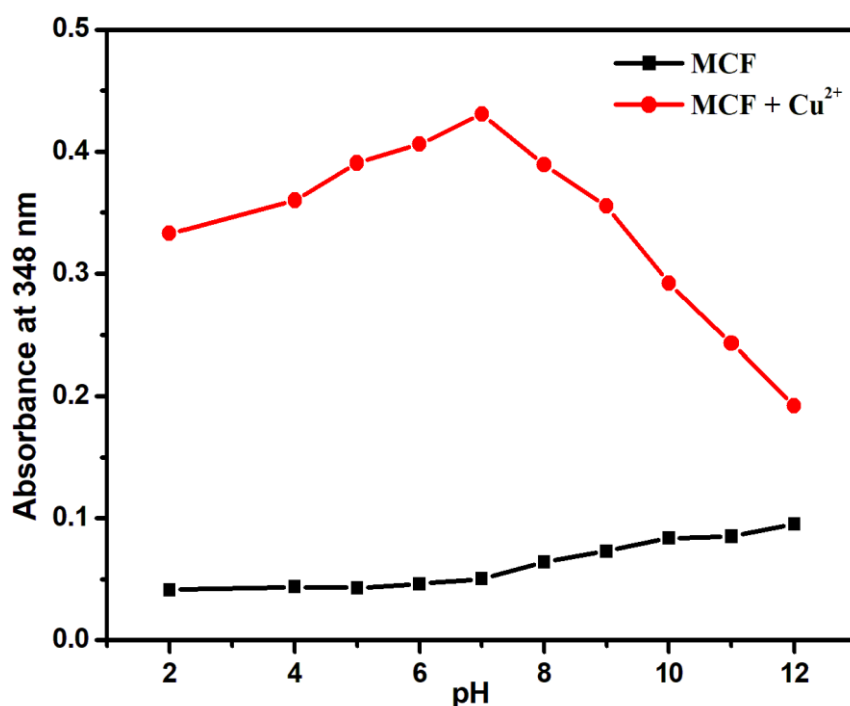


Fig.VI.11. Effect of pH to the absorption spectra of **MCF** and **MCF + Cu^{2+}** complex.

VI.3.3. Binding mechanism of **MCF** towards Cu^{2+}

To investigate the mechanism of binding of the probe (**MCF**) towards Cu^{2+} ions the $^1\text{H-NMR}$ titration studies were carried out. During the $^1\text{H-NMR}$ titration the $^1\text{H-NMR}$ spectrum of **MCF** changed upon the addition of Cu^{2+} soluble with the $\text{d}^6\text{-DMSO}$ solvent. The $^1\text{H-NMR}$ titration shows the broadening of the all proton signals of the chromone moiety ranging from the triplet at 7.53 ppm to singlet at 8.29 ppm; similar observations were also seeming to be happened for the protons of benzothiazole ring ranging from the doublet at 6.39 ppm to doublet at 7.00 ppm respectively; after adding 0.5 equiv. Cu^{2+} in $\text{d}^6\text{-DMSO}$. Upon addition of 1.0 equiv. Cu^{2+} ; all the respective proton signals of both chromone and benzothiazole rings merge to a broad singlet (**Fig.VI.12**). It's also important to notice that the singlet (-NH-) at 7.06 ppm disappears once

1.0 equiv. of Cu^{2+} is added, indicating that Cu^{2+} binds via -N-H proton of the benzothiazole ring. This observation supports the interaction of **MCF** with the Cu^{2+} ions.

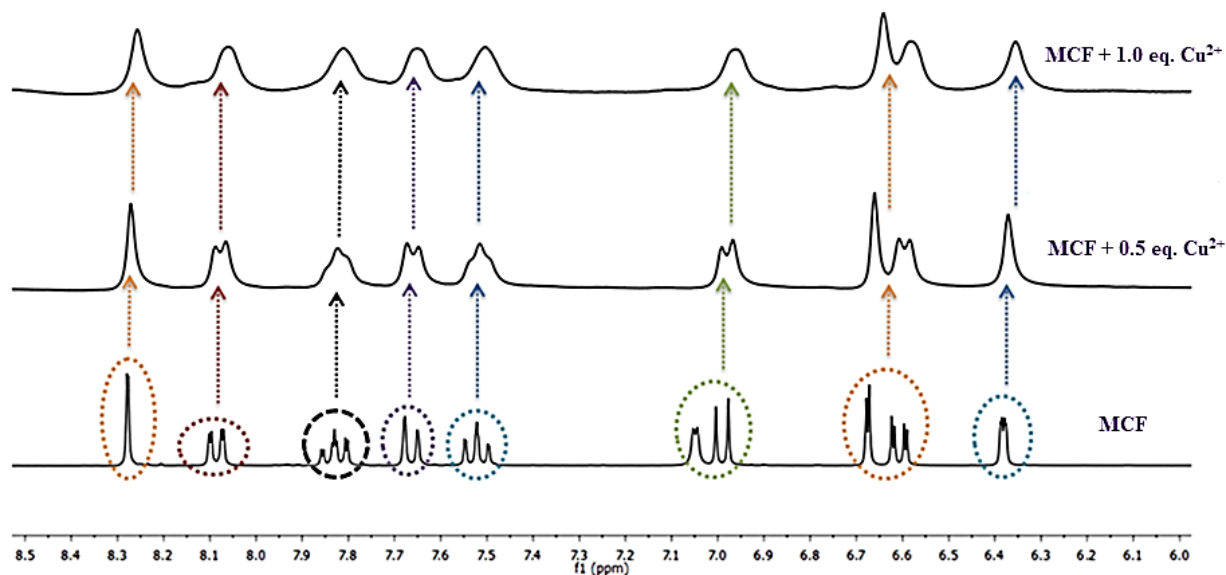


Fig.VI.12. The ^1H NMR (300 MHz, $\text{d}_6\text{-DMSO}$) titration spectra of **MCF** in presence of Cu^{2+} ion.

In FT-IR spectrum of **MCF** (**Fig.VI.4**) there is a sharp peak of -NH at 3308 cm^{-1} which was completely disappeared in the FT-IR spectrum of Cu^{2+} complex of **MCF** (**Fig.VI.13**). Hence this observation confirmed the formation of Cu^{2+} complex with the replacement of proton from benzothiazolyl -NH.

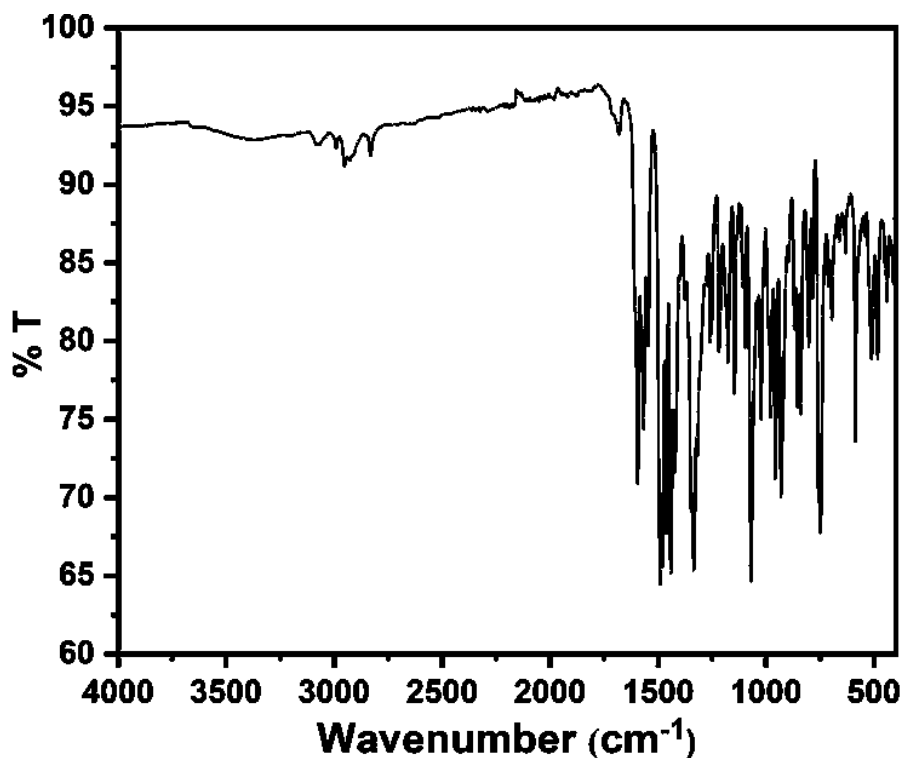
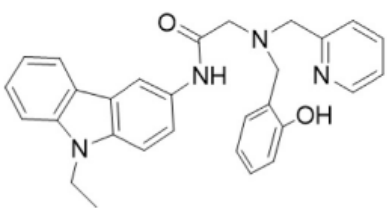
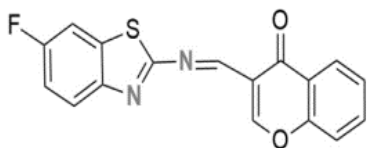
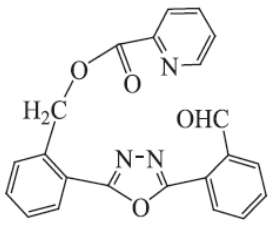
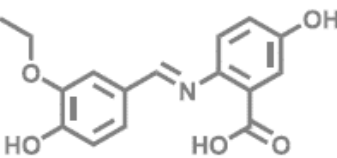
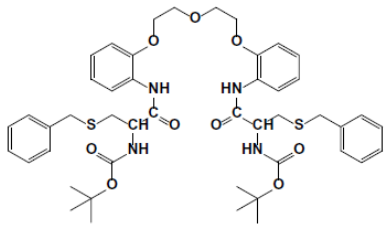
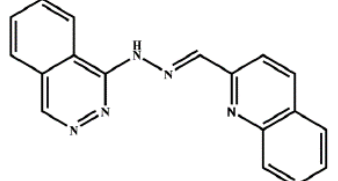
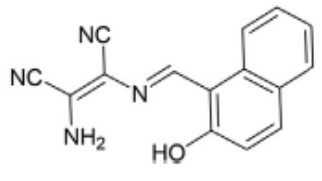
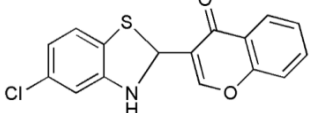


Fig.VI.13. FT-IR spectrum of Cu²⁺ complex of MCF

The probe, MCF shows efficient selectivity towards Cu²⁺ ions and the results have been compared (Table VI.1) with the recently published articles and it is found that the performance of the probe, MCF is better than some recently published articles.

TableVI.1. Correlation table of different parameters of some recently published work on Cu²⁺ sensing.

Probe	Solvent	LOD (M)	Reference
	DMF-buffer solution (1:1, v/v, 10 mM bis-tris, pH 7.0).	2.9×10^{-6} M	[53]
	THF: Ethanol	0.273×10^{-6}	[54]

	CH ₃ CN	4.48 × 10 ⁻⁶	[55]
	EtOH-H ₂ O (v/v, 8:2) (HEPES 0.01 M, pH = 7.4) solution.	0.39 × 10 ⁻⁶	[56]
	CH ₃ CN	6.6 × 10 ⁻⁶	[57]
	Bis-tris buffer (10 mM, pH 7).	2.1 × 10 ⁻⁶	[58]
	10 mM bis-tris buffer/ DMSO (7:3, v/v)	2.4 × 10 ⁻⁶	[59]
	ethanol-water (99:1, v/v)	0.6 × 10 ⁻⁶	This work

VI.3.4. Reversibility study

A probe's propensity to turn in the opposite direction is crucial for practical uses. The reversibility of MCF was determined by using the chelating agent ethylenediaminetetraacetic acid (EDTA) via UV-Vis titration. As shown in **Fig.VI.14** upon the addition of EDTA to the solution containing MCF+Cu²⁺ mixture, the absorption spectra of free MCF were restored with the change in color from yellowish brown (MCF+Cu²⁺) to colorless (free MCF) takes place. Again, when to this solution Cu²⁺ was added then the solution turns into yellowish brown which reflects in the absorption spectra (**Fig.VI.14**). Significantly this observation was repeatedly

happened with the alternative addition of Cu^{2+} and EDTA. This observation due to the formation of a stable EDTA-Cu complex with the release of free MCF. This fact reveals that the sensor MCF can be repeatedly used to recognize Cu^{2+} ions.

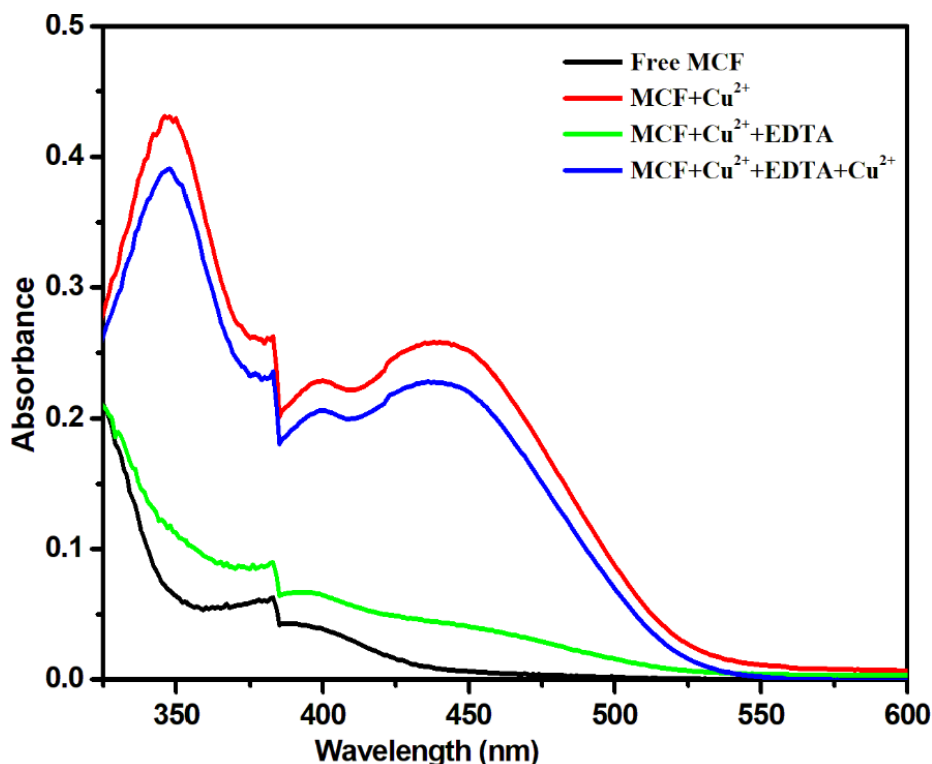


Fig.VI.14. The absorbance spectra of MCF after the alternative addition of Cu^{2+} and EDTA.

VI.3.5. Application on test paper kit

In an ethanol/water (99:1, v/v) medium, the selectivity of MCF towards several metal ions, including Na^+ , Cr^{3+} , Fe^{3+} , Al^{3+} , Ni^{2+} , Cd^{2+} , Fe^{2+} , Zn^{2+} , Cu^{2+} , Co^{2+} , Pb^{2+} , Mn^{2+} , Ba^{2+} , Mg^{2+} , and K^+ has been tested. It displayed a very obvious preference for copper ions, as seen with the naked eye. Only Cu(II) displayed a striking color shift (Fig.VI.15) from colorless to yellowish brown when probe was subjected to a succession of distinct metal ions in ethanol/water (99:1, v/v). Contrarily, no discernible color change was visible in the other metal ions.



Fig.VI.15. Naked eye view of **MCF** in presence of different metal ions in ethanol/water (99:1, v/v) medium.

Test strip was employed to look at the real-world applicability of **MCF**. A filter paper with the regular size was absorbed into the EtOH-H₂O (99:1, v/v) solution of **MCF** and then dried well in air. Significantly the apparent color shift was noticed after being sprayed with Cu^{2+} solution to that **MCF** coated paper, as illustrated in **Fig.VI.16**. These findings illustrate that the **MCF**-coated test papers are a practical and easy-to-use tool for monitoring Cu^{2+} ions in real-life specimens.

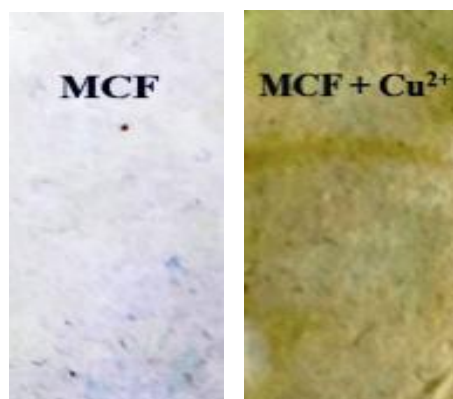


Fig.VI.16. Color changes of the test paper containing **MCF** and **MCF + Cu^{2+}** .

VI.4. Conclusion

From the above discussion, we have designed and synthesised a chromone based molecule, **MCF** which has exhibited an efficient and selective sensor for the detection of Cu^{2+} ion colorimetrically in ethanol-water (99:1, v/v) medium. The probe **MCF** showed the limit of

detection (LOD) for Cu²⁺ ions as 0.6 μM. The free **MCF** is colourless but upon the addition of Cu²⁺ ions the solution turns to yellowish brown which can be easily distinguished by naked eye view and this colour change also reflected in the UV-Vis spectroscopic experiment. The 1:1 stoichiometry of binding between the probe **MCF** and Cu²⁺ was determined from Job's plot analysis and the binding constant (K_a) also evaluated as 4.9346 × 10⁴ M⁻¹. The reversibility of sensing towards Cu²⁺ ions was examined by using the EDTA solution and the result showed that the **MCF** can be used as an excellent reversible colorimetric sensor for Cu²⁺ ions. Additionally, **MCF** coated test paper was prepared and it can used to detect Cu²⁺ ions successfully.

VI.5. References:

- [1]. E. Madsen, J.D. Gitlin, *Annu. Rev. Neurosci.*, 30 (2007) 317-337.
- [2]. T. Hirayama, G.C. Van de Bittnera, L.W. Gray, S. Lutsenko, C.J. Chang, *Proc. Natl. Acad. Sci.*, 109 (2012) 2228-2233.
- [3]. J.C. Lee, H.B. Gray, J.R. Winkler, *J. Am. Chem. Soc.*, 130 (2008) 6898-6899.
- [4]. Y.H. Hung, A.I. Bush, R.A. Cherny, *J. Biol. Inorg. Chem.*, 15 (2010) 61-76.
- [5]. C. Vulpe, B. Levinson, S. Whitney, S. Packman, J. Gitschier, *Nat. Genet.*, 3 (1993) 7-13.
- [6]. S.G. Kaler, *Nat. Rev. Neurol.*, 7 (2011) 15-29.
- [7]. L. Breydo, V.N. Uversky, *Metallomics*, 3 (2011) 1163-1180.
- [8]. J. Liu, M. Yu, X.C. Wang, Z. Zhang, *Spectrochim. Acta A.*, 93 (2012) 245-249.
- [9]. V.K. Gupta, A.K. Singh, M.R. Ganjali, P. Norouzi, F. Faridbod, N. Mergu, *Sens. Actuators B.*, 182 (2013) 642-651.
- [10]. S. Yagi, S. Nakamura, D. Watanabe, H. Nakazumi, *Dyes Pigm.*, 80 (2008) 98-105.
- [11]. J. Jiang, C. Gou, J. Luo, C. Yi, X. Liu, *Inorg. Chem. Commun.*, 15 (2012) 12-15.
- [12]. V.K. Gupta, N. Mergu, A.K. Singh, *Sens. Actuators B.*, 202 (2014) 674-682.
- [13]. V.K. Gupta, A.K. Singh, L.K. Kumawat, *Sens. Actuators B.*, 204 (2014) 507-514.

- [14]. J.M. You, H. Jeong, H. Seo, S. Jeon, *Sens. Actuators B.*, 146 (2010) 160-164.
- [15]. V.K. Gupta, N. Mergu, L.K. Kumawat, A.K. Singh, *Sens. Actuators B.*, 207 (2015) 216-223.
- [16]. J. Homola, *Chem. Rev.*, 108 (2008) 462-493.
- [17]. A. Piriya VS, P. Joseph, K. Daniel SCG, S. Lakshmanan, T. Kinoshita, S. Muthusamy, *Mater. Sci. Eng. C.*, 78 (2017) 1231-1245.
- [18]. L. Breydo, V.N. Uversky, *Metallomics.*, 3 (2011) 1163-1180.
- [19]. X. Zhou, J. Nie, B. Du, *ACS Appl. Mater. Interfaces.*, 9 (2017) 20913-20921.
- [20]. Y.L. Hung, T.M. Hsiung, Y.Y. Chen, Y.F. Huang, C.C. Huang, *J. Phys. Chem. C.*, 114 (2010) 16329-16334.
- [21]. N. Narayanaswamy, T. Govindaraju, *Sens. Actuators B.*, 161 (2012) 304-310.
- [22]. L.J. Tang, F. Li, M. Liu, R. Nandhakumar, *Spectrochim. Acta A.*, 78 (2011) 1168-1172.
- [23]. N. Shao, J.Y. Jin, H. Wang, Y. Zhang, R.H. Yang, W.H. Chan, *Anal. Chem.*, 80 (2008) 3466-3475.
- [24]. H. Zhou, J. Wang, Y. Chen, W. Xi, Z. Zheng, D. Xu, Y. Cao, G. Liu, W. Zhu, J. Wu, Y. Tian, *Dyes Pigm.*, 98 (2013) 1-10.
- [25]. Y. Fang, Y. Zhou, Q. Rui, C. Yao, *Organometallics*, 34 (2015) 2962-2970.
- [26]. A.R.S. Ross, M.G. Ikonomou, J.A.J. Thompson, K.J. Orians, *Anal. Chem.*, 70 (1998) 2225-2235.
- [27]. Q. Shang, Z. Zhou, Y. Shen, Y. Zhang, Y. Li, S. Liu, Y. Zhang, *ACS Appl. Mater. Interfaces.*, 7 (2015) 23672-23678.
- [28]. R. Sitko, P. Janik, B. Zawisza, E. Talik, E. Margui, I. Queralt, *Anal. Chem.*, 87 (2015) 3535-3542.
- [29]. H.Y. Chang, T.M. Hsiung, Y.F. Huang, C.C. Huang, *Environ. Sci. Technol.*, 45 (2011) 1534-1539.
- [30]. P. Kumar, K.H. Kim, V. Bansal, T. Lazarides, N. Kumar, *J. Ind. Eng. Chem.*, 54 (2017) 30-43.
- [31]. Y. Wu, X. Liu, Q. Wu, J. Yi, G. Zhang, *Sens. Actuators B Chem.*, 246 (2017) 680-685.

- [32]. A.J. Beneto, A. Siva, *Sens. Actuators B Chem.*, 247 (2017) 526-531.
- [33]. A. Mohammadi, S. Yaghoubi, *Sens. Actuators B Chem.*, 251 (2017) 264-271.
- [34]. A. Mohammadi, M. Kianfar, *J. Photochem. Photobiol. A.*, 367 (2018) 22-31.
- [35]. M. B. Maity, D. Talukdar, B. Dutta, G. Bairy, N. Murmu, G. Das, C. Sinha., *Inorganica Chim. Acta.*, 545 (2023) 121276.
- [36]. G.H. Park, I.H. Hwang, E.J. Song, H. Kim, C. Kim, *Tetrahedron*, 70 (2014) 2822-2828.
- [37]. A.K. Manna, J. Mondal, K. Rout, G.K. Patra, *J. Photochem. Photobiol.*, A 367 (2018) 74-82.
- [38]. M. B. Maity, B. Dutta, A. Rahaman, N. Sahu, D. P. Mandal, S. Bhattacharjee, C. Sinha, *J. Mol. Struct.*, 1250 (2022) 131870.
- [39]. H. Li, X. Sun, T. Zheng, Z. Xu, Y. Song, X. Gu, *Sens. Actuators B Chem.*, 279 (2019) 400-409.
- [40]. D. Vashisht, K. Kaur, R. Jukaria, A. Vashisht, S. Sharma, S.K. Mehta, *Sens. Actuators B Chem.*, 280 (2019) 219-226.
- [41]. B. Pang, C. Li, Z. Yang, *Spectrochim. Acta A Mol. Biomol. Spectrosc.*, 204 (2018) 641-647.
- [42]. S. Bhardwaj, N. Maurya, A.K. Singh, *Sens. Actuators B Chem.*, 260 (2018) 753-762.
- [43]. R. Rahman, S. Yu, S.K. Khalil, Y.P. Wu, S. Koppireddi, Z.T. Li, H. Wang, D. Zhang, *Sens. Actuators B Chem.*, 263 (2018) 594-604.
- [44]. Y. Wang, Z.Y. Ma, D.L. Zhang, J.L. Deng, X. Chen, C.Z. Xie, X. Qiao, Q.Z. Li, J.Y. Xu, *Spectrochim. Acta A Mol. Biomol. Spectrosc.*, 195 (2018) 157-164.
- [45]. A. Gaspar, M.J. Matos, J. Garrido, E. Uriarte, F. Borges, *Chem. Rev.*, 114 (2014) 4960-4992.
- [46]. J. Reis, A. Gaspar, N. Milhazes, F. Borges, *J. Med. Chem.*, 60 (2017) 7941-7957.
- [47]. F. Arjmand, Z. Afsan, T. Roisnel, *RSC Adv.*, 8 (2018) 37375-37390.
- [48]. Y. Lee, S. Basith, S. Choi, *J. Med. Chem.*, 61 (2017) 1-46.
- [49]. R. Kouser, A. Rehman, S. M. A. Abidi, F. Arjmand, S. Tabassum, *J. Mol. Struct.*, 1256 (2022) 132533.

- [50]. N. Tomer, A. Goel, V. D. Ghule, R. Malhotra, *J. Mol. Struct.*, 1227 (2021) 129549.
- [51]. N. Mergu, V. K. Gupta, *Sens. Actuators B Chem.*, 210 (2015) 408-417.
- [52]. D. Peralta-Domínguez, M. Rodriguez, G. Ramos-Ortiz, J. L. Maldonado, D. Luna-Moreno, M. Ortiz-Gutierrez, V. Barba, *Sens. Actuators B Chem.*, 225 (2016) 221-227.
- [53]. G.J. Park, G.R. You, Y.W. Choi, C. Kim, *Sens. Actuators B Chem.*, 229 (2016) 257-271.
- [54]. R. Kouser, A. Rehman, S. M. A. Abidi, F. Arjmand, S. Tabassum, *J. Mol. Struct.*, 1256 (2022) 132533.
- [55]. L. Wang, X. Gong, Q. Bing, G. Wang, *Microchem. J.*, 142 (2018) 279-287.
- [56]. B. Shruthi, H. D. Revanasiddappa, B. Jayalakshmi, A. Syed, A. M. Elgorban, R. Eswaramoorthy, R. G. Amachawadi, C. Shivamallu, S. P. Kollur, *Inorg. Chem. Commun.*, 150 (2023) 110467.
- [57]. N.A. Morais, L. Fernandes, J. Ariana-Machado, J.L. Capelo, C. Lodeiro, E. Oliveira, *Inorg. Chem. Commun.*, 86 (2017) 299-303.
- [58]. J.J. Lee, Y.W. Choi, G.R. You, S.Y. Lee, C. Kim, *Dalton Trans.* 44 (2015) 13305-13314
- [59]. S. A. Lee, J. J. Lee, J.W. Shin, K. S. Min, C. Kim, *Dyes Pigm.*, 116 (2015) 131-138.

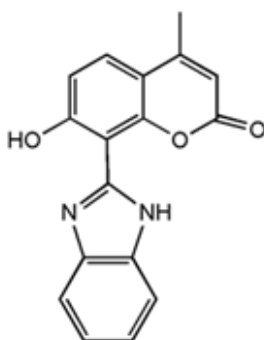
Chapter VII

Conclusion

VII.1. Conclusion

The above discussion in the chapters has concluded that the research work is focused mainly on the synthesis, structural characterisation and exploration of their ion sensing properties and photochromism in one case. To execute this idea, some fluorophore appended Schiff bases have been designed which have been used for the detection of various bio-relevant metal ions and one azoimidazole based Hg(II) complex which have shown photo-mechanical activity by *trans-cis* isomerization those can be used as an optical sensor. The discussed chemosensors can detect metal ions at a very low concentration (μM) level. The synthesized chemosensors have been used for the various biological as well as analytical applications.

VII.2. Double advantages of Benzimidazolyl-hydroxy-coumarinyl diad -“turn-on” sensing of Al^{3+} and preventing metastasis in cancer (Chapter II)



(HL)

8-(1H-Benzoimidazol-2-yl)-7-hydroxy-4-methyl-chromen-2-one

8-(1H-Benzoimidazol-2-yl)-7-hydroxy-4-methyl-chromen-2-one (HL), a benzimidazolyl-hydroxy-coumarinyl diad, serves as fluorescent turn-on Al^{3+} -sensor (Fig.VII.2.1, Fig.VII.2.2) in acetonitrile-water (2:1, v/v) of pH, 7.2 (HEPES buffer) medium. The intensity of emission on binding with Al^{3+} is enhanced by twelve times of probe with limit of detection (LOD) 0.62 μM . The structure of the probe has been established by the spectroscopic data (FT-IR, ^1H NMR,

Mass spectra) and is confirmed by Single Crystal X-ray structure determination. The coordination environment of the complex, $[\text{Al}(\text{L})(\text{NO}_3)_2(\text{H}_2\text{O})(\text{NCCH}_3)]$, has been supported by Mass, FT-IR, NMR spectra and the Job's plot supports 1:1 composition. The anti-metastatic potential of **HL** on Human skin carcinoma (A431) and Human lung carcinoma (A549) cells are examined. Wound healing and Zymography assay suggest that **HL** has anti-migratory properties. The RT-PCR and Immunoblotting data suggest that **HL** down-regulates the expression of mesenchymal markers (Vimentin, Snail, Slug, MMP, and MMP9) and induces the expression of the epithelial marker (E-Cadherin) (Fig.VII.2.3).



Fig.VII.2.1. In acetonitrile-water (2:1, v/v) of pH, 7.2 (HEPES buffer) UV chamber **HL** persists colour in presence of Al^{3+} but disappears in presence of all other metals.

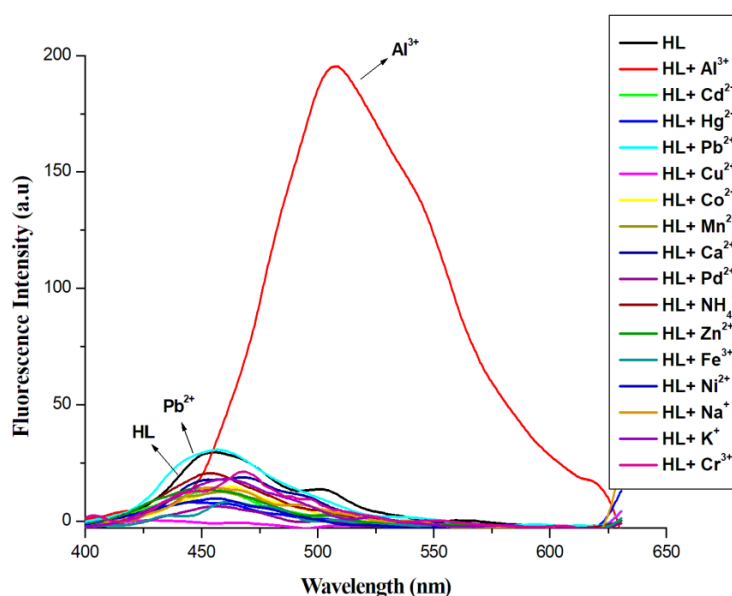


Fig.VII.2.2. Fluorescence spectra of **HL** in acetonitrile-water (2:1, v/v) of pH, 7.2 (HEPES buffer) in presence of different cations.

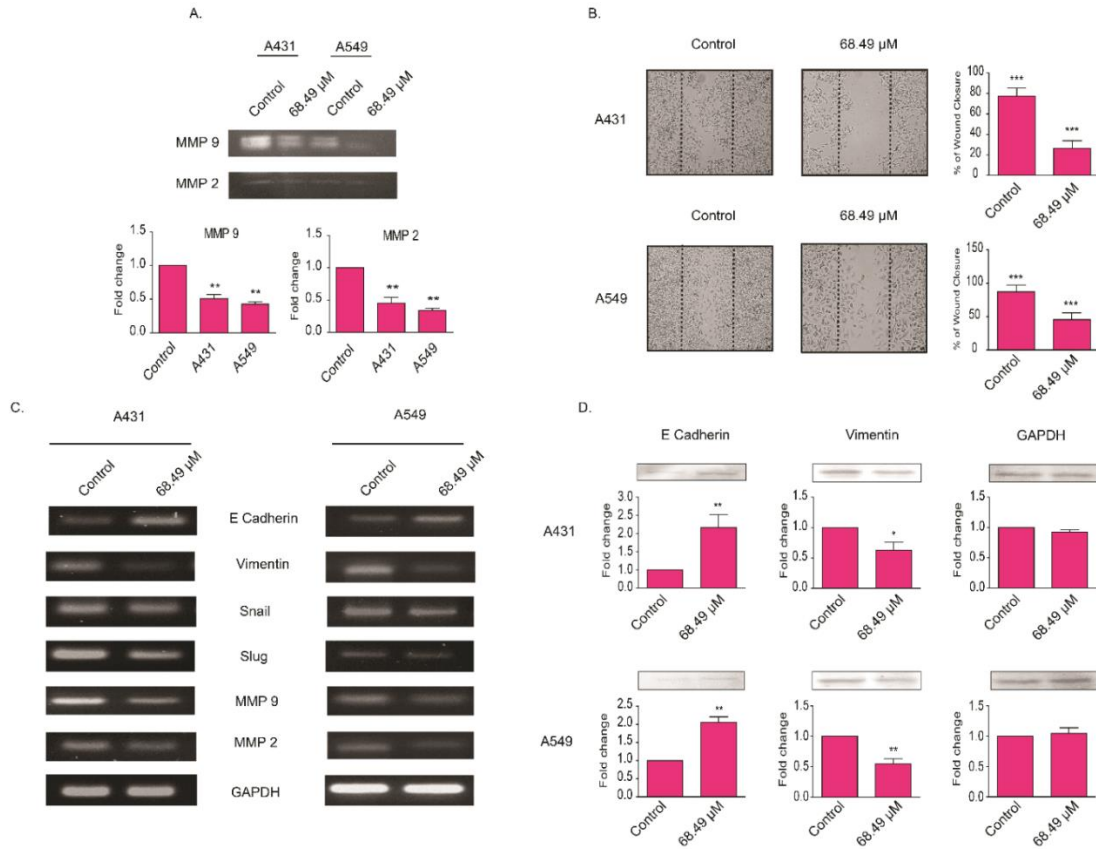
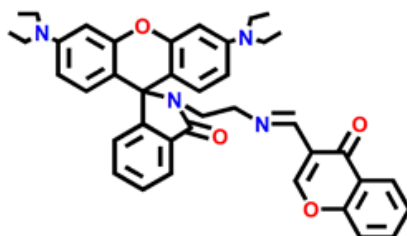


Fig.VII.2.3. HL inhibits the migration of carcinoma cell lines. (A) Effect of **HL** on the activity of matrix metalloproteinase enzyme by gelatin zymography. The MMP2 and MMP9 bands were displayed. (B) Wound healing assay displaying the migration of cells in 24 hours, with and without treatment with **HL** and the bar plots displaying % of wound coverage by cells. (C) The effect of **HL** on the EMT markers done by RT-PCR. (D) Effect of **HL** on E-Cadherin and Vimentin protein expression and bar plots represents the fold change in expression normalized with GAPDH. The data were represented as mean \pm SD and performed in triplicate.

VII.3. Application of a Rhodamine-Chromone Schiff Base Probe for the Sensing of Fe^{3+} , Al^{3+} , Cr^{3+} at Low Concentration and Exploration of the Anticancer Activity and Bio-imaging. (Chapter III)



(RFC)

Rhodamine appended chromone Schiff base (**RFC**), with two fluorogenic motifs, has been characterized through various spectroscopic techniques. The probe exhibits efficient sensitivity towards trivalent metal ions (Al^{3+} , Cr^{3+} and Fe^{3+}) (**Fig. VII.3.1**) in existence of other competitive analytes. The fluorescent intensity is enhanced by 350 fold (Fe^{3+}), 250 fold (Al^{3+}) and 220 fold (Cr^{3+}), respectively (**Fig. VII.3.2**) in methanol-water (99:1,v/v; HEPES buffer, pH, 7.2) medium. Rhodamine derivative (**RFC**) upon interact with Fe^{3+} , Al^{3+} , and Cr^{3+} ions the cleavage of spirolactam ring occurs followed by the change in colour takes place. After the cleavage of the spirolactam ring the donor atoms (O, N) come from amidic moiety of **RFC** may initiate noncovalent interaction with trivalent cations (Fe^{3+} , Al^{3+} , and Cr^{3+}). The limits of detection (LOD) ($3\sigma/M$ method; σ = standard deviation; M = slope) are 0.0051 ppm (Fe^{3+}), 0.0029 ppm (Al^{3+}) and 0.0052 ppm (Cr^{3+}); which are impressive and much below the WHO recommended data. The material may be employed for the fabrication of a detection device (**Fig. VII.3.3. (a)**). In addition to this, the compound has been utilized for cell imaging (**Fig. VII.3.3. (b)**) in presence of these three cations. The action of probe on MCF-7 (human breast cancer) cell lines demonstrates IC_{50} , 2.53 μM that is far better than activity against WI-38 (normal cell line) (IC_{50} , 393.7 μM). The drug (**RFC**) minimizes the cellular proliferation and has significant

wound healing capacity (**Fig. VII.3.4**) of the infected tissue with MCF-7 cells. The probe shows significant nuclear fragmentation with increase in the expression of apoptotic markers. Growth inhibition analysis in 3D tumor spheroid model showed the inhibition of breast cancer MCF-7 cells.

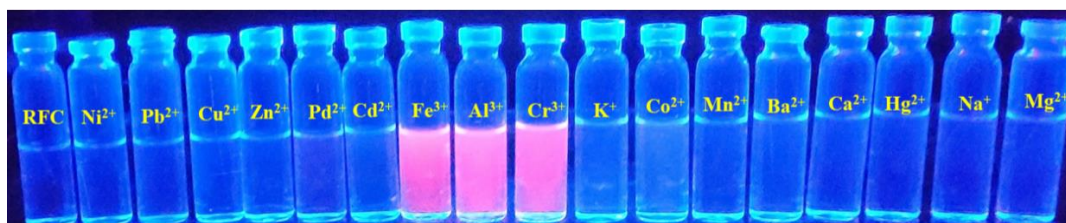


Fig. VII.3.1. Vial image in UV chamber of the probe **RFC** in presence of different cations in methanol-water (99:1 v/v; HEPES buffer, pH, 7.2)

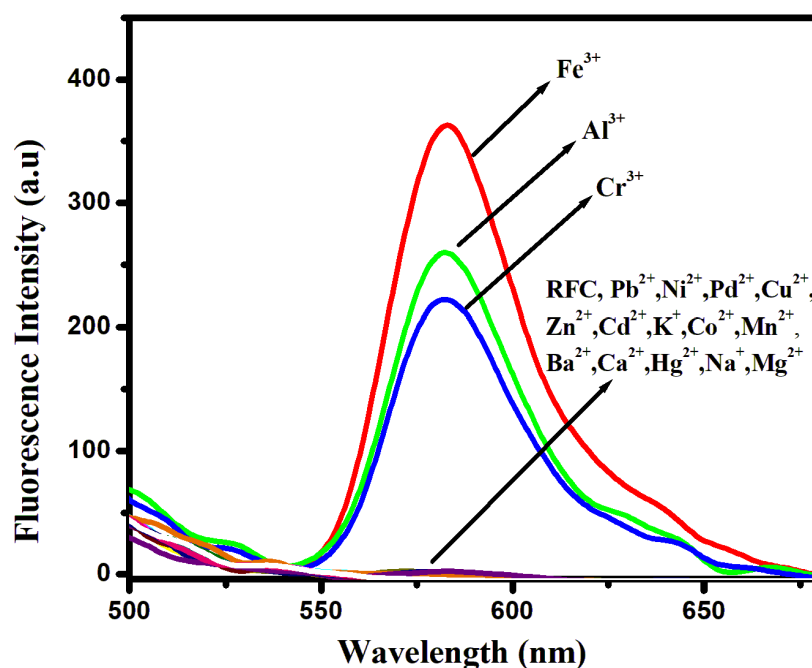


Fig. VII.3.2. Emission spectra of the probe **RFC** in methanol-water (99:1, v/v; HEPES buffer, pH, 7.2) in presence of various metal ions.

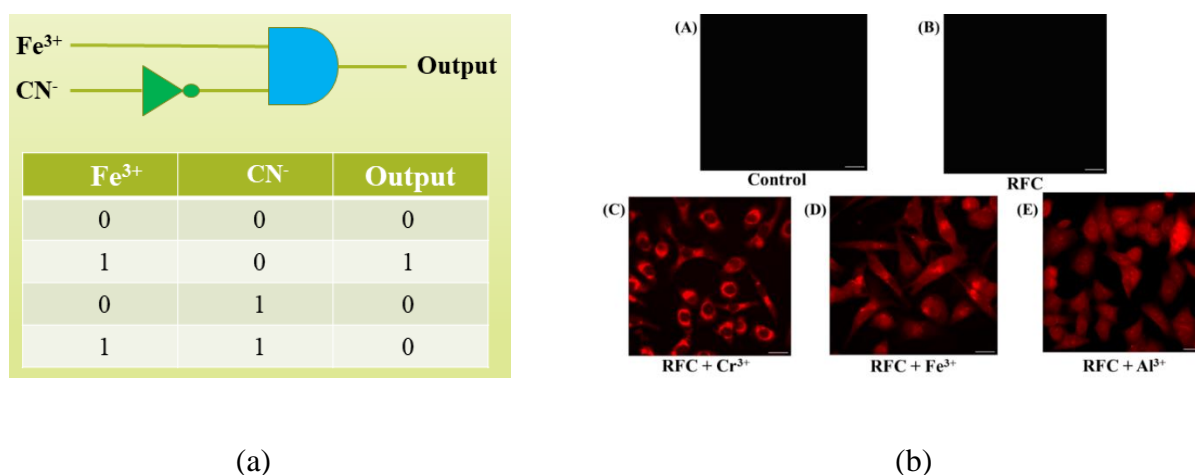


Fig. VII.3.3. (a) General representation of an INHIBIT logic gate and truth table for two inputs: Fe^{3+} and CN^- and single output at 583 nm. (b) The cell imaging study of **RFC** in the presence of Al^{3+} , Cr^{3+} and Fe^{3+} ions on the MCF-7 cell line.

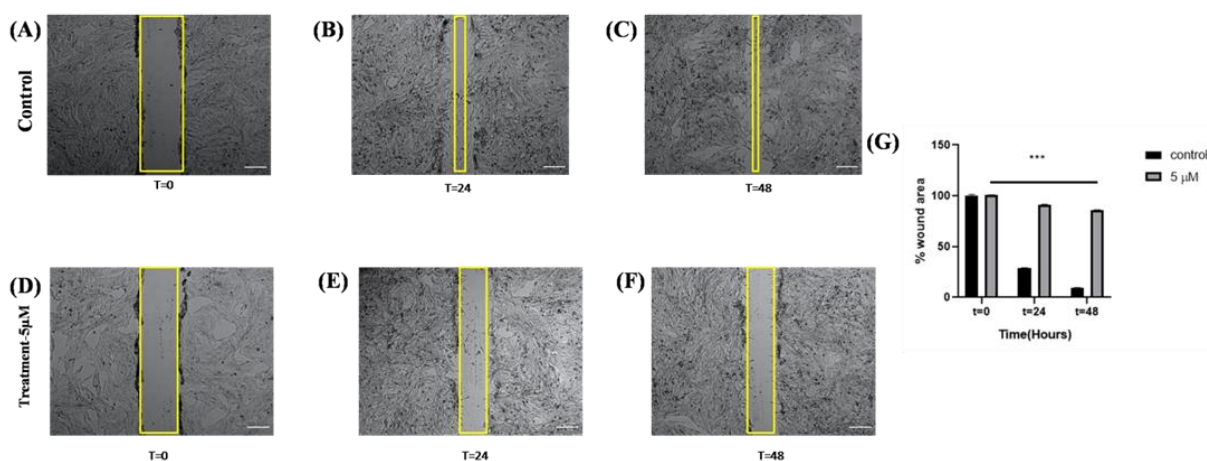
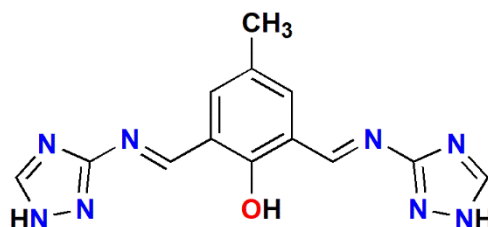


Fig. VII.3.4. Wound healing assay carried out in MCF-7 cells treated with 5 μM **RFC** probe. (A-F) Significant inhibition of the closure of the wound is observed in treated cells as compared to the untreated control. The scale bar corresponds to 100 μm . (G) Graph showing reduction in wound healing area on treatment with **RFC** as compared to untreated control where the wound almost completely closes at 48 h. The error bars correspond to the standard error of the value after performing the experiment in triplicates. (n=3) (Two-way ANOVA, *** $p < 0.001$).

VII.4. Use of Diformyl-triazolo Schiff base for Zn²⁺ Sensing and intracellular Live Cell Imaging. (Chapter IV)



(PTR)

4-Methyl-2, 6-bis-[(1H-[1,2,4] triazol-3-ylimino)-methyl]-phenol

4-Methyl-2, 6-bis-[(1H-[1,2,4] triazol-3-ylimino)-methyl]-phenol (**PTR**) has been synthesized and characterised by spectroscopic data (ESI-MS, UV-Vis, FT-IR, NMR spectra). The probe, **PTR** showed prominent UV-Visible spectra, upon the addition of Zn²⁺ ions the distinguishable colour change takes place (**Fig. VII.4.1. (a)**) in DMSO-water (99:1,v/v; HEPES buffer, pH, 7.2) medium. The probe, **PTR**, emits at 610 nm upon excitation at 380 nm and the emission is strongly intensified on interacting with Zn²⁺ ion (**Fig. VII.4.1. (b)**) in DMSO-water (99:1, v/v; HEPES buffer, pH, 7.2) solution even in presence of fifteen other cations (Cu²⁺, Mn²⁺, Co²⁺, Ni²⁺, Pd²⁺, Cd²⁺, Pb²⁺, Hg²⁺, Fe³⁺, Cr³⁺, Al³⁺, Na⁺, K⁺, Ba²⁺, Ca²⁺) and the emission band has been shifted to 530 nm. The limit of detection of Zn²⁺, 0.30 μM is much lower than WHO recommended value (76 μM). The significant and distinguishable solid-state emission of the probe **PTR** and the **PTR-Zn²⁺** complex (**Fig. VII.4.2**) makes the probe more effective towards the detection of Zn²⁺ ion in naked eye. The binding constant (K_d) is 4.2585 × 10⁴ M⁻¹. Selective and sensitive chemosensing behaviour of **PTR** to Zn²⁺ has been explained by switching off ESIPT quenching of the keto-enol tautomerisation of the probe along with the chelation enhancement of fluorescence (CHEF) by binding with Zn²⁺. The Job's plot and NMR titration have been extended to measure the 1:1 molar composition [**PTR+Zn²⁺**]. Intracellular Zn²⁺ ions

in living cells of HEK293 (PBS: Phosphate Buffer Saline, pH-7.2) have also been identified by the probe, **PTR**, using fluorescence microscopic imaging technique (**Fig. VII.4.3**).

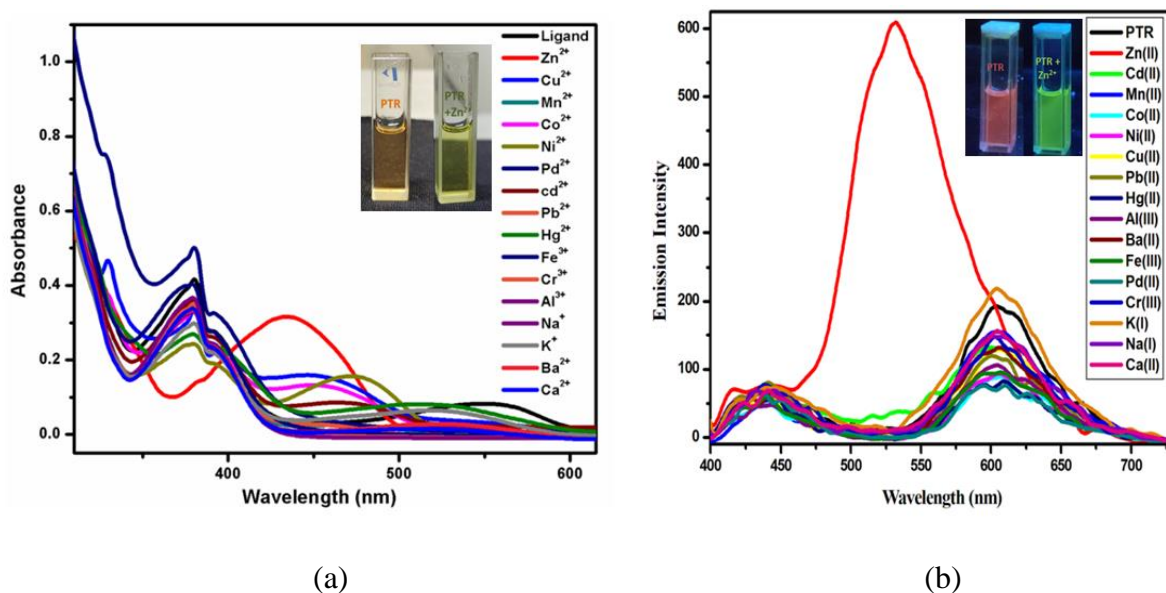


Fig. VII.4.1. (a) UV-vis absorption spectra of **PTR** (25 μM) with various cations in DMSO-water (99:1, v/v; HEPES buffer, pH, 7.2) medium. (b) Emission spectra of the probe **PTR** (25 μM) in presence of different metal ions upon excitation at 380 nm in DMSO-water (99:1, v/v; HEPES buffer, pH, 7.2) medium.

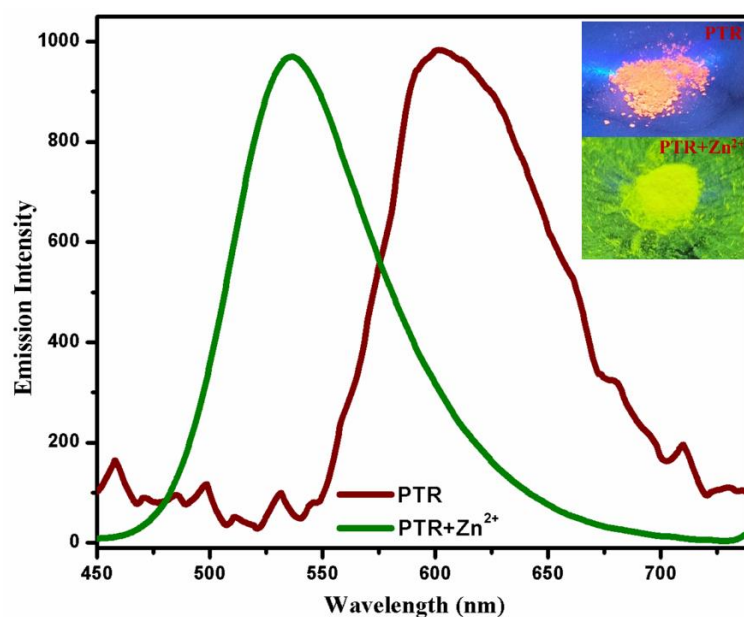


Fig. VII.4.2. The solid state emission spectra of the probe **PTR** and **PTR + Zn²⁺** complex

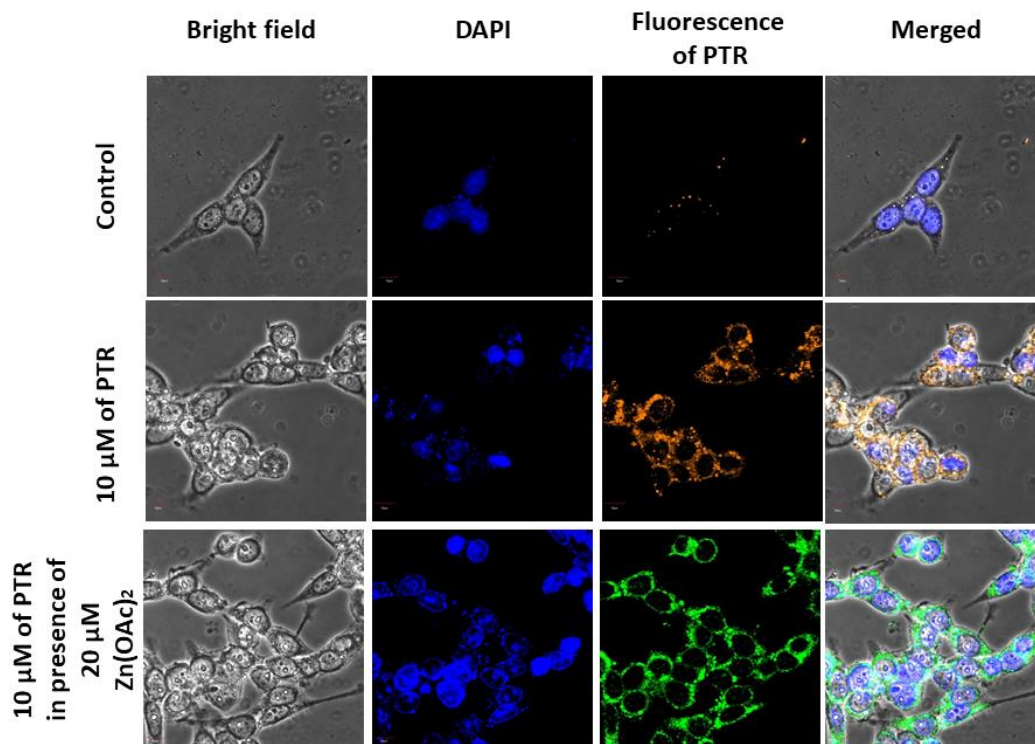
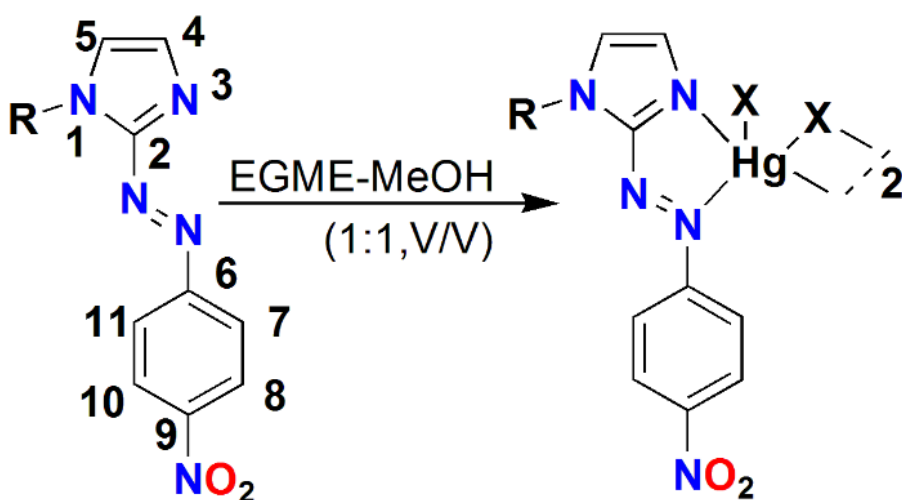


Fig. VII.4.3. Confocal microscopy images of HEK293 cells in presence of **PTR** and **PTR**+ Zn^{2+} .

VII.5. Structure and Photoisomerisation of Halo-bridged dimeric Mercury (II) complexes of 1- alkyl-2-(p-nitro-phenylazo) imidazoles. (Chapter V).

Mercury (II) complexes, $[\text{Hg}(\text{p-NO}_2\text{aaiR})(\mu\text{-X})(\text{X})_2]$ (**2-4**) of p-NO₂-aaiR [1-Alkyl-2-(p-nitro-phenylazo) imidazole, (**1**), where R = -CH₃ (**1a**), -C₂H₅ (**1b**) and X = Cl (**2**), Br (**3**), I (**4**)] (**Scheme VII.5.a**) have been studied by spectral data. The X-ray crystallography study in case of $[\text{Hg}(\text{p-NO}_2\text{aai-CH}_3)(\mu\text{-I})(\text{I})_2]$ (**4a**) has revealed the distorted dinuclear halobridge tetra-atomic puckered rhombohedral Hg(II) structure (**Fig. VII.5.1**). The ligand, p-NO₂aaiR shows trans (E) - cis (Z) isomerisation both in free and coordination state in the complex on shocking UV light in the solution phase. The Z-to-E transformation is carried out by thermal treatment while photoisomerization is carried out very slowly on visible light absorption and $\phi_{\text{E} \rightarrow \text{Z}}$ (quantum yields for E-to-Z isomerisation) is higher for free ligand compare to the complex

phase. The isomerisation rate shows the sequence, $[\text{Hg}(\text{p-NO}_2\text{ aaiR})(\mu\text{-I})(\text{I})_2]$ (**4**) < $[\text{Hg}(\text{p-NO}_2\text{ aaiR})(\mu\text{-Br})(\text{Br})_2]$ (**3**) < $[\text{Hg}(\text{p-NO}_2\text{ aaiR})(\mu\text{-Cl})(\text{Cl})_2]$ (**2**) which is also the sequence of molecular mass of the complexes. Light absorption in UV wavelength ($\lambda_{\text{max}}, 364\text{ nm}$) causes *trans*-(*E*-isomer) to *cis*-(*Z*-isomer) isomerisation (**Scheme VII.5.b**). For free ligand methanol solution of ligand is used while the complex is sparingly soluble in MeOH so DMF solution is used. The absorption at UV region is decreased ((**Fig. VII.5.2. (a), (b)**) with following increase at the longer wavelength portion of the spectrum till a stationary state is reached.



p-NO₂aai-CH₃ (**1a**), *p*-NO₂aai-C₂H₅ (**1b**), $[\text{Hg}(\textit{p}\text{-NO}_2\text{aai-CH}_3)(\mu\text{-Cl})(\text{Cl})_2]$ (**2a**), $[\text{Hg}(\textit{p}\text{-NO}_2\text{aai-C}_2\text{H}_5)(\mu\text{-Cl})(\text{Cl})_2]$ (**2b**) $[\text{Hg}(\textit{p}\text{-NO}_2\text{aai-CH}_3)(\mu\text{-Br})(\text{Br})_2]$ (**3a**), $[\text{Hg}(\textit{p}\text{-NO}_2\text{aai-C}_2\text{H}_5)(\mu\text{-Br})(\text{Br})_2]$ (**3b**) $[\text{Hg}(\textit{p}\text{-NO}_2\text{aai-CH}_3)(\mu\text{-I})(\text{I})_2]$ (**4a**), $[\text{Hg}(\textit{p}\text{-NO}_2\text{aai-C}_2\text{H}_5)(\mu\text{-I})(\text{I})_2]$ (**4b**)

Scheme VII.5.a. Synthetic route of Hg (II)- halide complexes.

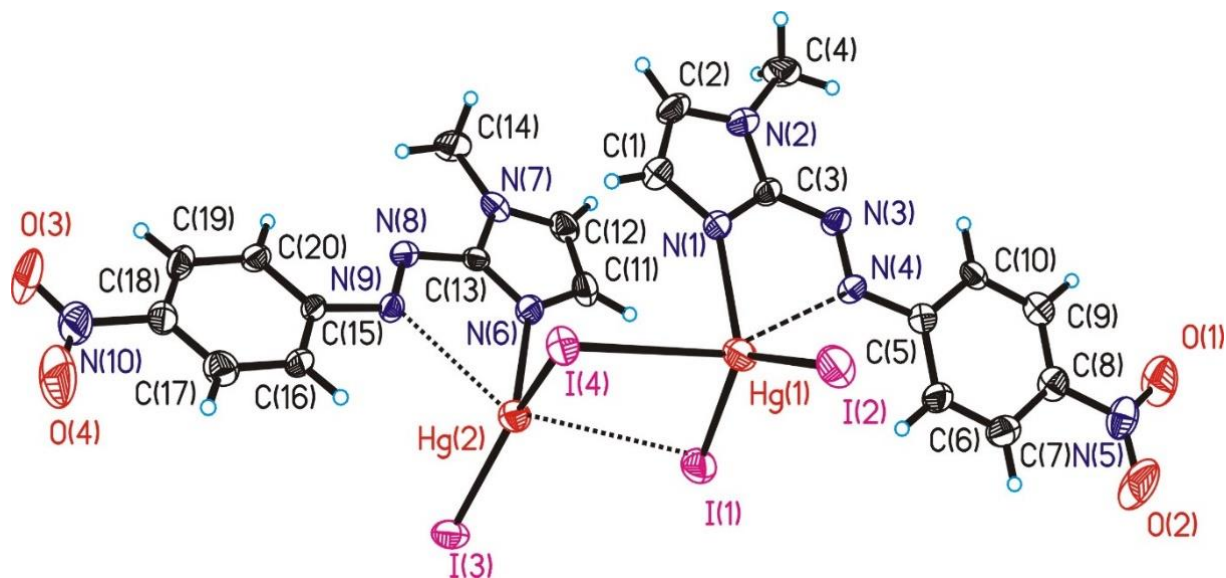
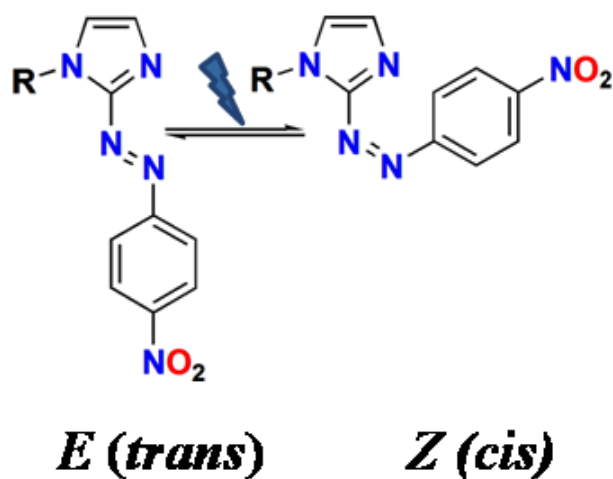


Fig. VII.5.1. Asymmetric unit of compound $[\text{Hg}(p\text{-NO}_2\text{ai-CH}_3)(\mu\text{-I})(\text{I})_2]$ (**4a**)



Scheme VII.5.b. Isomerisation of 1-alkyl-2-(*p*-nitro-phenylazo)imidazole, *p*-NO₂aiR, (**1**)

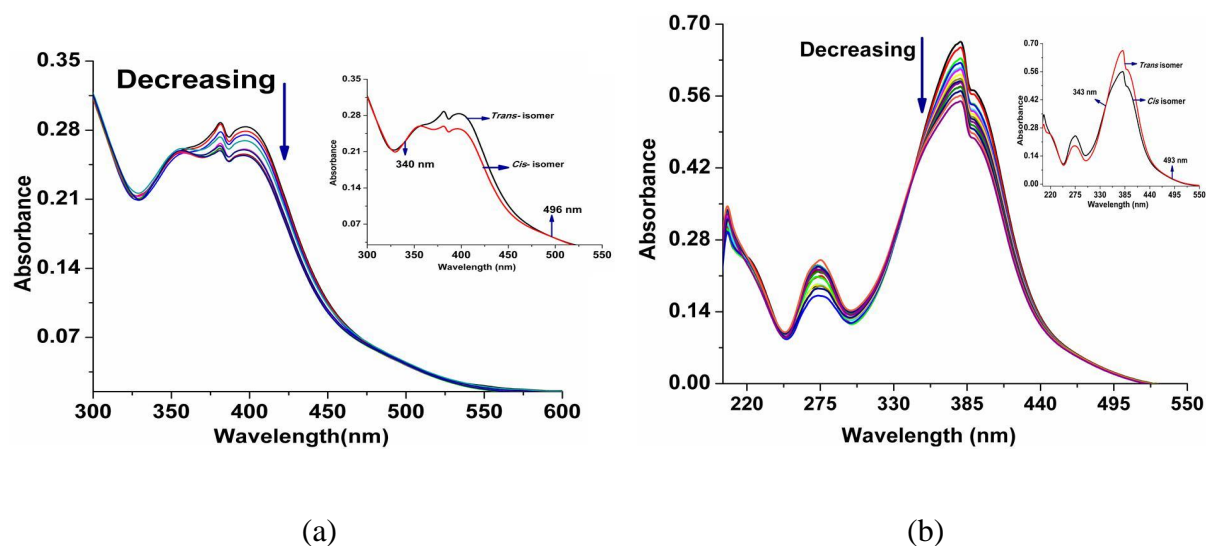
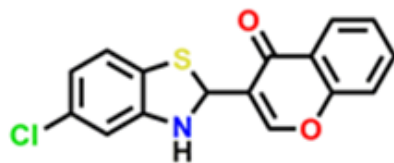


Fig. VII.5.2. (a) Evolution of absorption of *p*-NO₂aaiMe (**1a**) in MeOH upon irradiation at 364 nm at 3 min interval at 25°C. (b) Evolution of absorption of [Hg(*p*-NO₂aai-CH₃)(μ-I)(I)]₂ (**4a**) in DMF upon irradiation at 368 nm at 5 min interval at 25°C.

VII.6. Use of chromone based probe as colorimetric sensor for the detection of Cu²⁺ ion: design of test paper kit. (Chapter VI).



(MCF)

3-(5-chloro-2,3-dihydrobenzo[*d*]thiazol-2-yl)-4*H*-chromen-4-one

A chromone-based molecule, 3-(5-chloro-2,3-dihydrobenzo[*d*]thiazol-2-yl)-4*H*-chromen-4-one (**MCF**) has been spectroscopically characterised (FT-IR, UV-Vis, ESI-MS, NMR) and has been used for the chromogenic selective recognition of Cu²⁺ ion (**Fig.VII.6.1**) in EtOH-H₂O (99:1, v/v) medium. The sensor shows excellent selectivity towards Cu²⁺ ion at very low limit of detection, 0.6 μM in presence of competitive ions which is much lower than the permissible

limit (20 μM) in drinking water recommended by the World Health Organization (WHO). From the Job's plot it has been concluded that the probe MCF binds Cu^{2+} with 1:1 molar ratio. The binding constant ($4.9346 \times 10^4 \text{ M}^{-1}$) of MCF towards Cu (II) ion was determined by using the Benesi-Hildebrand equation. The reversibility of MCF was determined by using the chelating agent ethylenediaminetetraacetic acid (EDTA) via UV–Vis titration and the probe MCF can be repeatedly (Fig.VII.6.2) used to recognize Cu^{2+} ions. The naked eye change from colourless to yellowish brown of MCF solution upon addition of Cu^{2+} ion ((Fig.VII.6.3. (a)) in presence of different competitive metal ions is very convincing and helps to design paper kits ((Fig.VII.6.3. (b)).

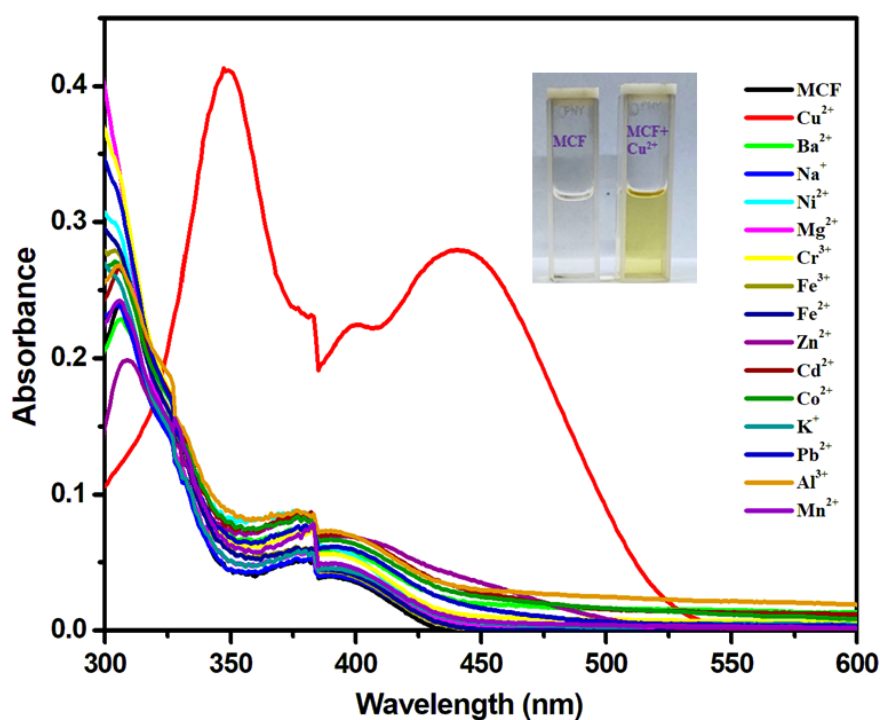


Fig.VII.6.1. UV–vis absorption spectra of MCF (25 μM) with various cations in ethanol/water (99:1, v/v) medium.

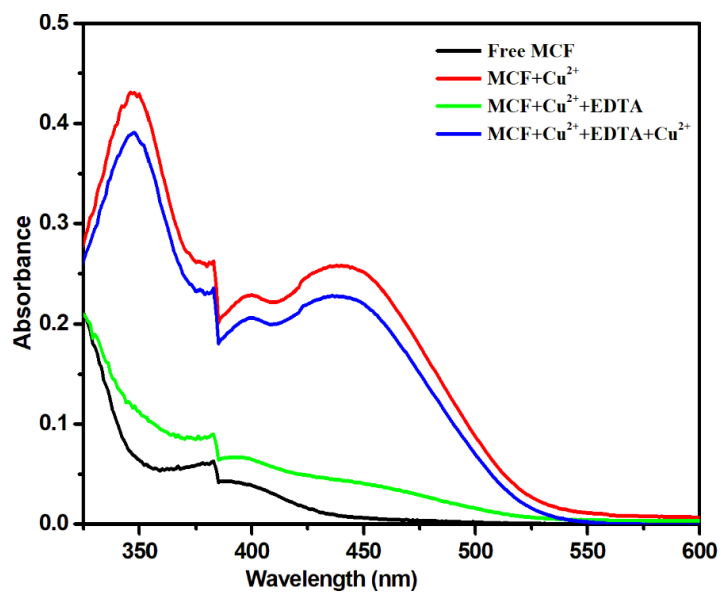


Fig.VII.6.2. The absorbance spectra of MCF after the alternative addition of Cu²⁺ and EDTA.

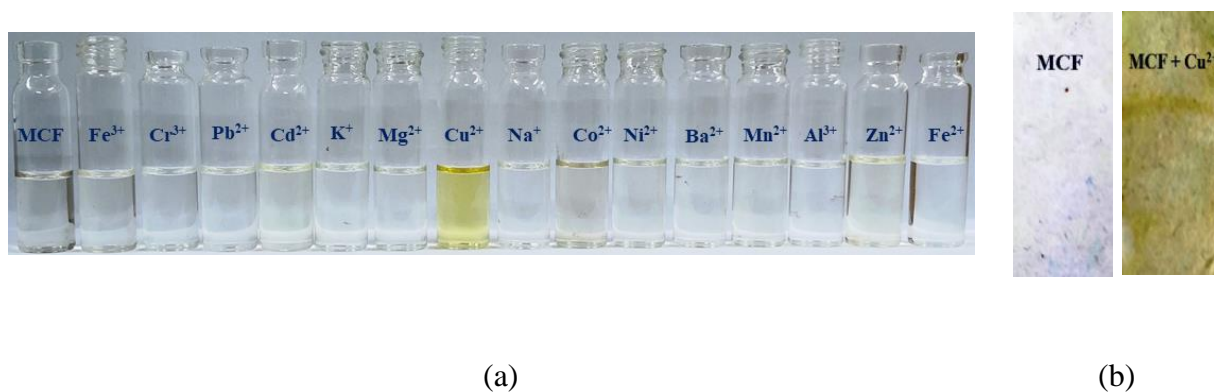


Fig.VII.6.3. (a) Naked eye view of MCF in presence of different metal ions in ethanol/water (99:1, v/v) medium. (b) Color changes of the test paper containing MCF and MCF + Cu²⁺.

List of Publications

1. **Mukul Bikash Maity**, Basudeb Dutta, Ashikur Rahaman, Nilima Sahu, Deba Prasad Mandal, Shamee Bhattacharjee, Chittaranjan Sinha., **Double advantages of Benzimidazolyl–hydroxy-coumarinyldiad - “turn-on” sensing of Al³⁺ and preventing metastasis in cancer**, J. Mol. Struct., 1250 (2022) 131870.
2. **Mukul Bikash Maity**, Debojit Talukdar, Basudeb Dutta, Gurupada Bairy, Nabendu Murmu, Gaurav Das, Chittaranjan Sinha., **Application of a Rhodamine-chromone Schiff base probe for the sensing of Fe³⁺, Al³⁺, Cr³⁺ at low concentration and exploration of the anticancer activity and bio-imaging.**, Inorganica Chim. Acta, 545 (2023) 121276.
3. **Mukul Bikash Maity**, Suprava Bhunia, Arka Patra, Panchanan Sahoo, Snehasis Mishra, Chittaranjan Sinha, **Use of Diformyl-triazolo Schiff base for Zn²⁺ Sensing and intracellular Live Cell Imaging**, Appl. Organomet. Chem., DOI: <https://doi.org/10.1002/aoc.7179>.

Accepted in June 8, 2023, First published: 22 June 2023.

4. Debashis Mallick ,**Mukul Bikash Maity** , Chandana Sen , Basudeb Dutta, Suman Kundu and Chittaranjan Sinha., **Structure and photochromism of halo-bridged dimeric mercury (II) complexes of 1-alkyl-2-(p-nitro-phenylazo)imidazoles.**, J. Indian Chem. Soc., 97 (2020) 1478-1486.

Conference Attended

1. Poster Presentation:

Poster Title: Coumarinyl Schiff base chemosensor for Al³⁺ sensing.

“Emerging Trends in Chemical Sciences” (January 07, 2020) organized by Department of Chemistry, Jadavpur University, Kolkata – 700032.

2. Participation: Participated in ten national and International conferences.

Awards and Recognition

1. NET- JRF (Council of Scientific & Industrial Research (CSIR), India. CSIR award no.: 09/096(0943)/2018-EMR-I)

Copyrights and Permission

1. Chapter II

Reprinted (adapted) with permission from Journal of Molecular Structure, 1250 (2022) 131870

2. Chapter III

Reprinted (adapted) with permission from Inorganica Chimica Acta, 545 (2023) 121276.

3. Chapter IV

Reprinted (adapted) with permission from Applied Organometallic Chemistry,

DOI: <https://doi.org/10.1002/aoc.7179>

3. Chapter V

Reprinted (adapted) with permission from Journal of the Indian Chemical Society, 97 (2020) 1478-1486.



RightsLink



Home



Help ▾



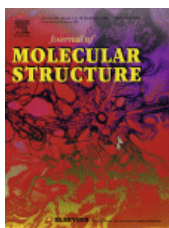
Live Chat



Sign in



Create Account



Double advantages of Benzimidazolyl-hydroxy-coumarinyl diad - “turn-on” sensing of Al³⁺ and preventing metastasis in cancer

Author:

Mukul Bikash Maity, Basudeb Dutta, Ashikur Rahaman, Nilima Sahu, Deba Prasad Mandal, Shamee Bhattacharjee, Chittaranjan Sinha

Publication: Journal of Molecular Structure**Publisher:** Elsevier**Date:** 15 February 2022

© 2021 Elsevier B.V. All rights reserved.

Journal Author Rights

Please note that, as the author of this Elsevier article, you retain the right to include it in a thesis or dissertation, provided it is not published commercially. Permission is not required, but please ensure that you reference the journal as the original source. For more information on this and on your other retained rights, please visit: <https://www.elsevier.com/about/our-business/policies/copyright#Author-rights>

[BACK](#)[CLOSE WINDOW](#)



RightsLink



Home



Help ▾



Live Chat



Sign in



Create Account



Application of a Rhodamine-chromone Schiff base probe for the sensing of Fe³⁺, Al³⁺, Cr³⁺ at low concentration and exploration of the anticancer activity and bio-imaging

Author:

Mukul Bikash Maity, Debojit Talukdar, Basudeb Dutta, Gurupada Bairy, Nabendu Murmu, Gaurav Das, Chittaranjan Sinha

Publication: Inorganica Chimica Acta**Publisher:** Elsevier**Date:** 24 January 2023

© 2022 Elsevier B.V. All rights reserved.

Journal Author Rights

Please note that, as the author of this Elsevier article, you retain the right to include it in a thesis or dissertation, provided it is not published commercially. Permission is not required, but please ensure that you reference the journal as the original source. For more information on this and on your other retained rights, please visit: <https://www.elsevier.com/about/our-business/policies/copyright#Author-rights>

BACK

CLOSE WINDOW

JOHN WILEY AND SONS LICENSE TERMS AND CONDITIONS

Jun 26, 2023

This Agreement between Mr. Mukul Bikash Maity ("You") and John Wiley and Sons ("John Wiley and Sons") consists of your license details and the terms and conditions provided by John Wiley and Sons and Copyright Clearance Center.

License Number	5576391361042
License date	Jun 26, 2023
Licensed Content Publisher	John Wiley and Sons
Licensed Content Publication	Applied Organometallic Chemistry
Licensed Content Title	Use of diformyl-triazolo Schiff base for Zn ² sensing and intracellular live cell imaging
Licensed Content Author	Mukul Bikash Maity, Suprava Bhunia, Arka Patra, et al
Licensed Content Date	Jun 22, 2023
Licensed Content Volume	0
Licensed Content Issue	0
Licensed Content Pages	11
Type of Use	Dissertation/Thesis
Requestor type	Author of this Wiley article
Format	Print and electronic
Portion	Full article
Will you be translating?	No
Title	Use of diformyl-triazolo Schiff base for Zn ² sensing and intracellular live cell imaging
Institution name	Jadavpur University
Expected presentation date	Jun 2024
Requestor Location	Mr. Mukul Bikash Maity Jadavpur University 188, Raja S.C. Mallick Rd. Kolkata, 700032 India Attn: Mr. Mukul Bikash Maity
Publisher Tax ID	EU826007151
Total	0.00 USD
Terms and Conditions	

TERMS AND CONDITIONS

This copyrighted material is owned by or exclusively licensed to John Wiley & Sons, Inc. or one of its group companies (each a "Wiley Company") or handled on behalf of a society with which a Wiley Company has exclusive publishing rights in relation to a particular work (collectively "WILEY"). By clicking "accept" in connection with completing this licensing transaction, you agree that the following terms and conditions apply to this transaction (along with the billing and payment terms and conditions established by the Copyright Clearance Center Inc., ("CCC's Billing and Payment terms and conditions"), at the time that you opened your RightsLink account (these are available at any time at <http://myaccount.copyright.com>).

Terms and Conditions

- The materials you have requested permission to reproduce or reuse (the "Wiley Materials") are protected by copyright.
- You are hereby granted a personal, non-exclusive, non-sub licensable (on a stand-alone basis), non-transferable, worldwide, limited license to reproduce the Wiley Materials for the purpose specified in the licensing process. This license, **and any CONTENT (PDF or image file) purchased as part of your order**, is for a one-time use only and limited to any maximum distribution number specified in the license. The first instance of republication or reuse granted by this license must be completed within two years of the date of the grant of this license (although copies prepared

before the end date may be distributed thereafter). The Wiley Materials shall not be used in any other manner or for any other purpose, beyond what is granted in the license. Permission is granted subject to an appropriate acknowledgement given to the author, title of the material/book/journal and the publisher. You shall also duplicate the copyright notice that appears in the Wiley publication in your use of the Wiley Material. Permission is also granted on the understanding that nowhere in the text is a previously published source acknowledged for all or part of this Wiley Material. Any third party content is expressly excluded from this permission.

- With respect to the Wiley Materials, all rights are reserved. Except as expressly granted by the terms of the license, no part of the Wiley Materials may be copied, modified, adapted (except for minor reformatting required by the new Publication), translated, reproduced, transferred or distributed, in any form or by any means, and no derivative works may be made based on the Wiley Materials without the prior permission of the respective copyright owner. **For STM Signatory Publishers clearing permission under the terms of the [STM Permissions Guidelines](#) only, the terms of the license are extended to include subsequent editions and for editions in other languages, provided such editions are for the work as a whole in situ and does not involve the separate exploitation of the permitted figures or extracts,** You may not alter, remove or suppress in any manner any copyright, trademark or other notices displayed by the Wiley Materials. You may not license, rent, sell, loan, lease, pledge, offer as security, transfer or assign the Wiley Materials on a stand-alone basis, or any of the rights granted to you hereunder to any other person.
- The Wiley Materials and all of the intellectual property rights therein shall at all times remain the exclusive property of John Wiley & Sons Inc, the Wiley Companies, or their respective licensors, and your interest therein is only that of having possession of and the right to reproduce the Wiley Materials pursuant to Section 2 herein during the continuance of this Agreement. You agree that you own no right, title or interest in or to the Wiley Materials or any of the intellectual property rights therein. You shall have no rights hereunder other than the license as provided for above in Section 2. No right, license or interest to any trademark, trade name, service mark or other branding ("Marks") of WILEY or its licensors is granted hereunder, and you agree that you shall not assert any such right, license or interest with respect thereto
- NEITHER WILEY NOR ITS LICENSORS MAKES ANY WARRANTY OR REPRESENTATION OF ANY KIND TO YOU OR ANY THIRD PARTY, EXPRESS, IMPLIED OR STATUTORY, WITH RESPECT TO THE MATERIALS OR THE ACCURACY OF ANY INFORMATION CONTAINED IN THE MATERIALS, INCLUDING, WITHOUT LIMITATION, ANY IMPLIED WARRANTY OF MERCHANTABILITY, ACCURACY, SATISFACTORY QUALITY, FITNESS FOR A PARTICULAR PURPOSE, USABILITY, INTEGRATION OR NON-INFRINGEMENT AND ALL SUCH WARRANTIES ARE HEREBY EXCLUDED BY WILEY AND ITS LICENSORS AND WAIVED BY YOU.
- WILEY shall have the right to terminate this Agreement immediately upon breach of this Agreement by you.
- You shall indemnify, defend and hold harmless WILEY, its Licensors and their respective directors, officers, agents and employees, from and against any actual or threatened claims, demands, causes of action or proceedings arising from any breach of this Agreement by you.
- IN NO EVENT SHALL WILEY OR ITS LICENSORS BE LIABLE TO YOU OR ANY OTHER PARTY OR ANY OTHER PERSON OR ENTITY FOR ANY SPECIAL, CONSEQUENTIAL, INCIDENTAL, INDIRECT, EXEMPLARY OR PUNITIVE DAMAGES, HOWEVER CAUSED, ARISING OUT OF OR IN CONNECTION WITH THE DOWNLOADING, PROVISIONING, VIEWING OR USE OF THE MATERIALS REGARDLESS OF THE FORM OF ACTION, WHETHER FOR BREACH OF CONTRACT, BREACH OF WARRANTY, TORT, NEGLIGENCE, INFRINGEMENT OR OTHERWISE (INCLUDING, WITHOUT LIMITATION, DAMAGES BASED ON LOSS OF PROFITS, DATA, FILES, USE, BUSINESS OPPORTUNITY OR CLAIMS OF THIRD PARTIES), AND WHETHER OR NOT THE PARTY HAS BEEN ADVISED OF THE POSSIBILITY OF SUCH DAMAGES. THIS LIMITATION SHALL APPLY NOTWITHSTANDING ANY FAILURE OF ESSENTIAL PURPOSE OF ANY LIMITED REMEDY PROVIDED HEREIN.
- Should any provision of this Agreement be held by a court of competent jurisdiction to be illegal, invalid, or unenforceable, that provision shall be deemed amended to achieve as nearly as possible the same economic effect as the original provision, and the legality, validity and enforceability of the remaining provisions of this Agreement shall not be affected or impaired thereby.
- The failure of either party to enforce any term or condition of this Agreement shall not constitute a waiver of either party's right to enforce each and every term and condition of this Agreement. No breach under this agreement shall be deemed waived or excused by either party unless such waiver or consent is in writing signed by the party granting such waiver or consent. The waiver by or consent of a party to a breach of any provision of this Agreement shall not operate or be construed as a waiver of or consent to any other or subsequent breach by such other party.
- This Agreement may not be assigned (including by operation of law or otherwise) by you without WILEY's prior written consent.
- Any fee required for this permission shall be non-refundable after thirty (30) days from receipt by the CCC.

- These terms and conditions together with CCC's Billing and Payment terms and conditions (which are incorporated herein) form the entire agreement between you and WILEY concerning this licensing transaction and (in the absence of fraud) supersedes all prior agreements and representations of the parties, oral or written. This Agreement may not be amended except in writing signed by both parties. This Agreement shall be binding upon and inure to the benefit of the parties' successors, legal representatives, and authorized assigns.
- In the event of any conflict between your obligations established by these terms and conditions and those established by CCC's Billing and Payment terms and conditions, these terms and conditions shall prevail.
- WILEY expressly reserves all rights not specifically granted in the combination of (i) the license details provided by you and accepted in the course of this licensing transaction, (ii) these terms and conditions and (iii) CCC's Billing and Payment terms and conditions.
- This Agreement will be void if the Type of Use, Format, Circulation, or Requestor Type was misrepresented during the licensing process.
- This Agreement shall be governed by and construed in accordance with the laws of the State of New York, USA, without regards to such state's conflict of law rules. Any legal action, suit or proceeding arising out of or relating to these Terms and Conditions or the breach thereof shall be instituted in a court of competent jurisdiction in New York County in the State of New York in the United States of America and each party hereby consents and submits to the personal jurisdiction of such court, waives any objection to venue in such court and consents to service of process by registered or certified mail, return receipt requested, at the last known address of such party.

WILEY OPEN ACCESS TERMS AND CONDITIONS

Wiley Publishes Open Access Articles in fully Open Access Journals and in Subscription journals offering Online Open. Although most of the fully Open Access journals publish open access articles under the terms of the Creative Commons Attribution (CC BY) License only, the subscription journals and a few of the Open Access Journals offer a choice of Creative Commons Licenses. The license type is clearly identified on the article.

The Creative Commons Attribution License

The [Creative Commons Attribution License \(CC-BY\)](#) allows users to copy, distribute and transmit an article, adapt the article and make commercial use of the article. The CC-BY license permits commercial and non-

Creative Commons Attribution Non-Commercial License

The [Creative Commons Attribution Non-Commercial \(CC-BY-NC\) License](#) permits use, distribution and reproduction in any medium, provided the original work is properly cited and is not used for commercial purposes.(see below)

Creative Commons Attribution-Non-Commercial-NoDerivs License

The [Creative Commons Attribution Non-Commercial-NoDerivs License \(CC-BY-NC-ND\)](#) permits use, distribution and reproduction in any medium, provided the original work is properly cited, is not used for commercial purposes and no modifications or adaptations are made. (see below)

Use by commercial "for-profit" organizations

Use of Wiley Open Access articles for commercial, promotional, or marketing purposes requires further explicit permission from Wiley and will be subject to a fee.

Further details can be found on Wiley Online Library <http://olabout.wiley.com/WileyCDA/Section/id-410895.html>

Other Terms and Conditions:

v1.10 Last updated September 2015

Questions? E-mail us at customercare@copyright.com.



President

Prof. Ganapati D. Yadav

Institute of Chemical Technology, Mumbai

Honorary Secretary

Prof. Sudip K. Das

University of Calcutta

Honorary Treasurer

Prof. Avijit Ghosh

Heritage Institute of Technology, Kolkata

To whom it may concern

Title: Structure and photochromism of halo-bridged dimeric mercury(II) complexes of 1-alkyl-2-(p-nitro-phenylazo)imidazoles

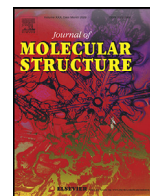
Authors: Debashis Mallick, Mukul Bikash Maity, Chandana Sen, Basudeb Dutta, Suman Kundu and Chittaranjan Sinha

Journal publication: Journal of the Indian Chemical Society, vol. 97(9b) 1478-1486 (2020).

The Indian Chemical Society hereby grants Authors the necessary permission to reproduce the material mentioned above to the terms and conditions as follows,

- i. Acknowledge: if any part of the material to be used (like Table or figure) has appeared in your other publication, it must be acknowledged (with full acknowledgement of the original article).
- ii. The permission is granted for translation to any other language.
- iii. Authors can share their preprints anywhere at any time for scholarly purpose.
- iv. Authors can use the published material in their thesis or dissertation in either print or electronic form. If the thesis be published commercially, please reapply for permission. .

Professor Sudip K Das
Honorary Secretary
Indian Chemical Society



Double advantages of Benzimidazolyl–hydroxy-coumarinyl diad - “turn-on” sensing of Al³⁺ and preventing metastasis in cancer

Mukul Bikash Maity^a, Basudeb Dutta^{a,b}, Ashikur Rahaman^c, Nilima Sahu^a, Deba Prasad Mandal^c, Shamee Bhattacharjee^c, Chittaranjan Sinha^{a,*}

^a Department of Chemistry, Jadavpur University, Kolkata 700032, India

^b Department of Chemistry, Aliah University, Kolkata 700156, India

^c Department of Zoology, West Bengal State University, Kolkata 700126, India



ARTICLE INFO

Article history:

Received 21 August 2021

Revised 25 October 2021

Accepted 2 November 2021

Available online 5 November 2021

Keywords:

Benzimidazolyl-hydroxy-coumarinyl

X-ray structure

Al³⁺-sensor

Carcinoma

Anti-metastatic potential

Epithelial marker

ABSTRACT

8-(1H-Benzoimidazol-2-yl)-7-hydroxy-4-methyl-chromen-2-one (**HL**), a benzimidazolyl–hydroxy-coumarinyl diad, serves as fluorescent turn-on Al³⁺-sensor in acetonitrile-water (2:1, v/v) of pH, 7.2 (HEPES buffer) medium. The intensity of emission on binding with Al³⁺ is enhanced by twelve times of probe with limit of detection (LOD) 0.62 μM. The structure of the probe has been established by the spectroscopic data (FT-IR, ¹H NMR, Mass spectra) and is confirmed by Single Crystal X-ray structure determination. The co-ordination environment of the complex, [Al(L)(NO₃)₂(H₂O)(NCCH₃)], has been supported by Mass, FT-IR, NMR spectra and the Job's plot supports 1:1 composition. The anti-metastatic potential of **HL** on Human skin carcinoma (A431) and Human lung carcinoma (A549) cells are examined. Wound healing and Zymography assay suggest that **HL** has anti-migratory properties. The RT-PCR and Immunoblotting data suggest that **HL** down-regulates the expression of mesenchymal markers (Vimentin, Snail, Slug, MMP, and MMP9) and induces the expression of the epithelial marker (E-Cadherin).

© 2021 Published by Elsevier B.V.

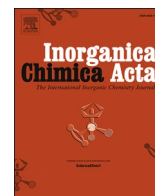
1. Introduction

Towards achievement of sustainable health - quality of air, water, essential goods, pharmaceuticals, cosmetics etc. are very important. So, quality control of the food products and other consuming materials, along with precise and accurate analytical determination are significant. Different high value analytical techniques and instruments are used in this regard in the R & D sector of the industries and research institutes. Fluorescence sensing [1–7] is one of the widely accepted techniques that is widely used due to high selectivity, sensitivity, simple instrumentation technique, low cost etc. By the way sensing of biologically active metal ions has practical utility on the issues of human health. aluminum (Al), third most abundant metal present in the earth's crust (8% of its mass) [8], has used in large quantity in domestic purposes, cooked food supply and transportation. Al(III) ingestion causes diverse abnormality in human body such as neurotoxicity, Alzheimer's and Parkinson's diseases, and also obstructs the protein transportation in respiratory system, softening of bone, anemia in living actualities etc. [9,10]. Al(III) impedes the acceptance of Ca²⁺ and inhibits to delay the growth rate of biological systems. Moreover, the

harmfulness of Al(III) is a threat towards aquatic lives and slows down the agriculture production in acidic lands. Dose-response impact of Al(III) shows adverse effects with respect to human health and plant growth. As a consequence, developing of new and practical multigesturing chemosensor for Al³⁺ is very important. Till date, several analytical techniques are available for recognition of Al³⁺ including titrimetric, chromatography, atomic absorption spectra, mass spectrometry, electrochemical detection, and Al-NMR technologies. Fluorescence spectroscopic technique is considered in recent literature as one of the most powerful analytical technique [11–15]. Many fluorescent based probes have been considered and some of them are utilized successfully in Al-neurochemistry. Most of the molecules have been constructed on quinoline, pyridyl, bipyridyl, coumarinyl, imine, pyrene, nitrobenzoxadiazole, carbazole, naphthalimide, benzoxazole, pyrazoline, tripyrrins, BINOL, fluorescein, rhodamine fluorophores [16–21], benzimidazolyl [22] and coumarinyl [23–29] groups are strongly fluorogenic motifs and inclusion of these two in a single molecule may prepare analytically and biologically useful agent which may be applied for optical detection of metal ions. Besides, coumarin belongs to interesting class of natural ingredients and shows anticancer, anticoagulant and antioxidant activity [30]. Benzimidazolyl motif serves as fungicides, anthelmintic, anticancer, anti-tubercular, anti-HIV and inhibits microtubule assembly [31]. Therefore, a molecular diad with

* Corresponding author.

E-mail address: crsjuchem@gmail.com (C. Sinha).



Application of a Rhodamine-chromone Schiff base probe for the sensing of Fe^{3+} , Al^{3+} , Cr^{3+} at low concentration and exploration of the anticancer activity and bio-imaging

Mukul Bikash Maity^a, Debojit Talukdar^b, Basudeb Dutta^c, Gurupada Bairy^a, Nabendu Murmu^b, Gaurav Das^b, Chittaranjan Sinha^{a,*}

^a Department of Chemistry, Jadavpur University, Jadavpur, Kolkata 700 032, India

^b Department of Signal Transduction and Biogenic Amines, Chittaranjan National Cancer Institute (CNCI), Bhowanipore, Kolkata 700026

^c Department of Chemical Sciences, Indian Institute of Science Education and Research, Kolkata, Mohanpur, West Bengal 741246, India

ARTICLE INFO

Keywords:

Rhodamine-chromone Schiff base
Turn-on sensing by $\text{Fe}(\text{III})$, $\text{Cr}(\text{III})$, $\text{Al}(\text{III})$
LODs are much less than WHO recommendation
Stops MCF-7 growth
Bioimaging

ABSTRACT

Strategic design of fluorescent probe for the recognition of ions/molecules at very low concentration by fluorescence sensing is one of the stimulating current research topics with reference to health and sustainability. Towards this objective, Rhodamine based chemosensors are playing extraordinary protagonist. In this work, a Rhodamine appended chromone Schiff base (**RFC**), with two fluorogenic motifs, has been characterized through various spectroscopic techniques. The probe exhibits efficient sensitivity towards Analytical Group IIIA ions (Al^{3+} , Cr^{3+} and Fe^{3+}) in existence of other competitive analytes. The fluorescent intensity is enhanced by 350 fold (Fe^{3+}), 250 fold (Al^{3+}) and 220 fold (Cr^{3+}), respectively in methanol-water (99:1,v/v; HEPES buffer, pH, 7.2) medium. The limits of detection (LOD) ($3\sigma/M$ method; σ = standard deviation; M = slope) are 0.0051 ppm (Fe^{3+}), 0.0029 ppm (Al^{3+}) and 0.0052 ppm (Cr^{3+}); which are impressive and much below the WHO recommended data. In addition to this, the compound has been utilized for cell imaging in presence of these three cations. The action of probe on MCF-7 (human breast cancer) cell lines demonstrates IC_{50} , 2.53 μM that is far better than activity against WI-38 (normal cell line) (IC_{50} , 393.7 μM). The drug (**RFC**) minimizes the cellular proliferation and has significant wound healing capacity of the infected tissue with MCF-7 cells. The probe shows significant nuclear fragmentation with increase in the expression of apoptotic markers. Growth inhibition analysis in 3D tumor spheroid model showed the inhibition of breast cancer MCF-7 cells.

1. Introduction

The detection of cations in ecological as well as biological prominence is one of the issues of sustainable development.[1–3] The sensing application of organic molecules has exalted scientific, technological, and medicinal issues.[4–6] However, the design of a multifunctional fluorogenic probe is also a major concern. The ‘turn-on’ fluorescence property is practically more reliable than ‘turn-off’ to the probe-analyte interaction because of higher preciseness, sensitivity, and accuracy for direct laboratory-to-land application.[7–10] The interaction of metal ions has been directly controlled by the binding sites of chemosensor and hence the prominence of the fluorescence intensity.[11–13].

Recently, the novel colorimetric and luminescent detection processes have been recognized in the sustainable development issues because of

their efficacy in the critical phase of biology and environment in reference to the quantitative identification of non-biodegradable hazardous ions and persistent organic pollutants.[14–17] Principally, the following procedures may be intricate for the signaling manifestation of molecular chemosensors: photoinduced charge transfer (PCT), chelation-enhanced fluorescence (CHEF), PET (Photoinduced Electron Transfer) and RET (Resonance Energy Transfer) accompanying, in particular, the HSAB (Hard and Soft Acid Base) principle[18–20]. The quantities of the analyte in the sample are the decisive cause for the regularization of ecological progression or the initiation of noxiousness. Hence, the trace level recognition of analyte concentration is a most trustworthy analytical task.[21–23].

In this regard, the detection of very low concentration of trivalent metal ions (Analytical Group-III A) is vastly stimulating. These metal

* Corresponding author.

E-mail address: crsjuchem@gmail.com (C. Sinha).

Use of diformyl-triazolo Schiff base for Zn²⁺ sensing and intracellular live cell imaging

Mukul Bikash Maity¹  | Suprava Bhunia¹  | Arka Patra¹  |
Panchanan Sahoo²  | Snehasis Mishra²  | Chittaranjan Sinha¹ 

¹Department of Chemistry, Jadavpur University, Kolkata, India

²School of Materials Science and Nanotechnology, Jadavpur University, Kolkata, India

Correspondence

Chittaranjan Sinha, Department of Chemistry, Jadavpur University, Jadavpur, Kolkata 700 032, India.
Email: crsjuchem@gmail.com

A diformylphenol Schiff base of triazole-amine, 4-methyl-2, 6-bis-[(1H-[1,2,4] triazol-3-ylimino)-methyl]-phenol (**PTR**) has been synthesised and characterised by spectroscopic data (ESI-MS, UV-vis, FT-IR, NMR spectra). The probe, **PTR**, emits at 610 nm upon excitation at 380 nm and the emission is strongly intensified on interacting with Zn²⁺ ion in DMSO-water (99:1, v/v; HEPES buffer, pH, 7.2) solution even in the presence of 15 other cations (Cu²⁺, Mn²⁺, Co²⁺, Ni²⁺, Pd²⁺, Cd²⁺, Pb²⁺, Hg²⁺, Fe³⁺, Cr³⁺, Al³⁺, Na⁺, K⁺, Ba²⁺, Ca²⁺) and the emission band has been shifted to 530 nm. The limit of detection of Zn²⁺, 0.30 μM is much lower than WHO recommended value (76 μM). The binding constant (K_d) is 4.2585 × 10⁴ M⁻¹. Selective and sensitive chemosensing behaviour of **PTR** to Zn²⁺ has been explained by switching off ESIPT quenching of the keto-enol tautomerisation of the probe along with the chelation enhancement of fluorescence (CHEF) by binding with Zn²⁺. The Job's plot and NMR titration have been extended to measure the 1:1 M composition [**PTR** + Zn²⁺]. The energy calculation by the DFT computation of keto and enol isomers supports easy tautomerisation and helps ESIPT quenching by proton transfer. Intracellular Zn²⁺ ions in living cells of HEK293 (PBS: phosphate buffer saline; pH, 7.2) have also been identified by the probe, **PTR**, using fluorescence microscopic imaging technique.

KEYWORDS

emission in visible region, ESIPT, intracellular imaging, triazole Schiff base probe, Zn²⁺ sensing

1 | INTRODUCTION

Zinc is a useful element in the progress of civilization since ancient times. Zn (II) is the second most abundant micronutrient (first is Iron) and plays a vital role in the growth and development of the human body. It regulates neural signal transmission,¹ immune function,² mammalian reproduction and others.³⁻⁵ The deficiency of Zn²⁺ ions cause severe harmful effect on the eye and skin, and the excessive presence of it causes Parkinson's,⁶⁻⁸

Alzheimer's^{9,10} and many other diseases. Although Zn²⁺ (d¹⁰) is redox innocent but its structural integrity, cooperation to other ions, structural flexibility, easy participation in substitution reaction and so forth contributes key function towards large number of enzyme catalyses.^{11,12} Therefore, the analytical detection of Zinc is an important task for sustainable health maintenance planning. There are several quantitative techniques such as gravimetric, volumetric, electroanalytical, spectroscopic and so forth. The simplest, easiest, selective and sensitive

Structure and photochromism of halo-bridged dimeric mercury(II) complexes of 1-alkyl-2-(*p*-nitro-phenylazo)imidazoles

Debashis Mallick^{*a}, Mukul Bikash Maity^b, Chandana Sen^c, Basudeb Dutta^d, Suman Kundu^e and Chittaranjan Sinha^b

^aDepartment of Chemistry, Mrinalini Datta Mahavidyapith, Kolkata-700 051, India

^bDepartment of Chemistry, Jadavpur University, Kolkata-700 032, India

^cDepartment of Chemistry, Sripat Singh Collge, Murshidabad-742 123, West Bengal, India

^dDepartment of Chemistry, Aliah University, New Town, Kolkata-700 156, India

^eDepartment of Chemistry, Ramakrishna Mission Residential College, Kolkata-700 103, India

E-mail: dmchemmdm51@gmail.com

Manuscript received online 09 July 2020, accepted 25 August 2020

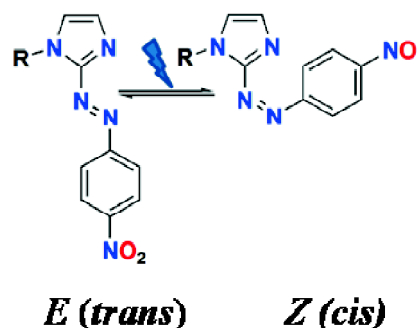
Mercury(II) complexes, $[\text{Hg}(p\text{-NO}_2\text{aaiR})(\mu\text{-X})(\text{X})_2]$ (**2-4**) of *p*-NO₂-aaiR [1-alkyl-2-(*p*-nitro-phenylazo)imidazole (**1**), where R = -CH₃ (**1a**), -C₂H₅ (**1b**) and X = Cl (**2**), Br (**3**), I (**4**)] have been studied by spectral data. X-Ray crystallography study in case of $[\text{Hg}(p\text{-NO}_2\text{aai-CH}_3)(\mu\text{-I})(\text{I})_2]$ (**4a**) has revealed the distorted dinuclear halobridge tetra-atomic puckered rhombohedral geometry. The ligand, *p*-NO₂-aaiR shows *trans(E)-cis(Z)* isomerisation both in free and coordination state on shocking UV light in the solution phase. The *Z*-to-*E* transformation is carried out by thermal treatment while photoisomerization is carried out very slowly on visible light absorption and $\phi_{E \rightarrow Z}$ (quantum yields for *E*-to-*Z* isomerisation) is superior for free ligand than the complex phase. The isomerisation rate follows $[\text{Hg}(p\text{-NO}_2\text{aaiR})(\mu\text{-I})(\text{I})_2]$ (**4**) < $[\text{Hg}(p\text{-NO}_2\text{aaiR})(\mu\text{-Br})(\text{Br})_2]$ (**3**) < $[\text{Hg}(p\text{-NO}_2\text{aaiR})(\mu\text{-Cl})(\text{Cl})_2]$ (**2**) which is also the sequence of molar mass of the compounds. The energy gap calculation of the optimized structures by DFT (Density Functional Theory) also supports this conjecture.

Keywords: Photochromism, *p*-nitro-phenylazo-imidazole, Hg(II), X-ray, DFT.

Introduction

The structural change of some aromatic-azo compounds^{1,2} by absorbing light has massive applications in the field of molecular machines³, data storage⁴, bio-conjugates⁵, polymers towards optical stimuli-response⁶, nanomaterials^{7,8} etc. The prospect of azobenzene in this field is inspiring to focus on group of azo molecules, arylazoimidazoles, in particular². Photochromism of 1-alkyl-2-(arylo)imidazole^{9,10} and some of their complexes are published¹¹⁻¹⁴. For detail investigation on the influence of substituent on the photoisomerisation, a nitro (-NO₂) functionalised azoimidazole, 1-alkyl-2-(*p*-nitro-phenylazo)imidazole, *p*-NO₂-aaiR (**1**) (R = -CH₃ (**1a**), -C₂H₅ (**1b**)) and its Hg(II) complexes are synthesized. The spectroscopic techniques are used for the characterisation of ligands and compounds. The single crystal X-ray structure determination is help ful for the establishment of structure of one of the complexes only. Through this

work, the isomerisation rates and quantum yields are compared between free ligand and coordination phase in the complex in presence of different halides. Theoretical study has been attempted to describe the light induced structural change.



Scheme 1. Isomerisation of 1-alkyl-2-(*p*-nitro-phenylazo)imidazole, *p*-NO₂-aaiR, (**1**).